



HAL
open science

Investigation of the performances of an ECR charge breeder at ISOLDE: a study of the $1+ n+$ scenario for the next generation ISOL facilities

Mélanie Marie-Jeanne

► **To cite this version:**

Mélanie Marie-Jeanne. Investigation of the performances of an ECR charge breeder at ISOLDE: a study of the $1+ n+$ scenario for the next generation ISOL facilities. Accelerator Physics [physics.acc-ph]. Université Joseph-Fourier - Grenoble I, 2009. English. NNT : . tel-00363928

HAL Id: tel-00363928

<https://theses.hal.science/tel-00363928>

Submitted on 25 Feb 2009

HAL is a multi-disciplinary open access archive for the deposit and dissemination of scientific research documents, whether they are published or not. The documents may come from teaching and research institutions in France or abroad, or from public or private research centers.

L'archive ouverte pluridisciplinaire **HAL**, est destinée au dépôt et à la diffusion de documents scientifiques de niveau recherche, publiés ou non, émanant des établissements d'enseignement et de recherche français ou étrangers, des laboratoires publics ou privés.

Université Joseph Fourier - Grenoble I
Ecole Doctorale de Physique

Thèse présentée pour le titre de Docteur en Physique pour l'Instrumentation

Mélanie MARIE-JEANNE

**Investigation des performances d'un élévateur de l'état de charge par ECR à
ISOLDE: une étude du scénario $1^+ \rightarrow n^+$ pour les installations ISOL de la
prochaine génération**

INVESTIGATION OF THE PERFORMANCES OF AN ECR CHARGE BREEDER AT ISOLDE:
A STUDY OF THE $1^+ \rightarrow n^+$ SCENARIO FOR THE NEXT GENERATION ISOL FACILITIES



Thèse dirigée par Ana LACOSTE et Pierre DELAHAYE

Soutenue le 6 Février 2009 au CERN, à Genève

Jury:

Président:	Georg BOLLEN
Rapporteurs:	Yorick BLUMENFELD Oliver KESTER
Examineurs:	Charles BARTON Thierry LAMY
Directrice de thèse:	Ana LACOSTE
Co-directeur de thèse:	Pierre DELAHAYE

Acknowledgments

Until now, I have always received more supportive and constructive remarks than discouraging words. One of the greatest rewards of this work was to mix with a large number of interesting characters during the last three years. Therefore I am truly thankful to all the people who made this project possible in so many ways.

First of all, I would like to thank the members of the jury for examining this report, especially Yorick Blumenfeld and Oliver Kester for their comprehensive reading. I am also obliged to Georg Bollen for crossing so many miles to take the chair at my defence, thus putting just enough pressure on my performance to make the best out of it. I am similarly indebted to Charles Barton and Oliver Kester for taking the trip again this time, like the numerous times before.

I am sincerely grateful to Ana Lacoste, Pierre Delahaye, Peter Butler and Karsten Riisager for giving me the opportunity to conduct my research project at ISOLDE. I felt that their full trust and support could only add to my motivation. I have a special thought for Pierre's careful guidance during my study years. From him I learned to use every second of my (beam)time to make things happen !

I truly appreciated the precious advices of Thierry Lamy and Thomas Thuillier, who did a wonderful job introducing me to the ECRIS technology at the "Service des Sources d'Ion" of Grenoble. I am also thankful to Erik Heijne for following the progress of my work at CERN from the very beginning.

Nothing could have been achieved without the help of the numerous people who gave me a hand precisely when it was needed. Therefore I give credit

to Joakim Cederkäll and Ulli Köster for helping me to build such interesting projects

within my thesis, and to the other collaborators from the IS397 and IS458 experiments for sharing their experience with me.

to Erwin, Fredrik, Jarno, Magnus, Nicolas, Pascal, Sophie, Tim, the whole ISOLTRAP team, and many other members of the ISOLDE team for finding the time to help me in the experimental hall even during rush periods.

to the ISOLDE target group, and particularly to magicians such as Bernard, Daniel and Ermano, for saving so many pieces of equipment as well as their final design.

to Catherine, Céline, France, Ingrid, Jenny, Sandrine, Valérie for making my life much easier on the administrative side.

Because friends and family are definitely needed to survive a PhD thesis, I am indebted

to all the “corridor” friends for many welcome breaks: Anna, Anne-Gaëlle, Chabouh, Dennis, Elian, Gry, Hanna, Herta, Joris, Karl, Liviu, Magda, Martin “Bonjour !”, Pekka, Romain, Sarah, Sandrina, Sven, Tania, and many others.

to all the “long-distance” friends for many soothing week-ends: Alixe, Aurélie, Elisa, Marty, Nadine, Séverine, Yoann, Yohan and many more.

to my parents, Hélène, Jean and the rest of the family for preserving my diet balance with a reasonable amount of real food.

Finally, there are persons who deserve all my gratitude for leading me to who I am today.

Thanks to my parents for arousing my curiosity as a child and for giving me this will to always learn more.

Thanks to the few professors who, due to their communicative passion, oriented me towards the path of science.

Thanks to my sister for patiently listening to my science presentations.

Thanks to Fabien for teaching me how to take a much broader view of problems... and for helping me to keep a life outside of work.

Abstract

The work I describe here was performed at ISOLDE, CERN. It aimed at giving an objective report of the current performances of Electron Cyclotron Resonance (ECR) ion sources used as charge breeders, with both stable and radioactive ion beams. As a prerequisite, some technical developments were undertaken to improve the setup and to lead the tests with optimal conditions. A major part of these developments concerns beam purity, and is detailed in this thesis. Then, the program of measurements of the charge breeding efficiencies of various isotopes was completed with different charge breeding modes. I analyzed the results of these experiments and compared them to the current performances of other types of charge breeding methods. At the end, some conclusions are drawn from this investigation in perspective of the choices to make for future ISOL postaccelerators. The discussion is extended to the immediate application of ECR charge bred radioactive ion beams to physics experiments, for which I proposed and performed additional tests.

Le travail que je décris ici fut effectué à ISOLDE, au CERN. Il vise à établir un rapport objectif des performances actuelles des sources d'ions à Résonance Electronique Cyclotronique (ECR) utilisées en tant qu'élevateurs d'état de charge, à la fois avec des faisceaux d'ions stables et radioactifs. Au préalable, on a entrepris quelques développements techniques pour améliorer le dispositif et conduire les tests dans des conditions optimales. Ce rapport détaille la majeure partie de ces développements qui concerne la pureté du faisceau. Puis, le programme de mesure des efficacités d'élevation d'état de charge pour divers isotopes fut achevé avec des modes de fonctionnement différents. J'ai analysé les résultats de ces expériences et les ai comparés aux performances actuelles des autres méthodes d'élevation d'état de charge. Finalement, je présente les conclusions que l'on peut tirer de cette étude concernant les choix à effectuer pour les futurs post-accelérateurs dans les installations de type ISOL. La discussion s'étend aux applications immédiates, pour les expériences de physique, des faisceaux radioactifs d'ions épluchés par ECR, pour lesquelles j'ai proposé et effectué des tests supplémentaires.

Contents

Acknowledgements	iii
Abstract	v
Contents	ix
List of tables	xi
List of figures	xv
List of symbols	xvii
List of acronyms and abbreviations	xix
Introduction	1
<i>Introduction (français)</i>	7
1 Motivation and scientific context	11
1.1 Charge breeding for postaccelerated RIBs	11
1.2 Multi-ionization techniques	13
1.2.1 Stripping cells	13
1.2.2 EBIS	16
1.2.3 ECRIS	19
1.3 The ECR charge breeder test bench	24
1.3.1 The facility: ISOLDE	24
1.3.2 The charge breeder: PHOENIX ECR Booster	25
1.3.3 Experimental methods	28
1.4 Aim of the PhD study	38

<i>Résumé du chapitre 1 (français)</i>	41
2 Charge breeding experiments	45
2.1 Online results with stable ions	45
2.1.1 Optimizing the injection in continuous mode	45
2.1.2 Tests with the trapping mode	50
2.2 Online results with radioactive ions	52
2.2.1 Tests with noble gases of various (A,Z)	52
2.2.2 Effect of the chemical properties of isobars	53
2.2.3 Trapping of daughter nuclides in the ECR plasma	58
2.3 Summary of the performance study tests	66
<i>Résumé du chapitre 2 (français)</i>	67
3 Proposals to improve the PHOENIX ECR Booster	71
3.1 Limitations of the current setup	71
3.1.1 Stable background	71
3.1.2 X-ray shielding	72
3.1.3 Radioactive background	73
3.1.4 Light ion injection	73
3.2 Improvements needed for an objective comparison with the EBIS devices	74
3.2.1 Capture efficiency	74
3.2.2 High charge states	74
3.2.3 Quality of the extracted beam	75
3.2.4 Operation and maintenance	75
3.3 Projects for the technical upgrade of the PHOENIX ECR Booster	75
3.3.1 60kV upgrade	75
3.3.2 Towards a UHV charge breeder	77
3.3.3 Project of a new mass and energy separator	80
<i>Résumé du chapitre 3 (français)</i>	89
4 Perspectives of the $1^+ \rightarrow n^+$ ECR charge breeding	91
4.1 Discussion of the results of the performance study	91
4.1.1 Comparison with other charge breeding techniques	91
4.1.2 Consequences for the type of postaccelerator	91
4.2 Future for physics experiments	94
4.2.1 Possibilities for beam purification	94
4.2.2 Application to a case in nuclear astrophysics	95
<i>Résumé du chapitre 4 (français)</i>	103
Conclusion	105

Conclusion (français)	107
A Routines for GO4 and ROOT analysis	111
A.1 On-line monitoring with GO4	111
A.1.1 Data encoding with the f_user.c routine	112
A.1.2 Structure of the *.lmd data file	114
A.2 Analysis with ROOT	115
A.2.1 Unpacking the data with the CreateHisto.cpp routine	115
A.2.2 Fitting the coincidence spectra with the FitHisto.cpp routine	124
A.2.3 Sorting the results with the Analyze.cpp routine	125
B Beam calculations for the new mass and energy separator	127
B.1 Available beamline elements	127
B.2 Transfer matrices with COSY INFINITY	129
B.3 Ion distribution with Matlab	136
B.4 Control system with LabView	140
C Latest proposal of experiment with the PHOENIX ECR charge breeder	143
Bibliography	153

List of Tables

1.1	Performances of stripping cells	15
1.2	Performances of EBIS charge breeders	18
1.3	Performances of ECR charge breeders	23
1.4	Specifications of the mass analyzing magnet	27
1.5	Power supplies for the PHOENIX Booster	28
1.6	Typical parameter settings in continuous mode	30
1.7	Typical parameter settings in pulsed mode	31
1.8	Sources of systematic errors	37
3.1	Isotopic separator costs	87
4.1	Comparative table of performances	92
B.1	List of elements available for the separator	128
B.2	Specifications of the new magnetic and electrostatic sectors	129

List of Figures

1	Chart of nuclides	1
2	Mass measurement with highly-charged ions	2
3	Application of highly-charged ions to the formation of single dopant arrays	3
4	Picture of the PHOENIX Booster ECR charge breeder	5
1.1	Geometrical transverse emittance definition	12
1.2	Analogy between various multi-ionization techniques	13
1.3	Principle of the stripping cell	14
1.4	Principle of the EBIS charge breeding	16
1.5	Electron Cyclotron Resonance condition	19
1.6	Magnetic mirror in the ECRIS	20
1.7	Principle of the ECR charge breeding	21
1.8	Scheme of the axial ECR plasma potential	21
1.9	Layout of ISOLDE experimental hall	25
1.10	Layout of the experimental test bench	26
1.11	Cross-section drawing of the PHOENIX Booster	27
1.12	Beam ON - beam OFF method	29
1.13	Example of pulsed extraction from the ECR charge breeder	32
1.14	Detection efficiency for the gammas and for the betas	33
1.15	Scheme of the detection setup	33
1.16	Picture of the detection setup	34
1.17	Scheme of the detection electronics	35
1.18	Measurement cycles in pulsed mode and in continuous mode	35
1.19	Data acquisition events encoding	36
2.1	Detection of charge bred stable beams of ^{238}U and ^{40}Ar	46
2.2	ΔV curve for injection of stable elements	47
2.3	Efficiency of plasma capture	48

2.4	Charge breeding efficiencies for various stable species	49
2.5	Afterglow pulse of $^{238}\text{U}^{26+}$	50
2.6	Afterglow charge breeding efficiencies for stable elements	51
2.7	Signature of $^{48}\text{Ar}^{9+}$	52
2.8	Beta-gated gamma spectrum for isobars of mass 142	53
2.9	ΔV curve for the injection of isobars	54
2.10	Scheme of a hot plasma ion source	55
2.11	Gamma yield spectrum for mass 142 isobars	56
2.12	Release curve for ^{142}Cs	56
2.13	Charge state distributions for mass 142 isobars	57
2.14	^{61}Mn release curve	58
2.15	^{61}Mn beta decay curve	60
2.16	Charge breeding times for ^{61}Mn	60
2.17	^{61}Fe beta decay curve	61
2.18	^{61}Fe activity as a function of the trapping time	63
2.19	^{61}Fe activity as a function of time	64
2.20	^{61}Mn and ^{61}Fe charge breeding efficiencies	65
3.1	Stable background in the ECRIS	71
3.2	Pictures of the X-ray shielding	72
3.3	TAC spectrum	73
3.4	Pictures of the 60 kV upgrade	76
3.5	Scheme of the 60 kV platform grounding	76
3.6	Carbon extraction tube	77
3.7	Scheme of the conductance for vacuum improvement	78
3.8	Pumping system on the test bench	79
3.9	Mass spectra with reduced extracted current	79
3.10	Energy spread in a mass spectrum	80
3.11	Expected improvements on the A/q spectrum	81
3.12	Scheme of beam transport	82
3.13	Determination of the mass resolving power	83
3.14	Determination of the energy resolving power	83
3.15	Final isotopic separator layout	85
3.16	X-Y distribution of the beam on focal planes	86
4.1	Principle of the molecular beam technique	94
4.2	R-process path nuclides	95
4.3	Neutron-rich nuclides detection scheme	97
4.4	Pictures of the neutron-rich nuclides detection setup	97
4.5	Timing of the neutron-rich nuclides measurement cycle	98
4.6	Charge breeding efficiencies for ^{94}Rb , ^{132}Sn and ^{133}Sn	99
4.7	Neutron decay measured for $^{134}\text{Sn}^{21+}$	100

List of Figures

4.8	Gamma lines for the $^{118}\text{In}^{15+}$ contamination measured after the ECR	101
A.1	GO4 graphical user interface	111
A.2	Schematic representation of the analysis program	115
B.1	Triplets measured dimensions	127
B.2	Power supplies control via Profibus	140
B.3	LabView interface for the power supplies control system	141

List of symbols

a	divergence along the x axis (in radian)
A	atomic mass number (in atomic mass units)
$(A/q)/\Delta(A/q)$	mass resolving power (no dimension)
b	divergence along the y axis (in radian)
B	magnetic field of the mass analyzer (in Gauss)
Δt_{delay}	delay before the start of a measurement file (in minutes)
$\Delta\Phi$	electrostatic well created by the high density of electrons in the center of the plasma (in Volts)
ΔV	difference of potential between the 1^+ source and the ECR charge breeder (in Volts)
η_{n+}	charge breeding efficiency for a given charge state n (no dimension)
η_{total}	capture efficiency or sum of the charge breeding efficiencies for all charge states (no dimension)
Φ	plasma potential (in Volts)
f_c	electron cyclotron frequency (in GHz)
f_{RF}	external (klystron) radiofrequency (in GHz)
K	kinetic energy (in MeV for Appendix C)
$(K/q)/\Delta(K/q)$	energy resolving power (no dimension)
m	mass (in atomic mass units)
$\delta m/m$	mass resolving power (no dimension)
q	charge state number (no dimension)
q_{max}	most abundant charge state of the distribution (no dimension)
$P_{(x,y,z)}$	quantity of motion (and its projections on the coordinates axes)
P_n	probability of beta-delayed neutron emission (no dimension)
t	time of flight (in seconds)
$T_{1/2}$	half-life (in seconds)
t_{BGon}	beam injection duration (in seconds)
τ_{cb}	charge breeding time (in milliseconds)

$t_{collect}$	duration for ions collection on tape (in seconds)
τ_{conf}	confinement time of the ion in the magnetic field (in milliseconds)
t_{decay}	duration for decay measurement (in seconds)
t_{delay}	delay between the end of the beam injection and the tape move, to collect all charge bred ions released by the ECR plasma (in milliseconds)
t_{init}	delay between the proton pulse and the beam injection start (in milliseconds)
τ_{ioniz}	ionization time (in milliseconds)
t_{mov}	time needed for tape move from collection point to measurement point (in seconds)
t_{start}	starting time for a measurement file
t_{stop}	stopping time for a measurement file
u	atomic mass unit (approximately $1.7 \cdot 10^{-27}$ kg)
v	particle velocity (in meter per second)
V_{1+}	potential of the 1^+ source (in kVolts)
V_{ECR}	potential of the ECR charge breeder plasma chamber (in kVolts)
x	position along the x axis (in meter)
y	position along the y axis (in meter)
Z	number of protons for a given element (no dimension)

List of acronyms and abbreviations

ADC	Analog-to-Digital Converter
AFM	Atomic-Force Microscopy
AMS	Accelerator Mass Spectrometry
BGoff	Measurement period where the beam gate is OFF and FC3 is not inserted
BNL	Brookhaven National Laboratory
CERN	European Organization for Nuclear and Particle Physics Research
CFD	Constant Fraction Discriminator
collect	Measurement period where the beam gate is ON
CS	Charge State
CW	Continuous Wave
DAQ	Data AcQuisition
DC	Direct Current (or “continuous” current)
EBIS	Electron Beam Ion Source
ECL	Emitter-Coupled Logic
ECR	Electron Cyclotron Resonance
ECRIS	Electron Cyclotron Resonance Ion Source
EL	Einzel Lens
ETFSI	Extended Thomas-Fermi plus Strutinsky Integral
EURISOL	EUROpean Isotope Separation On-Line radioactive nuclear beam facility
EURONS	the integrated infrastructure initiative for EUROpean Nuclear Structure research
FEBIAD	Forced Electron Beam Ion Arc Discharge
FC	Faraday Cup
FCin	Measurement period where the beam gate is OFF and FC3 is inserted
FWHM	Full-Width at Half Maximum
GANIL	Grand Accélérateur National d’Ions Lourds

GHM	General Heavy Masses (beamline)
GLM	General Lower Masses (beamline)
GPS	General Purpose Separator
GUI	Graphical User Interface
HRS	High Resolution Separator
ISAC	Isotope Separator and ACcelerator
ISN	Institut des Sciences Nucléaires
ISOL	Isotope Separation On Line
ISOLDE	Isotope Separator On Line (DE)
KEK-JAERI	KEK - Joint Project on High Intensity Proton Accelerators
LINAC	LINear ACcelerator
LPSC	Laboratoire de Physique Subatomique et Corpusculaire
MAXEBIS	MAX-Electron Beam Ion Source
MBS	Module Buffer Stream
MINIMAFIOS	MINI-Machine A Faisceau d'IONS Strippés
NASA	National Aeronautics and Space Administration
NIM	Nuclear Instrument Module
LBNL	Lawrence Berkeley National Laboratory
LPSC	Laboratoire de Physique Subatomique et Corpusculaire
ORNL	Oak Ridge National Laboratory
OLE	Object Linking and Embedding
OPC	OLE for Process Control
PC	Personal Computer
PHOENIX	Production Hautement Optimisée d'Electrons, de Noyaux Ionisés et de rayons X
PROFIBUS	PROcess FIeld BUS
QED	Quantum ElectroDynamics
REX-EBIS	Radioactive beam EXperiment Electron Beam Ion Source
REX-ISOLDE	Radioactive beam EXperiment at ISOLDE
REXTRAP	Radioactive beam EXperiment cooling TRAP
RF	RadioFrequency
RHIC	Relativistic Heavy Ion Collider
RIA	Rare Isotope Accelerator
RIB	Radioactive Ion Beam
RILIS	Resonance Ionization Laser Ion Source
SPIRAL (1 or 2)	Système de Production d'Ions Radioactifs Accélérés en Ligne (1 or 2)
TAC	Time to Amplitude Converter
TIS	Target-Ion Source (unit)
TOF	Time-Of-Flight
TTL	Transistor-Transistor Logic

List of acronyms and abbreviations

TRIUMF	TRI-University Meson Facility
UHV	Ultra-High Vacuum
VME	VERSA-Module Europe

Introduction

The exploration of the nuclear chart has raised the issue of producing nuclides always further from the valley of stability (see Figure 1 and [1]). In the various Radioactive Ion Beam (RIB) facilities around the world, special efforts are made to produce and extract efficiently radioactive isotopes, and to transport them towards experiments.

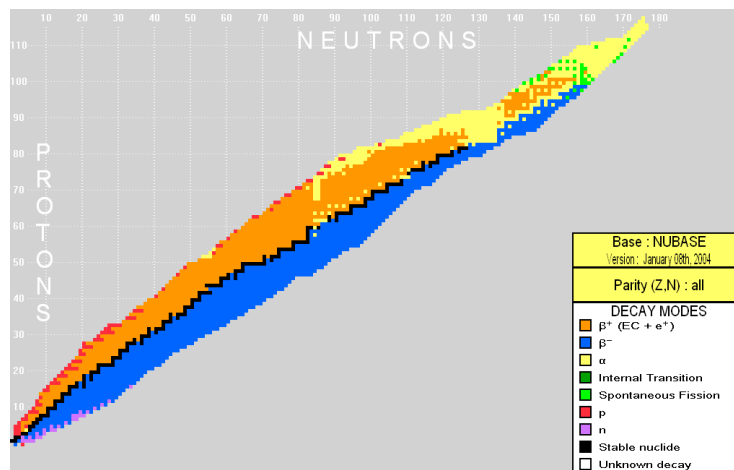


Figure 1: Chart of nuclides as given by [2]. The ensemble of stable isotopes, called valley of stability, is drawn in black. The rest constitutes the ensemble of the radioactive nuclides.

In the latter step, ionization plays a crucial role. Due to its electric charge, one can manipulate an ion inside electric and magnetic fields. Charged particles can be accelerated, deflected, and selected according to their charge, mass or velocity, to form an ion beam. Being able to charge breed one charge state rather than another allows control on the beam energy or trajectory, for a given acceleration voltage.

In itself, producing different charge states of a same isotope is of interest for fundamental science, due to the fact that the additional charges can enhance some effects in the atomic structure that are hardly detectable otherwise. Indeed, highly-charged ions have become tools to probe our universe at every scale. At a sub-atomic level, the structure of small ensembles of electrons around different nuclides can be studied to probe Quantum ElectroDynamics (QED), one of the most advanced quantum field theories in electromagnetism nowadays [3]. High precision fundamental measurements such as the measurements of atomic masses (see Figure 2 and [4, 5]) and of fundamental constants [6] have progressed with the use of highly-charged ions, and provide information for the determination of nuclear properties or for the search for physics beyond the standard model. In astrophysics, the lifetime shortening of given isotopes when they are in a highly ionized state directly effects on the determination of the age of the universe [7]. The production of spectra of highly-charged ions in the laboratory also allows one to simulate the conditions corresponding to X-ray transitions of astrophysical interest [8]. Measurements of electron-ion recombination rates for different charge states of the ion lead to improved stellar plasma modeling [9]. At our scale, such interactions are also of importance to understand processes in future fusion reactor plasmas [10]. More research to improve our quality of life, such as the study of the risks associated to radiation on biological systems, uses techniques based on highly charged ions [11].

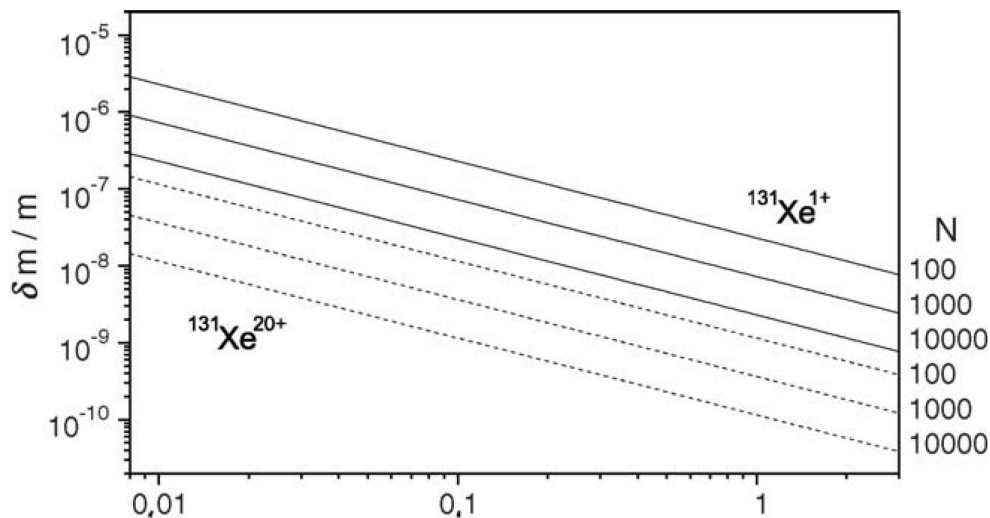


Figure 2: Mass measurement with highly-charged ions as taken from [5]: “Relative statistical mass uncertainty $\delta m/m$ [...] for $^{131}\text{Xe}^{1+}$ (solid lines) and $^{131}\text{Xe}^{20+}$ (dashed lines) as a function of the observation time T_{obs} and for different total ion numbers N .”

Furthermore, with a given accelerating potential higher beam energies can be reached with highly-charged ions, and this is very advantageous for postaccelerated beams applications. Nowadays, highly-charged ions are postaccelerated for medical purposes such as cancer tumor treatment [12, 13], for industrial tests such as wear studies [14], for the development of electronics nanomaterial (see Figure 3) and nanoprobes [15], or for various nuclear physics experiments where the implantation depth should be controlled (as for example in [16]).

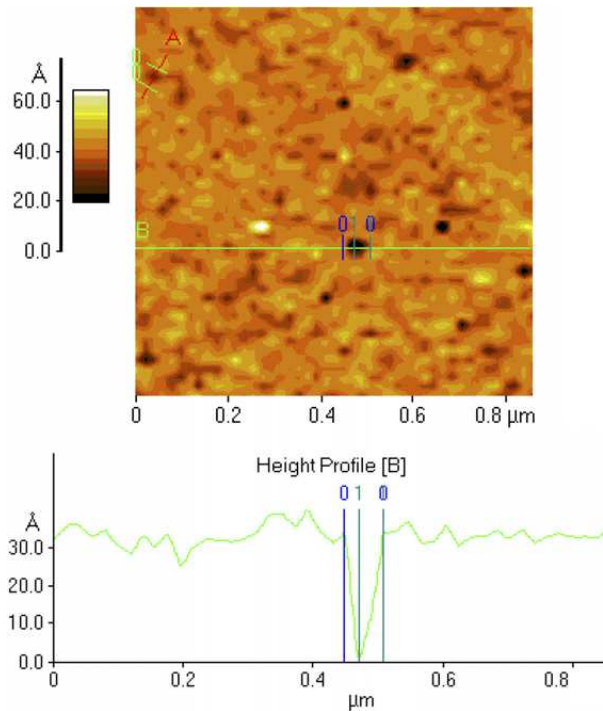


Figure 3: Application of highly-charged ions to the formation of single dopant arrays on diamond surfaces as given in [17]: “[Atomic-Force Microscopy (AFM)] images of defects on the surface of a “flat” [insulating] diamond [...] induced by single Xe^{44+} ions”. The study of single ion impacts on insulating or semi-conducting material is essential to the development of a precise technique for the formation of optically active defects in ordered arrays.

Although a few cases exist where a pure electrostatic post-acceleration would be sufficient to reach energies necessary for the experiments [18], most issues in nuclear physics and in astrophysics require much higher energies. Therefore, charge breeding is part of the beam preparation, required for the post-acceleration of the radioactive nuclides in a LINear ACcelerator (LINAC) or a cyclotron. Lately, it has also become part of the beam purification processes, as it allows the removal of contaminants from the radioactive ion beam in some specific cases [19, 20].

Various solutions exist for charge breeding of stable ion beams. However, charge breeding raises a few challenges when it comes to radioactive ion beams (RIBs). Issues such as beam purity, charge breeding efficiency, and charge breeding times for a wide range of isotopes become highly important when the yields are low. Moreover, the ratio between the mass A of the ion and the highest charge state q that can be reached should match the acceptance of the post-accelerator. It is foreseen that next generation post-accelerators, for example at ISOLDE [21], will be designed for beams of up to a factor 5 higher intensity, so charge breeders should eventually be able to handle intense injected beams of up to a few 10^{13} radioactive ions per second [22]. Finally, safety regulations in a RIB facility increase the level of constraints for the maintenance of equipment. Therefore, the robustness and the easy maintenance of the charge breeder are crucial points. The complexity of operation should also be taken into account for a continuous run in an operational facility.

The choice to study an Electron Cyclotron Resonance (ECR) ion source as a charge breeder was motivated by its relative robustness and the fact that no efficiency drop was observed up to a few tens of microamperes of injected beam [23]. With such a high acceptance, the ECR charge breeder appeared as a much simpler setup than the Electron Beam Ion Source (EBIS) charge breeder, which requires a preparation stage to cool and bunch the injected beam [24]. This work presents the results obtained with the Daresbury Laboratory (UK) ECR charge breeder, which is installed as a test bench in the ISOLDE facility at CERN, Geneva, as shown on Figure 4. It aims at the investigation of the ECR charge breeding performances with a wide range of radioactive ions produced at ISOLDE.

The first chapter of this thesis describes briefly the various multi-ionization techniques currently used in RIB facilities, and more in detail the ECR charge breeder chosen for the study. Then, the experimental results with both stable and radioactive ions are given in the second chapter. In the third chapter, technical improvements to the ECR charge breeder are proposed. Finally, the results are compared with the ones from other types of charge breeders in the fourth chapter, and perspectives for physics applications are discussed as well. The final conclusion gives an outlook of the role of ECR charge breeding in next generation RIB facilities.

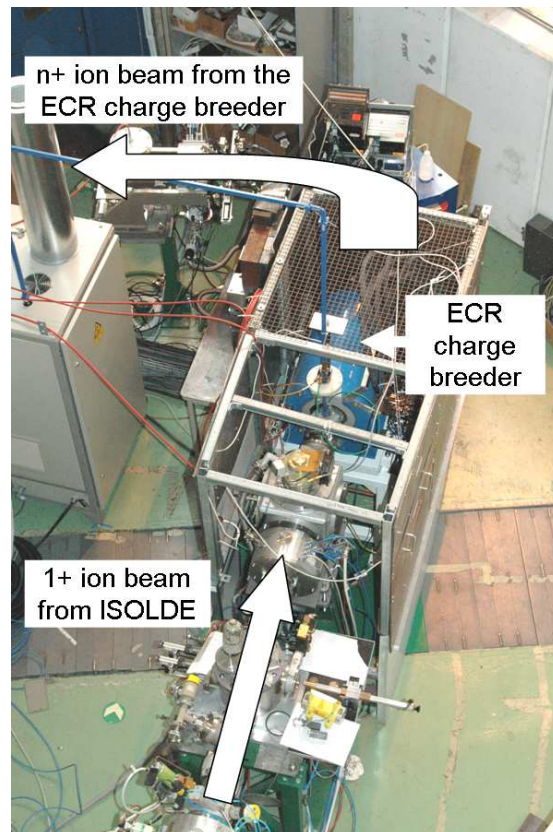


Figure 4: Picture of the Daresbury Laboratory (UK) ECR charge breeder, or so-called PHOENIX Booster, on its test bench at ISOLDE, CERN.

Introduction

Avec l'exploration de la carte des noyaux est apparue la problématique de la production de noyaux toujours plus éloignés de la vallée de stabilité (voir Figure 1 et [1]). Les diverses installations de production de faisceaux d'ions radioactifs dans le monde s'efforcent tout particulièrement de produire et d'extraire les isotopes radioactifs de manière efficace afin de les transporter vers les expériences.

Pour cette dernière étape, l'ionisation joue un rôle crucial. En raison de son état de charge, on peut manipuler l'ion par des champs électriques et magnétiques. On peut accélérer, défléchir et sélectionner les particules chargées selon leur état de charge, leur masse ou leur vitesse, pour former un faisceau d'ions. L'aptitude à produire un état de charge plutôt qu'un autre donne, pour une tension d'accélération fixée, le contrôle sur l'énergie ou la trajectoire du faisceau.

En soi, la production des différents états de charge d'un même isotope présente un intérêt en science fondamentale, car les charges additionnelles peuvent accentuer des effets de la structure atomique qui ne sont pas détectables autrement. En effet, les ions multichargés sont devenus des outils pour l'étude de notre univers à toutes les échelles. Au niveau subatomique, l'étude de petites structures électroniques autour de noyaux différents permet de tester la théorie de l'électrodynamique quantique relativiste (QED), l'une des théories quantiques des champs de l'électromagnétisme les plus avancées à l'heure actuelle [3]. Les mesures fondamentales de haute précision comme les mesures de la masse atomique (voir Figure 2 et [4, 5]) et les mesures de constantes fondamentales [6] ont progressé avec l'utilisation des ions multichargés, et procurent des informations pour la détermination des propriétés du noyau, ou pour la recherche au-delà du modèle standard. En astrophysique, certains isotopes ont une durée de vie plus courte lorsqu'ils sont dans un état hautement ionisé, ce qui influe sur la détermination de l'âge de l'univers [7]. La production des spectres d'ions multichargés en laboratoire permet de simuler les conditions de transition X présentant un intérêt en astrophysique [8]. Des mesures des taux de recombinaison entre électrons et ions d'états de charge différents améliorent la modélisation des plasmas stellaires

[9]. A notre échelle, de telles interactions importent pour comprendre les processus de fonctionnement des futurs réacteurs de fusion [10]. D'autres recherches pour améliorer notre qualité de vie mettent en jeu des techniques utilisant les ions multichargés, comme l'étude des risques des radiations pour les systèmes biologiques [11].

En outre, on peut atteindre des énergies de faisceau plus élevées avec des ions multichargés, ce qui est très avantageux pour les applications des faisceaux post-accélérés. De nos jours, les ions multichargés sont post-accélérés à des fins médicales, telles que le traitement de tumeurs cancéreuses [12, 13], pour des tests industriels tels que les études d'usure [14], pour le développement de nanomatériaux (voir Figure 3) et de nanosondes [15] en électronique, ou pour des expériences variées de physique nucléaire qui requièrent le contrôle de la profondeur d'implantation (comme par exemple pour [16]).

Bien qu'il existe quelques cas pour lesquels une post-accélération électrostatique suffirait à atteindre les énergies nécessaires aux expériences [18], la plupart des problématiques en physique nucléaire et en astrophysique requièrent des énergies beaucoup plus élevées. Par conséquent, l'élévation de l'état de charge fait partie de la préparation de faisceau requise pour post-accélérer les noyaux radioactifs dans un ACcélateur LINéaire (LINAC) ou un cyclotron. Récemment, elle est également devenue partie intégrante des procédés de purification du faisceau, en permettant la suppression de contaminants du faisceau d'ions radioactifs dans certains cas spécifiques [19, 20].

Des solutions variées existent pour élever l'état de charge des faisceaux d'ions stables. Cependant, l'élévation de l'état de charge devient un défi avec les faisceaux d'ions radioactifs. Des problèmes tels que la pureté du faisceau, l'efficacité et la durée du processus pour une grande variété d'isotopes sont d'autant plus importants que les taux de production sont faibles. En outre, le rapport entre la masse A de l'ion et le plus élevé des états de charge atteints q doit correspondre à l'acceptance du post-accélérateur. On prévoit de concevoir la prochaine génération de post-accélérateurs (tel que celui d'ISOLDE [21]) pour des faisceaux jusqu'à cinq fois plus intenses, donc les élévateurs d'état de charge devront pouvoir gérer des faisceaux injectés jusqu'à quelques 10^{13} ions radioactifs par seconde [22]. Finalement, les règles de sûreté dans une installation de production de faisceaux d'ions radioactifs augmentent le niveau des contraintes concernant la maintenance de l'équipement. L'utilisation d'un élévateur de l'état de charge robuste et simple à entretenir est donc cruciale. Dans le cas d'une utilisation continue pour une installation opérationnelle, on doit également prendre en compte la simplicité d'opération.

Le choix d'étudier une source d'ion à Résonance Electronique Cyclotronique (ECR) en tant qu'élévateur d'état de charge se justifie par sa relative solidité et par le fait qu'on n'a observé aucune baisse de l'efficacité jusqu'à quelques dizaines de microampères de faisceau injecté [23]. Avec une si grande acceptance, l'élévateur d'état de charge ECR pourrait constituer un dispositif plus simple que la Source d'Ion à Bombardement Electronique (EBIS), qui nécessite une étape de préparation pour refroidir et pulser le faisceau [24]. Ce travail présente les résultats obtenus avec

l'élevateur d'état de charge ECR du laboratoire de Daresbury (GB), qui est installé sur un banc de test au complexe ISOLDE au CERN, à Genève, comme le montre la Figure 4. Il est destiné à l'étude des performances d'élévation d'état de charge par ECR avec une grande variété d'ions radioactifs produits à ISOLDE.

Le premier chapitre de cette thèse décrit brièvement les diverses techniques de multi-ionisation qu'utilisent actuellement les complexes de faisceaux d'ions radioactifs, et plus en détail l'élevateur d'état de charge ECR choisi pour l'étude. Puis le second chapitre donne les résultats expérimentaux avec à la fois les ions stables et les ions radioactifs. Le troisième chapitre propose des améliorations techniques à l'élevateur de charge ECR. Finalement le quatrième chapitre compare les résultats avec ceux des autres types d'élevateurs d'état de charge, et expose également des perspectives pour les applications en physique. La conclusion finale donne un aperçu du rôle de l'élévation de l'état de charge par ECR dans la prochaine génération de complexes pour faisceaux d'ions radioactifs.

Chapter 1

Motivation and scientific context

1.1 Charge breeding for postaccelerated RIBs

As mentioned in the introduction, postaccelerated RIBs present a wide interest for industrial and medical applications, as well as for nuclear physics research. But in order to produce the great variety of isotopes required, two issues should be considered: can all beams be efficiently postaccelerated, and at what cost ?

First, the A/q acceptance of the post-accelerator defines the usable mass range, with A the mass of the isotope and q its charge state. For example, at the ISAC facility at TRIUMF (Vancouver, Canada) an A/q below 7 is desired [25], while REX-ISOLDE (CERN, Geneva) requires an A/q below 4.5 [26]. The new SPIRAL2 facility at GANIL (Caen, France) will be designed to accelerate in a first step ions with A/q below 3 [27]. In all those cases, the direct use of singly charged ions would limit post-acceleration to the very light masses. Increasing the charge state of the ions equals to extending the usable mass range for post-acceleration. As efficient ion sources at Isotope Separation On-Line (ISOL, see subsection 1.2.1)-type facilities mainly produce singly charged ions [28], the process of increasing the charge state from 1^+ to n^+ (the so-called “ $1^+ \rightarrow n^+$ ” method) is preferred to a direct multi-ionization at the production target.

The charge breeding performances are evaluated according to various criteria:

- The **acceptance** of the charge breeding method corresponds not only to the singly charged ion beam emittance (see Figure 1.1), but also to the beam intensity and to the range of masses that the charge breeder can handle.
- The **A/q range** of the charge bred elements should tend to high charge states, i.e. low A/q values, which are more likely to match low acceptances of post-accelerators. In the following, one calls q_{max} the most abundant charge state of the distribution [29].
- The **charge breeding efficiency** η_{n+} for a given charge state n is calculated by:

$$\eta_{n+} = \frac{\text{number of multiply charged ions extracted}}{\text{number of singly charged ions injected}} = \frac{1}{n} \frac{I_{n+}}{I_{1+}}$$

where I_{1+} is the injected singly charged ion current, I_{n+} is the extracted ion current for the

charge state n considered. Thus the **total breeding efficiency** η_{total} for a given element is:

$$\eta_{total} = \sum_{i=1}^{\infty} \eta_{i+}$$

- The **charge breeding time** τ_{cb} for a given charge state is defined as the time to reach 90% of the maximum current for that charge state with respect to the instant when the singly charged ion beam was injected [30]. As the charge breeding time shortens, the losses by radioactive decay are minimized.
- The **emittance of the charge bred beam** should be considered to minimize further losses and to optimize mass and energy selection after the charge breeder.

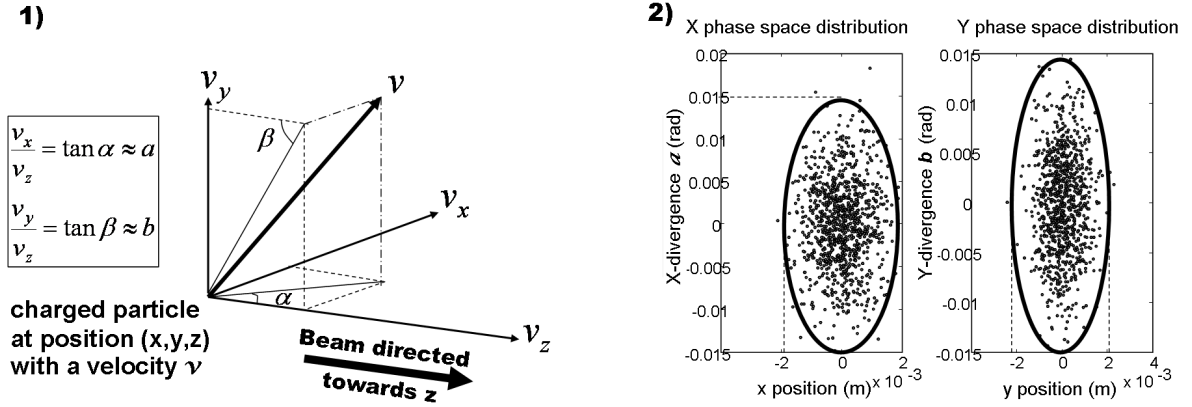


Figure 1.1: Geometrical beam emittance definition.

- 1) Considering the position and velocity coordinates of a charged particle in a beam propagating towards the z direction, one defines the divergence coordinates of the ion, a and b .
- 2) The beam is represented according to the position and divergence coordinates sets (x, a) and (y, b) composing the phase space. The total geometrical emittance is defined by the area of the elliptical beam projection in the phase space. Here, 99% of the projected beam exhibits an emittance of $30\pi \cdot \text{mm} \cdot \text{mrad}$.

Second, the cost of post-acceleration should include not only the cost of the post-accelerator itself, but also the cost of the charge breeding stage. In the case of a LINAC, the higher charge state allows a lower voltage DC accelerator, i.e. shorter devices, to provide the same ion beam energy. The consequences are even more advantageous for cyclotrons, as the beam energy is then proportional to the square of the charge. The compactness of the post-accelerator and of the charge breeder reduces the final cost. More criteria such as the robustness of the charge

breeder to radiation damage, the frequency of maintenance operations, and the required preparation stages are also to be taken into account for cost estimates.

A large-scale study of charge breeding techniques was started in Europe through two projects supported by the European Commission: EURONS and EURISOL [31]. While EURONS aims at optimizing all steps of existing breeding processes [32], EURISOL includes a feasibility and design study of a new generation of charge breeders with orders of magnitude greater capacity and throughput in order to accumulate, cool, bunch and purify the high intensity radioactive ion beams of the “next-generation” European ISOL facility [33].

1.2 Multi-ionization techniques

In the following section, the three main charge breeding techniques schematically represented in Figure 1.2 are described, and their current best achievements are presented.

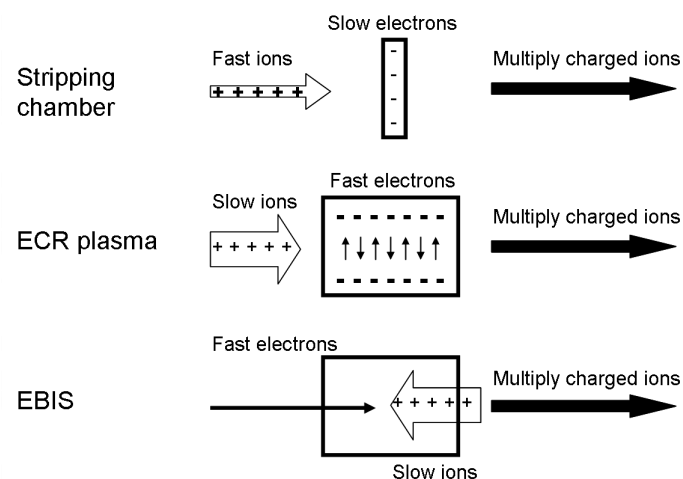


Figure 1.2: Analogy between various multi-ionization techniques: the stripping cell (constituted of a thin foil or a gaseous cell), the ECR plasma, or the EBIS. The scheme was adapted from [34].

1.2.1 Stripping cells

Stripping cells principle

Stripping cells allow to multi-ionize a beam of fast ions, by collision with comparatively “slow” electrons of the cell (see Figure 1.2). The stripper can be constituted of a solid foil [35, 36] or of

gaseous material [37, 38]. For example, thin carbon foils are now widely used at the terminal of tandem accelerators (see Figure 1.3). The resulting charge state distribution and beam quality depend on the initial energy of the beam and on the cell thickness, and were extensively studied for the last thirty years with various stripper media [39, 40, 41, 42]. Several stripping cells can be alternated with accelerating stages to reach almost fully-stripped charge states, especially in the case of light ion beams ($A < 40$, see [43]).

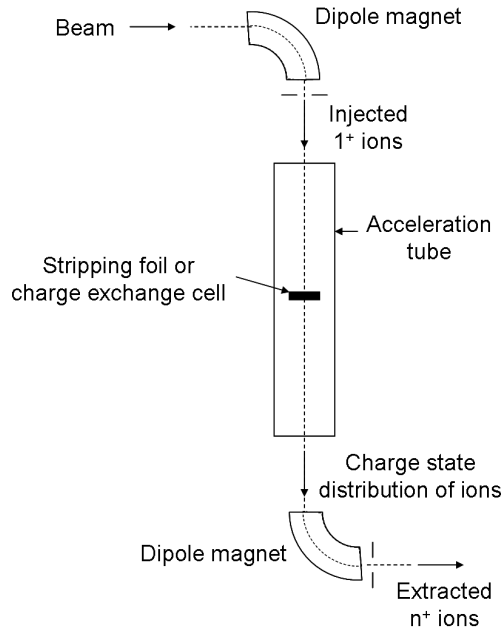


Figure 1.3: Principle of the stripping cell. In the case of tandem accelerators, injected ions are negatively charged, and by charge exchange in the stripping cell, they become positively (and highly) charged. Accelerating high voltage is then applied at a terminal, where the stripping cell is positioned.

Stripping cells status of research and development

Due to the specificities of the various electron stripper media, it can be challenging to optimize either the beam transmission, the resulting charge state distribution and beam quality, or the lifetime of the stripper.

Gas strippers have no lifetime limitation because they can be continuously refilled. However they are space-consuming, and the resulting beam energy spread can lead to further losses in the post-acceleration stage [37]. Latest studies favour thin solid strippers to achieve a higher average charge state distribution and a rather good beam quality [44]. However, thin foils have

a limited lifetime depending on the preparation and mounting methods, the level of impurities, or the radiation effects leading to the formation of holes [45]. Solutions to extend their lifetime can be similar to the ones applied on high-power targets: gas cooling, or supporting the foils on a rotating wheel [46]. For the low-energy applications, recent progress in nanotechnology is actively used to search for new methods of producing stronger stripper foils with aerial densities [47]. Liquid strippers were until recently mentioned [44] as an alternative dense and recirculating stripper with controllable thickness, but no conclusive result was published yet [48].

Electron stripper media also contribute to the development of methods for the purification of radioactive ion beams. For example, isobars can be accelerated and fully stripped, so that they are separated when undergoing energy selection [43, 35]. Another application is the production of pure neutron-rich isotopes by extracting them as molecular beams from the target, and later breaking them with the stripper [43]. Tentative tests were also performed to use the gas stripper of a tandem accelerator as a target for inverse-kinematics reactions of interest in astrophysics [38].

Stripping cells performances and weaknesses

Next generation RIB facilities aim at producing radioactive beam intensities of the order of a few microamperes [22], and much higher stable beam intensities. The next generation Facility for Rare Isotope Beams (FRIB, formerly RIA: Rare Isotope Accelerator) in the USA foresees the acceleration of a 5 particle-microampere ($\text{p}\mu\text{A}$) stable beam current of ^{238}U . Latest design studies consider solutions with solid strippers of low Z materials, in order to achieve the higher average charge state distribution [44]. Therefore, only solid stripper performances will be compared here to those from other charge breeding techniques. Table 1.1 gives some indication about charge states and efficiencies achieved with radioactive ions stripping, starting with singly or multiply charged projectiles. More measurements can be referred to in data tables [49, 42, 41, 40].

	Thickness (mg/cm^2)	Projectile	Energy (MeV/u)	q_{max}	η (%)	Reference
Carbon foil	0.6	^{238}U	10.5	72+	* * 14.8	[44]
	0.9	$^{238}\text{U}^{58+}$	24.1	77+	18.13	[49]
	16	$^{238}\text{U}^{73+}$	85	88+	*22.5	[44]
Beryllium foil	1.3	^{238}U	10.5	74+	* * 14.7	[44]
	2.35	$^{238}\text{U}^{58+}$	24.1	81+	24.72	[49]
	37	$^{238}\text{U}^{73+}$	85	88+	*24	[44]

Table 1.1: Performances of stripping cells for intermediate energies. For measurements by [49], the thickness of the foil is, on purpose, not adapted to the charge-state equilibrium reached. In the RIA concept, a broader band of charges is accelerated to allow higher particle intensity [50]. Therefore, the given efficiency values for the most abundant charge state q_{max} are averaged on the four (*) or five (**) highest charge state fractions of the distribution.

Advantages are that this charge breeding technique has been well-studied for the last thirty years, and achieves rather good transmission and charge breeding efficiencies. Such a solution well suits short-lived species as there is no charge breeding time to take into account. As a drawback however, it requires a pre-acceleration stage to at least 150 keV/u for solid strippers to be efficient [51], and thus prior multi-ionization at low energy in some cases. For the foreseen intensities in next-generation facilities, radioprotection problems related to the replacement of solid stripping foil could also add to the final cost (see [36, 44], and subsection 4.1.1).

1.2.2 EBIS

EBIS principle

The EBIS [52] is composed of an axial magnetic field created by a long solenoid and of an axial electrostatic potential generated by cylindrical electrodes. An electron gun produces an intense electron beam, focused and compressed by the strong magnetic field. The injected singly charged ions are guided in the center by the magnetic field lines and radially contained by the electron beam space charge. They are axially confined by the electrostatic trap, where they undergo stepwise multi-ionization by colliding with the energetic electron beam. Finally, the electrostatic potential is lowered to release the multiply charged ions.

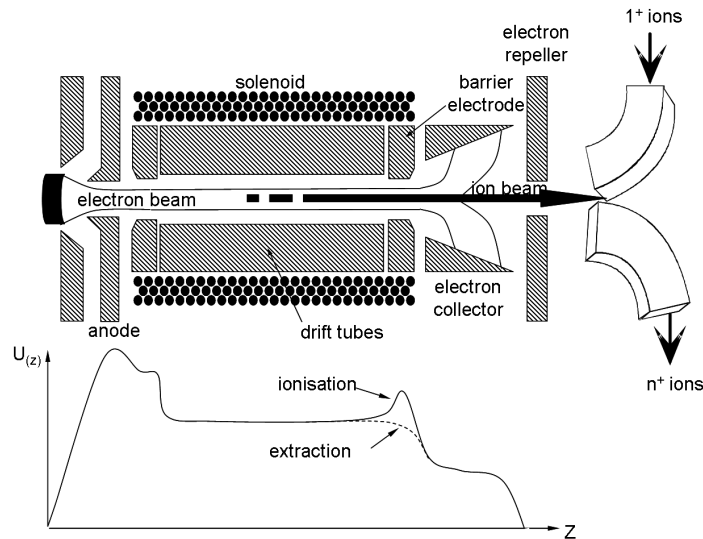


Figure 1.4: Principle of the EBIS charge breeding. Picture adapted from [34]. The top scheme shows a longitudinal cut of the EBIS charge breeder. The bottom scheme shows the corresponding electrostatic potential along the electron beam axis, for ions trapping (solid line) and for ions extraction (dotted line).

The success of the method requires a good alignment of the electron beam with the axis of the magnetic field and of the drift tube [53]. It is advantageous to inject the singly charged ion beam per bunches in order to achieve high injection efficiencies and narrow charge state distribution. The injected beam should have a low emittance in order to match the low EBIS acceptance [54]. Moreover, a time structure is needed in the injection-extraction scheme as ions are injected and extracted through a unique opening (see Figure 1.4). Therefore, the EBIS requires a preparation stage, for example with a Penning trap [55], to accumulate, cool and bunch the singly charged ion beam.

The EBIS is maintained under Ultra-High Vacuum (UHV), about 10^{-11} mbar for the REXEBIS [51], in order to avoid the electron-beam compensation with ions from the residual gas [52], prolong the lifetime of the cathode [56] and lower the extracted stable background [54].

EBIS status of research and development

A historical review of the progresses on EBIS can be found in [57], and highlights of the developments of EBIS as injectors for heavy ion post-acceleration are given in [58].

Currently, the only operational EBIS charge breeder on-line is the REXEBIS [59] located at ISOLDE, which provides highly-charged RIBs for post-acceleration at the REX-ISOLDE facility [60]. Charge breeding tests are also conducted on the MAXEBIS test bench at GSI, in Germany [61] in the frame of European studies on charge breeding techniques [31]. Tests are in progress with the TestEBIS at Brookhaven National Laboratory (BNL) in the USA to check the feasibility of the design for the new EBIS heavy ion preinjector to provide beams for the Relativistic Heavy Ion Collider (RHIC) and the NASA Space Radiation Laboratory (NSRL) [62]. Finally a new high-current EBIS is being designed at the National Superconducting Cyclotron Laboratory in the USA to ensure both high acceptance and fast charge breeding [63].

Recent developments on EBIS charge breeders tend towards higher magnetic fields (5T at MAXEBIS against 2 T at REXEBIS) and higher electron beam intensities (a goal of 10 A for TestEBIS routine operation, with the possibility to increase the electron beam intensity to 20 A, against 250 mA currently at REXEBIS). In order to deliver more “continuous” beams slow extraction modes are tested, with low repetition rates and enlarged extracted pulses [64]. Shorter injection rates are also tested, and the so-called REXEBIS “accu-mode” allowed a successful injection and charge breeding of a 500 pA continuous low-emittance beam [59].

EBIS performances and weaknesses

The REXEBIS and the MAXEBIS are both part of the European investigation programs for RIBs charge breeding techniques mentioned in section 1.1. Preliminary results of the EURISOL study are online [64], and some of the values were gathered in (Table 1.2).

The EBIS charge breeder allows to reach relatively high charge states with short charge breeding times independently from the isotope chemistry, as ionization takes place far from the chamber walls [54]. Because of the UHV, the equilibrium charge-state mainly depends on the electron beam density and the charge breeding time. So fully stripped charge states can be reached, provided that the electron beam energy is high enough for stripping the deepest levels [57]. Moreover, the total extracted current and stable background level remain extremely low, allowing a good mass separation of the charge bred beam [26]. Additional suppression of contaminants can be achieved by mass-selective cooling in the preparation stage [55, 65, 66], or by the use of molecular ions that are sent into the EBIS to be broken by the electron beam, thus suppressing molecular sidebands [67, 68]. Charge bred ions are extracted with a kick off potential, resulting in a low-emittance beam [52, 24].

	Isotope	Cooling time (ms)	τ_{cb} (ms)	Total time (ms)	q_{max}	η (%)	Reference
Actinide	$^{238}U^+$ (stable)	500	498	998	52+	4.3	[64, 69]
Light ion ($A < 30$)	$^7Li^+$ (stable)	20	18	38	3+	6	[64]
	$^{23}Na^+$ (stable)	30	28	58	9+	10	[64]
Molecule	$^{27}Al(F)^+$ (stable)	20	10	30	7+	16.7	[64]
	$^{70}Se(CO)^+$ (radioactive)	60	58	118	19+	3	[59, 64]
Alkaline	$^{39}K^+$ (stable)	20	12	32	10+	15	[64]
	$^{133}Cs^+$ (stable)	200	198	398	33+	3	[64]
Metal	$^{67}Cu^+$ (radioactive)	100	68	168	19+	12.6	[64]
	$^{116}Cd^+$ (stable)	250	248	498	31+	9.6	[64]
Noble gas	$^{136}Xe^+$ (stable)	200	198	398	34+	8.7	[64]

Table 1.2: Best performances of EBIS charge breeding for various categories of stable and radioactive isotopes and their most abundant charge state q_{max} . One distinguishes the 1^+ beam cooling time and the charge breeding time in the EBIS τ_{cb} . Efficiencies η include the cooling efficiency of about 50%, 25% only for Li cooling ([64]).

However, the total time for charge breeding should take into account the cooling time, which effects the decay losses of radioactive ions. In the case of REXEBIS, space charge effects in the preparation Penning trap REXTRAP limit the acceptance to 10^7 ions/s for a maximal cooling efficiency [69], i.e. a few tens of picoamperes of injected beam. In practice, the data from Table 1.2 are given for an injected current of 1 pA to 100 pA of singly charged ions. For a given electron beam density, charge breeding times increase with Z and so does the accumulating times in REXTRAP, resulting in a drop of efficiencies for heavier ions [31]. Moreover the cathode producing the electron beam has a limited lifetime, 3 to 4 months for a LaB₆ cathode [59], and regular replacement requires some extra cost and radiation risk.

1.2.3 ECRIS

ECRIS principle

The ECRIS [70] is composed of superposed radial and axial magnetic fields, a microwave RadioFrequency (RF) and a low-pressure ionized gas. The cyclotron motion of the buffer gas free electrons along the magnetic field lines is resonantly excited by the applied RF (see Figure 1.5). The electrons stochastically gain energy and ionize the atoms from the rest gas by collisions, thus rapidly igniting a plasma [71]. The magnetic field configuration is not closed, allowing efficient ion extraction through the loss cones (Figure 1.6). The extraction can be bunched by abruptly turning off the RF feeding, as explained in 1.3.3.

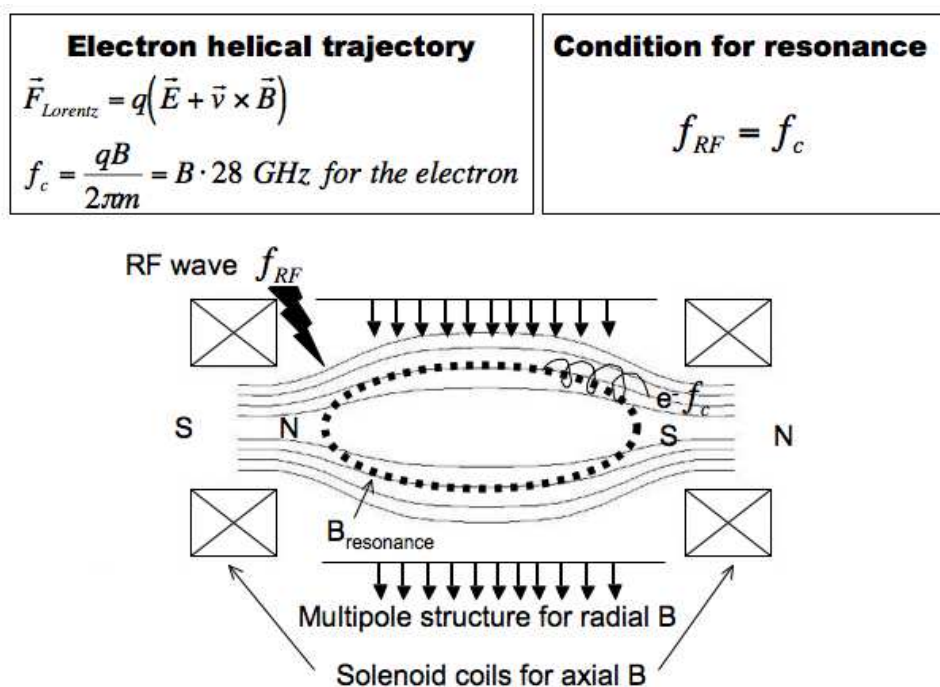


Figure 1.5: Principle of the Electron Cyclotron Resonance as inspired from [71]. The magnetic field configuration of an ECRIS is viewed from a axial cut. Free electrons move helically along the magnetic field lines with the electron cyclotron frequency f_c . At the specific location where the resonance condition is fulfilled, their motion can be resonantly excited by an external RF wave of frequency f_{RF} .

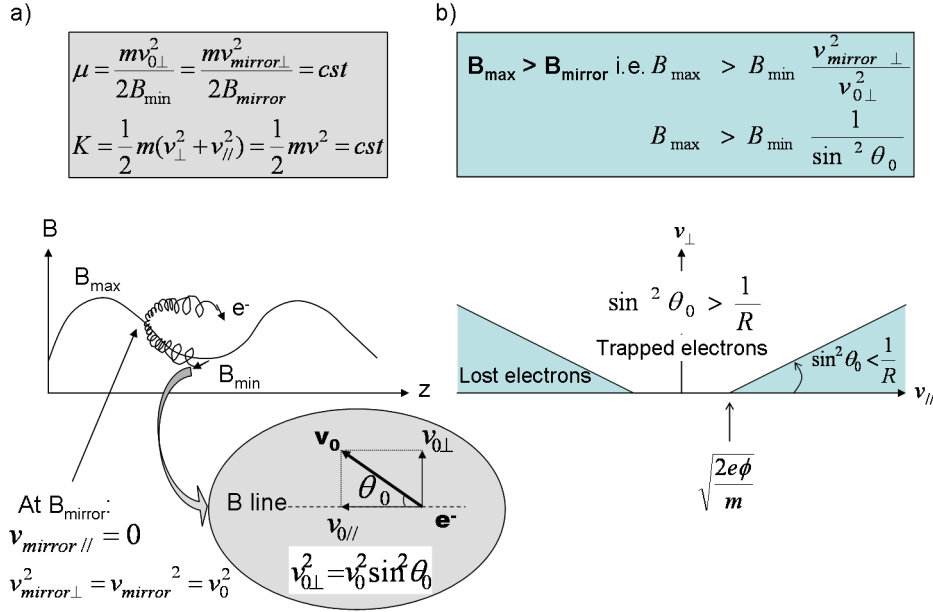


Figure 1.6: Principle of the magnetic mirror inside the ECRIS as inspired from [71].

- a) The magnetic moment μ and the kinetic energy K being respectively invariant, the velocities of one electron at B_{\min} and B_{mirror} are related.
- b) The magnetic mirror point exists for electrons whose initial θ angle was higher than $\sqrt{\frac{1}{R}}$, where R is the mirror ratio $\frac{B_{\max}}{B_{\min}}$. Other electrons with enough energy to overcome the plasma potential ϕ are lost in a cone.

Used as a charge breeder (Figure 1.7), the plasma chamber is put at an electrostatic potential to stop the injected beam and post-accelerate the n^+ beam. The capture by the plasma of the singly charged injected ions was demonstrated in [72] to depend on their energy, one of the challenges of the method. The ions should have a sufficient kinetic energy to overcome the positive plasma potential [71], but still of the same order as the energy of the plasma ions (about a few eV according to [73]). In that case, they are thermalized by Coulomb collisions [71], and trapped in the electrostatic well $\Delta\Phi$ created by the high density of electrons in the center of the plasma [71]. Therefore, the difference ΔV between the 1^+ ion beam acceleration potential and the potential applied to the plasma chamber should be tuned accordingly (see Figure 1.8, [74, 75]). The ΔV range allowing plasma capture is a good approximation of $\Delta\Phi$, of the order of a few tens of Volts [72].

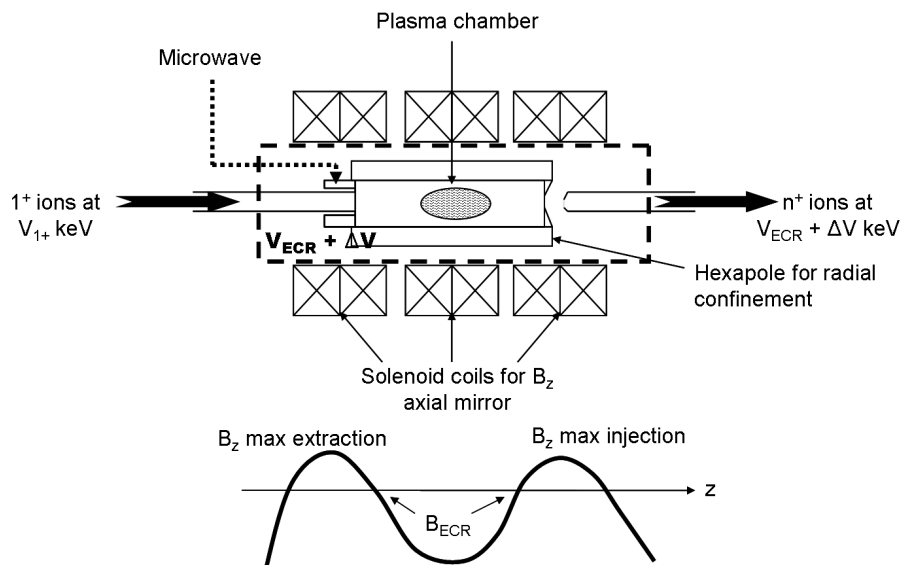


Figure 1.7: Principle of the ECR charge breeding.

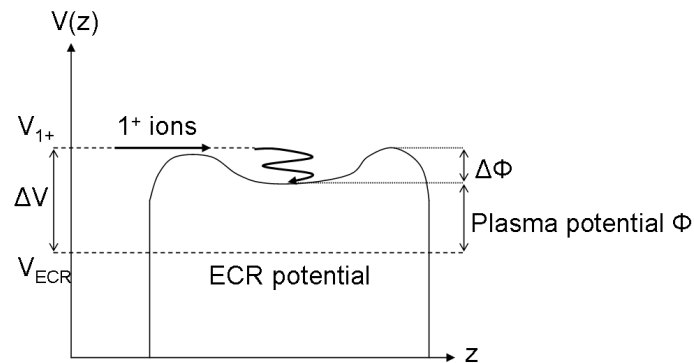


Figure 1.8: Scheme of the axial ECR plasma potential as inspired by [76], describing how singly charged ions are decelerated from their potential V_{1^+} , overcome the plasma potential barrier and are trapped in the ECR plasma (see text for details). V_{ECR} is the potential applied on the ECR plasma chamber.

Hot electrons in the plasma contribute to the successive ionization of the injected ions in outer shells by electron impact or in inner shells by Auger effect and by the so-called "shake-off" phenomena where many secondary electrons are emitted [71]. At the same time, ion cooling effects, such as charge exchanges with the rest gas or radiative electron captures limit the stepwise ionization process [71]. The charge breeding time τ_{cb} of a given charge state n^+ convolutes the time needed for the stepwise ionization τ_{ioniz} and a confinement time τ_{conf} due to the magnetic field. The reachable charge state is defined by the balance between electronic density and τ_{conf} [70]. Indeed, as long as τ_{ioniz} remains much shorter than τ_{conf} , higher charge states can be reached. However, τ_{conf} being equal to or longer than τ_{ioniz} , it usually acts as a limiting factor, during which charge exchanges and radiative recombination happen and limit the achievable charge state [77]. Recent studies of τ_{cb} have underlined the existence of collision phenomena which are not well understood yet [78, 25]. Research is ongoing to simulate, for example with a Monte Carlo code [79], how ions are decelerated, captured in the ECR plasma, multi-ionized and extracted.

ECRIS status of research and development

A history of ECRIS designs can be found in [70], and issues for the next generation are summarized in [80]. In order to reach higher charge states and increase the charge breeding efficiencies in ECRIS, the number of ion recombination should be diminished, and the electron density should be increased (according to scaling laws given in [71]). Current research is ongoing in these two directions: the minimization of losses by plasma leak or ion recombination, and the enhancement of the electron cyclotron resonance to generate a higher density of electrons in the plasma. In the first case, the optimization of the magnetic confinement [81] and of the quality of vacuum components [82] respectively tend to minimize electron losses and charge exchanges. On the other hand, the development of superconducting ECRIS for a high magnetic confinement [83, 84] and the dimensioning of new ECRIS to accept high RF power and frequency [85] or multi-frequency heating to increase the fraction of absorbed RF [86, 83] follow the trend of denser ECR plasmas.

Presently, ECR charge breeders are very similar to ECR ion sources, as the dimensions and the magnetic field structure were inspired from ion sources designs. However, the transformation of an ECRIS into an ECR charge breeder has raised new challenges. Investigation of the plasma capture [72], of the continuous and pulsed modes [87], and numerous tests of various masses, chemical elements and intensities of injected ions [23] were already studied with stable beams. Promising results led a few RIB facilities to consider the ECR charge breeder as an adequate injector for post-accelerators.

Currently, ECR charge breeders are being developed for instance at the Variable Energy Centre of Calcutta in India [88] and at GANIL in Caen, France [89]. One of them, the KEK-JAERI ECR charge breeder in Japan, is already on-line and operational since 2005 [82], providing stable and radioactive charge bred ions to the post-accelerator.

More specifically, charge breeding experiments with PHOENIX-type ECR charge breeders, i.e. with a similar design as the PHOENIX Booster used for the thesis work, are performed on

test benches with stable beams at LPSC Grenoble [90] and at TRIUMF Vancouver [25]. A third PHOENIX ECR charge breeder is on-line at ISOLDE, CERN, as a test bench for charge breeding experiments with stable and radioactive ion beams [91, 29].

Recent developments on ECR charge breeders concentrate on the background reduction and the improvement of the extracted beam emittance, for example at TRIUMF for the foreseen online installation [25, 92]. Besides the investigation of the charge breeding performances, direct applications to physics experiments are tested, especially in the domain of beam purification (see more details in subsection 2.2.1, section 4.2 and Appendix C).

ECRIS performances and weaknesses

Considering ECR charge breeders only, a non-exhaustive list of the best performances is given in Table 1.3.

	Isotope	τ_{cb} (ms)	q_{max}	η (%)	Reference
Actinide	$^{238}U^+$ (stable)	100	26+	2	[29]
Light ions	$^{20}Ne^+$ (stable)	–	4+	7.5	[23]
	$^{23}Na^+$ (stable)	–	6+	1.3	[23]
Molecule	$^{139}La(O)^+$ (stable)	–	23+	2.7	[93]
Alkaline	$^{39}K^+$ (stable)	100	10+	1.7	[29]
	$^{39}K^+$ (stable)	–	6+	6.5	[23]
	$^{133}Cs^+$ (stable)	200	26+	1.7	[29]
Metal	$^{56}Fe^+$ (stable)	–	10+	2.4	[23]
	$^{109}Ag^+$ (stable)	–	17+	3	[23]
	$^{116}Sn^+$ (stable)	200	21+	6.3	[29]
	$^{126}In^+$ (radioactive)	–	16+	2.3	[82]
	$^{209}Bi^+$ (stable)	330	28+	2.3	[29]
Noble gas	$^{40}Ar^+$ (stable)	–	9+	13.5	[78]
	$^{84}Kr^+$ (stable)	–	12+	10.4	[78]
	$^{92}Kr^+$ (radioactive)	–	12+	8.2	[82]
	$^{129}Xe^+$ (stable)	–	20+	7.4	[82]
	$^{132}Xe^+$ (radioactive)	230	21+	6.2	[29]
Afterglow	$^{85}Rb^+$ (stable)	520	15+	2.5	[94]
	$^{86}Kr^+$ (stable)	500	13+	1	[29]
	$^{132}Xe^+$ (radioactive)	600	18+	2.2	[29]

Table 1.3: Performances of ECR charge breeding for various categories of elements in continuous mode, and the first tests of the “afterglow” pulsed mode (details about the afterglow in 1.3.3). τ_{cb} is the charge breeding time, q_{max} the most abundant charge state and η the charge breeding efficiency for this charge state.

Highlights of the ECR charge breeding are the high acceptance in injected beam emittance (up to 55π .mm.mrad for 90% of $2.8 \mu\text{A}$ injected Ar at 18 keV [95]) and current (no drop in efficiency observed up to $20 \mu\text{A}$ of Pb^{2+} injected [96]), and the great robustness due to the configuration of the charge breeder (no filament nor electron gun). The charge capacity was experimentally evaluated as more than $20 \mu\text{A}$, i.e. 10^{14} ions with the 14.5 GHz PHOENIX [96]. The highly-charged beam emittance after mass-separation varies from 10 to 20π .mm.mrad (10π .mm.mrad measured for Zn^{11+} at 19.5 keV [95]).

The drawback is the high current due to the use of buffer gas, which induces a high stable background after the analyzing magnet [25]. Moreover, fully stripped ions cannot be produced with the ECR due to the balance between recombination and ionization rates during the confinement time. There is still a lack of data with light ion injection, currently not achieved with the ECRIS, for an objective comparison with the other charge breeding techniques (see subsection 3.1.4).

1.3 The ECR charge breeder test bench

1.3.1 The facility: ISOLDE

Experimental tests are performed at the ISOLDE facility [97] at CERN, Geneva, where up to now 939 isotopes of 68 elements have been produced through the Isotope Separator On-Line (ISOL) method [98]. Up to $2 \mu\text{A}$ of a 1.4 GeV proton beam impinge a thick solid target to produce fission, spallation and fragmentation reactions. One can favour fission over fragmentation by shooting the proton beam on a tantalum neutron converter positioned close to the target. The volatile nuclear reaction products are released from the high-temperature target into an ion source via chemically selective processes [28, 99]. Then, they are extracted at up to 60 kV as a radioactive ion beam, and undergo on-line mass selection before being accelerated towards the experiments.

As shown on Figure 1.9, two isotope separators on-line with independent Target-Ion Source (TIS) units are available at ISOLDE: the General Purpose Separator (GPS) and the High-Resolution Separator (HRS). The GPS consists of one magnetic dipole and an electrostatic switchyard allowing the simultaneous extraction of three mass separated beams, respectively in the General Heavy Masses (GHM), General Central Masses, and General Lower Masses (GLM) beamlines. The Central Masses beamline gathers together with HRS separator, feeding the major experimental installations, whereas the GHM and GLM beamlines are attached to the GPS TIS system only.

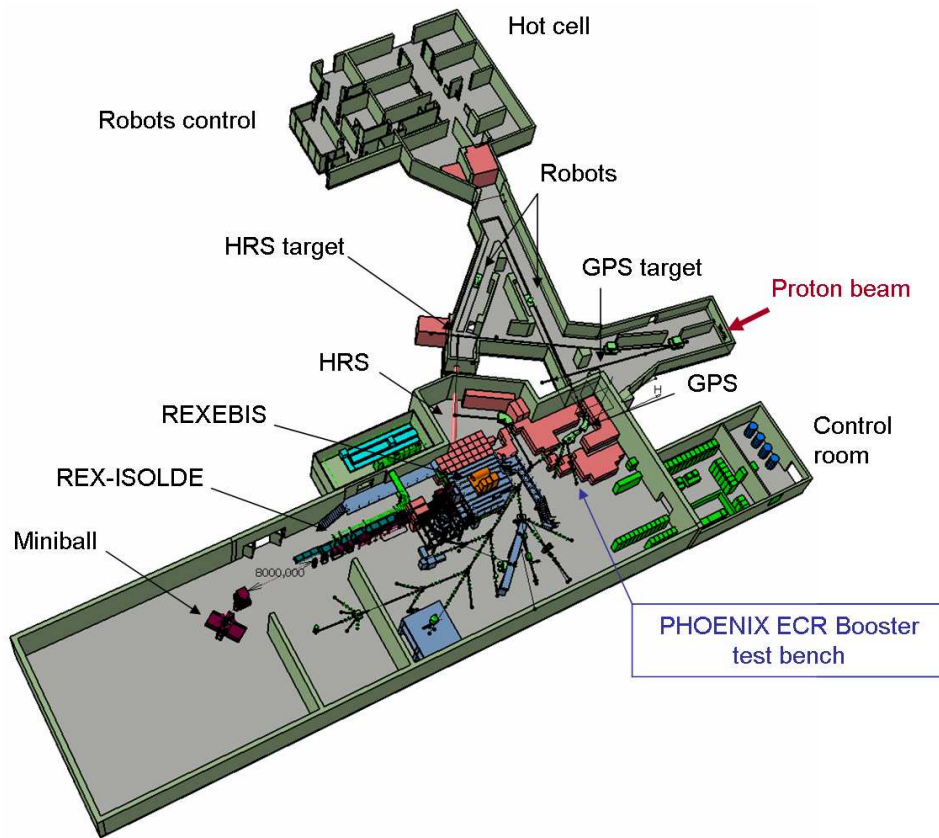


Figure 1.9: Layout of ISOLDE experimental hall. The proton beam impinges either the GPS target or the HRS target. The ECR charge breeder is located on the GHM beamline, so it can benefit from GPS beams only.

1.3.2 The charge breeder: PHOENIX ECR Booster

Experiments described in chapter 2 were performed with an ECR charge breeder of PHOENIX type [95] installed as a test bench on the General Heavy Masses (GHM) beamline.

Because of its location, the test bench can benefit from GPS beams only, but beam can be taken on GHM in parasitic mode at the same time as main users of the central beamline. Masses of interest should be within a 15% deviation of the central mass, but the full mass range can be accessed when main users run with HRS and no other user runs with GPS. If full proton intensity is not required for HRS runs, the protons can then be shared between the HRS and GPS targets.

The experimental test bench layout is shown on Figure 1.10. Although vacuum in GHM is around $5 \cdot 10^{-7}$ mbar, the use of a conductance (see 3.3.2) between the collection chamber and Faraday Cup (FC) 2 allows to keep a vacuum of 10^{-7} mbar in the setup while running. Optimization of the beam towards the entrance of the charge breeder is checked by measuring the current on FC1 and FC2. As the 1^+ beam energy is fixed by the extraction potential of GPS ionization source, one tunes the ΔV (subsection 1.2.3) by varying the electrostatic potential applied to the ECR plasma chamber. Fine tuning of the plasma capture is achieved with double Einzel Lens (EL) 1.

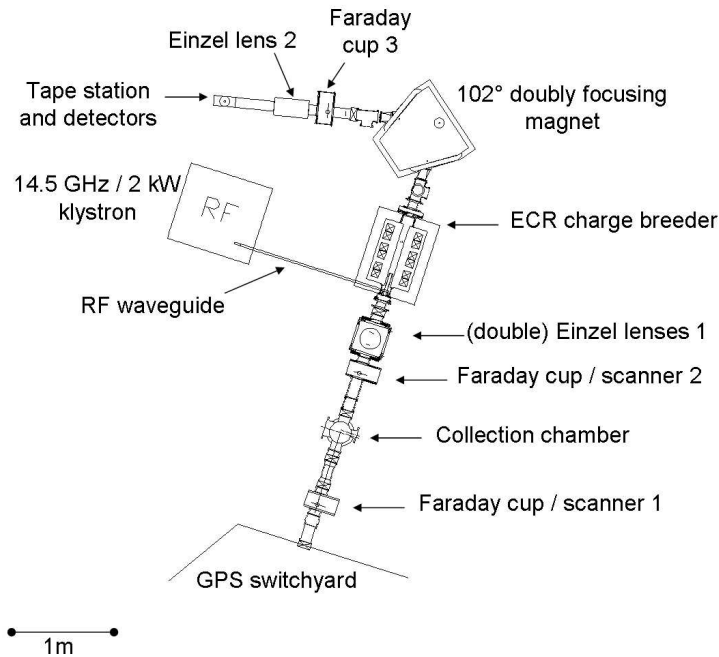


Figure 1.10: Layout of the experimental test bench. More details in the text.

A cross-section drawing of the PHOENIX ECR charge breeder is shown on Figure 1.11. It has a one-liter stainless steel plasma chamber [90] surrounded by a 1.1 T - hexapole for radial confinement. Three solenoid coils are used to produce an axial mirror ratio close to 2 (Figure 1.6). Such dimensions allow the injection of a 14.5 GHz microwave (Figure 1.5) up to 1 kW power. O_2 is injected through a controlled gas leak to support the plasma, as it is quite adapted to masses over 40 [70] and ignites without much RF power. The setup allows a 60 kV operation (see subsection 3.3.1 for more details), but a decision was taken to perform the measurements at 30 kV only due to time constraints with the 60 kV conditioning. Ions leak through the 8 mm-diameter hole of a Dural plasma electrode, are accelerated on a distance of 38 mm and extracted as a beam through the 13 mm-diameter extraction hole of the puller. For most beams, a potential voltage close to 15 kV is applied on EL1 and EL2.

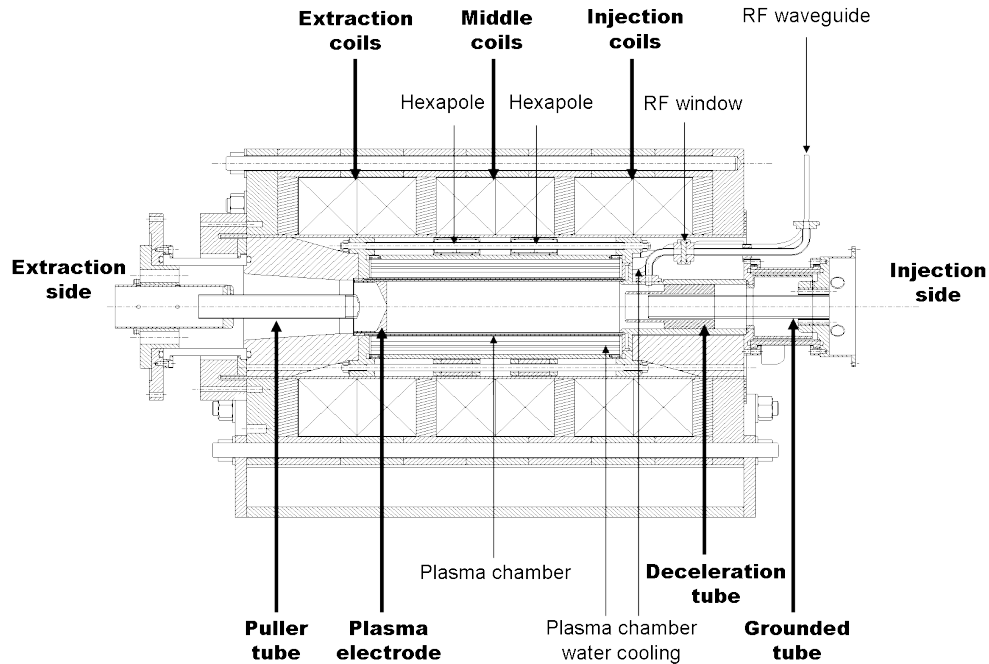


Figure 1.11: Cross-section drawing of the PHOENIX Booster, adapted from a LPSC technical scheme by C. Fourel. Buffer gas is injected just before the injection flange, therefore the gas leak entry does not appear on the scheme.

SIGMAPHI ref.	13928
Number of spire windings per coil	36
Deflection angle	102°
Bending radius	350 mm
B field at nominal current	300 G
Entrance angle	33.5°
Exit angle	33.5°
Pole gap	70 mm
Nominal voltage	44 V
Nominal current	250 A
Waterflow rate at 12 bars	7 L/min
Temperature rise	22°C
Magnet resistance at 20°C	170 mΩ
Manufacturing date	12/03/97

Table 1.4: Specifications of the mass analyzing magnet as given by the manufacturer (SIGMAPHI).

After extraction, a 102° doubly focusing magnet (Table 1.4) achieves charge state selection, with a slits opening letting 90% of the beam through. Due to the effects of hysteresis of the magnet, the A/q calibration at a given energy is systematically checked with the intense peaks of oxygen. Stable beam is measured on FC3 and compared to FC2 measurements to calculate the charge breeding efficiency. When working with radioactive ions, the intensity of the current is also checked on FC3 before directing the ions towards the tape station and detection setup (1.3.3) at the end of the line, to avoid damaging the tape.

A LabView [100] Graphical User Interface (GUI) developed by LPSC Grenoble allows the control of most power supplies (Table 1.5) and parameters of the test bench, such as the platform electrostatic potential value, the three independant coils current for the axial magnetic confinement, the buffer gas leak rate, and the value of the current in the analyzing magnet corresponding to the selected A/q ratio. The interface (Figure 1.12) also displays the current read from the various FCs through a Keithley 485 picoammeter (more details in [29]). A program performs mass scans within ranges fixed by the user.

Beamline element	Part	Current/bias range	Power supply reference
PHOENIX Booster	Injection coils	1200 A - 55 V	Bruker BLMPSMON255/1200C401
	Middle coils	500 A - 40 V	Bruker B_MN38/500
	Extraction coils	1200 A - 55 V	Bruker BLMPSMON255/1200C401
	High-voltage platform	65 kV - 20 mA	FUG HCP1400-65000
	14.5 GHz radiofrequency	0 - 2 kW	SAIREM GXP20KP/RI1249
Mass analyzer	Coils	100 A - 60 V	DELTA ELEKTRONIKA SM60-100
Einzel lenses	EL1	30 kV - 1.5 mA	Glassman PS/EL30P01.5-22
	EL2	35 kV - 10 mA	FUG HCN350-35000

Table 1.5: Power supplies for the PHOENIX Booster test bench.

1.3.3 Experimental methods

In this section, various methods used for the experiments described in chapter 2 are detailed.

The beam ON - beam OFF method

Typical currents from the ECR charge breeder are of the order of $500 \mu\text{A}$ on the extraction side, mainly induced by stable elements with a constant background of the order of 10 nA between the peaks (subsection 3.1.1). Therefore, it is a challenge to detect charge bred currents of the order of at most a few hundreds of picoamperes. The “beam ON - beam OFF” method is used to

detect stable charge bred species over the continuous background level. By pulsing the beam gate according to a TTL signal of typically 0.25 Hz, singly charged ions are injected and accumulated in the ECR plasma for a given duration. The current of extracted charge bred ions is pulsed accordingly with a delay due to the charge breeding time (Figure 1.12), and can be measured on FC3 provided that it is more intense than the continuous background fluctuations. This method is used in the ΔV tuning to determine the optimal parameters of the plasma capture. It requires the ECR plasma to be stable in order to minimize the continuous current fluctuations.

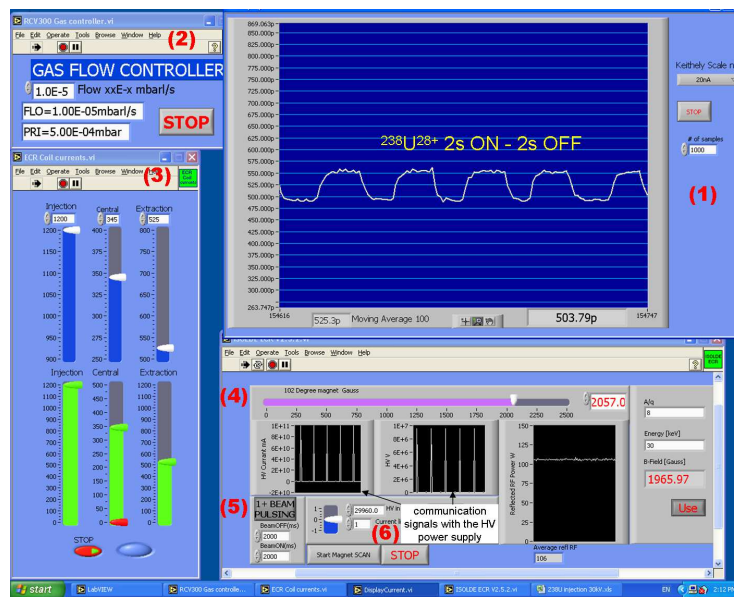


Figure 1.12: Example of a beam ON - beam OFF screenshot for $^{238}\text{U}^{28+}$. The ECR plasma behaves like a capacitance, releasing the charge bred ions with a time constant corresponding to the charge breeding time (1). The various panels allow to control the buffer gas flow (2), the coils currents (3), the dipole current (4), the injected beam pulsing (5) and the high voltage (6).

Continuous mode and pulsed mode

As mentioned in the previous description (1.2.3), when the RF is applied as a continuous wave (CW), the ECR plasma ignition is sustained, and charge bred ions are extracted continuously through the extraction loss cone (Figure 1.6). They are released after a time that depends both on the tuning of the charge breeder (axial confinement and RF power) and on possible chemical interactions with the plasma chamber walls. A charge breeding time down to 100 ms was observed depending on the adjustments of the source (Table 1.6). Therefore, the continuous mode is not appropriate for the charge breeding of short-lived radioisotopes with half-lives less than 100 ms.

Beamline element	Parameter	Setting	How to tune
PHOENIX Booster	Injection coils current	1100 A	
	Middle coils current	335 A	Optimized on $^{40}\text{Ar}^{6+}$ and $^{238}\text{U}^{26+}$ with FC3
	Extraction coils current	650 A	
	Platform high-voltage	29880 V - 1 mA	ΔV (120 V) obtained from the measurement of ^{142}Xe ΔV curve
	14.5 GHz radiofrequency power	400 W	Stable regime with a low reflected power (here 70 W)
	Buffer gas leak rate	$1 \cdot 10^{-4}$ mbar·L/s	Variations of the injection pressure are visible on the gauge
Mass analyzer	B field value	1693.5 G	Scaled from a close A/q stable peak ($^{16}\text{O}^{3+}$)
Einzel lenses	EL1 voltage	14 kV	Optimized on $^{40}\text{Ar}^{6+}$ and $^{238}\text{U}^{26+}$ measured with FC3
	EL2 voltage	19 kV	Optimized on $^{40}\text{Ar}^{6+}$ measured with a FC inserted at the collimator just before the tape

Table 1.6: Typical parameter settings for the PHOENIX Booster in continuous mode. Values are given for the injection of a ^{142}Xe beam extracted as $^{142}\text{Xe}^{24+}$ towards the tape station.

Beamline element	Parameter	Setting	How to tune
PHOENIX Booster	Injection coils current	1190 A	
	Middle coils current	310 A	Afterglow optimized on $^{84}\text{Kr}^{15+}$ and $^{238}\text{U}^{26+}$ with FC3
	Extraction coils current	620 A	
	Platform high-voltage	29952 V - 0.8 mA	ΔV (48V) optimized with the injection of ^{238}U and ^{88}Rb
	14.5 GHz radiofrequency power	500 W	Stable regime with a low reflected power (here 60 W)
	Buffer gas leak rate	$8 \cdot 10^{-6}$ mbar·L/s	Variations of the injection pressure are visible on the gauge
Mass analyzer	B field value	1572 G	Scaled from a close A/q stable peak ($^{16}\text{O}^{3+}$)
Einzel lenses	EL1 voltage	14 kV	Optimized on $^{238}\text{U}^{26+}$ measured with FC3 and on $^{88}\text{Rb}^{15+}$ beta count rate
	EL2 voltage	19 kV	Optimized on $^{88}\text{Rb}^{15+}$ beta count rate

Table 1.7: Typical parameter settings for the PHOENIX Booster in pulsed mode. Values are given for the injection of a ^{61}Mn beam extracted as $^{61}\text{Mn}^{12+}$ towards the tape station.

However, a pulsed mode can be achieved by pulsing the RF according to a TTL signal. As the RF is turned off, the ECR plasma collapses, and the charge bred ions are released as a single pulse called “afterglow peak”, which seems more pronounced for heavy ions ([76], Figure 1.13). 90% of the afterglow intensity can be released in less than 10 ms [94], thus reducing τ_{cb} down to 20 ms ([75]). Up to now, half of the efficiency achieved with the CW mode can be reached in the afterglow [23]. Typical parameter settings to operate the PHOENIX Booster in pulsed mode are given in Table 1.7.

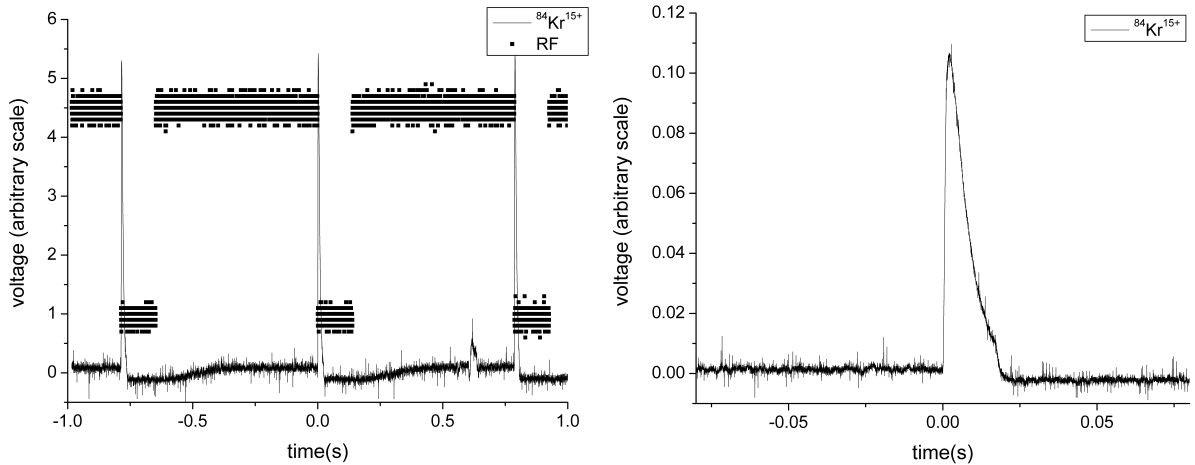


Figure 1.13: Example of pulsed extraction of $^{84}\text{Kr}^{15+}$. A RF power of 600 W was applied. The RF was switched on for 1 s and switched off for 150 ms according to the shown TTL signal. A Full-Width at Half Maximum (FWHM) of 10 ms is observed on the afterglow pulse.

Detection setup and measurement cycle

The measurements with radioactive ions presented in chapter 2 were performed with a detection setup consisting of a tape station, a germanium detector with 0.7% efficiency at 800 keV gamma-ray energy and a 5 mm-thick NE102 scintillator cup with 49% efficiency for beta detection (Figure 1.14).

Radioactive ions are collimated and implanted on the aluminized Mylar tape. Gammas and betas from the radioactive decay are both detected through the kapton window (see Figure 1.15 and Figure 1.16), and both signals are sent through the Time to Amplitude Converter (TAC) for beta-gamma coincidence selection (Figure 3.3). The energy of the gamma signal is also recorded in the Data Acquisition (DAQ) system for ions identification (Figure 1.17). The tape is moved between two cycles for the remaining activity removal.

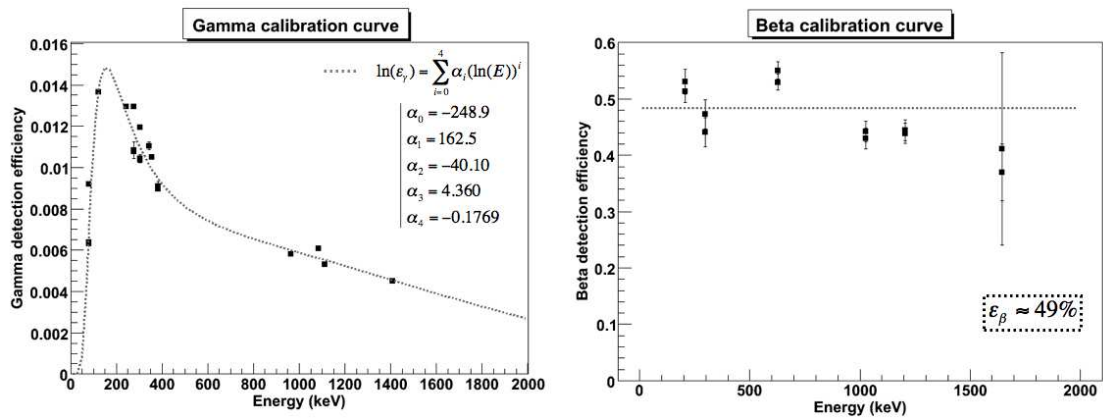


Figure 1.14: Detection efficiency for the gammas and for the betas. The gamma efficiency ϵ_γ is fitted with a fourth-order polynomial of logarithms of the energy E (dashed line). An average value of the ratios of beta-gated gamma peaks over rough gamma peaks is taken for determining the beta efficiency ϵ_β .

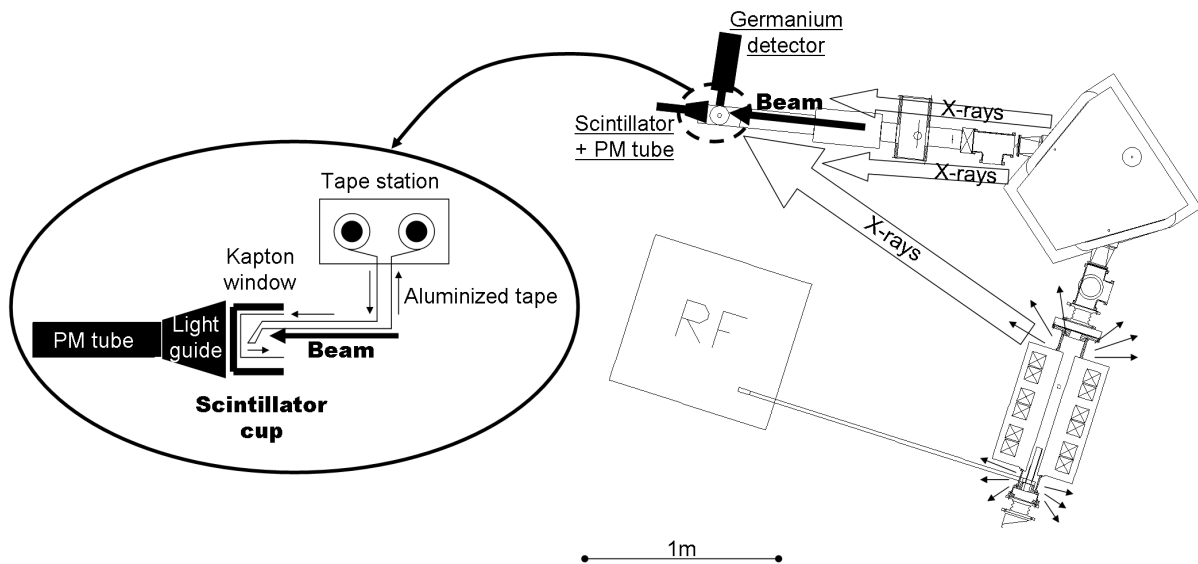


Figure 1.15: Scheme of the detection setup with the tape station. See text for details.

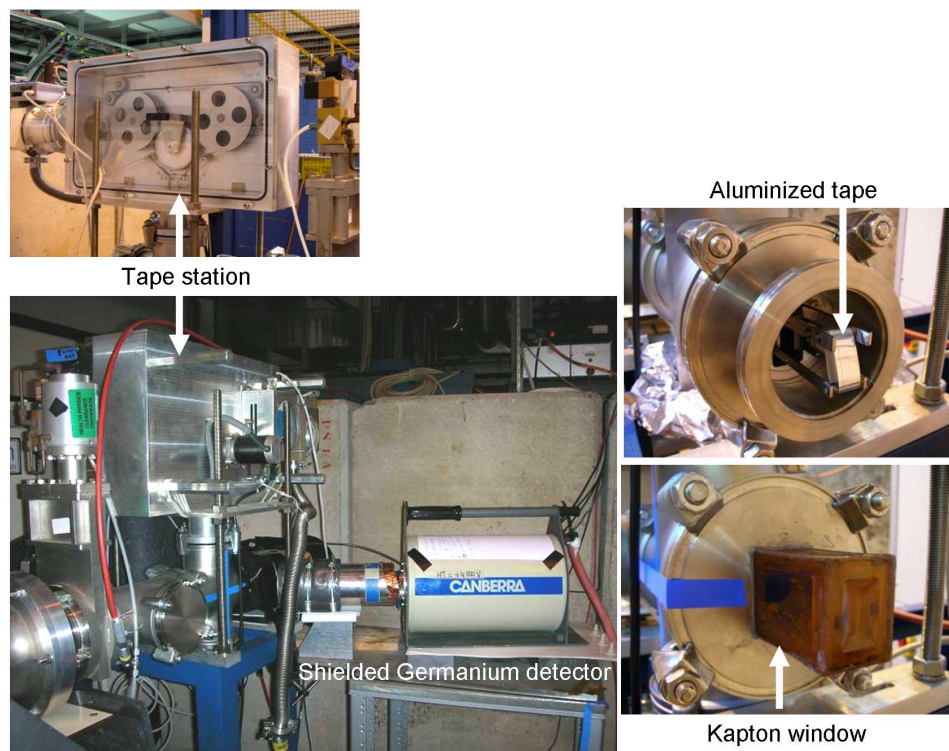


Figure 1.16: Pictures of the detection setup, also published in [101]. See text for details.

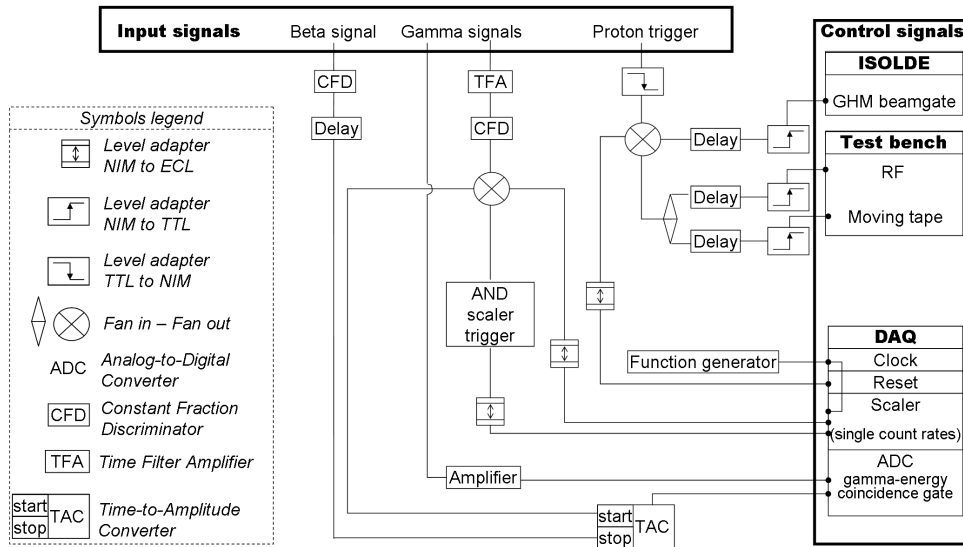


Figure 1.17: Scheme of the detection electronics showing signal processing from the detector preamplifiers to the DAQ and control signals.

The cycle in continuous mode differs from the one used in pulsed mode (Figure 1.18). Successive cycles with the same parameter conditions constitute one measurement period. In the following, periods where the beam gate is open will be called **collect** period. Measurements of the background are performed in two ways: with the beam gate closed to check what is still coming out from the ECR plasma when no ions are injected (**BGoff** periods), and with FC3 inserted (Figure 1.10) to measure long-lived activity deposited on the sides of the tape (**FCin** periods).

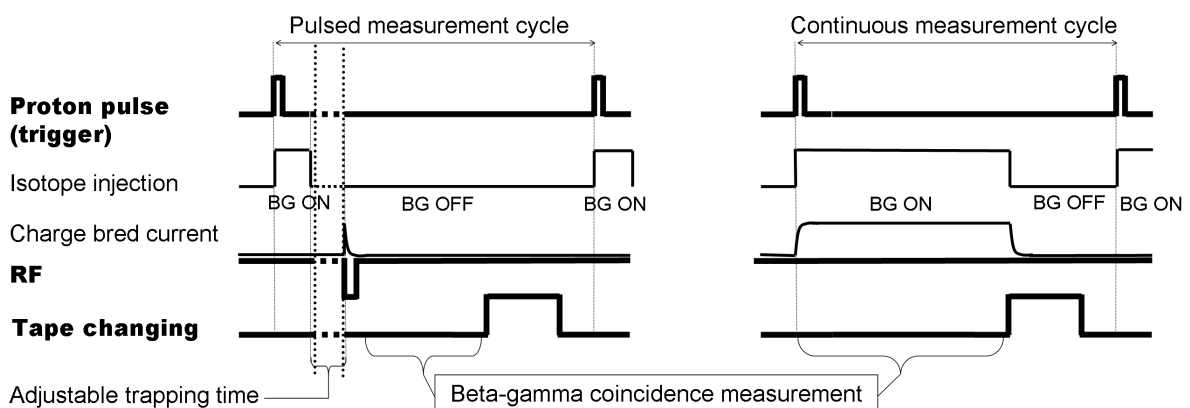


Figure 1.18: Scheme of the measurement cycles in pulsed mode and in continuous mode.

Analysis method

The DAQ system is recording events encoded as shown in Figure 1.19. A ROOT-based [102] GUI called GO4 and developed by GSI (Darmstadt, Germany) is used for on-line monitoring, and provides the fitting tools for an interactive off-line analysis [103].

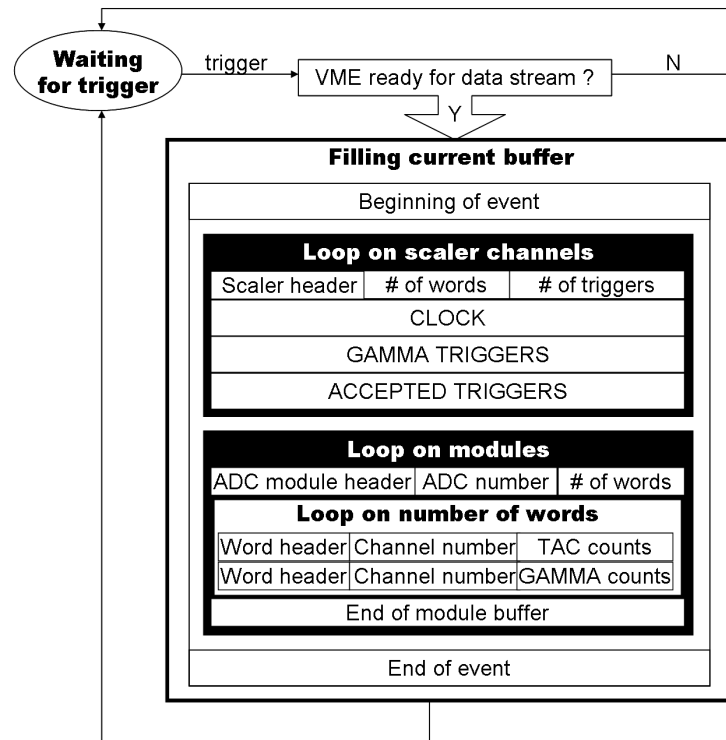


Figure 1.19: Data acquisition events encoding. The data file is structured in events typically encoded as shown for the purpose of our experiments.

The data analysis required the development of specific routines in the GO4 and later in the ROOT environment for the data unpacking (Appendix A). Dead time induced by the electronics was estimated from the ratio of the total gamma triggers with the total of “busy” signals from the scaler (see Figure 1.17), indicating the number of accepted triggers. Gamma spectra, beta-gamma coincidence spectra and beta decay curves were obtained as shown in Figure 1.17, and their background level suppressed. Gamma lines provided identification of the various species, and confirmation was obtained from the fit of the beta decay curves with the half-life value. Charge breeding efficiencies were determined from the beta-gamma coincidence counts. Additional information such as the confinement and charge breeding times could be obtained from the fit of the beta decay curves. Expected sources of systematic errors are gathered in Table 1.8.

Measurement with	Uncertainty on	Source	
Stable beam	1 ⁺ injected current	<ul style="list-style-type: none"> • drifts with time, isotope and target lifetime • -25% if GHM slits inserted • read with +200 pA noise on GHM FC 	
		Radioactive beam	<ul style="list-style-type: none"> • drifts with time, isotope and target lifetime
		true coincidences	<ul style="list-style-type: none"> • background from beam deposited on collimator and tape sides (wrong dipole setting, wrong slits opening) • +10% false coincidences selected on TAC spectrum • multiple counting of events due to low threshold setting
	durations in cycle (Figure 1.18)	<ul style="list-style-type: none"> • tuned with the precision of the timer range 	
	detection efficiencies	<ul style="list-style-type: none"> • measured at some distance from exact tape implantation point 	

Table 1.8: Expected sources of systematic errors for the calculation of charge breeding efficiencies for radioactive and stable beam.

1.4 Aim of the PhD study

Although many tests were already performed with ECR charge breeders with stable ions, on-line measurements with radioactive ions are necessary to address the issues which are specific to RIB facilities:

- the charge breeding of low yields of radioactive isotopes
- the extraction of a pure beam of highly-charged radioactive ions from the ECR charge breeder
- the efficient suppression of contaminants
- the interaction of various chemical elements with the plasma chamber walls
- the decay of isotopes trapped in the ECR plasma
- the radioprotection constraints in case of maintenance

Moreover, even weak intensities of radioactive ions can be identified with the tape station setup. Therefore, the PHOENIX ECR charge breeder is a unique test bench for testing on-line the performances of such a setup. One can switch from one mass to another, with a wide range of choices, and compare the charge breeding efficiencies for various elements (different Z values) and various masses (different A values).

Required developments for an objective comparison

For an objective comparison with other on-line charge breeders such as the REX-EBIS, technical developments were undertaken during my PhD work.

- Although the setup cannot be modified to fit the same UHV standards as the REX-EBIS, the vacuum in the beamline could still be improved. I partly addressed this issue during the thesis (subsection 3.3.2) prior to the measurements.
- Moreover, the REX-EBIS already benefits from an extracted beam with a good emittance and a very low stable background (less than 0.1 pA according to [64]). I studied a solution to the problem of the stable background with the ECR (subsection 3.1.1) during the thesis (subsection 3.3.3 and Appendix B), but the needed modifications were not undertaken.
- Finally, the REX-EBIS operates at 60 kV, which is the maximum acceleration voltage at ISOLDE. I took part to the developments started during the thesis to upgrade the PHOENIX ECR to a 60 kV operation (subsection 3.3.1) and thus obtain more available beams for tests.

Required comparative tests

As many tests from the performance study (IS397 proposal [91, 104]) started in 2003 could not be performed within the given shifts, an addendum was proposed and accepted in 2005 [105]. I was involved in the measurements required to complete the addendum, i.e. in the beamtimes for the study of the pulsed mode, the trapping of daughter nuclides within the ECR plasma, and the study of the effects of chemistry on the charge breeding process. I also took in charge the analysis of these measurements.

As a conclusion to the PhD work, a proposal of experiment for which I was spokesperson was prepared and defended for testing the application of the ECR charge breeding techniques for an astrophysics experiment. It was accepted and I could organize a first test experiment with the help of a new collaboration. The preliminary results presented in this thesis come from a last data analysis which I could undertake before submitting this manuscript.

Résumé du chapitre 1: Motivation et contexte scientifique

*Les faisceaux d'ions radioactifs accélérés offrent un intérêt croissant pour la médecine, l'industrie, et la recherche. Cependant, il n'existe pas encore d'accélérateur capable de gérer toute la variété des faisceaux d'ions produits. **Des techniques de multi-ionisation permettent d'étendre la gamme des faisceaux que peuvent accepter les postaccélérateurs.** Ces techniques utilisent la collision entre les ions simplement chargés du faisceau et des électrons libres, selon trois variantes représentées schématiquement en Figure 1.2:*

- ***La technique des “Stripping Cells”** est largement répandue depuis maintenant plus de trente ans [39]. Elle produit des ions multichargés avec une efficacité élevée (Table 1.1) et elle est au centre de plusieurs développements innovants [47, 35, 43, 38]. Des mesures récentes montrent que cette technique supporte des faisceaux incidents de quelques microampères d'intensité [44]. Son principal désavantage demeure le coût à engager pour la préparation et la pré-accelération du faisceau, ainsi que pour la maintenance des cellules de stripping lors d'un usage à haute intensité. Il ne s'agit pas d'une solution compacte.*
- ***L'utilisation de l'EBIS** pour la pré-injection d'ions multi-ionisés dans les accélérateurs connaît un certain essor [57, 58] en raison des excellents résultats en terme d'efficacité et de rapidité de l'élévation de la charge ([54], voir les exemples de la Table 1.2). En revanche, l'EBIS nécessite une maintenance qui peut se révéler délicate dans un complexe de production de faisceaux d'ions radioactifs. En outre sa limitation intrinsèque de capacité de charge se traduit par une limite de l'intensité des ions multichargés produits.*
- ***Enfin, la source ECR** connaît depuis une dizaine d'années des développements pour être transformée en élévateur de charge [72, 87]. Les performances actuelles avec des faisceaux intenses d'ions stables [23] encouragent le développement des élévateurs de charge ECR pour les futures installations de production des faisceaux d'ions exotiques. Depuis 2001, un élévateur de charge ECR est dédié à des tests avec des faisceaux radioactifs au CERN*

[91, 29], et sert de support expérimental pour cette étude. Il s'agit également de la solution qui a été proposée pour les intensités d'EURISOL [22].

Les constituants essentiels de la source ECR sont une haute tension pour décélérer le faisceau d'ions incident, une onde Haute Fréquence (HF) pour allumer un plasma, et un champ magnétique pour le confinement du plasma (voir Figure 1.7). Dans le plasma, il existe une zone où le mouvement giratoire des électrons le long des lignes de champ magnétique est en résonance avec l'onde HF (voir Figure 1.5): c'est la Résonance Electronique Cyclotronique, ou ECR. Les électrons qui traversent cette zone gagnent stochastiquement l'énergie suffisante pour ioniser les ions du plasma lors de collisions [71].

Selon que le faisceau injecté est constitué d'ions stables ou d'ions radioactifs, des méthodes expérimentales spécifiques sont mises en place. L'injection des ions stables est pulsée (méthode "beam ON - beam OFF" illustrée en Figure 1.12) afin de détecter au-dessus du seuil du bruit de fond les créneaux correspondants des ions multichargés extraits de l'ECR. Dans ce cas, la source ECR fonctionne en mode continu, c'est-à-dire que l'onde HF est appliquée en permanence. En mode pulsé, l'onde HF est appliquée de manière discontinue. Lorsque l'onde HF n'est plus appliquée, les électrons rapides s'échappent du plasma, le plasma ECR s'éteint et les ions qui étaient confinés sont relâchés d'un seul coup: il s'agit du pic "afterglow"([76], voir Figure 1.13). Ce mode est particulièrement adapté à la multi-ionisation des isotopes de courte durée de vie [94, 75].

Le travail de thèse fut mené au complexe de séparation des isotopes en ligne (Isotope Separation On-Line ou ISOL) du CERN, nommé ISOLDE [97]. On y produit une grande variété d'isotopes stables et radioactifs par des réactions de fission, spallation ou fragmentation d'un faisceau de protons de 1.4 GeV sur une cible épaisse. Les produits sont extraits de la cible, ionisés, puis accélérés à un potentiel maximal de 60 kV vers les expériences.

Un élévateur de charge ECR, la source de "Production Hautement Optimisée d'Electrons, de Noyaux Ionisés et de rayons X", dite PHOENIX [95], a été installé sur une ligne de test expérimentale après la séparation en masse du faisceau d'ions simplement chargés. La ligne de faisceau est représentée en Figure 1.10. Un dipôle magnétique sélectionne l'état de charge du faisceau d'ions multichargés extrait de l'ECR. Le courant des ions stables multichargés est mesuré dans une cage de Faraday, tandis que les ions radioactifs sont implantés sur un dérouleur de bande pour être identifiés et sélectionnés par la détection des coïncidences bêta-gamma.

La source PHOENIX est particulièrement dédiée à l'étude des performances d'une source ECR utilisée en élévateur de charge avec des ions radioactifs. En effet, **malgré les nombreuses études réalisées avec des faisceaux stables, certaines conditions spécifiques aux faisceaux exotiques n'ont jamais été testées.**

Premièrement, l'acceptance en termes d'émittance, d'intensité et de masse du faisceau d'ions incident doit être testée avec une grande variété d'isotopes. Dans cette perspective, un banc de test en ligne dans un complexe de production tel que ISOLDE est un atout.

En outre, le problème de la contamination prend toute son importance lorsqu'on travaille avec des faisceaux d'ions radioactifs. Des intensités faibles, des probabilités de décroissance radioactive variées, un bruit de fond non négligeable d'isotopes neutres diffusant dans les lignes de faisceau, compliquent la production efficace d'un faisceau pur d'ions multichargés.

Les tests expérimentaux doivent permettre de comparer l'efficacité et la rapidité de l'élévation de la charge pour divers éléments chimiques, diverses masses, et diverses intensités de faisceaux stables et radioactifs. Un addendum au programme de tests démarré en 2003 a été proposé et accepté en 2005 [105]. Celui-ci vise notamment à compléter les connaissances concernant: les processus chimiques intervenant dans l'élévation de charge, les conséquences de la décroissance radioactive sur la capture des ions dans le plasma ECR, et le fonctionnement en mode pulsé (voir chapitre 2). Ces sujets sont abordés dans la thèse.

Le but du travail de thèse est donc de compléter l'investigation des performances de l'élévateur de charge ECR PHOENIX avec des ions radioactifs, ainsi que d'étudier les possibilités d'application des faisceaux d'ions radioactifs multichargés par l'ECR à des expériences de physique.

Les tests expérimentaux auxquels j'ai participé et dont j'ai analysé les résultats (voir chapitre 2) visent tout d'abord à mesurer l'efficacité et la rapidité de l'élévation de la charge pour divers isotopes. La structure en temps du faisceau extrait (continu ou pulsé) doit également être étudiée.

Ensuite, on constate qu'une comparaison objective des performances ECR avec celles des autres techniques de multi-ionisation requiert l'amélioration du dispositif existant, notamment un vide de meilleure qualité et une meilleure séparation en masse et en énergie du faisceau extrait. J'ai entrepris la majeure partie de ces développements dans le cadre de ma thèse (voir chapitre 3).

Finalement, à la lumière des nouveaux résultats, je compare les performances ECR à celles des autres techniques de multi-ionisation. J'effectue un bilan quant aux applications immédiates ou à moyen-terme de l'élévateur d'état de charge PHOENIX. En tant que porte-parole d'une expérience d'application à l'astrophysique, j'ai pu organiser au sein d'une nouvelle collaboration un dernier temps de faisceau. Je présente les résultats d'une analyse préliminaire de ce test, que j'ai pu effectuer avant de rendre ce manuscrit.

Chapter 2

Charge breeding experiments

A summary of all measurements undertaken within the IS397 program between 2004 and 2008 is provided in this chapter. Measurements performed in 2006 and 2007 are part of the PhD work.

2.1 Online results with stable ions

At ISOLDE, a wide variety of stable ion beams are produced with intensities high enough to be measured on Faraday cups. Most of them are coming directly from the TIS units, either present in the target material or in the support gas of the 1^+ plasma ion source. In some cases, specific mass markers are additionally used for setting up the 1^+ source or tuning the beam lines. The transmission through ISOLDE beamlines, from GPS to the injection side of the PHOENIX is therefore always estimated from the stable beam current on FCs. Only electrostatic quadrupoles are used for transport, therefore the tuning is considerably simplified as it is valid for all masses. Moreover, measurements with stable ions allow fine tuning of the injection with the Einzel lenses and of the optimal ΔV . This method is called “blind tuning” as one uses the settings with the stable beam to later inject the radioactive ions, and it was demonstrated for gaseous ions in [31]. Thus, stable beam optimization constitutes a prerequisite to any measurement with radioactive ions.

2.1.1 Optimizing the injection in continuous mode

Various TIS units were used for the stable beam measurements.

- A UC_x target was coupled with a Forced Electron Beam Ion Arc Discharge (FEBIAD)-type plasma ion source [106] and a heated transfer line (or so-called “hot plasma” ion source) to produce Kr and Xe in 2004, and U, In and Ar in 2007. A similar source was coupled to a Pb / Bi target to provide beams of Pb, Bi, and Xe in 2005.
- A surface ionization source was coupled to a UC_x target to produce U in 2006, to a Ta target to deliver K and Cs beams in 2005, and to a LaO target to produce La and Sn beams the same year. In the last case, “the lasers of the ISOLDE [Resonance Ionization Laser Ion Source] RILIS were resonantly ionizing the Sn beams” [29, 107].

For all the runs, oxygen was used as a buffer gas to support the ECR plasma.

The beam ON - beam OFF method (see 1.3.3) suppresses the steady ECR background from the charge bred ion current (Figure 2.1). Therefore, the errors on the following charge breeding efficiencies (Figure 2.4) arise from both readings of the charge bred ion current and of the A/q background. The injection optics are optimized for the highest intensity on the LabView monitoring (Figure 2.1) in parallel with the ΔV scan. Settings are taken on a charge state expected to show the best signal to background ratio.

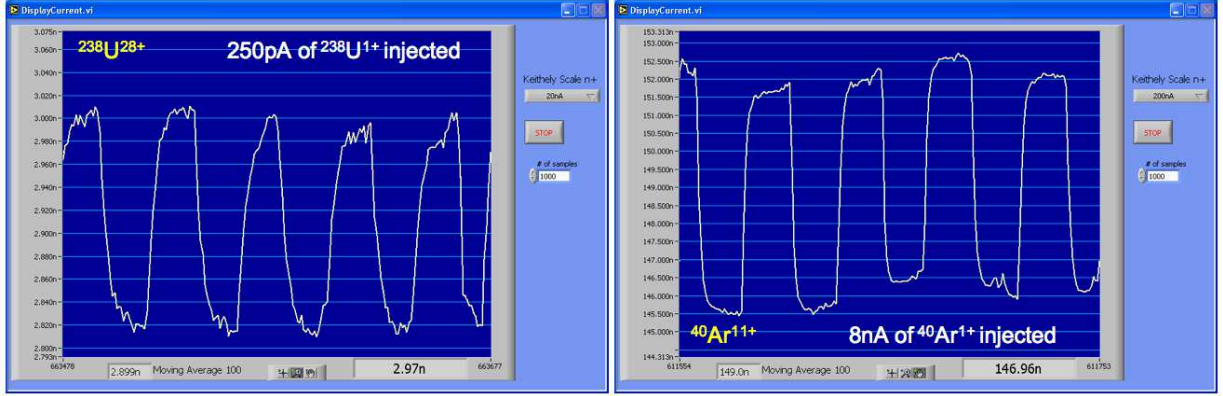


Figure 2.1: Detection of charge bred stable beams of ^{238}U and ^{40}Ar , injected in cycles 2 s ON-2 s OFF (see 1.3.3). The extracted currents of $^{238}\text{U}^{28+}$ and $^{40}\text{Ar}^{11+}$ are measured as a function of time and monitored through the LabView-based control system (see subsection 1.3.2). The left scale is in nA.

The shapes of the ΔV curves are consistent with the results of previous runs (Figure 2.2) and with measurements at other facilities [23, 82]. For positive values of the ΔV , the 1^+ beam energy is not sufficient to overcome the ECR plasma potential. As soon as the 1^+ beam reaches the plasma potential, it is captured. For further negative values of the ΔV , the injected ions have higher energies than the mean energy of the plasma ions, and Coulomb collisions are not sufficient to thermalize them. If lost by the plasma, condensable elements stick to the cold plasma chamber walls. The narrow ΔV curves for condensable elements allows a rough estimate of the plasma sheath potential drop along the beamline axis ($\Delta\Phi$) to be about 25 V, taking the full-width at half-maximum (FWHM). On the contrary, noble gases are released from the walls and recycled into the ECR plasma: this explains the “plateau” shape of the curve as soon as capture starts. For much higher values of the 1^+ beam energy, the proportion of charge bred ions decreases again as one shoots through the plasma. The workable range for noble gases can be approximated to 300 V from the $^{134}\text{Xe}^{22+}$ data.

A shorter “plateau” of 100 V was observed at KEK-JAERI for Xe [78], as well as narrower peaks for condensable elements (only 4 V width for Ba [82]), for a non-PHOENIX type ECR charge breeder. However, widths of condensable element peaks were estimated to 10 V with

a PHOENIX at LPSC Grenoble [23]. Tests performed with the MINIMAFIOS charge breeder suggest that the high pressure in the GHM beamline could increase the number of collisions and recombinations with residual gas, thus inducing more energy spread in the 1^+ injected beam and contributing to the widening of the ΔV curves.

For plasma sources, the potential of the injected beam V_{1^+} equals the 30 kV ISOLDE line acceleration voltage summed with the anode voltage, of the order of 100 - 200 V. One expects ΔV curves to be relatively reproducible for a given isotope (A,Z) and ion source. Although some components of the PHOENIX charge breeder were exchanged between 2005 and 2006 (subsection 3.3.1), the measurements performed with the hot plasma source still match. A shift remains between the peaks of $^{238}\text{U}^{29+}$ and of $^{39}\text{K}^{8+}$ produced with the surface ionization source, most probably due to their mass difference. Moreover, it is not clear whether gas and condensable elements can be captured in the same conditions with an optimal efficiency, as the mass difference should also be taken in account. For this reason, measurements with isobars are needed, i.e. measurements with radioactive ions (see subsection 2.2.2).

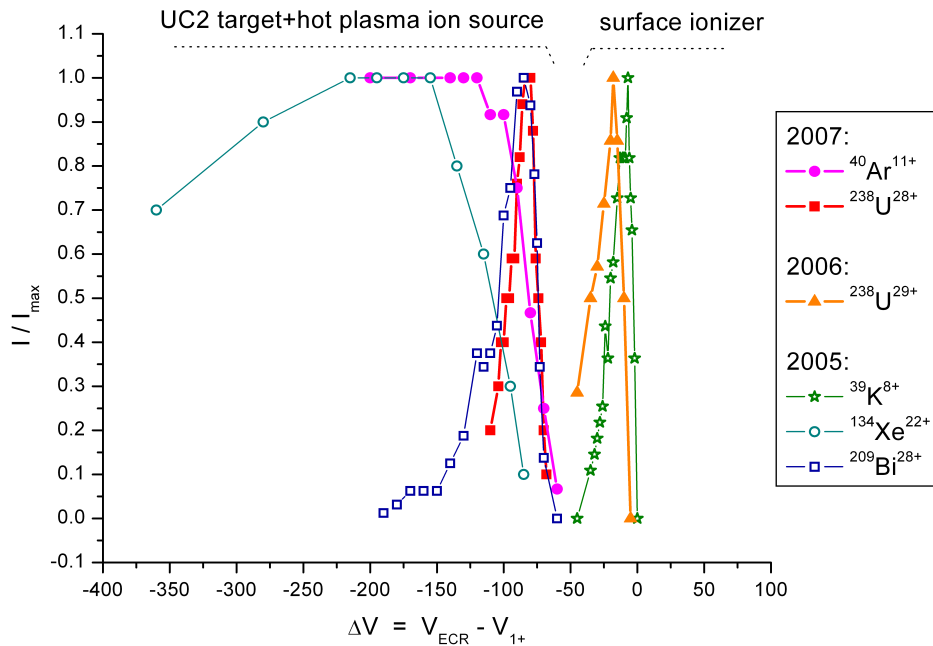


Figure 2.2: ΔV curve for the injection of stable elements. Error bars are not shown, but are estimated to 10% in average for the ^{238}U measurement performed in 2007.

The global charge breeding efficiency provides a measurement of the plasma capture efficiency. An average minimum of 10% for plasma capture is achieved for all species. Much higher performances are obtained with noble gases because of the recycling effect. More than 50% total capture obtained for ^{40}Ar indicates that this measurement might not be reliable, as one should lose charge bred ions from both sides of the ECR. Global efficiencies for metals were measured at different times, therefore no mass dependence as in [23] is observed.

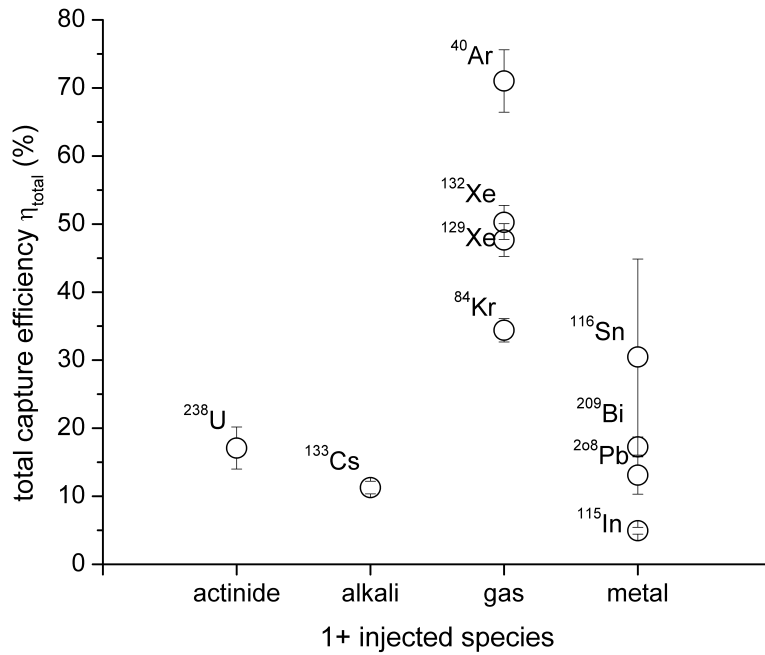


Figure 2.3: Efficiency of plasma capture. Non-measurable charge states efficiencies, such as those mixed with charge states of the buffer gas, were extrapolated from the shape of the charge state distribution. Error bars correspond to the sum of errors on each charge state efficiency. More details in text.

The charge state distribution for each isotope is given in Figure 2.4. Values are missing for the charge states overlapping oxygen or carbon. Efficiencies obtained for the various charge states of ^{238}U are close to previous values obtained for ^{208}Pb and ^{209}Bi in the region $6.5 < A/q < 9.5$. Although values close to $A/q=4$ have bigger error bars due to a high background of $^{16}\text{O}^{4+}$ and $^{12}\text{C}^{3+}$, charge breeding efficiencies measured for ^{40}Ar after the experiment period in 2007 are surprisingly high, with 15.9% of $^{40}\text{Ar}^{9+}$. For comparison, [19] reports an offline 9% efficiency for $^{40}\text{Ar}^{8+}$ and [78] reports 13.5% of $^{40}\text{Ar}^{9+}$ online. Measurements with the same conditions earlier during the run showed an achievement of half of the efficiencies. Both injected Ar were measured

on FC2 with the charge breeder switched off to avoid backstreaming current. Many possible explanations exist for this discrepancy. The ECR plasma was most probably much stabler at the end of the run, and the pressure much lower in the GHM beamline, allowing better charge breeding conditions. However, the 1^+ current was lower after the run, maybe inducing more errors in the reading of the ISOLDE FCs. Special care was taken for measurements published in [29] to check on oxygen peaks that the stable background was not pulsed as well with the beam ON - beam OFF method, but such precaution was not taken for measurements in 2007 and may include an offset on read current.

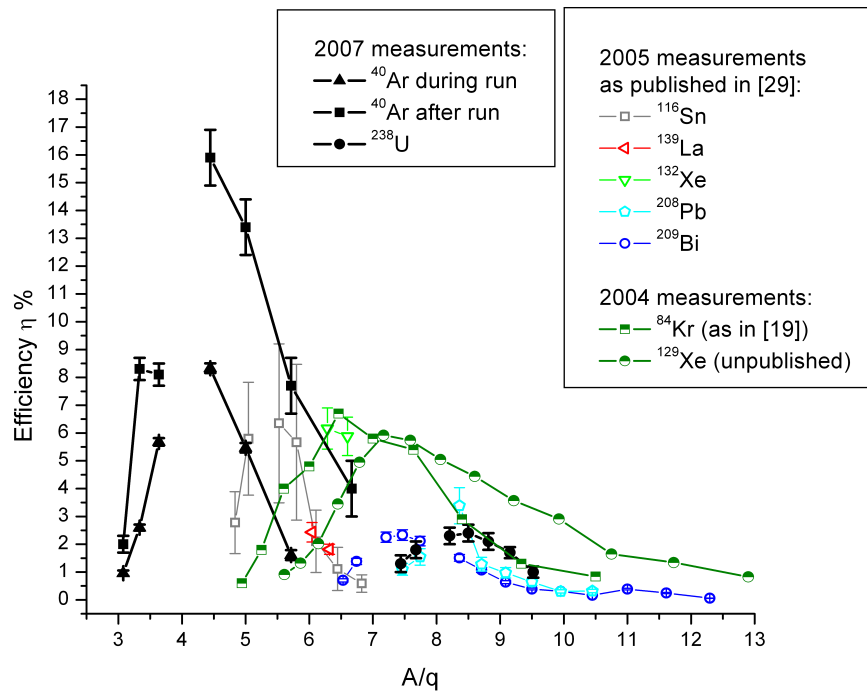


Figure 2.4: Charge breeding efficiencies for various stable species. Plotted values of the year 2005 runs are taken from [29].

2.1.2 Tests with the trapping mode

Tests with the trapping mode and stable beam were performed in 2007 prior to the trapping of daughter nuclides in the ECR plasma (subsection 2.2.3). The afterglow mode was optimized with the injection of ^{84}Kr ions, as previously shown on Figure 1.13, and with the injection of ^{238}U ions (see Figure 2.5). The aim of the tuning was to condition a stable afterglow pulse, reproducible over long measurement times, and with a short tail. Due to beamtime constraints, it was decided not to measure the whole charge state distribution in afterglow mode, but to proceed with the radioactive ion beam injection. Tests reported with the same setup by [29] gave charge breeding efficiencies of the order of 2.2% for $^{86}\text{Kr}^{13+}$ and 1% for $^{132}\text{Xe}^{18+}$ (see Figure 2.6).

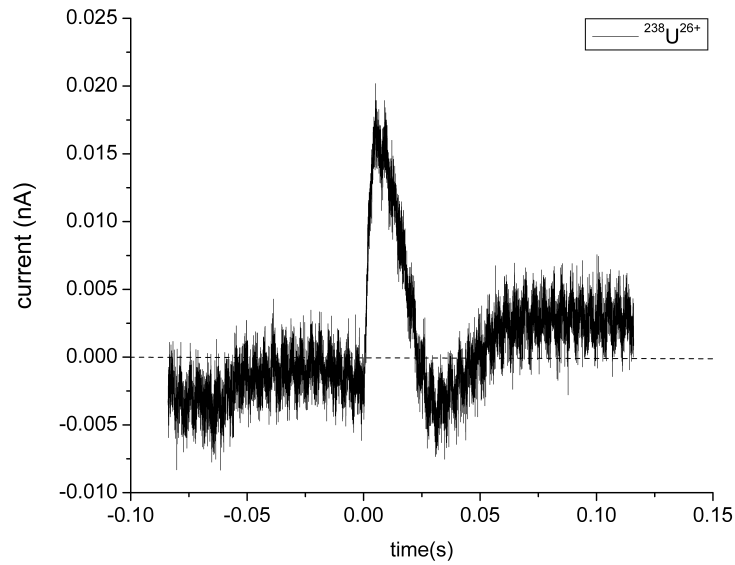


Figure 2.5: Afterglow pulse of $^{238}\text{U}^{26+}$. A RF power of 600W was applied. Injected $^{238}\text{U}^{1+}$ current was 1 nA. The extracted current was measured with and without the injection of ^{238}U in order to subtract the plasma background. This plot shows the $^{238}\text{U}^{26+}$ afterglow pulse once the background was subtracted.

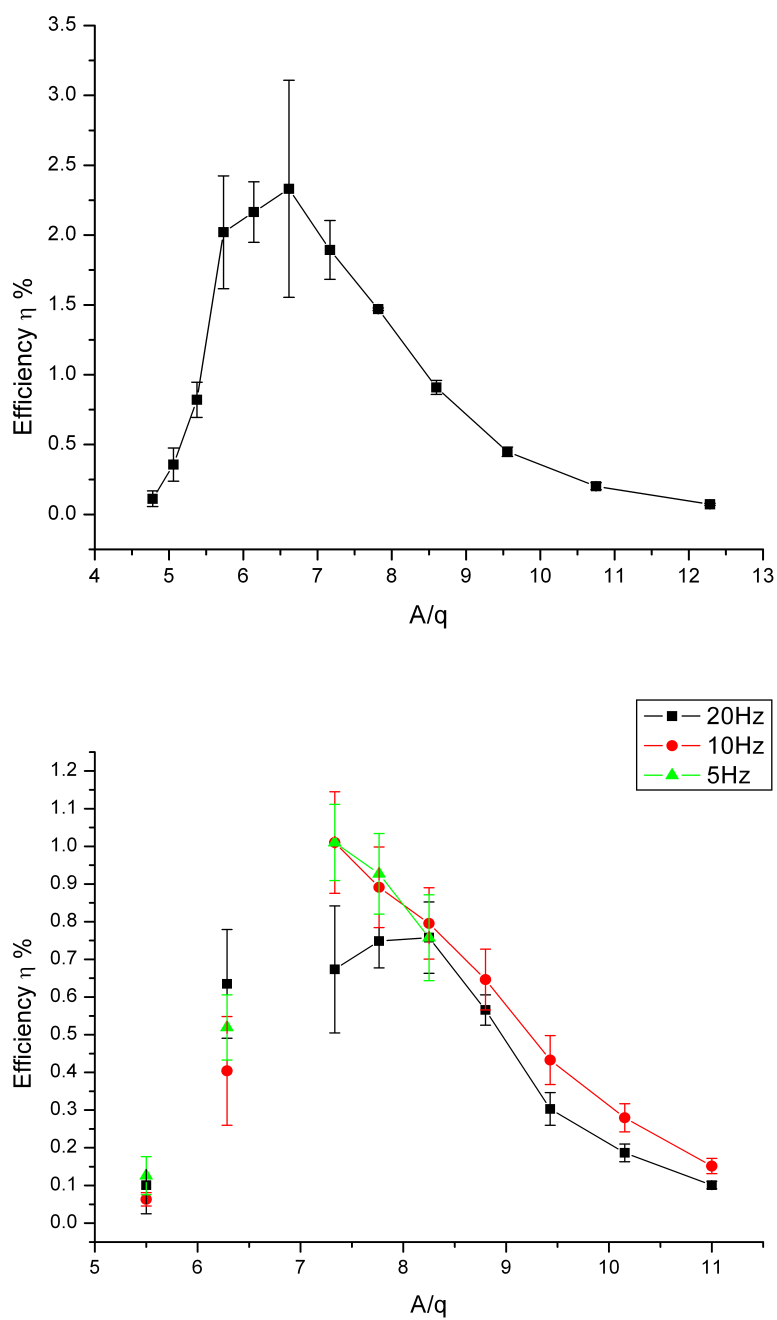


Figure 2.6: Afterglow efficiencies as given in [29]: “Charge breeding efficiencies measured for ^{86}Kr (10 Hz frequency, [top]) and ^{132}Xe injected beams [bottom]”.

2.2 Online results with radioactive ions

2.2.1 Tests with noble gases of various (A,Z)

Tests performed by the collaboration prior to the PhD work made use of the specific properties of the ECR charge breeding for noble gases. [19] presents an application of ECR charge breeding to the study of the decay properties of the ^{48}Ar nuclide of astrophysical interest [108]. This neutron-rich isotope was produced at ISOLDE with a UC_x target coupled with a plasma ion source and a cooled transfer line to select gases (or so-called “cold plasma ion source”). A high contamination of doubly charged ^{96}Kr and triply charged ^{144}Xe was selected at the same A/q ratio as the singly charged ^{48}Ar . In the charge breeder, the charge state distributions of Kr and Xe are shifted towards higher A/q values compared to Ar. Therefore, the choice of the charge state of Ar could improve its ratio over the Kr and Xe background. ^{48}Ar was injected and charge bred to $^{48}\text{Ar}^{9+}$. The obtained beta-gated gamma spectra (Figure 2.7) shows ^{48}Ar decay lines that could not be detected previously with such a setup.

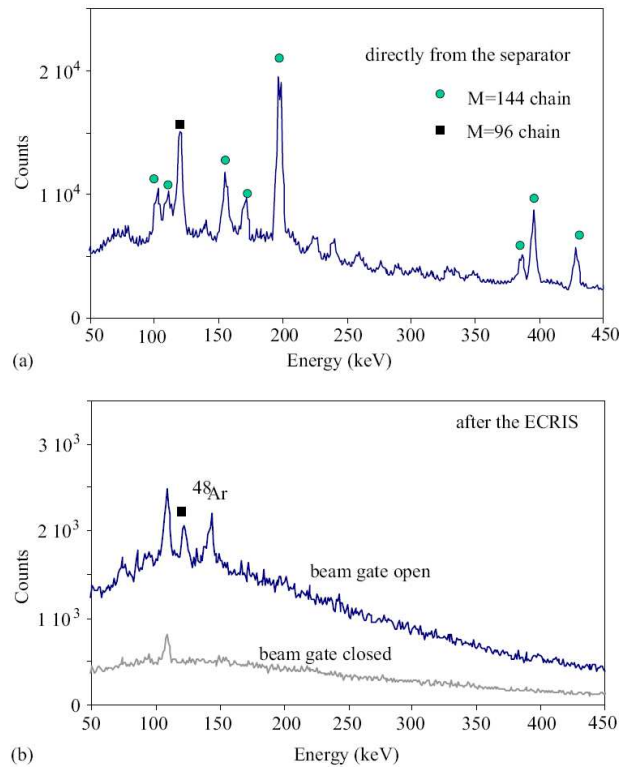


Figure 2.7: Signature of $^{48}\text{Ar}^{9+}$ as given in [19]: “(a) The β -gated γ -spectrum collected for the $^{48}\text{Ar}^+ / ^{96}\text{Kr}^{2+} / ^{144}\text{Xe}^{3+}$ beam admixture directly from the GPS separator (b) The β -gated γ -spectrum collected for the same admixture after the ECRIS. [...] The background spectrum corresponding to the closed separator beam gate is also shown”.

2.2.2 Effect of the chemical properties of isobars

It was observed with stable beam injection that the shape of the plasma capture curve depends on the type of chemical element injected. For a given 1+ ion source, the capture curve of a given element is quite reproducible, and seems to depend on the mass only (Figure 2.2). By injecting radioactive isobars, one suppresses the mass dependence and allows to investigate the chemical effects only. One expects the capture to start at a same reproducible ΔV for a given 1+ ion source and a given isotope mass.

^{142}Xe ($T_{1/2}=1.22$ s (2) [109]) and ^{142}Cs ($T_{1/2}=1.689$ s (11) [109]) isotopes were produced with proton pulses impinging every 7.2 s on a UC_x target coupled with a hot plasma ion source, and injected into the ECR set up in continuous mode. The charge bred isotopes were detected with the setup described in 1.3.3. The measurements were synchronized with the proton pulses. They were done simultaneously with the collection and implantation for 5 s, then the beam gate was closed during the tape move (approximately 1 s) and until the next proton pulse.

The decay of ^{142}Xe feeds the detected ^{142}Cs , which in turn decays into ^{142}Ba ($T_{1/2}=10.6$ min (2) [109]), decaying into ^{142}La ($T_{1/2}=91.1$ min (5) [109]). One observes on all coincidence spectra (Figure 2.8) that a high amount of ^{142}Xe feeds the whole decay chain. Unfortunately, the ^{142}Xe gamma lines intensities are only known relative to the main 572 keV line, and incomplete yield measurements did not allow the calculation of absolute charge breeding efficiencies, as detailed in the following.

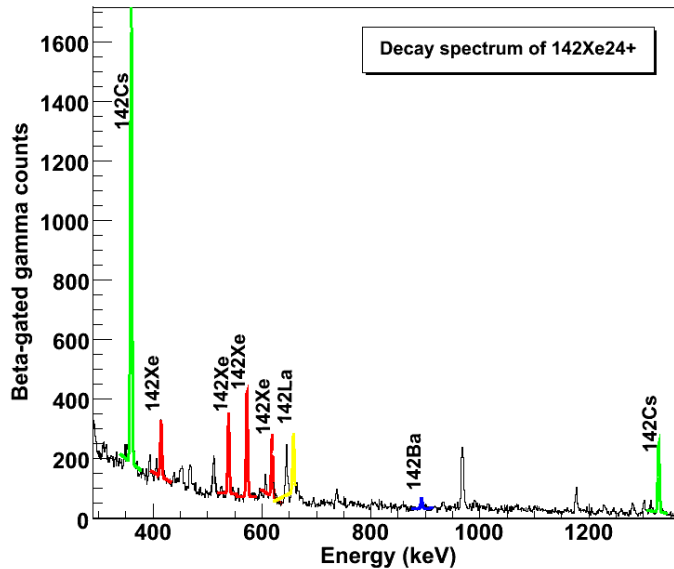


Figure 2.8: Beta-gated gamma spectrum for isobars of mass 142. Gamma peaks used for analysis are labeled by isotope.

Optimizing the injection

A quick charge state scan with the beta count rate indicated that the charge state distributions were peaked around 24^+ (Figure 2.13), on which the injection was optimized. The ΔV scan (Figure 2.9) reveals the well-known “plateau” shape for the injection of Xe, and corresponds to the energy of the 1^+ beam extracted from the hot plasma ion source with a 120 V bias at the anode, around $\Delta V = -120$ V as expected from the stable beam tuning with ^{40}Ar . The Cs ΔV curve was plotted by subtracting the high contribution from the Xe decay, estimated on the range $\Delta V \leq -150$ V and $\Delta V \geq -40$ V to about 10% of the charge bred Xe. One main narrow injection peak is observed for Cs at -55 V, and could correspond to a fraction of Cs undergoing surface ionization on the walls of the plasma ion source (Figure 2.10). The FWHM is consistent with the workable ΔV range measured for condensable species with stable beam (subsection 2.1.1), approximately 25 V. Stable beam tuning with ^{238}U gave a peak at -85 V from ionization in the hot plasma ion source, and one could possibly expect a second Cs peak within a few tens of Volts range. A few data points at -120 V indicate the possibility of a second injection peak of Cs from the hot plasma ion source.

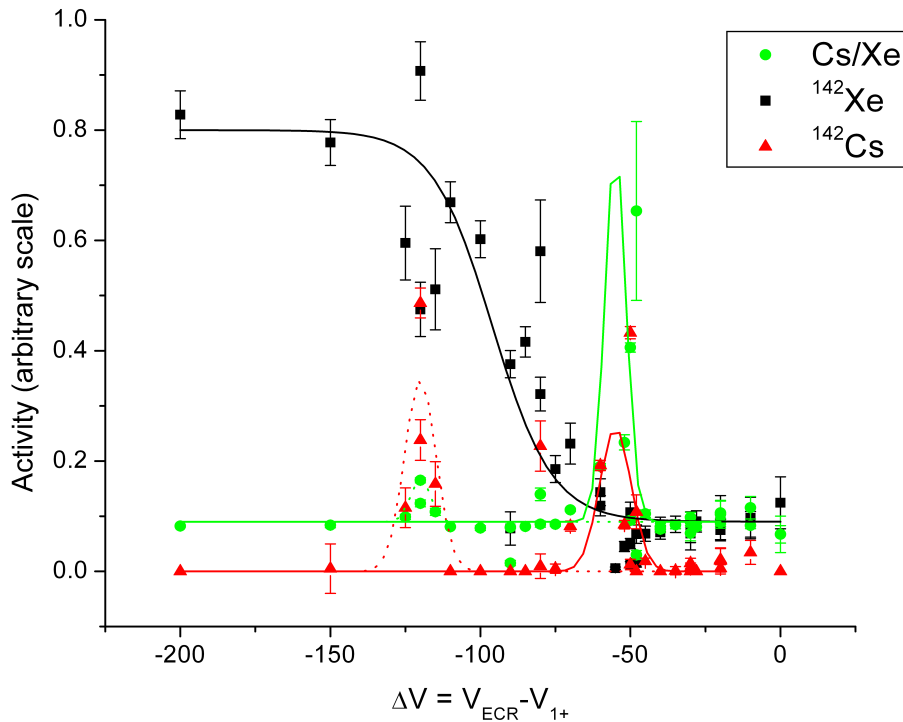


Figure 2.9: ΔV curve for the injection of isobars. The respective beta-gated gamma counts for Cs and Xe are normalized to their maximal value. Error bars arise from the fit of the beta-gated gamma spectra only.

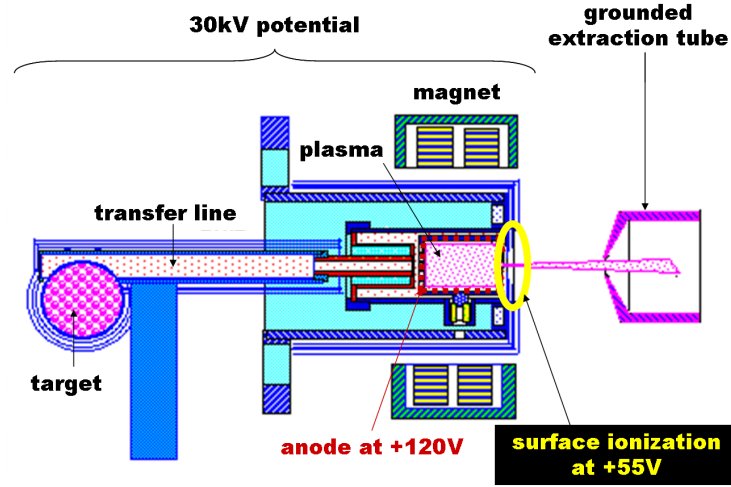


Figure 2.10: Scheme of a hot plasma ion source. In the case of the ^{142}Cs measurements, surface ionization could happen at +55 V.

Yield calculation

Yield measurements were performed with a Eurysis germanium detector and a beta counter at the ISOLDE tape station set after GPS [110]. For unexplained reasons, most gamma spectra do not show any ^{142}Xe line (Figure 2.11), although plenty can be seen after the ECR charge breeder. As ^{142}Xe decays into ^{142}Cs , the yield measurements might have been performed with too much delay with respect to the proton pulse, so that only the ^{142}Cs contribution was seen. However, as ^{142}Xe is seen after the charge breeder, it must have been produced in the target in the first place. Therefore it was wrongly assumed that only ^{142}Cs came out of the target during the yield measurement, in order to calculate a tentative yield for ^{142}Cs . The release curve was plotted in Figure 2.12, considering a 90% beta detection efficiency at ISOLDE tape station, 1 s of tape transport and 83% transmission of the beam from GPS to the tape station. It was fitted with a sum of exponential functions as explained in [111, 112]:

$$f(t) = A_{norm} \cdot (1 - \exp(-\lambda_r t)) \cdot (\alpha \cdot \exp(-\lambda_f t) + (1 - \alpha) \cdot \exp(-\lambda_s t)) \cdot \exp(-\lambda t),$$

where A_{norm} is a normalization factor, λ is the decay constant and λ_r , λ_f and λ_s are parameters of the fit and are related to diffusion and effusion processes. The contribution from fast-decaying ^{142}Xe was excluded from the fit, and $f(t)$ was integrated over the first 5 s after proton impact. Production of ^{142}Cs out of the target was estimated to $2.55 \cdot 10^6$ isotopes/ μC . Measurements were partly performed with $1 \cdot 10^{13}$ protons per pulse and with $2.3 \cdot 10^{13}$ protons per pulse, so either with $2.55 \cdot 10^6$ or with $5.9 \cdot 10^6$ ^{142}Cs isotopes produced per proton pulse.

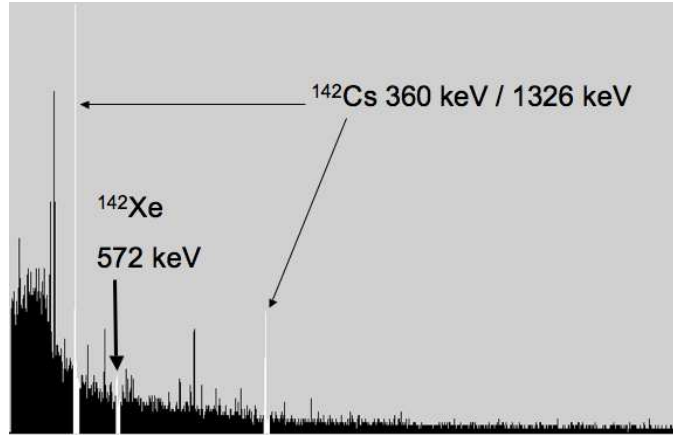


Figure 2.11: Gamma yield spectrum for mass 142 isobars measured and analyzed with the *Genie2K* software [113]. The ^{142}Xe peak is much lower than expected.

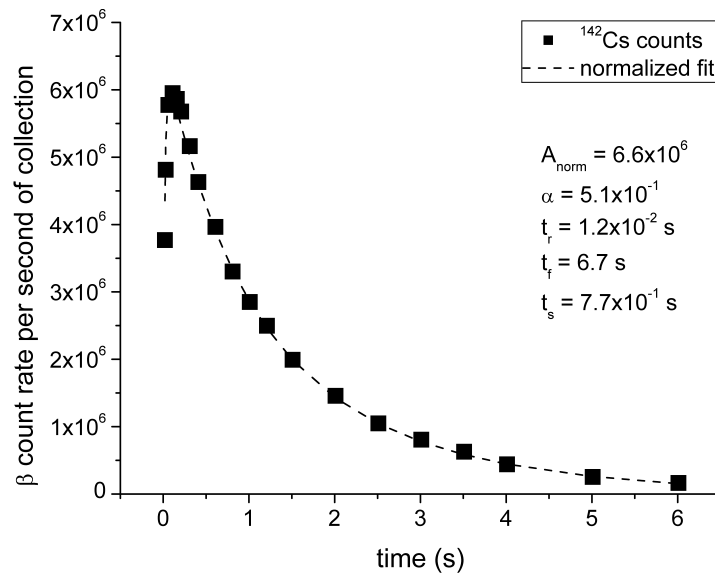


Figure 2.12: Release curve for ^{142}Cs . The parameters A_{norm} and $t_i = \ln(2)/\lambda_i$, $i=\{r,s,f\}$, of the fit are given for the dashed curve.

No absolute yield could be calculated for ^{142}Xe , as the intensity of the transition from the ground state of ^{142}Xe to the one of ^{142}Cs is not known. From the ratio of the total intensities of ^{142}Xe gamma lines over ^{142}Cs gamma lines, one assumes that the ^{142}Xe intensity was a factor 20 less than the ^{142}Cs intensity.

Charge state distributions

Charge state distributions for ^{142}Cs and ^{142}Xe are given in Figure 2.13. Production rates could not be calculated (see above), so no absolute efficiency is given. Charge state distributions are plotted with an arbitrary vertical scale on Figure 2.13. ^{142}Cs count rates for the various charge states were measured for $\Delta V = -55$ V, and the fraction coming from the decay of ^{142}Xe was suppressed. Count rates for ^{142}Xe were measured for $\Delta V = -120$ V.

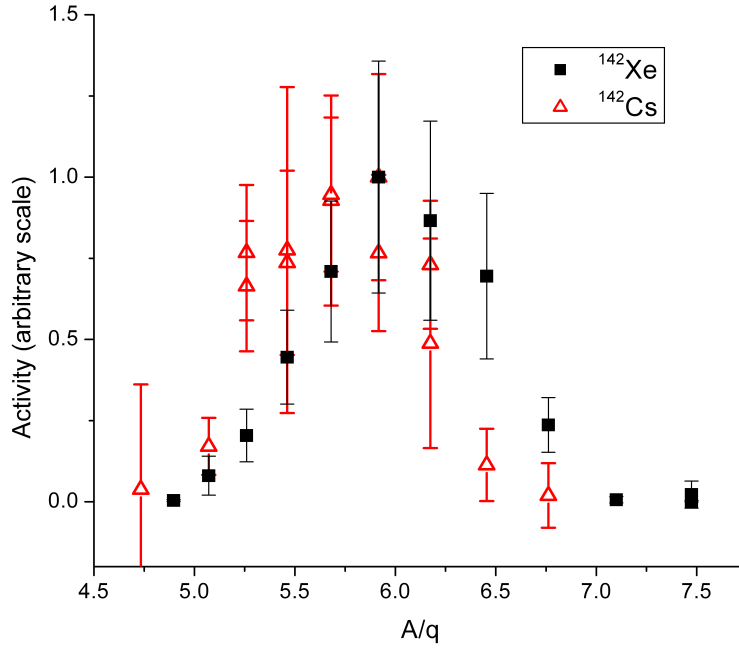


Figure 2.13: Charge state distributions measured in continuous mode for ^{142}Xe and background-suppressed ^{142}Cs at the optimum ΔV for each isotope. Error bars arise from the fit of the beta-gated gamma spectra only.

2.2.3 Trapping of daughter nuclides in the ECR plasma

In some specific cases, beams of isotopes that are not directly accessible with the ISOL production method can be produced from the beta decay of their mother nuclides. One possible method is the trapping of the mother nuclides for several half-lives. Such a technique was used by the ISOLTRAP experiment using Penning traps to measure the mass of neutron-rich iron isotopes [114] that are not directly produced at the ISOLDE facility [115]. In order to estimate the efficiency for trapping and charge breeding a daughter nuclide within the ECR plasma, a similar experiment was performed with the PHOENIX booster.

Experimental method

The experimental method was detailed in [101] and is summarized here. ^{61}Mn isotopes were produced by the bombardment of a UC_x target by pulses of $2 \cdot 10^{13}$ protons every 16.8 s and ionized by RILIS [107]. About $5.1 \cdot 10^6$ $^{61}\text{Mn}^+$ ions were injected per proton pulse (Figure 2.14) during 880 ms into the PHOENIX booster configured in trapping mode. The measurements were performed by repeating the pulsed mode cycle described in Figure 1.18 with given conditions. The trapping time could be varied around the half-life of ^{61}Mn , i.e., 670 (40) ms [109].

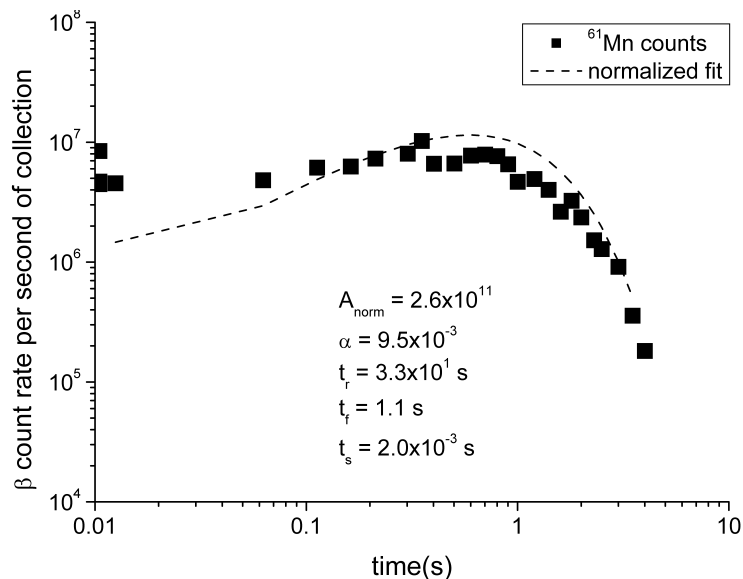


Figure 2.14: ^{61}Mn release curve. It is fitted as explained in 2.2.2 with the indicated parameters (dashed line).

^{61}Mn decays to ^{61}Fe which has a half-life of 5.98 (0.06) min [109]. After a sufficient trapping time, some charge bred ^{61}Fe ions are possibly released within the afterglow pulse. The analyzing magnet was set to select mass 61 with a 12^+ charge state, and the beam was directed to the tape station setup (1.3.3).

For a given trapping time, one successively measured:

- the collected ^{61}Mn and possibly trapped ^{61}Fe isotopes for a 30 min **collect1** period,
- the ^{61}Fe background on the sides of the tape for a 12 min **FCin1** period,
- the collected ^{61}Mn and possibly trapped ^{61}Fe isotopes for a 30 min **collect2** period,
- the possible ^{61}Fe isotopes recycled in the ECR plasma after injection for a 15 min **BGoff** period
- the ^{61}Fe background on the sides of the tape for a 12 min **FCin2** period.

During the **collect** periods, one sums the beta statistics gated on the ^{61}Mn main gamma lines, 206.8 keV and 628.6 keV, to obtain the ^{61}Mn beta decay curve (Figure 2.15). Two phases can be distinguished:

When GHM beam gate is open, the number of ^{61}Mn ions released by the ECR dN_{ECR} is proportional to the number of injected ions delayed by the confinement time. If $\tau_{cb} < T_{1/2}$, one can write:

$$dN_{ECR} = N_{ECR0} \cdot (1 - e^{-t/\tau_{cb}}) dt$$

with N_{ECR0} the current of ions injected into the ECR, which is constant for the first 900 ms after the proton pulse according to Figure 2.14.

When GHM beam gate is closed:

$$dN_{ECR} = N_{ECR0} \cdot e^{-t/\tau_{cb}} dt$$

The number of ions on the tape follows the differential equation:

$$dN_{tape} = dN_{ECR} - \lambda \cdot N_{tape} dt$$

with λ the decay constant for a given isotope and $N(t)$ the number of these isotopes implanted. By fitting ^{61}Mn beta decay curve with this expression, one obtains $\tau_{cb} \sim 500$ ms (± 50 ms) (Figure 2.16), so ^{61}Mn ions are in average charge bred and extracted before they decay. The afterglow pulse at 2.3 s is not visible on the decay curve on Figure 2.15.

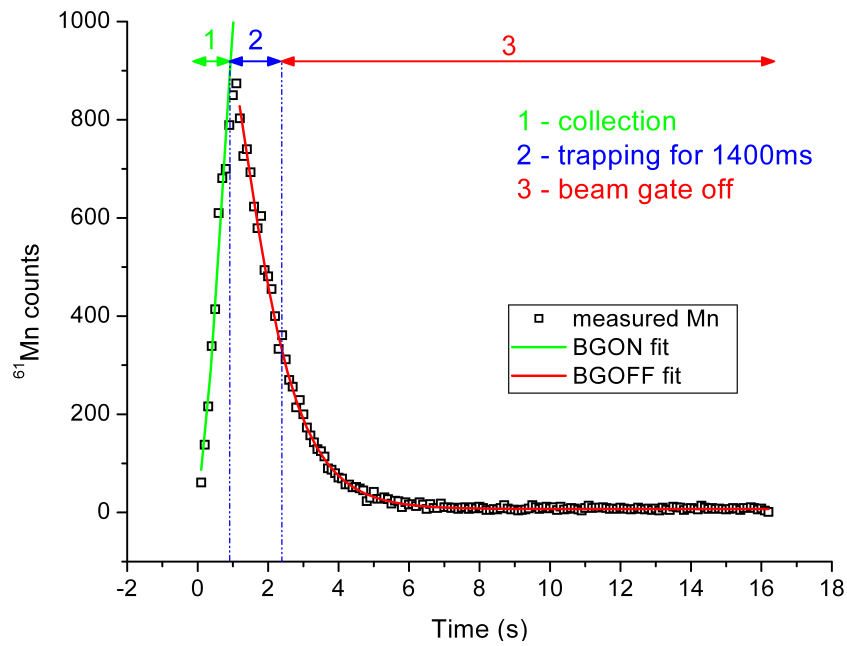


Figure 2.15: ^{61}Mn decay curve for 1400 ms trapping time.

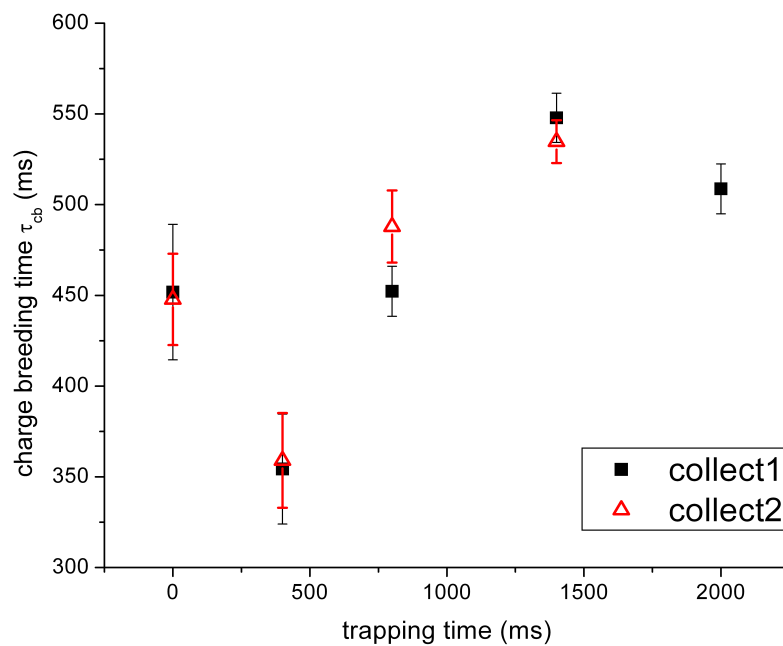


Figure 2.16: Charge breeding times for ^{61}Mn obtained for the fit of both sets of collection. The interruption of proton pulses during the collections with a 400 ms trapping time might explain why $\tau_{cb(400ms)}$ is slightly off the average value.

By summing the beta statistics gated on the ^{61}Fe gamma lines, one plots the ^{61}Fe beta decay curves for each measurement period one after the other (Figure 2.17). The measurement is vetoed during the tape move. The curves follow the decay of ^{61}Mn during both injection periods. When FC3 is inserted, one measures the fraction of ^{61}Fe implanted on the tape sides, which was not removed with the tape. For trapping times of 400 ms and 800 ms, the number of ^{61}Fe counts measured with the beam gate closed drops when FC3 is inserted, possibly showing that some $^{61}\text{Fe}^{12+}$ was still coming out of the ECR plasma even when the beam gate was closed for a few minutes. No such drop is observed for trapping times of 0 s and 1400 ms, suggesting that the plasma stability was not the same for all measurements.

Moreover, averaging effects might also cause such drops in Figure 2.17. In order to check that ^{61}Fe is effectively coming from the ECR plasma and to estimate in which proportion, a careful suppression of the counts from the tape sides should be performed.

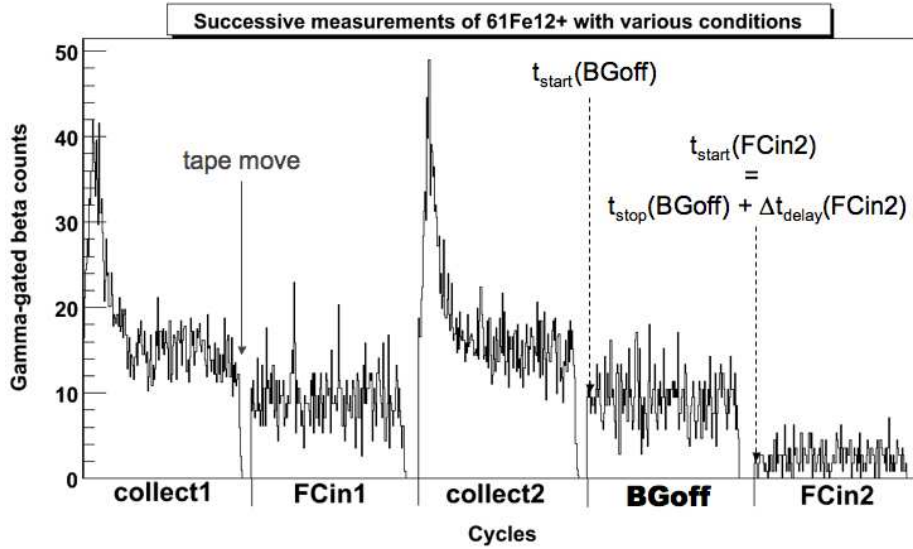


Figure 2.17: ^{61}Fe decay curve for 800 ms trapping time. The various periods were normalized over the same measurement time, approximately 10 min. No correction was made for the decay of ^{61}Fe between each file.

Background suppression for the **BGoff** measurements

A first possibility is to suppress the background from the ^{61}Fe counts integrated on the **BGoff** period. The background mainly originates from the fraction of the collected beam implanted on the tape sides, which can be estimated either from **FCin1** or from **FCin2** measurement period.

If $\Delta t_{\text{delay}(\text{FCin1})}$ is the duration before the start of the **FCin1** file, $t_{\text{start}(\text{collect1})}$ and $t_{\text{stop}(\text{collect1})}$ respectively the beginning and the end of the **collect1** file, the ratio

$$\frac{N_{\text{FCin1}} \cdot e^{-\lambda \cdot (\Delta t_{\text{delay}(\text{FCin1})} + t_{\text{stop}(\text{collect1})} - t_{\text{start}(\text{collect1})})}}{N_{\text{collect1}}}$$

gives the fraction of the collected beam implanted on the tape sides. The fraction of ^{61}Fe released from the ECR plasma N_{Fe} can then be expressed as:

$$(1) \quad N_{Fe} \sim N_{\text{BGoff}} - N_{\text{collect2}} \cdot \frac{N_{\text{FCin1}} \cdot e^{-\lambda \cdot (\Delta t_{\text{delay}(\text{FCin1})} + t_{\text{stop}(\text{collect1})} - t_{\text{start}(\text{collect1})})}}{N_{\text{collect1}}} \cdot e^{-\lambda \cdot (t_{\text{start}(\text{collect2})} - t_{\text{stop}(\text{collect2})} + \Delta t_{\text{delay}(\text{BGoff})})}$$

with $\Delta t_{\text{delay}(\text{BGoff})}$ the time between the end of **collect2** and the start of **BGoff**.

It should also correspond to:

$$(2) \quad N_{Fe} \sim N_{\text{BGoff}} - N_{\text{FCin2}} \cdot e^{-\lambda \cdot (\Delta t_{\text{delay}(\text{FCin2})} + t_{\text{stop}(\text{BGoff})} - t_{\text{start}(\text{BGoff})})}$$

Unfortunately, one observes in some cases that $N_{\text{collect1}} > N_{\text{collect2}}$ although the background should contribute to a higher N_{collect2} (Figure 2.18). This can be due to fluctuations in ISOLDE production rates. Therefore the calculation of N_{Fe} from the integrated counts is not chosen.

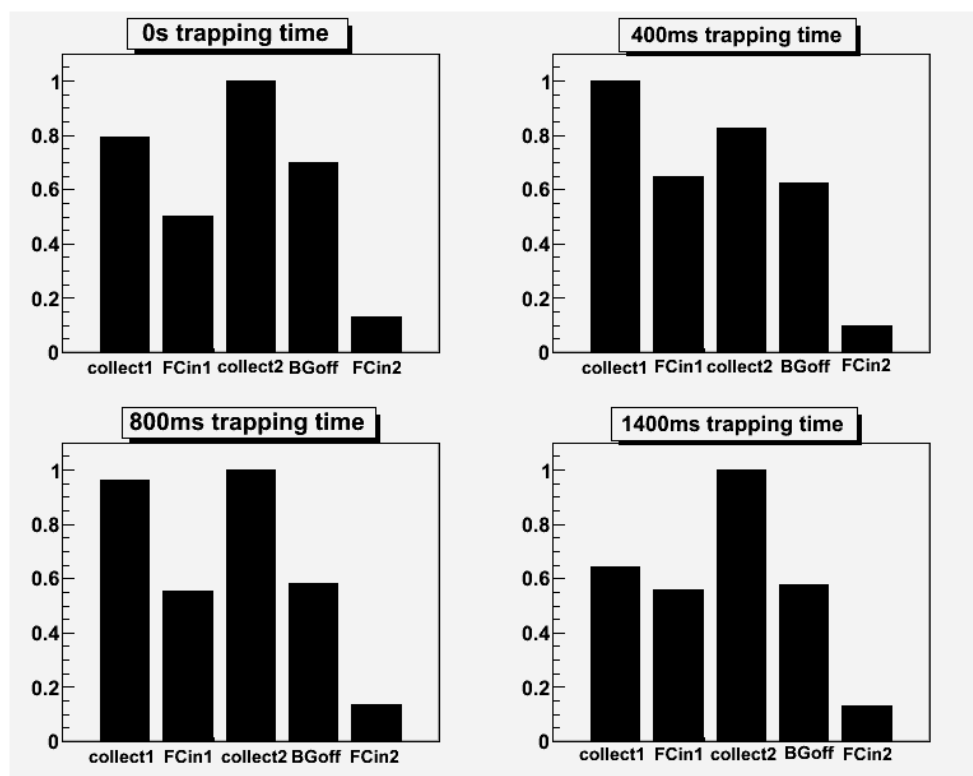


Figure 2.18: ^{61}Fe activity as a function of the trapping time. ^{61}Fe relative activities are given for each measurement period on the horizontal axis, and corrected for the decay between each file. The vertical axis give arbitrary units. One notes that **collect2** does not collect more activity than **collect1** for a 400 ms trapping time.

A second method is to sum measurements for each proton pulse signal every 16.8 s (Figure 2.19) in order to suppress in each the decay background generated by the previous collection. However, high statistical fluctuations do not allow a good estimation of the low fraction of ^{61}Fe collected from the ECR plasma, and of the fraction of ^{61}Fe from the decay of implanted ^{61}Mn on the sides of the tape. Therefore, a simple fit of the ^{61}Fe decay during **BGoff** and **FCin** is used to compare both initial activities at $t_{\text{start}(\text{BGoff})}$:

$$(3) A_{Fe} \sim A_{\text{BGoff}}(t_{\text{start}(\text{BGoff})}) - A_{\text{FCin2}}(t_{\text{start}(\text{BGoff})}).$$

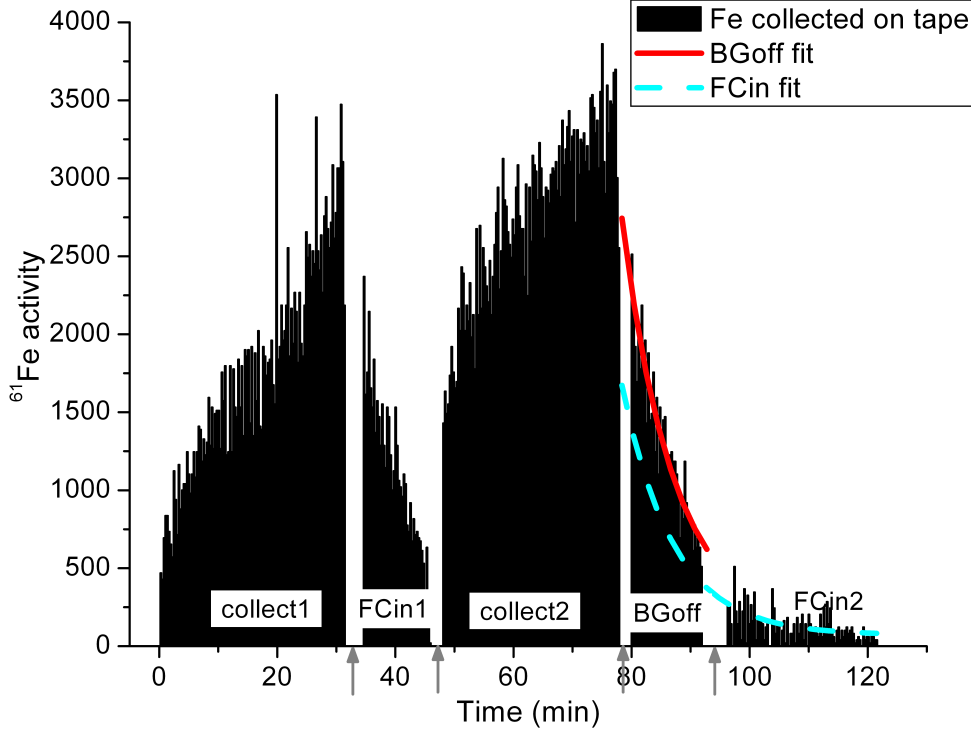


Figure 2.19: ^{61}Fe activity as a function of time for a 1400 ms trapping time. The ^{61}Fe decay is independently fitted for **BGoff** and **FCin2** in order to determine which fraction of the initial ^{61}Fe activity at the beginning of the **BGoff** measurement might be released by the ECR plasma. Delays between measurements are taken into account in the time reconstitution (gray arrows).

Efficiencies as a function of the trapping time

One fits the beta-gated gamma spectra (subsection A.2.2) to calculate the charge breeding efficiencies for ^{61}Mn . Charge breeding efficiencies for ^{61}Fe are calculated from (3). Figure 2.20 shows the results as a function of the trapping time. The higher efficiency for $^{61}\text{Mn}^{14+}$ could indicate that measurements were not performed on the maximum of the charge state distribution. One notes that charge bred $^{61}\text{Mn}^{12+}$ efficiencies increase even with trapping times greater than $T_{1/2}$, showing that the configuration of the ECR Ion Trap (ECRIT) mode was not optimal. No deflection system was used to prevent the implantation of beam released during the trapping time. Therefore, the increase of the ^{61}Mn charge breeding efficiencies are due to the longer time of the applied RF and thus less perturbation of the plasma as for the continuous mode. The values of the efficiencies are also closer to what can be achieved in continuous mode (Figure 2.4). As almost no ^{61}Fe seems to be released for charge breeding times lower than 1400 ms, one cannot conclude whether ^{61}Fe comes from the long-term trapping of decaying ^{61}Mn in the ECR plasma, or from some recycling effect from the plasma chamber walls. Considering the time scale, the ^{61}Fe signal probably corresponds to recycling from the plasma chamber walls.

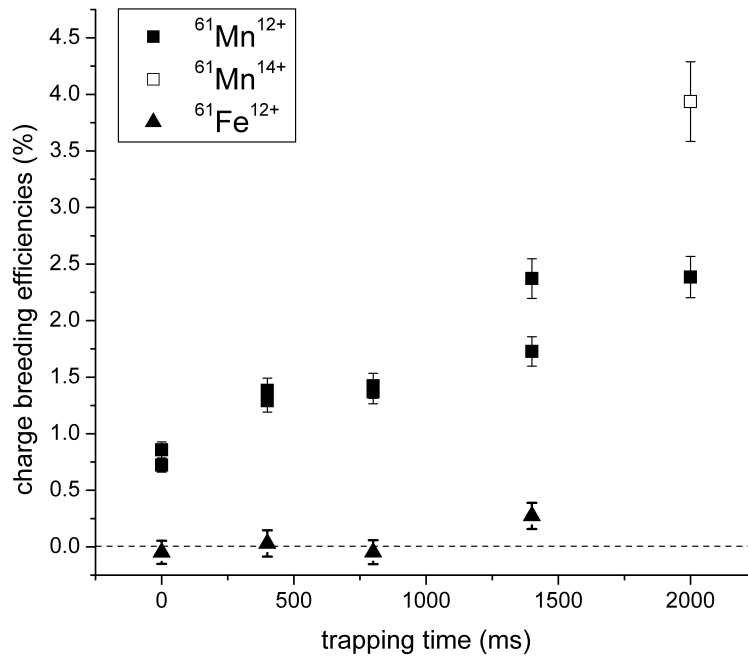


Figure 2.20: ^{61}Mn and ^{61}Fe charge breeding efficiencies as a function of the trapping time. No $^{61}\text{Fe}^{12+}$ is released for trapping times of 0 s and 800 ms. Error bars include errors on the ^{61}Mn yield, on the detection efficiencies and from the fit of the beta-gated gamma spectra.

2.3 Summary of the performance study tests

Measurements performed with stable isotopes in continuous mode reveal a great reproducibility of the optimal plasma capture conditions for a given target and 1^+ ionizer couple (Figure 2.2), but with a dependence on the mass of the charge bred isotope and of the ECR plasma settings. The workable ΔV range seems correlated to the shape of the plasma, and can be widened according to the size of the ECR zone. A minimum capture efficiency of 10% is achievable for all chemical species, and more than 30% for noble gases getting recycled from the plasma chamber walls (Figure 2.3). Charge state distributions were shown to be quite reproducible as well for given settings of the magnetic field, with an optimal charge breeding efficiency for masses over 40 of about 3% for condensable elements in the range $7 < A/q < 9$ and of about 9% for noble gases in the range $4 < A/q < 7$ (Figure 2.4). Up to half of these efficiencies could be reached in pulsed mode (Figure 2.6).

Experiments with radioactive ions have shown how important the blind tuning of the ions injection with stable isotopes is: the reproducible charge state distributions of noble gases of various Z allowed to suppress a fraction of the radioactive beam contamination (subsection 2.2.1), and the ΔV curve shapes measured with radioactive ions are similar to the ones measured with stable ions for the same 1^+ ion source (subsection 2.2.2). Measurements of the ΔV values for ^{142}Cs and ^{142}Xe did not confirm that the plasma capture only depends on the isotope mass for a given 1^+ source. More tests are needed to check whether the optimal ΔV value can be predicted out of existing curves for stable isotopes of the same chemical type. The afterglow blind tuning is not as positive either: although properly conditioned with stable Kr and U (Figure 1.13, Figure 2.5), measurements with radioactive ^{61}Mn revealed bad trapping conditions (subsection 2.2.3). A systematic comparison of the injection conditions should be performed with stable and radioactive ions having the same chemical properties.

Charge breeding of RIBs provided some more information about the plasma capture process. In the case of hot plasma ion sources, one can expect that condensable elements with a high surface ionization efficiency get extracted with a different beam energy, as confirmed in recent tests by [116]. Provided that one optimizes the beam on the right peak, this can be advantageously used to suppress isobaric contamination.

The tentative trapping of daughter nuclides in the ECR plasma did not give conclusive results (2.2.3): the global fraction of captured ^{61}Mn remains unknown and the charge bred ^{61}Fe cannot be clearly dissociated from the ^{61}Fe background on the sides of the tape with such low efficiencies. The trapping of decaying $^{61-62}\text{Mn}$ inside REXTRAP was tested in June 2008 to estimate the fraction of trapped and charge bred $^{61-62}\text{Fe}$ in the beam, prior to Coulomb excitation study on the MINIBALL setup [117]. Whereas the trapping conditions in REXTRAP need some further investigation, it was observed that ^{61}Fe could be successfully produced by keeping the ^{61}Mn for long times in the REXEBIS, where a higher magnetic confinement is achieved [118, 119].

Résumé du chapitre 2: Expériences d'élévation de l'état de charge

Les tests de performance de la source PHOENIX sont effectués avec des faisceaux d'ions stables (ou considérés comme stables en raison de leur longue durée de vie) et des faisceaux d'ions radioactifs.

Les mesures réalisées avec des faisceaux d'ions stables servent à évaluer le pourcentage de transmission du faisceau à travers les lignes d'ISOLDE, depuis le séparateur GPS jusqu'à l'entrée de la source PHOENIX. On vérifie également les conditions d'injection et de capture du faisceau 1^+ par le plasma ECR, en mode continu ou pulsé, à l'aide de la méthode de variation du ΔV décrite dans le chapitre précédent. On a déjà observé que les conditions de capture variaient selon le type de source 1^+ utilisée et l'espèce chimique de l'ion injecté, mais également selon sa masse. Les mesures de ΔV des isotopes ^{39}K , ^{40}Ar , ^{134}Xe , ^{208}Bi et ^{238}U avec la source ECR en mode continu ont confirmé ces observations (Figure 2.2):

- Les éléments condensables sont capturés par le plasma sur la plage étroite du $\Delta\Phi$, environ 25 V à la largeur à mi-hauteur du pic.
- Les gaz nobles sont recyclés des parois froides de la chambre plasma, ce qui étend la plage de capture à environ 300 V.

Bien que les mesures soient réalisées avec la même source 1^+ , les courbes des isotopes de même catégorie chimique diffèrent légèrement. Ceci peut être dû à des variations de l'ionisation dans la source 1^+ , du réglage du plasma ECR, ou des masses des isotopes. Afin d'éliminer les effets liés à la masse, des tests furent effectués avec des faisceaux radioactifs et l'injection de cocktails d'isobares (subsection 2.2.2). Concernant les efficacités de capture, un minimum de 10% du faisceau incident est injecté et capturé par le plasma quel que soit l'élément, et plus de 30% du faisceau peut être capturé dans le cas de gaz nobles. On obtient une distribution d'état de

charge de ^{238}U proche de celle du ^{208}Bi avec 2.4% de $^{238}\text{U}^{28+}$. En revanche, les valeurs obtenues pour ^{40}Ar , avec 15.9% de $^{40}\text{Ar}^{9+}$, sont bien plus élevées que celles publiées dans [78, 19, 29], et éventuellement à confirmer par d'autres mesures. En mode pulsé, on rapporte seulement les distributions d'état de charge mesurées dans [29].

Les mesures réalisées avec des faisceaux d'ions radioactifs avaient pour but d'estimer:

- l'effet de l'ensemble (A, Z) sur la forme de la distribution d'état de charge pour des gaz nobles
- la conséquence des propriétés chimiques sur le processus de capture ECR pour des isobares
- l'efficacité de piégeage dans le plasma ECR des produits de décroissance radioactive

L'expérience rapportée dans [19] utilise la différence des distributions en état de charge de l'argon, et de ses contaminants krypton et xénon produits en grande quantité pour favoriser la proportion de l'argon sur le reste. En sélectionnant $^{48}\text{Ar}^{9+}$ avec le dipôle magnétique, le rapport de ^{48}Ar avec ses contaminants ^{96}Kr et ^{144}Xe devient favorable à l'observation des raies de décroissance de ^{48}Ar présentant un intérêt en astrophysique.

Les deux expériences suivantes furent réalisées pendant le travail de thèse.

Le processus de capture pour des isobares fut étudié avec les isotopes ^{142}Xe et ^{142}Cs produits à partir d'une cible de carbure d'uranium couplée avec une source plasma à tube de transfert chauffé. Les mesures de ΔV confirment les résultats obtenus en faisceau stable avec des espèces condensables ou des gaz nobles, et ont révélé la coexistence de deux faisceaux d'énergies différentes: un potentiel de 120 V au-dessus de la tension de l'ensemble cible-source d'ISOLDE correspond au faisceau issu de la source plasma, tandis qu'un potentiel de 55 V correspond à une ionisation de surface sur les parois de la source plasma. ^{142}Xe était principalement produit par ionisation plasma, et ^{142}Cs par ionisation de surface. L'existence d'un second pic de ^{142}Cs à -120 V par ionisation plasma n'est pas confirmée. La distribution d'état de charge était centrée sur le 24^+ pour les deux espèces. La quantité exacte de ^{142}Xe produit n'étant pas connue, aucun ordre de grandeur des efficacités de ^{142}Xe et ^{142}Cs n'est donné.

L'efficacité de piégeage du ^{61}Mn et de son produit de décroissance ^{61}Fe dans le plasma ECR fut testée avec le mode pulsé. Les isotopes de ^{61}Mn furent produits avec une cible de carbure d'uranium, ionisés par RILIS [107], et injectés pendant 880 ms dans la source configurée pour le piégeage. Le temps de piégeage fut varié autour du temps de vie de ^{61}Mn . Pour des temps supérieurs à $T_{1/2}$, ^{61}Fe est produit dans le plasma ECR, élevé à l'état de charge 12^+ et sélectionné par l'aimant dipolaire. τ_{cb} est estimé à 500 ms (± 50 ms) à partir de la courbe de décroissance de $^{61}\text{Mn}^{12+}$. Pour estimer la part de $^{61}\text{Fe}^{12+}$ provenant de l'ECR, il est nécessaire de supprimer le bruit de fond créé par le ^{61}Fe implanté sur les côtés de la bande. On compare l'activité initiale de $^{61}\text{Fe}^{12+}$ lorsqu'aucun faisceau de ^{61}Mn n'est injecté avec l'activité initiale

mesurée lorsque FC3 est insérée. Il n'y a que pour un temps de piégeage de 1400 ms qu'on a une contribution de $^{61}\text{Fe}^{12+}$ provenant de l'ECR. Le pic afterglow n'est pas visible sur les courbes de décroissance, et les efficacités de $^{61}\text{Mn}^{12+}$ augmentent avec des temps de piégeage supérieurs à $T_{1/2}$ (Figure 2.20), ce qui montre que le mode de piégeage n'était pas correctement configuré. Il est probable qu'une partie du $^{61}\text{Fe}^{12+}$ mesuré provienne plutôt d'un effet de recyclage des murs de la chambre plasma.

Les résultats des tests de performances du PHOENIX Booster avec des faisceaux stables ont montré la grande reproductibilité des conditions de capture plasma pour un ensemble cible-source donné, et des efficacités de capture et d'élévation de l'état de charge selon la nature chimique de l'isotope. Ces réglages avec des isotopes stables permettent de se faire une idée du comportement du faisceau radioactif dans l'élévateur d'état de charge. La prédiction précise des conditions optimales de capture et d'ionisation doit encore être testée avec des isotopes de même nature chimique. Dans le cas des isotopes efficacement produits par ionisation de surface, on peut éventuellement extraire d'une source plasma à ligne de transfert chauffée un même faisceau à deux énergies différentes (l'énergie d'ionisation dans le plasma et l'énergie d'ionisation de surface). Cela peut compliquer les réglages, ou bien se révéler avantageux: on peut choisir de capturer dans le plasma ECR l'une ou l'autre des espèces en présence et supprimer ainsi une partie de la contamination isobarique. La méthode de réglage de la capture avec des faisceaux stables n'est pas aussi concluante en mode pulsé. Malgré des conditions de piégeage correct avec des faisceaux stables de Kr et U, on ne parvient pas à piéger ^{61}Mn . En raison des faibles efficacités mesurées pour le ^{61}Fe , il est difficile d'estimer la part des effets de recyclage.

Chapter 3

Proposals to improve the PHOENIX ECR Booster

Due to its location or to its design, a number of technical limitations were identified on the ECR charge breeder test bench, that could prevent an objective comparison with the other existing charge breeding techniques. They are listed in section 3.1, and a non-exhaustive list of suggestions is given section 3.2 to improve the device. Finally, one presents a few projects of technical upgrade that were initiated during the PhD work.

3.1 Limitations of the current setup

3.1.1 Stable background

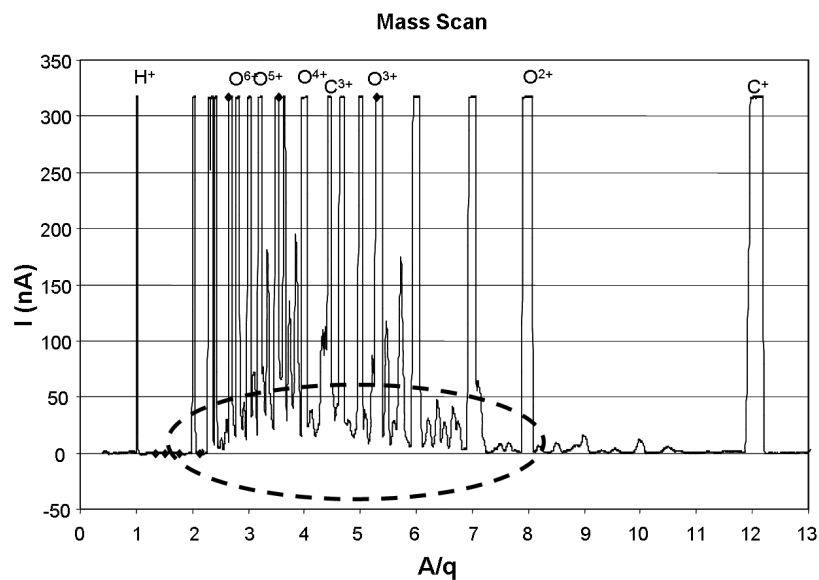


Figure 3.1: Zoom on the stable background (area circled by a dotted line) extracted from the ECRIS with a mass spectrum.

Due to charge exchanges in the extraction region with residual gas, the extracted beam shows an energy spread of a few eV per charge typically [51]. Therefore, the mass analyzer is not able to suppress sidebands of very abundant elements. Stable elements such as carbon, nitrogen and oxygen are naturally released from the beamline elements, and constitute a constant level orders of magnitude higher than radioactive current between the charge state peaks (see Figure 3.1), making difficult the identification and observation of the charge bred distribution for low intensity beams.

A first solution would be to improve the vacuum in the beamline in order to reduce the interacting residual gas. This can be achieved by the use of low-outgassing material for the beamline elements [69] and by increasing the pumping capacity in the extraction region. Such modifications were started during the thesis, as given later in subsection 3.3.2.

A second solution, which was successfully applied at TRIUMF (Vancouver, Canada) [25], would be to add energy selection to the mass separation of the extracted beam. The design for this new development was started during the thesis, and is detailed later in subsection 3.3.3 and Appendix B.

3.1.2 X-ray shielding

As explained in 1.2.3 and Figure 1.6, energetic electrons are lost within a certain cone both at the injection and extraction sides. Therefore, without the appropriate lead shielding, the detectors see a high count rate coming from the X-rays (see Figure 1.15). A non-negligible fraction of this X-ray background is also due to the brehmsstrahlung coming from the bending of the beam in the mass analyzer. Before each run, lead shielding was positioned around the detectors, around the hot points at the extraction and at the mass analyzer to reduce the X-ray background as much as possible (see Figure 3.2). Improvements were monitored with the DAQ system (see Figure 3.3).

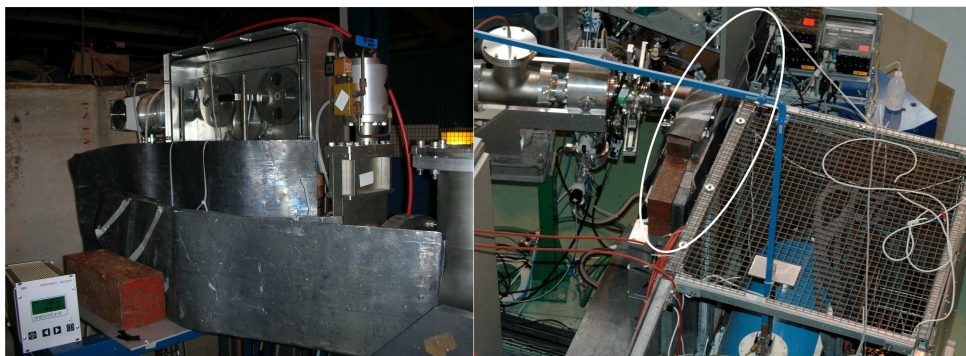


Figure 3.2: Pictures of the X-ray shielding.

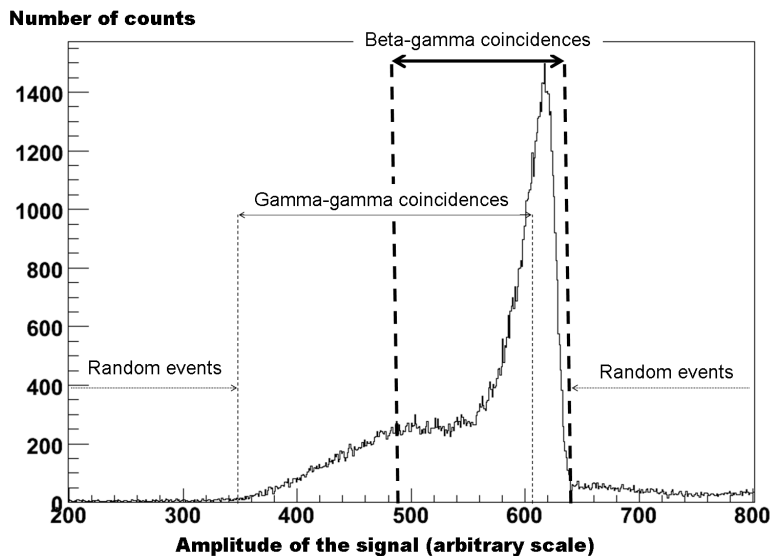


Figure 3.3: Example of TAC spectrum taken from [101]. In spite of the lead shielding, a non-negligible fraction of the counts comes from gamma-gamma coincidences with the high X-ray count rate.

3.1.3 Radioactive background

The internal background could be arising from two main sources, which should be quantified through data analysis.

The first one corresponds to neutral gases of radioactive elements that can diffuse out of GPS target through the beamlines and up to the ECR charge breeder. Such a background should be estimated from the gamma lines. Although it was reported in [19], it was never observed for these measurements.

The second source of background is the fraction of charge bred ions, especially isobars not separated by GPS, which are implanted on the sides of the aluminized tape and possibly have long-lived daughters. The part of this background can be calculated from the **FCin** measurements.

3.1.4 Light ion injection

Previous measurements have shown some problems concerning the injection and capture of a light ion beam by the ECR plasma. It is believed that the ΔV tuning is much more sensitive for light ions. One possible reason is a mismatch between the light ion velocity distribution when they are stopped, and the velocity distribution of the ions of the plasma. Therefore, light ions either fly through, or are reflected back by the plasma. Suggestions are that the grounded tube position should be varied inside the plasma sheath [23], or that a specific drift tube needs to

be designed for lighter ions, with eventually various segments allowing to better control the 1^+ ion beam deceleration [88, 92, 120]. A decision was taken not to address the challenge of the light ion injection during the limited time of the thesis, due to the required modifications on the deceleration tube.

3.2 Improvements needed for an objective comparison with the EBIS devices

The PHOENIX Booster was initially proposed as an alternative to the REXEBIS to feed the LINAC [91]. Pulses with FWHM less than 10 ms are needed, with a 10% duty factor. Such short pulses are achievable within the afterglow mode, however the trapping configuration did not prove to be optimal at 14 GHz (subsection 2.2.3). Moreover the A/q range reached with the PHOENIX Booster is still a little too high compared to the $A/q < 4.5$ required for the LINAC injector part [121].

Some more studies would be needed to test the reliability of the pulsed mode with the ECR charge breeder over long times. Going to higher RF frequencies might improve the afterglow effect [122], or even allow to use the so-called “preglow” mode [85]. Some more improvements needed to get the best out of the current charge breeder capabilities are reminded in this section. Most of them were proposed in [93], and as a letter of intent for “Ultra Pure and High Intensity Multiply Charged Radioactive Ion Beams” within the 7th european framework program (2007-2013) [123].

3.2.1 Capture efficiency

One could see how the plasma capture depends on the chemical properties of the injected element, and its capability of being recycled into the plasma. An idea of using a plasma chamber with hot walls to prevent lost condensable ions from sticking and recycle them into the plasma was proposed by [31]. Although such a system could ease the ΔV tuning and eventually widen the narrow capture range for condensable elements, no technical solution was designed up to now.

Moreover the current design of the ECR charge breeder is not optimized for the injection, and especially for the capture of light ions by the plasma. Previous measurements [74, 75, 95] have shown that the plasma capture is strongly correlated to the energy spread of the injected beam, and increases as the beam quality is improved. Therefore, the use of a cooled beam, for example from a RadioFrequency Quadrupole (RFQ), could improve the capture efficiency [93]. Moreover, the low transverse emittance of a cooled beam could ease the steering.

3.2.2 High charge states

The charge breeding performances are linked to the plasma performances, i.e. the electron density, the fraction of absorbed RF, and the recombination rate. In order to increase the electron density, a plasma chamber in aluminum [124, 64] or wall coating [80] can be used to favour

secondary electrons emission. A smaller injection hole would also increase the plasma density by lowering the backstream losses [82].

3.2.3 Quality of the extracted beam

The extracted beam should have a low emittance and a low background current. To lower the emittance, an optimized extraction system for handling large currents should be designed, probably by adding electrostatic lenses to focus the beam, as in TRIUMF [92]. However, the quality of vacuum is poor in an ECR charge breeder compared to the one in an EBIS, and induced charge recombinations also contribute to the high emittance of the ECR charge bred beam. Examples of solutions could be the use of non-outgasing material for the beamline, the cleaning of the plasma chamber and electrode by sand blaster, high pressure purified water or ultrasounds [82], or the coating of the plasma chamber with a getter material [78].

3.2.4 Operation and maintenance

During this work, one could observe how essential it is that the ECR charge breeder runs without interruption in order to obtain stable plasma working modes. Indeed, the RF absorption varies with the magnetic field tuning or the buffer gas pressure, and charge breeding performances could evolve accordingly during the first hours of setting up.

Moreover, for each new TIS unit, the many parameters of the ECR charge breeder should be tuned. For each setting, one should compensate for the hysteresis of the analysis magnetic field (B field) by systematically checking the position of the nearest stable background peak. The development of a control system with automatic procedures of tuning would ease the operation. Another solution could be to introduce a hall probe in the analysis magnet to get permanently proper values of the B field.

Another constraint of the actual setup is the high dose of X-rays induced close to the device, preventing from any intervention in the area when the charge breeder is running. As mentioned above, one should avoid switching off the ECR plasma, and therefore an efficient X-ray shielding should be installed. [125] proposed to shield the X-ray flux with a 2 mm Ta coating on the plasma chamber, but results were not conclusive so far [83].

3.3 Projects for the technical upgrade of the PHOENIX ECR Booster

3.3.1 60kV upgrade

As mentioned previously (subsection 1.3.1), the ISOLDE facility operates with a maximum acceleration voltage of 60 kV. In order to be able to operate at such a voltage, and thus benefit from more beams in parasitic mode, the ECR high voltage components were upgraded at the beginning of the PhD work [126].

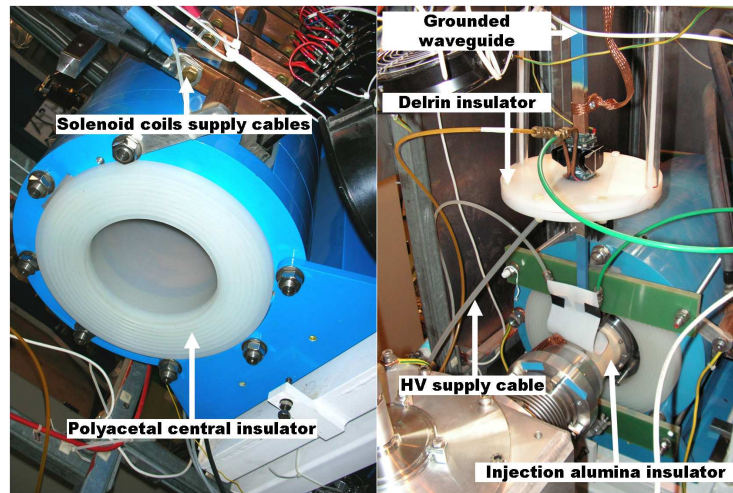


Figure 3.4: Pictures of the 60 kV upgrade.

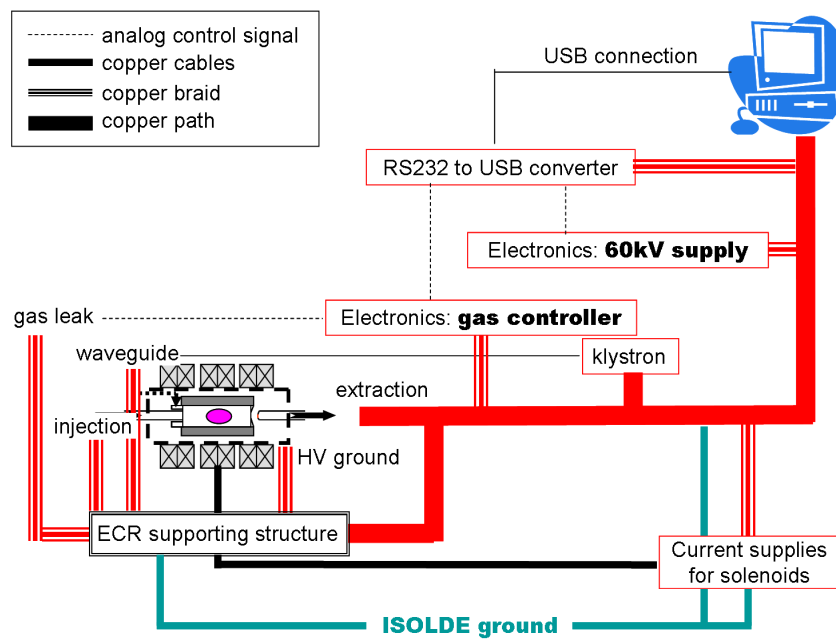


Figure 3.5: Scheme of the 60 kV platform grounding.

The former 30 kV FUG high voltage supply was replaced by the HCP-1400-65000 model from FUG, providing up to 65 kV and 20 mA, and was connected to the LabView control system and to the interlock safety system. Thicker central and extraction insulators were installed, respectively in polyacetal and permaglass materials. The injection and extraction alumina insulators were replaced for longer ones (Figure 3.4), and injection and extraction tubes lengths were adapted accordingly. All electronical devices, as well as the injection and extraction grounded beamlines, were connected to the 60kV ground (and to ISOLDE ground) through a copper path (Figure 3.5).

The commissioning of the 60 kV operation was slowed down by the existence of a Penning effect on the injection and extraction sides of the ECRIS. Energetic electrons escaping from the plasma through the loss cones (Figure 1.6) are accumulating on the injection and extraction tubes, creating a local negative potential that discharges through the grounded parts after a while. Induced sparkings cause instabilities in the plasma, and if frequently repeated, they affect fragile electronical devices.

Solutions to reduce the Penning effect should be investigated. For instance, the inox injection and extraction tubes could be replaced by carbon tubes (Figure 3.6) in order to avoid discharges. However, the charge state distribution is expected to tend towards lower charges because of charge recombinations with carbon. One could also add some capacitance to the grounding circuit to limit the damages of discharge currents on sensitive electronics.



Figure 3.6: Carbon extraction tube.

3.3.2 Towards a UHV charge breeder

Tests at LPSC Grenoble show a drastic reduction of the oxygen contamination by running their ECR charge breeder for one year without venting [31]. Evolving towards a UHV ECR charge breeder could solve most of the stable beam contamination problems. Tentatives to diminish the stable background current by improving the pumping system were tested.

Improving vacuum at the injection

Although the plasma ignition induces a strong pumping effect [70] in the beamline, the vacuum on the injection side remained quite high due to the bad quality of the GHM beamline vacuum, i.e. a few 10^6 mbars, thus favouring Penning discharges at the injection. A conductance tube (Figure 3.7) was designed and inserted between FC1 and FC2 (Figure 1.10) to improve differential pumping. The DN100 flange ensured that the tube was centered in the beamline. The pressure on the injection side could effectively be reduced to a few 10^7 mbars when connected to ISOLDE GHM beamline. No decrease of the transmission between FC1 and FC2, or for the tuning between GPS and FC1/FC2, was observed.

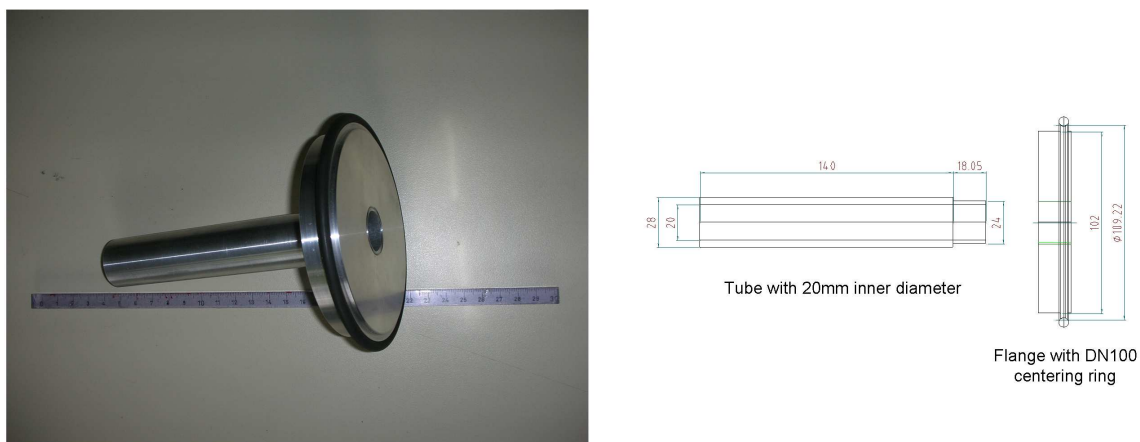


Figure 3.7: Scheme of the conductance for vacuum improvement on the injection side.

Pumping capacity

At the end of this work, the total pumping capacity was increased from 400 L/s to 1000 L/s on the injection side, from 540 L/s to 900 L/s on the extraction side before mass separation, and from 540 L/s to 640 L/s close to FC3. This resulted in a vacuum improvement of a few 10^7 mbars.

A notable 50% reduction of the total extracted current could be observed due to a higher pumping rate of the buffer gas at the injection, but microamperes of stable C and N contamination could still be found in the mass spectrum Figure 3.9. Tests performed with getter material at KEK [78] also showed more impressive results to remove stable contamination than the improvement of the pumping capacity.

During the last experiment presented in subsection 4.2.2, one could observe that the plasma was stable with these new conditions, and that charge breeding efficiencies remained comparable to the ones prior to the vacuum improvement.

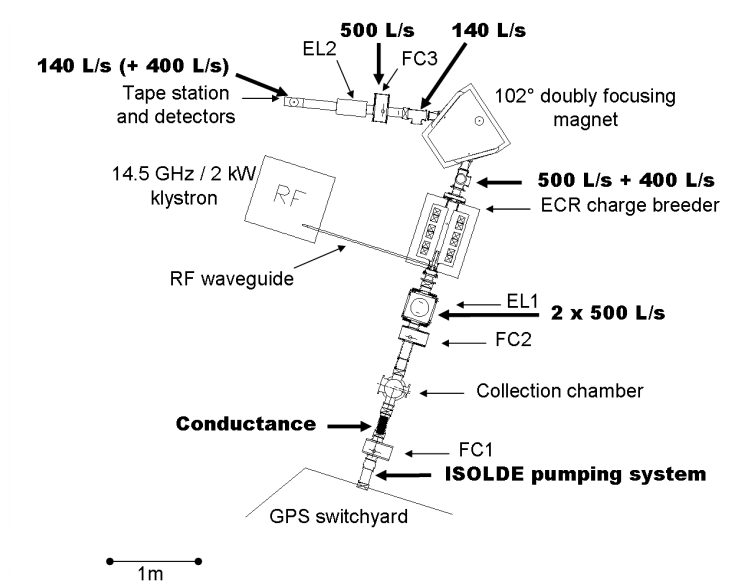


Figure 3.8: Pumping system on the test bench.

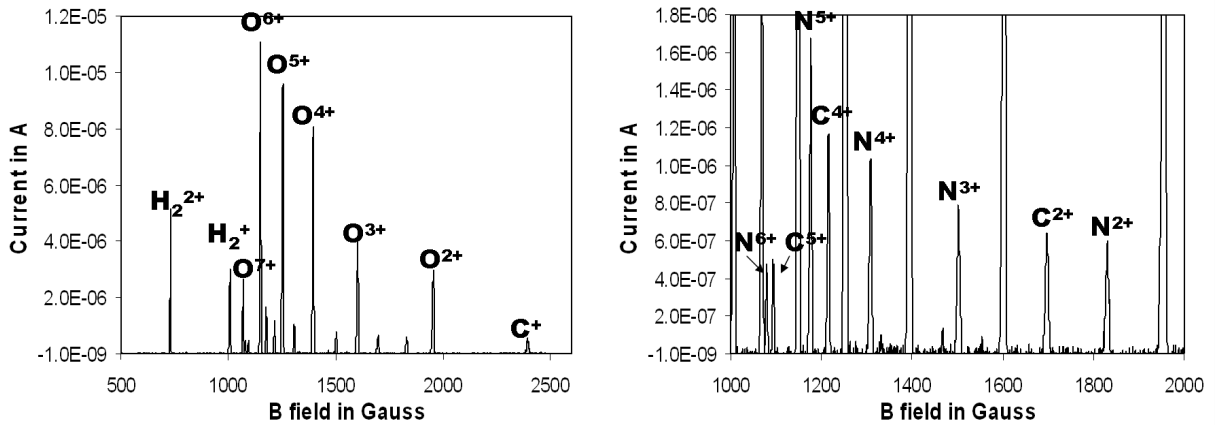


Figure 3.9: Mass spectra with reduced extracted current. $10 \mu\text{A}$ of O, $1.5 \mu\text{A}$ of N, $1.3 \mu\text{A}$ of C are extracted.

3.3.3 Project of a new mass and energy separator

Concept

A mass resolving power of $(A/q)/\Delta(A/q)=150$ was reported by [19] for the analysis magnet after the ECR charge breeder, when the extraction hole was 8 mm diameter. Since the 60 kV upgrade, the extraction diameter was raised to 13 mm and the resolving power was reduced to 50, as measured on latest mass spectra for a factor of suppression 20. The selection occurs provided that all ions extracted from the charge breeder have the same energy. However, charge exchanges at the very beginning of the extraction region, between the plasma electrode and the tip of the grounded extraction tube, prevent a uniform acceleration of all ions at the same potential.

From the expression of the magnetic rigidity in a constant magnetic field B_0 , one deduces the trajectory bending radius ρ_B :

$$\rho_B = \sqrt{\frac{2}{e^2 B_0^2}} \sqrt{\frac{A}{q}} \sqrt{\frac{K}{q}}$$

with K being the kinetic energy of the particle of mass A and charge state q , and e the Coulomb charge. For a given $\sqrt{A/q}$ ratio, the bent trajectories are spread according to a $\sqrt{K/q}$ distribution. This results in broader peaks in the spectrum. Thus, for a given $\sqrt{A_1/q_1}$ ratio, the peak flanks may hide another $\sqrt{A_2/q_2}$ peak. Intense peaks of contaminants in the beam might hinder the study of charge breeding efficiency (example Figure 3.10). Therefore mass separation can only be efficient after energy separation.

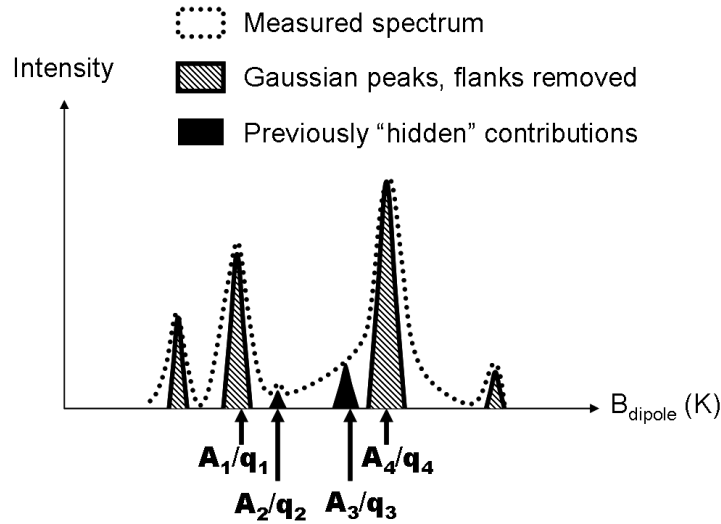


Figure 3.10: Example of energy spread in a mass spectrum. The efficiency for a given A/q cannot be determined with precision, but it can for given $(A/q, K)$ values.

A radially inhomogeneous electrostatic sector field could achieve energy-over-charge separation, i.e. separation according to the acceleration potential, independently from the mass. In the

case of an electrostatic sector composed of toroidal electrodes [127], the optical axis radius ρ_E is:

$$\rho_E = \frac{2}{eE_0} \frac{K}{q}$$

with E_0 the electrostatic field, constant on the circular trajectory.

The design chosen for the new mass and energy separator is similar to the one which was implemented in TRIUMF and showed successful results as on Figure 3.11. First a magnetic sector selects one charge state out of the high current extracted from the ECR, so that less than $1 \mu\text{A}$ of radioactive ion beam is sent through the electrostatic sector, thus reducing the space charge effects [25].

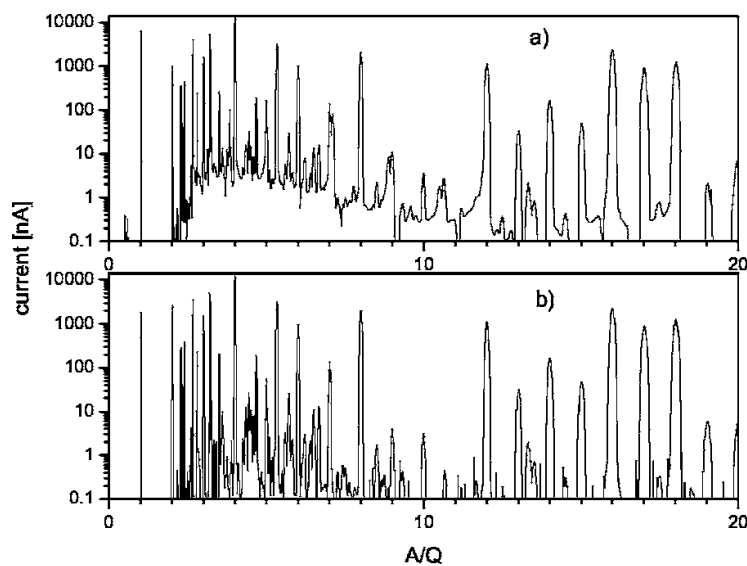


Figure 3.11: *Expected improvements on the A/q spectrum from [25]: “Mass spectra of background ions obtained with a) only magnetic separation and b) with additional electrostatic bender.”*

Beam calculations

The Department of Physics from the University of Lund recently dismantled their Accelerator Mass Spectrometry (AMS) setup on the Pelletron accelerator [128]. Most elements of the injection mass and energy isotopic separator were bought by ISOLDE for use on the ECR charge breeder experiment with radioactive ion beams. Therefore, beam calculations were performed with the geometry specifications of available elements. The separator itself is composed of a doubly focusing 90° dipole with a bending radius of 373.5 mm, a pole gap of 48 mm, and entrance and exit angles of 28.2° , and of a 90° electrostatic bender of radius 435 mm with spherical electrode plates separated by 43.5 mm.

Beam transport was simulated with the COSY INFINITY code dedicated to beam dynamics simulation and analysis [129] with the position of the elements taken as a free parameter. Optimization routines given in Appendix B were used to fit the optimal distances between elements (Figure 3.12). Three constraints had to be taken into account. First, a minimal distance of 900 mm is needed between the extraction electrode tip and the entrance of the magnetic analyzer to keep an efficient pumping capacity in that region. Second, the emittance of the beam extracted from the ECR charge breeder prior to mass separation has not been measured, so the various elements were positioned in the order allowing an acceptance as high as possible. Third, the system was designed as compact as possible due to space restrictions in the hall.

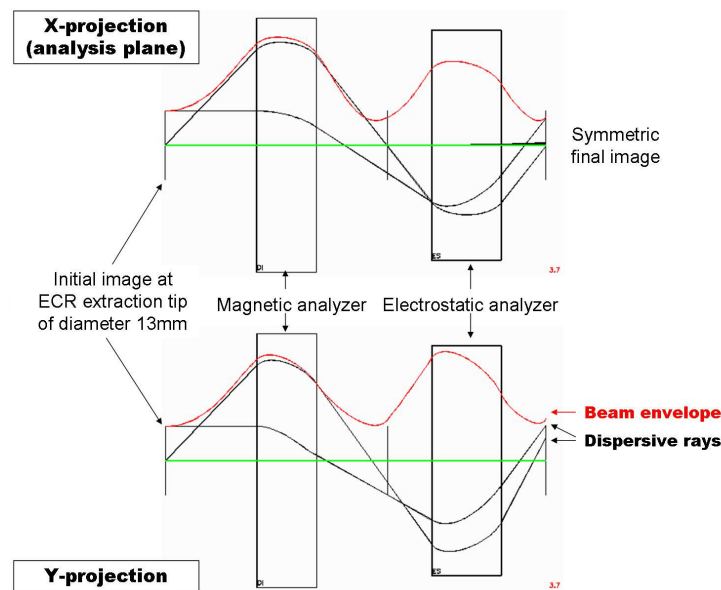


Figure 3.12: Scheme of beam transport through both analyzers projected in the X and Y planes for a maximal divergence of 20 mrad. Special care was taken to achieve symmetrical images at the focal points in the analysis plane X .

The position of the analyzers were optimized as shown on Figure 3.12 to achieve transmission of a beam with up to $130\pi \cdot \text{mm} \cdot \text{mrad}$ geometrical emittance. For comparison, emittances up to $100\pi \cdot \text{mm} \cdot \text{mrad}$ were reported for ECRIS devices [95], but highly charged states should produce a beam closer to $50\pi \cdot \text{mm} \cdot \text{mrad}$ or below (see chapter 1).

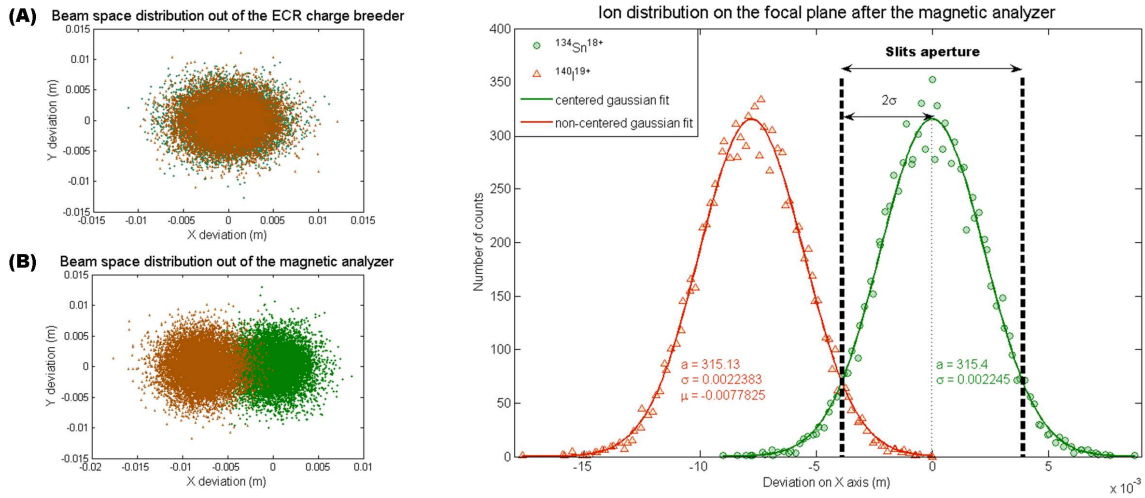


Figure 3.13: Determination of the mass resolving power for a factor of suppression 20: two peaks normally distributed are separated when resolved by $\pm 4\sigma$. Simulations were performed for two beams of 10,000 ions extracted through a 13 mm diameter hole (A) and separated by the mass analyzer (B).

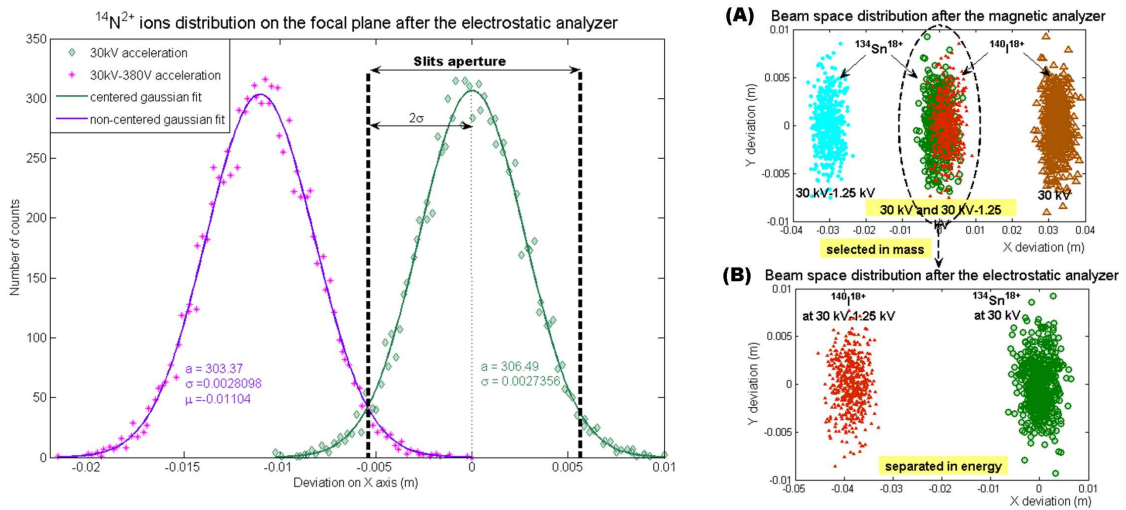


Figure 3.14: Determination of the energy resolving power for a factor of suppression 20 with beams of 10,000 ions extracted through a 13 mm diameter hole. (A) Although the mass analyzer properly separates beams of $^{134}\text{Sn}^{18+}$ and $^{140}\text{I}^{18+}$ at the same potential energy, peaks of $^{134}\text{Sn}^{18+}$ at 30 kV and $^{140}\text{I}^{18+}$ at 28.75 kV are overlapping. (B) The selected overlapping peaks of $^{134}\text{Sn}^{18+}$ at 30 kV and $^{140}\text{I}^{18+}$ at 28.75 kV can be resolved with additional energy separation.

Maps of the transport through each element were calculated up to sixth order including the chromatic effects as a function of the mass A , charge state q , and kinetic energy K parameters of the beam. No detectable modification was observed from third-order onwards. Those third-order matrixes were used in a Matlab program to simulate a cocktail beam of various isotopes undergoing separation in mass and energy, thus giving the resolving power of the system (Figure 3.13 and Figure 3.14). Calculations show that mass resolving power would be improved to $(A/q)/\Delta(A/q)=100$, while an energy resolving power of $(K/q)/\Delta(K/q)=80$ could be achieved. The mass separation would not yet be as good as the one achieved after the REXEBIS ($(A/q)/\Delta(A/q)=150$ according to [130]). The effect of beam divergence on the resolving power is negligible for the range of emittance considered. However, the beam diameter has a much stronger effect. For a thin beam of 2 mm diameter, the theoretical resolving power of the system would be $(A/q)/\Delta(A/q)\approx(K/q)/\Delta(K/q)\approx 370$.

Layout design

The most simple layout is composed of the magnetic bender followed by the electrostatic bender, and by a quadrupole triplet to add some flexibility for an eventual detection setup. Such an installation on the ground floor both in a U or Z-shape would achieve the performances calculated in 3.3.3. However space constraints in the hall would not allow to setup advanced detection equipment afterwards.

Latest considerations to relocate the ECR charge breeder pointed out the possibility of installing the isotopic separator upwards, so that detection equipment could sit on an existing platform close to the first extension wall (Figure 3.15). Such a system would need a longer separator to reach 3 m height, and it would induce a 20° angle between the ECR charge breeder line and the detection system line, around the vertical axis. A five-element layout achieves these specifications, but has a smaller acceptance than before due to the triplets (about $115\pi\cdot\text{mm}\cdot\text{mrad}$).

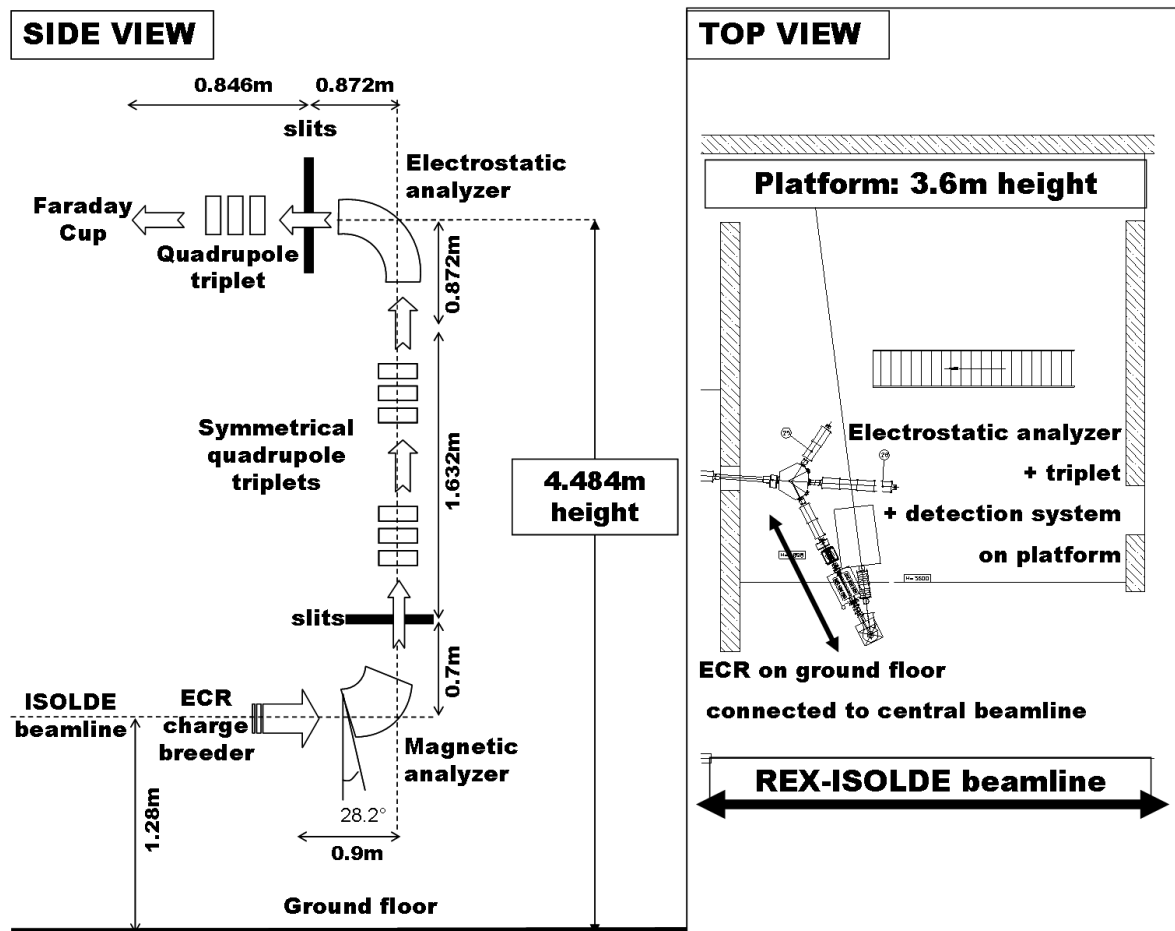


Figure 3.15: Final isotopic separator layout in ISOLDE hall.

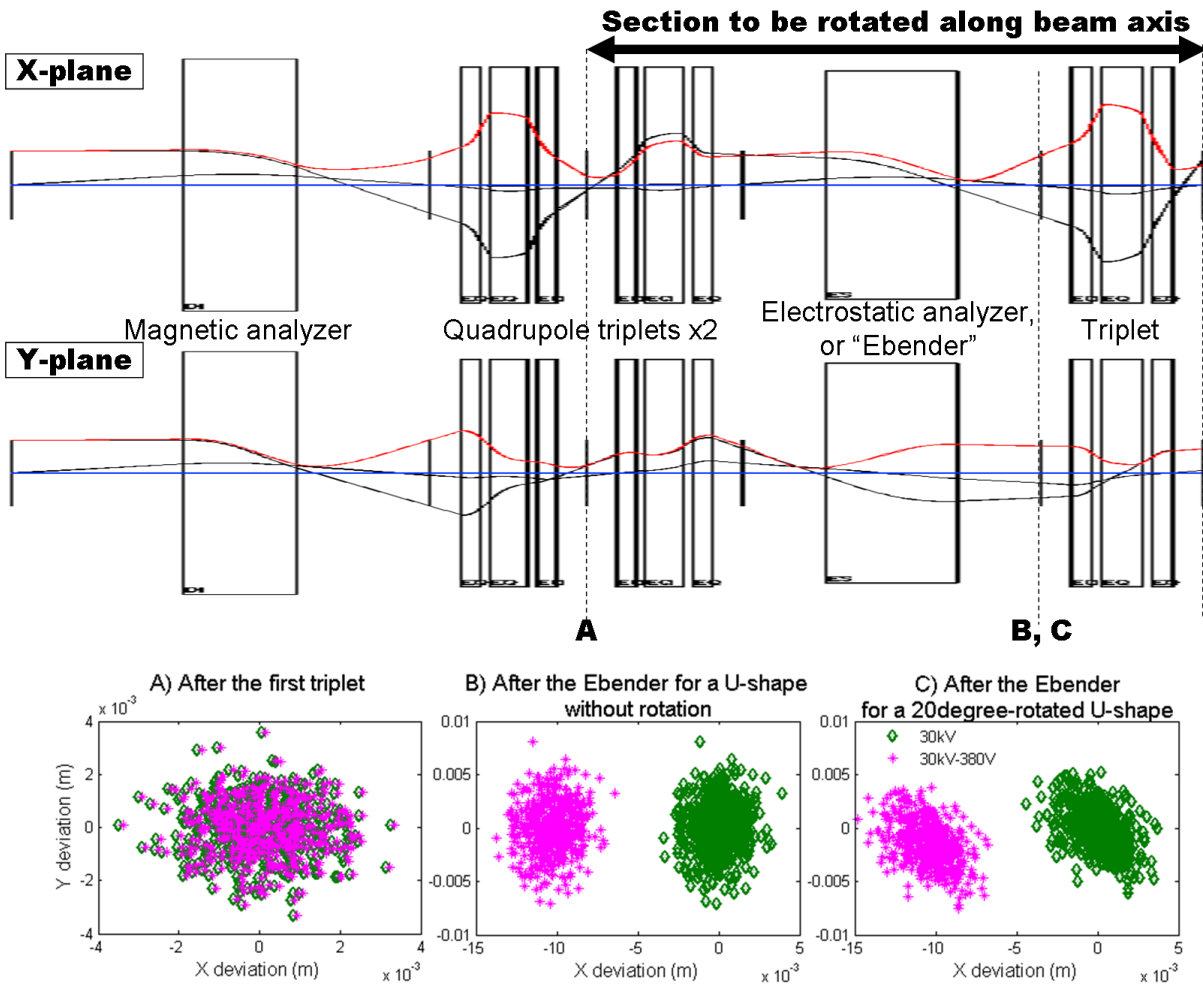


Figure 3.16: *X-Y distribution of the beam on focal planes. For an initial symmetrical beam (A), the energy analyzer is as efficient for the non-rotated layout (B) as for the 20° rotated layout (C).*

Two triplets are added between the magnetic bender and the electrostatic bender, and positioned to achieve a round beam projection in both phase spaces between the triplets (Figure 3.16). In that case, the magnetic bender and the first triplet are completely decoupled from the rest of the beam line, which can be rotated with any angle on the vertical beamline axis. One notes that the triplets focusing in the X-plane decreases the size of a parallel beam, thus slightly improving the energy resolving power. Therefore, the modification of the extraction system as suggested in subsection 3.2.3 could also improve the mass resolving power.

Cost estimate

Table 3.1 details the equipment already available and stored at ISOLDE, and the needed resources to complete the project. The supporting structure as discussed in 3.3.3 should be designed by an engineering department, in order to be validated for installation in the experimental hall. The isotopic separator should also be built and tested offline with an optimal control system. The power supplies for the various elements were already controlled and tested within a summer student project [131] through a Profibus connection to a borrowed computer, with a LabView-based control system (more details in Appendix B). However, dedicated equipment for the control system should be bought and the software finalized. Therefore one estimates the remaining work to about one year in total.

	Equipment detail	Cost (CHF)	Total (CHF)
Available	Sputter ion source $\times 1$	6,000	
	Magnetic and Electrostatic sectors	105,000	
	Triples $\times 2$	8,000	
	Electrostatic steerer $\times 1$	1,000	
	Slits and FCs $\times 2$	6,000	
	Cryogenic pumps, valves and compressors $\times 2$	80,000	
	Power supplies $\times 10$	30,000	
	Manpower for design (6 months PhD project + 1 month summer student project)	27,000	263,000
Remaining	Supporting structure design study	10,000	
	Supporting structure production	20,000	
	Complementary vacuum equipment	20,000	
	Control system (equipment + 1 month work)	10,000	
	Manpower for tests (2 people for 6 months)	50,000	110,000

Table 3.1: Estimated costs for the isotopic separator. An approximative value of the equipment already available and details of the missing elements for construction are given.

Résumé du chapitre 3: Propositions pour améliorer l'élevateur d'état de charge ECR

Lors des tests expérimentaux, plusieurs limitations du dispositif ont pu être constatées. Un courant élevé d'éléments stables provenant à la fois du gaz support et du dégazage des parois, un taux élevé de comptage des rayons X sur les détecteurs, des espèces neutres radioactives diffusant de la zone du séparateur ou une implantation des isotopes radioactifs à côté de la bande de déroulement, sont autant de facteurs qui contribuent au bruit de fond et limitent le nombre d'expériences réalisables. D'autre part, le PHOENIX Booster n'est pas utilisable en l'état actuel pour l'injection de faisceaux radioactifs dans le LINAC de REX-ISOLDE, car il produit des faisceaux sur une gamme A/q trop élevée et un mode afterglow optimal n'a pas pu être reproduit avec des isotopes radioactifs.

Plusieurs développements techniques contribueraient à améliorer les performances du système actuel. Les efficacités de capture bénéficieraient de refroidisseurs RF visant à réduire à la fois l'émittance du faisceau injecté et les pertes sur les parois de la chambre plasma. Des états de charge plus élevés pourraient être produits avec une chambre plasma dans un matériau émetteur d'électrons secondaires, ou avec un système visant à réduire le flux des électrons perdus par le trou d'injection. La qualité du faisceau produit en termes d'émittance et de pureté dépend fortement de la quantité de gaz résiduel dans la zone d'extraction du faisceau. Un meilleur vide est nécessaire, voire des éléments de ligne adaptés à l'ultravide et nettoyés pour réduire le dégazage. Enfin les conditions d'opération et de maintenance du dispositif sont loin d'être optimales pour faire fonctionner le PHOENIX Booster toute l'année. Le système de contrôle doit être doté de fonctions automatiques pour faciliter l'optimisation des nombreux paramètres, et un blindage aux rayons X permanent et compact doit être installé aux points déterminants pour faciliter l'accès à l'aire expérimentale pendant le fonctionnement.

Certains développements techniques ont été démarrés au cours du travail de thèse pour permettre une comparaison objective du banc de test du PHOENIX avec REXE-BIS. D'abord, les composants d'isolation de la plateforme et les alimentations en haute-tension furent échangés pour supporter une opération à 60 kV, la tension d'accélération maximale à ISOLDE. Les tests effectués pour augmenter progressivement la tension de fonctionnement jusqu'à 45 kV furent interrompus afin de planifier les temps de faisceau. Puis en raison de la qualité dégradée du vide du côté de l'injection, entraînant de nombreuses décharges, une conductance fut mise en place pour permettre un pompage différentiel, et l'ensemble du système de pompage de la ligne a été renouvelé. Enfin, la conception d'un nouveau système de séparation en masse et en énergie du faisceau d'ions multichargés fut démarrée.

Le système de séparation en masse et en énergie a pour but de pallier à l'élargissement des pics du spectre de masse dû à la dispersion en énergie du faisceau multichargé. Dans le cas de pics intenses, les isotopes d'intérêt peuvent être noyés dans la contamination. Des éléments provenant du démantèlement de l'injecteur du spectromètre de masse de Lund furent achetés par ISOLDE pour construire ce nouveau séparateur. Les positions des divers éléments disponibles furent établies, basées sur des calculs faisceaux avec les logiciels COSY INFINITY et Matlab. Avec le système d'extraction actuel du PHOENIX Booster, on pourrait atteindre des pouvoirs de résolution en masse $(A/q)/\Delta(A/q)=100$ et en énergie $(E/q)/\Delta(E/q)=80$, et accepter des faisceaux d'émittance élevée (jusqu'à $115\pi \cdot \text{mm} \cdot \text{mrad}$). La construction d'un tel système après le PHOENIX Booster nécessiterait le déplacement du banc de test vers une autre ligne d'ISOLDE disposant de plus d'espace. Le schéma d'installation le plus probable dans la configuration actuelle du hall expérimental est proposé, ainsi qu'une étude prévisionnelle des coûts et délais.

Chapter 4

Perspectives of the $1^+ \rightarrow n^+$ ECR charge breeding

In the following, the results presented in chapter 2 are placed in regards with the other charge breeding techniques. Possible applications of the ECR charge breeder for experiments are illustrated by the presentation of the latest results of an astrophysics experiment.

4.1 Discussion of the results of the performance study

4.1.1 Comparison with other charge breeding techniques

Table 4.1 summarizes the performances of solid stripping foils, of the REXEBIS including its preparation stage, and of the ISOLDE PHOENIX ECR Booster setup at ISOLDE to charge breed radioactive ions. One compares beam acceptance, extracted beam quality, charge breeding times and efficiencies, and constraints due to operation and costs. It should be noted that the REXEBIS is usually operated all year long, whereas the PHOENIX Booster was used for the performance test beamtimes only, i.e. four months per year. Therefore, the ECR charge breeding performances shown here might be improved, for example using the upgraded version of the PHOENIX charge breeder as developed by LPSC Grenoble for the SPIRAL2 project.

4.1.2 Consequences for the type of postaccelerator

Requirements for performant charge breeding in a RIB facility are:

- a maximum η_{m^+} (at least several percent of the injected beam)
- a short τ_{cb} (less than the half-life of the charge bred nuclide)
- adaptability to a wide range of 1^+ beams in terms of mass and quality

in order to provide beam to experiments with sufficient intensity.

Table 4.1 shows that the stripping foil remains by far the best charge breeding technique in terms of beam acceptance, charge breeding performances and quality of the charge bred beam. It is well-suited to charge breeding of pulsed or continuous beams of all isotopes, even very

		Solid stripping foil	REX(EBIS + TRAP)	PHOENIX ECR setup at ISOLDE	(*)Note
Injected beam	Emittance	all*	$<30\pi \cdot \text{mm} \cdot \text{mrad}$ [51]	$<55\pi \cdot \text{mm} \cdot \text{mrad}$ [23]	with adapted beam focusing to avoid damage
	Energy dispersion	all	$<50 \text{ eV}$ [55]	$<25 \text{ eV}$ for condensable, $<300 \text{ eV}$ for noble gases subsection 2.1.1	
	Structure Intensity	all up to $\sim 100 \mu\text{A}$ [51]	pulsed, continuous* $<100\text{pA}$ [132]*	pulsed, continuous up to $\sim 20 \mu\text{A}$ [96]*	with accu-mode (1.2.2) lower limit depends on background level
	Mass $T_{1/2}$	all >Time Of Flight (TOF)	all $>30 \text{ ms}$ [64] *	$A > 20$ [23] $>100 \text{ ms}$ in CW, $>30 \text{ ms}$ with afterglow [29] *	
Extracted beam	Emittance Dispersion Structure	\geq injected beam depends on thickness same as injected beam	$10\text{-}70\pi \cdot \text{mm} \cdot \text{mrad}$ [132] a few q.10eV pulsed	$15\text{-}100\pi \cdot \text{mm} \cdot \text{mrad}$ [23] a few q.10eV convolutes injected beam time structure and RF time structure	
	Optimal A/q Background	tunable with thickness none	>3 and <5 [133] $<0.1\text{pA}$ [132]	>4 and <8 (Figure 2.4) $\sim 10\text{nA}$ (Figure 3.1)	
Charge breeding	CS distribution τ_{cb}	tunable with thickness TOF	narrow $>30 \text{ ms}$ [64]	wide $>100 \text{ ms}$ in CW, $>30 \text{ ms}$ with afterglow	
	η_{n^+}	15% to 25%	5% to 15%	5% to 15% in CW, $<5\%$ with afterglow	
	full stripping	yes*	yes	no	with several stages for heavy ions
Operation	Complexity Maintenance	simple lifetime of the foil (up to 4.5 months reported in [36])	tuning of REXTRAP lifetime of the cathode (~ 3 to 4 months [69])	tuning of ΔV lifetime of the RF window/amplifier ($\sim 1 \text{ year}^*$)	as observed during this work
	Cost (manpower excluded)	Initial	pre-accelerator	1.1M\$ [132]	1M£*
Maintenance		foil replacement (10\$ to 30k\$)	cathode replacement (1k€), superconducting magnets cooling	RF window* replacement	cheap teflon window (0.05€) or standard quartz window (2k€)

Table 4.1: Comparative table of performances.

short-lived, with all intensities, and to feeding of all types of post-accelerator with a clean beam. However, efficiencies might become lower in the case of full-stripping of heavy ions, as many successive stages are needed. This might be compensated using multiple charge state acceleration [50].

The REXEBIS (taking into account its preparation stage REXTRAP) and the PHOENIX ECR show very similar performances concerning the charge breeding efficiencies and the emittance of the extracted beam. For both devices, the charge breeding of very short-lived isotopes is not efficient, and long-lived isotopes should be avoided to prevent contamination of the chamber. The EBIS remains the best way to feed a low duty cycle LINAC with clean beams of high charge state or fully-stripped ions of all masses. As for the PHOENIX ECR, it is more suited to charge breed intense high emittance beams and feed a CW LINAC or a cyclotron with moderate charge states.

For all-year runs in a RIB facility, a charge breeding system should also show:

- a simple operation (with reproducible procedures)
- a safe maintenance
- low running costs

The stripping foil system is convenient for facilities with no space restriction and high investment capabilities, as it requires a pre-accelerator and a RF bunch rotator to condition the beam [51]. However, it later shows the simplest operation and maintenance: the change of a foil was estimated to cause 5 h of downtime only, and 100 μ S of personal dose at TRIUMF [36].

The two-stages of the REXEBIS system make setting up more complex, but theoretically, next-generation EBIS dimensioned as the BNL TestEBIS would not require a preparation stage any more [64]. Interventions are less frequent but more time-consuming to replace the cathode. Instead of the LaB₆ cathode currently on use at REXEBIS [69], an IrCe cathode is foreseen for the TestEBIS, with an estimated lifetime of 20000 h [62].

Finally, the PHOENIX ECR is the most compact and cheapest solution. Reproducible working modes can be identified for tuning and the beam produced is stable over long times. Maintenance interventions are as time-consuming as on the EBIS, but less costly with the use of a cheap teflon RF window for the last years (following the successful example of LINAC3, both at 14.5 GHz and 18 GHz [134]).

4.2 Future for physics experiments

4.2.1 Possibilities for beam purification

In the current status, the PHOENIX Booster can provide high currents of charged bred beams to physics experiments. Some of the possible applications for nuclear physics, astrophysics and solid state physics were reviewed in [135, 136]. Most cases require beams of high purity for implantation or for low-background detection. In RIB facilities, isobaric contamination is a major problem as it might induce long-term contamination of the beamlines and of the high-resolution mass separators, and therefore of the experimental setups.

One technique to suppress noble gas isobaric contamination by ECR charge breeding was already described in subsection 2.2.1. Another possibility is to form molecules of the isotope of interest, thus shifting the mass selected by the mass separator towards a region with lower isobaric contamination. The molecule can be broken by charge breeding and the interesting isotope undergoes an additional mass separation which allows to choose a low-background charge state (Figure 4.1). Such an experiment was performed at Oak Ridge National Laboratory (ORNL) using a stripping cell to break the molecule [20] prior to mass selection and charge breeding the isotope of interest with a stripping foil. The advantage of using ECR charge breeding in such a process is to charge breed both the isotope of interest and the molecular sideband, thus minimizing the losses due to molecular sidebands keeping the charge after breakup. Molecular injection into the ECR charge breeder was already demonstrated with the charge breeding of ^{123}LaO , and no drop in the charge breeding efficiency of ^{123}La was observed compared to the results with the injection of atomic La beam [93]. Therefore, an experiment was proposed during the PhD work to demonstrate this method of purification using molecular beams [137, 138] (proposal attached in Appendix C), and is detailed in the following section.

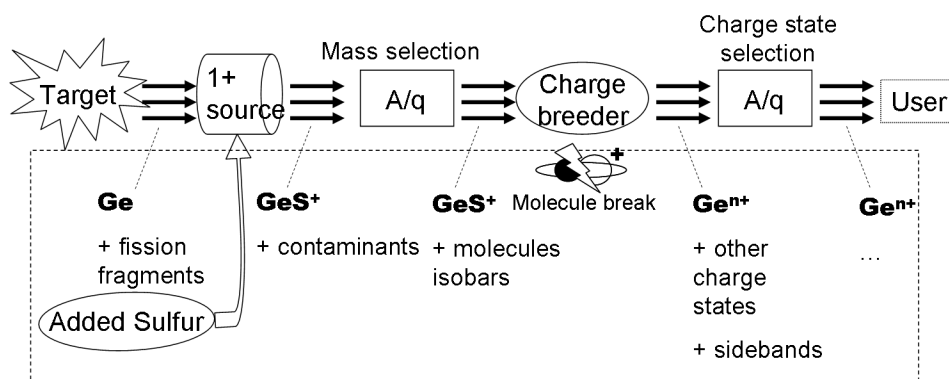


Figure 4.1: Principle of the molecular beam technique.

4.2.2 Application to a case in nuclear astrophysics

Physics case

At ISOLDE, neutron-rich isotopes in the intermediate mass range ($A=80$ to 150) can be produced with high yields by fission of an actinide target associated to a chemically non-selective plasma ion source. Thus, the whole isobaric chain is ionized, resulting sometimes in a high background of many different fission products that are extracted and mass-separated. As mentioned before, the question of isobaric contamination is crucial for the proper measurement of nuclear structure properties [139]. Although the RILIS can now be used for selective ionization of many metallic elements, many non-metallic and some metallic elements can be better separated in molecular form with a plasma ion source.

Approximately half of the heaviest isotopes in nature, beyond iron, are produced via neutron captures on very short time scales in neutron-rich environments, i.e. the so-called r-process. The beta decay properties of most neutron-rich isotopes close to the r-process path between the neutron closed shells are not experimentally measured. The isotopes abundance peaks are shaped by those decay properties, but cannot be explained by standard shell modelling. Many explanations exist, such as discrepancies between mass model predictions in the region of $Z=40$ and $N=75$ [140]. Currently, r-process nuclei can only be reached in the region of ^{129}Ag and ^{130}Cd [141] or at much lower N and Z . Therefore, one proposed to approach the discrepancy region starting from ^{85}Ge , ^{92}Se and ^{104}Sr (Figure 4.2), which can respectively be produced as GeS^+ , SeCO^+ and SrF^+ beams. The combined beta decay half-lives ($T_{1/2}$) and beta-delayed neutron emission probabilities (P_n) of these isotopes should provide a first rough characterization of the distribution of beta-strength in a beta decay.

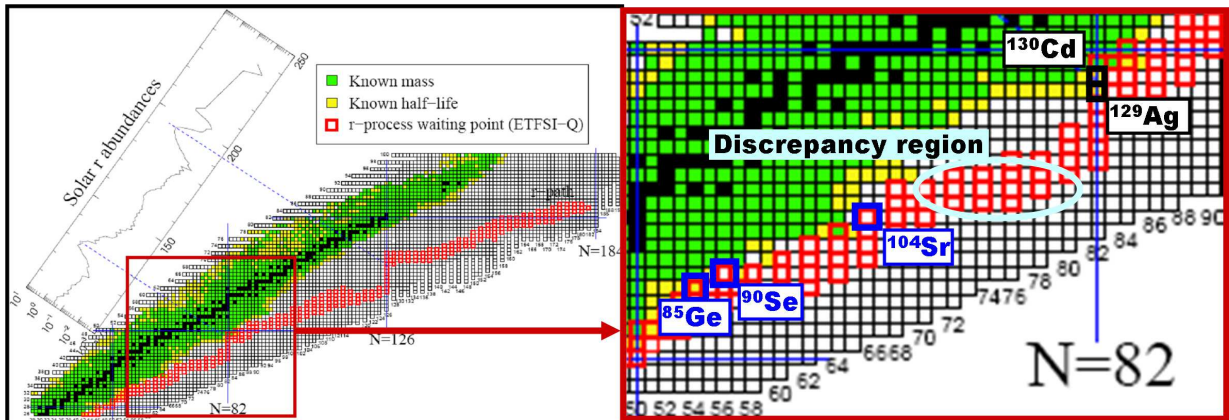


Figure 4.2: R-process path nuclides as given in [140]: “The figure shows the range of r-process paths, defined by their waiting point nuclei. After decay to stability the abundance of the r-process progenitors produce the observed solar r-process abundance distribution [...]. In this calculation a mass formula based on the ETFSI model and special treatment of shell quenching [...] has been adopted.”

Apart from the nuclear astrophysics interest, the measurement of the neutron-rich $^{84-90}\text{Ge}$, $^{90-98}\text{Se}$, and $^{102-110}\text{Sr}$ isotopes gross properties is so challenging that it was proposed as one of the EURISOL key experiments [142]. The measurement of any of these at an existing facility such as ISOLDE would be a great success. The development of the related techniques of production and separation is in this respect of high interest. The study of the gross properties could constitute a first step towards a deeper investigation of these neutron-rich isotopes through other experiments, for example such as mass measurement or using post-acceleration with REX-ISOLDE. The validation of this purification method is a major step for beam development as it is the only way to determine precisely the yields of the more exotic neutron-rich isotopes. Therefore, a first experiment was performed to demonstrate the performances of the cleaning by ECR charge breeding with less exotic GeS^+ and SeCO^+ beams, such as $^{82-83}\text{GeS}^+$ and $^{86-89}\text{SeCO}^+$.

Experimental setup

Neutron-rich Ge and Se isotopes can be produced with the same TIS unit, using respectively for the former a mass marker filled with ^{34}S and for the latter a gas leak of CO_2 . A ThO_2 target coupled with a hot plasma ion source would have been an oxidizing environment favorable to a more rapid release of Se isotopes and higher intensities for SeCO . A neutron converter was requested as well to suppress part of the symmetric fission products. However the experiment was performed with a reducing UC_x target coupled with a hot plasma ion source and no neutron converter. Therefore, no SeCO molecule could be observed, and special care had to be taken to avoid long-lived neutron-deficient contaminants in the setup.

The tape station system described in 1.3.3 was used with a longer kapton window nozzle fitting inside the tube of a neutron detector (Figure 4.3, Figure 4.4, [143]). Charge bred isotopes were implanted on the tape right after the collimator for a duration t_{collect} , and then moved 20 cm into the neutron detector barrel for the measurement of their decay for t_{decay} (Figure 4.5). A detailed description of the neutron detector can be found in [144]. The detection efficiency with 4 MeV neutrons from a $^{241}\text{Am-Be}(\alpha, n)$ source was estimated to 15% prior to the beamtime instead of an expected 19% efficiency, indicating that a few tubes among the twelve ^3He proportional counters were not working properly. A new scintillator box was machined in order to fit the geometry of the kapton window [143], and achieved 50% detection efficiency. Two germanium detectors were positioned respectively at the collection point and at the decay point. However only the detector at the decay point was actually used, as the other one stopped to work after a general powercut at ISOLDE at the beginning of the beamtime. The DAQ scaler triggered independently on the neutron, beta, and gamma signals. A 1 MHz clock signal was sent to one of the channels to timestamp events. Measurement was taken continuously for a certain period, and the modules were cleared by the “end of tape move” signal.

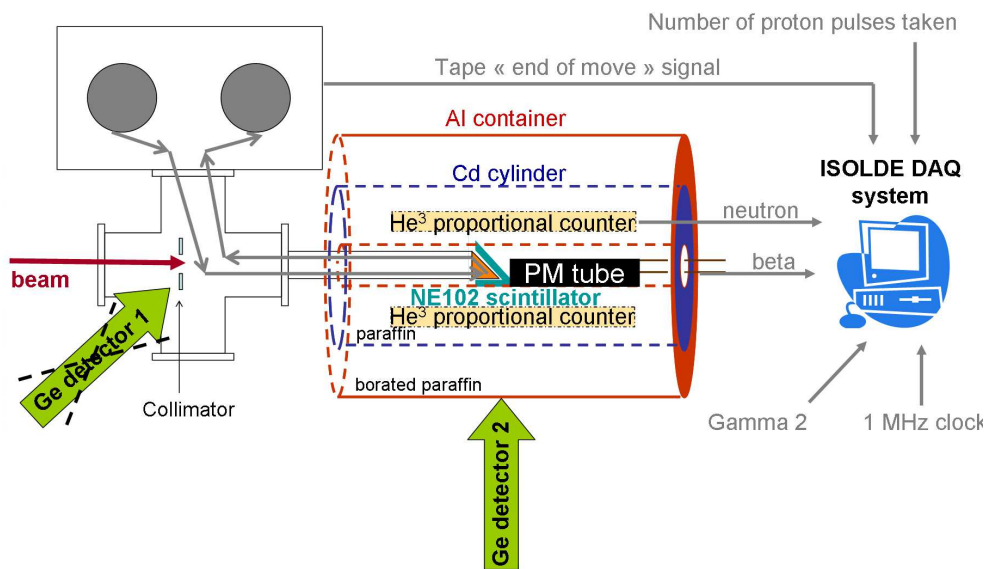


Figure 4.3: Neutron-rich nuclides detection scheme.

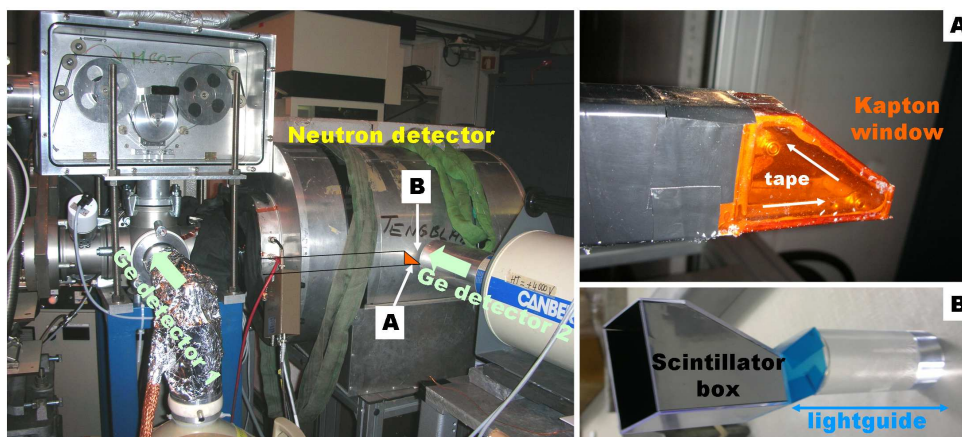


Figure 4.4: Pictures of the neutron-rich nuclides detection setup.

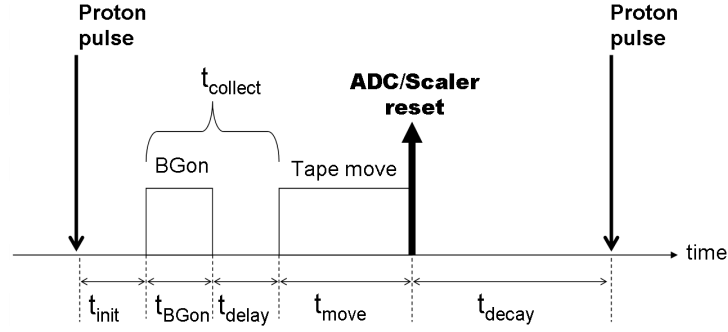


Figure 4.5: Timing of the neutron-rich nuclides measurement cycle. t_{init} and t_{BGon} are respectively set according to the release and the intensity of the radioactive isotope. In the case of very intense beams, i.e. very short t_{BGon} , a t_{delay} of 500 ms is added to allow the release of the charge bred isotopes from the plasma. The frequency of the proton pulses is adapted so that $t_{decay} \approx 5 \cdot T_{1/2}$.

Tuning procedure

The ECR charge breeder was working in a CW-mode. Transmission from GPS to FC2 was optimized with stable ^{40}Ar , ^{132}Xe (from the plasma ion source support gas) and ^{238}U to 52%, and the optimal ΔV found at -86 V. An intense beam of $9.5 \cdot 10^7$ at/ μC of radioactive ^{94}Rb ($T_{1/2}=2.702$ s (0.005), $P_n=10.01\%$ (23) [109]) was injected and charge bred to check that all parameters were optimal: EL1 voltage, B field value, EL2 voltage, and tape moving distance. All parameters were tuned according to the number of neutron counts, excepted the tape moving distance which had to be calibrated with the number of betas counted through the kapton window.

The requested stable ^{120}Sn mass marker to optimize the molecular beam injection did not come out with sufficient intensity. Therefore the tuning was directly performed using the beta counts from radioactive beams of $^{132}\text{Sn}^{34}\text{S}$ ($T_{1/2}=39.7$ s (0.5) [109]) and $^{133}\text{Sn}^{34}\text{S}$ ($T_{1/2}=1.45$ s (0.03), $P_n=0.0294\%$ (24) [109]), respectively produced with $1.8 \cdot 10^7$ at/ μC and $3.8 \cdot 10^5$ at/ μC .

Indicative charge breeding efficiencies obtained during the tuning are given in Figure 4.6. As the fluctuations of the neutron count rate are smaller, charge breeding efficiencies for ^{94}Rb were calculated from the neutron count rate averaged for each measurement cycle, i.e. per proton pulse. However, no neutron could be detected for ^{132}Sn and ^{133}Sn , so their efficiencies were deduced from the beta count rate. The average background per proton pulse was estimated with the beam gate closed. Later tunings with ^{94}Rb were performed with the optimal charge state 16^+ , and $^{132-135}\text{Sn}$ measurements were performed for the 21^+ charge state. The “94Rb_last” settings correspond to the preparation of ^{84}Ge measurement, where the charge state distributions were “detuned” towards lower charge states. Higher production rates might also explain the drop of the efficiencies. Comparisons with an experiment performed in parallel showed the possibility of

contamination in the beam, and that the ^{94}Rb yield might have been underestimated by a factor 10. Both effects could explain the very high efficiencies obtained for “94Rb”.

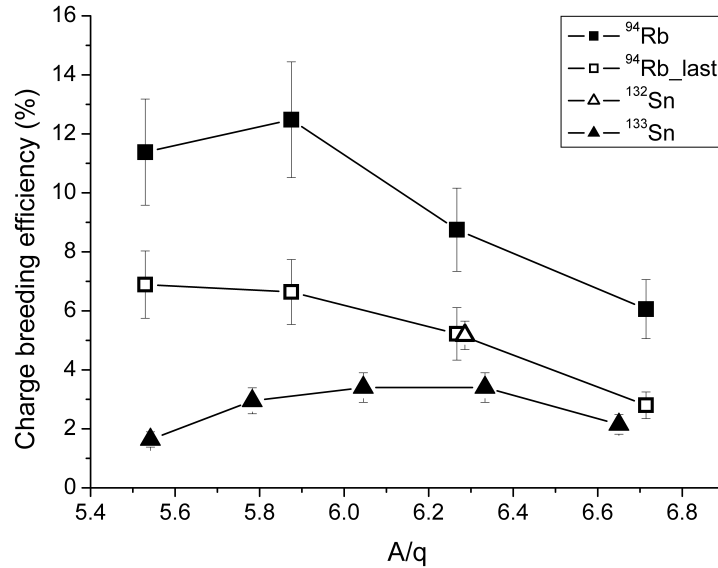


Figure 4.6: Charge breeding efficiencies for ^{94}Rb , ^{132}Sn and ^{133}Sn while testing the detection setup. Error bars include the error on the yield calculated from the release curve, the error on the neutron or beta count rate reading, and the error on the P_n in the case of the ^{94}Rb efficiencies. See text for more details.

Results of the molecular breaking up technique

$^{134}\text{Sn}^{34}\text{S}$ ($T_{1/2}=1.12$ s (0.08), $P_n=17\%$ (13) [109]) produced with $8.8 \cdot 10^4$ at/ μC and $^{135}\text{Sn}^{34}\text{S}$ ($T_{1/2}=530$ ms (20), $P_n=21\%$ (3) [109]) could be successfully injected into the ECR, broken up and charge bred. For charge states 21^+ and 23^+ , their decay could be measured at the detection setup and identified by fitting the beta decay curve. In the case of ^{134}Sn , the statistics were high enough to allow the fit of the neutron decay (Figure 4.7).

All the background contributions on the $^{134-135}\text{Sn}^{34}\text{S}$ beams have not been identified yet and are still under analysis. One expected the ^{134}Sn neutron spectra to be contaminated with ^{140}I ($T_{1/2}=0.86$ s (4), $P_n=9.3\%$ [145]), which could be selected at mass 168 as ^{140}ICO and which would be extracted from the target with a factor 10 lower intensity. However it could not be observed on yield measurements nor on gamma spectra after the ECR charge breeder.

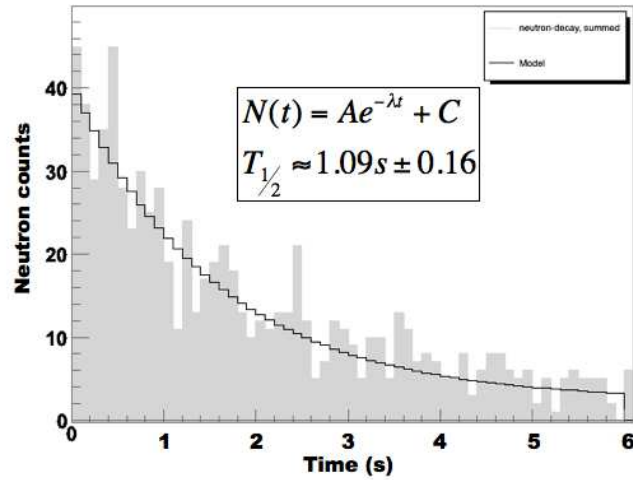


Figure 4.7: Neutron decay measured for $^{134}\text{Sn}^{21+}$. The result of the fit confirms that ^{134}Sn is the major contribution.

Results of the background suppression

$^{118}\text{Ag}/^{118}\text{In}$ is so intensely produced (about $1.4 \cdot 10^8$ at/ μC) that it makes the study of ^{84}Ge beta decay impossible. The most separated measurable peaks of $^{118}\text{In}^{15+}$ and $^{84}\text{Ge}^{11+}$ have a $\Delta(A/q)$ of 0.23. If they had similar intensities, the required resolving power would be only 40 and thus achievable with our current mass analyzer. However, even using the molecular sidebands, only a factor of suppression of 20 could be achieved for mass 118 contamination after the mass separation following the ECR (Figure 4.8), indicating that the mass resolving power was even worse than the $A/q/\Delta(A/q) \sim 50$ calculated previously (3.3.3).

A tentative long measurement of $^{84}\text{Ge}^{11+}$ was performed, but due to low statistics, no tendency could be identified on the neutron spectra. Moreover, a non-negligible part of the neutron counts was expected to come from ^{90}Br selected at mass 118 as $^{90}\text{BrCO}$, and charge bred to 12^+ . As the yields of $^{90}\text{BrCO}$ could not be measured, one could not perform a careful suppression of the background.

In order to study neutron-rich Ge isotopes, some more target development is needed to get enough statistics. The beta spectra might give some information, provided that the high intensity contaminants are suppressed. In such case, the installation of a new two-step separator as described in subsection 3.3.3 would benefit to the experiment by suppressing the $^{118}\text{In}^{15+}$ contamination on the $^{84}\text{Ge}^{11+}$ peak by a factor 10^6 if one achieves a mass resolving power of 70. For the calculated mass resolving power of 100, almost all the contamination could be suppressed on that peak.

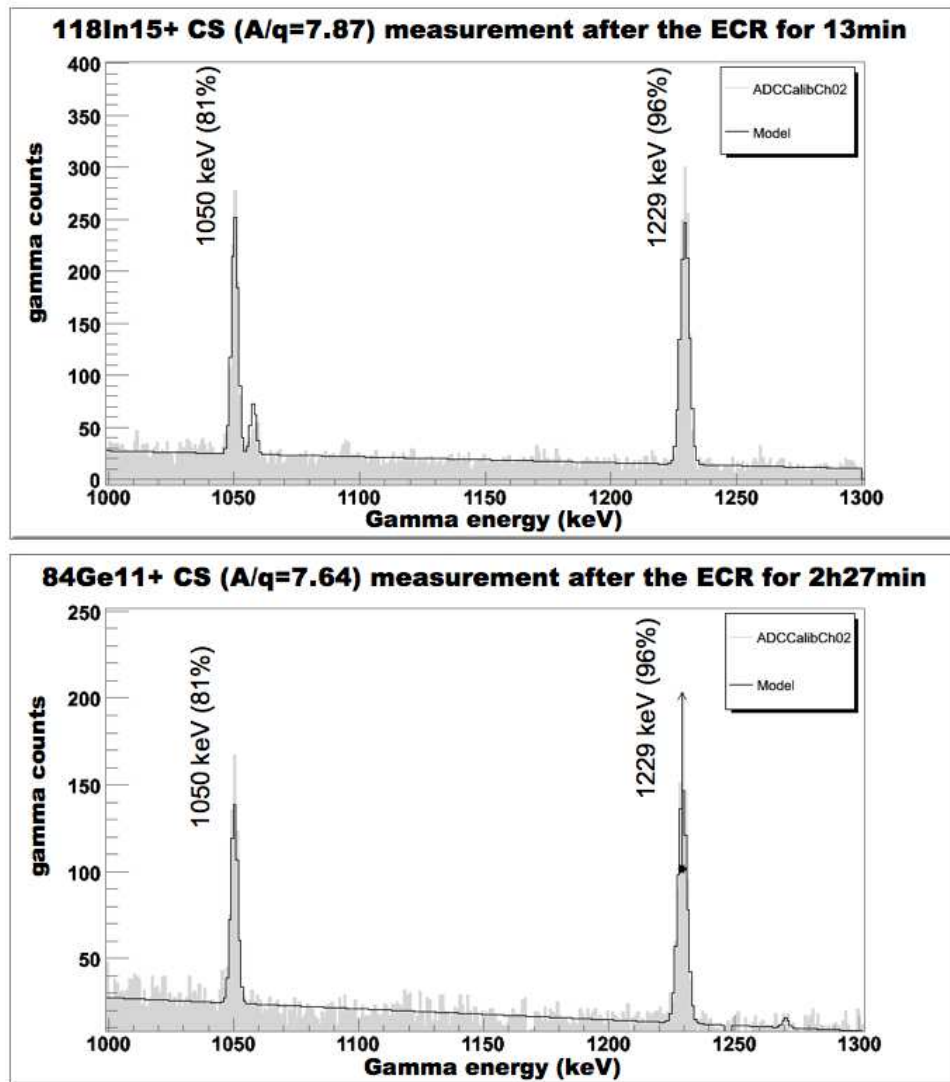


Figure 4.8: Gamma lines for the $^{118}\text{In}^{15+}$ contamination measured after the ECR. $^{118}\text{In}^{15+}$ is so abundant (top) that it overwhelms the count rate on the nearby A/q value where $^{84}\text{Ge}^{11+}$ is expected (bottom).

Résumé du chapitre 4: Perspectives de l'élévation $1^+ \rightarrow n^+$ de l'état de charge par ECR

Lorsqu'on compare les diverses techniques d'élévation de l'état de charge du point de vue des performances, les feuilles minces de "stripping" permettent d'obtenir efficacement des états de charge élevés quels que soient l'isotope, l'intensité ou l'émission du faisceau considéré, en mode continu ou pulsé. Les feuilles minces peuvent donc être utilisées pour n'importe quel type de postaccélération. REXEBIS (et son piège de préparation REXTRAP) et le PHOENIX Booster acceptent tous les deux des faisceaux continus ou pulsés, et produisent des faisceaux multichargés avec des efficacités et des temps comparables. Cependant on utilisera plutôt l'EBIS pour la production d'un faisceau pur d'états de charge très élevés destiné à être injecté dans un LINAC à fonctionnement pulsé par cycles lents. **Le système ECR sera le plus adapté pour élever à des états de charge modérés des faisceaux intenses de grande émission pour une postaccélération continue dans un LINAC ou un cyclotron.** Si l'on considère des critères plus pratiques comme les contraintes d'opération et de maintenance, les feuilles minces constituent un système très simple à maintenance fréquente, tandis que REXEBIS et le PHOENIX Booster ont un réglage plus complexe et requièrent des interventions plus rares. Le coût de mise en oeuvre le plus important concerne le "stripping", puisqu'un pré-accélérateur et des cavités pour la mise en forme du faisceau doivent être construits. REXEBIS (REXTRAP inclus) et le PHOENIX Booster ont requis un moindre coût initial. Selon le type de feuille mince utilisé, la maintenance du "stripper" est d'un prix comparable au remplacement trimestriel de la cathode de REXEBIS. **Le PHOENIX Booster apparaît comme la solution la plus robuste à la maintenance la moins coûteuse.**

Le PHOENIX Booster peut déjà fournir à nombre d'expériences de physique des faisceaux intenses d'ions multichargés à des états de charge modérés, particulièrement en rendant accessibles des faisceaux d'isotopes qui ne peuvent être obtenus

directement des lignes d'ISOLDE en raison d'un taux de contamination élevé ou d'une extraction difficile de la cible. Par exemple, une expérience fut proposée au cours de la thèse pour étudier les propriétés de décroissance bêta d'isotopes riches en neutron présentant un fort intérêt pour l'étude du processus r de nucléosynthèse en astrophysique. Ces isotopes sont difficiles à extraire de la cible sans un niveau important de contamination. En les produisant sous forme de molécules sélectionnées en masse avec GPS, puis en les cassant dans le PHOENIX Booster pour sélectionner uniquement l'isotope intéressant sous sa forme multichargée, on soustrait une grande partie du bruit de fond. L'expérience était destinée à démontrer le fonctionnement de cette méthode de purification utilisant le plasma ECR avec des isotopes moins exotiques, et à mesurer les propriétés de décroissance bêta des isotopes d'intérêt.

L'expérience a été effectuée dans le but de mesurer les propriétés fondamentales des noyaux de Ge et Se riches en neutrons impliqués dans le processus r dans la région comprise entre $N=50$ et $N=82$. Les isotopes Ge et Se sont respectivement extraits sous forme de molécules de GeS et SeCO. Cependant, la cible d' UC_x utilisée constituait un milieu réducteur plutôt défavorable à l'extraction du SeCO. C'est pourquoi on a cherché à démontrer la méthode de purification pour le premier isotope de Ge émetteur de neutrons: $^{84}\text{Ge}^{34}\text{S}$. Le dispositif de détection bêta-gamma-neutrons a d'abord été optimisé avec un faisceau de ^{94}Rb , puis avec l'injection de molécules de $^{132}\text{Sn}^{34}\text{S}$ et $^{133}\text{Sn}^{34}\text{S}$. La technique a pu être validée avec l'injection et le cassage de molécules de $^{134}\text{Sn}^{34}\text{S}$ dans le plasma ECR, et la détection de la courbe de décroissance neutron de $^{134}\text{Sn}^{21+}$. Les résultats ont montré que la technique fonctionne, cependant l'efficacité de la purification du faisceau reste principalement limitée par la résolution en masse du séparateur. En effet, le bruit de fond bêta des états de charge voisins de masse 118 reste élevé malgré un facteur de suppression de 20 sur le pic mesurable le plus proche ($\Delta(A/q)=0.23$) et le taux de comptage faible des neutrons du $^{84}\text{Ge}^{11+}$ ne permet pas de conclure. L'installation du nouveau séparateur de résolution en masse plus élevée pourrait permettre d'atteindre le facteur de suppression de 10^6 nécessaire à la détection des bêta du $^{84}\text{Ge}^{11+}$ au-dessus du bruit de fond.

Conclusion

ECR-type devices, which are already widely developed as injector ion sources for accelerators such as the Large Hadron Collider (LHC) or the SPIRAL2 facility, are now competing with various types of on-line charge breeders. In the next-generation facility race for beam purity and beam intensity, charge breeding of radioactive ions constitutes a real challenge. The tests undertaken in this work aimed at exploring the capabilities and limitations of a commercialized ECR charge breeder, the PHOENIX ECR Booster, to capture and charge breed various radioactive ion beams from ISOLDE.

Most measurements with stable ions were performed by other members of the collaboration prior to this work, and provided important information about charge breeding efficiencies, charge breeding times, and effects of the isotope mass on the capture performances. In my thesis work, I took part to many beamtimes to address specific issues that could only be answered with the use of radioactive ions:

- the validity of the “blind tuning” method, i.e. the applicability of the ΔV tuning with stable ions to radioactive species.
- the effects of the injected ions chemistry on the working range of the plasma capture, independently from the effects of mass, were tested by injecting (^{142}Xe , ^{142}Cs) isobars.
- the effects of the beta decay of injected ions in the ECR plasma, and its consequences on daughter nuclides trapping or recycling were investigated with the injection of ^{61}Mn decaying to ^{61}Fe .

I performed the data analysis from experiments run in 2006, 2007 and 2008. Results from the whole study program showed that the device was ready-to-use for intense beams of isotopes from the intermediate to heavy mass range ($A > 40$). It could provide continuous beams of average charge states ($4 < A/q < 7$) with several percents of efficiency, and measured charge breeding times were compatible with half-lives down to 500 ms. The working range of plasma capture could be clearly identified according to the chemistry of the injected isotope only. I could appreciate the reproducibility of tuning within a few tens of Volts for a given TIS unit throughout this work.

However former results for the pulsed extraction of charge bred stable ions could not be confirmed with radioactive ions due to a bad configuration of the ECRIT mode. Moreover, one could not conclude whether daughter nuclides were actually trapped in the ECR plasma or recycled from the plasma chamber walls over long times. Finally, the current design of the PHOENIX ECR Booster did not prove to be optimal concerning the injection of light ions ($A < 20$). Such developments are of high importance for next generation ISOL facilities as in the EURISOL scenario, in which the chosen charge breeder should accept a continuous beam of up to 10^{13} ions per second. For example, new solutions are currently searched for EBIS charge breeders to accept continuous beams of such high intensities.

Within my thesis, I chose to address the question of the purity of ECR charge bred beams. I made some effort to develop ways of reducing the intense contamination coming either from the plasma residual gas or from the injected beam. Among the many solutions presented, I investigated the installation of a new high resolution separator in mass and energy and proposed a design. I compared the existing techniques of beam manipulation with the ECR charge breeder to the needs of various fields in physics, and initiated the gathering of a new collaboration in order to test the possibilities of beam purification for astrophysics studies. Within this collaboration, I performed an experiment to suppress contamination from beams of neutron-rich ^{84}Ge , an isotope close to the r-process path, by injecting molecules of $^{84}\text{Ge}^{34}\text{S}$ into the ECR charge breeder, breaking the molecules in the ECR plasma, and selecting the charge bred ^{84}Ge only. The technique was successfully optimized with clean beams of $^{134}\text{Sn}^{34}\text{S}^+$. Unfortunately, the method could not be demonstrated with $^{84}\text{Ge}^{34}\text{S}$, as the statistics were low and as the resolving power of the mass analyzer was not sufficient to suppress the contamination from intense neighbouring charge states.

Currently, the ECR charge breeder seems more suited to post-acceleration with a CW-LINAC or a cyclotron, and thus complementary to EBIS-type charge breeders which provide with similar efficiencies pulsed beams of much higher charge states to pulsed LINACs. ECR beams development for experiments requires in priority the installation of an efficient mass and energy separator in order to benefit from ECR charge bred beams as clean as possible. The availability of ISOLDE beams at the PHOENIX ECR Booster test stand is ideal to investigate such possibilities.

Conclusion

Les appareils de type ECR, que l'on développe déjà largement en tant que sources d'ions pour l'injection des accélérateurs tels que le Grand Collisionneur de Hadrons (LHC) ou le complexe SPIRAL2, rivalisent maintenant avec les divers élévateurs d'état de charge en ligne. Dans la course aux faisceaux purs et intenses pour les installations de nouvelle génération, produire des ions radioactifs multichargés constitue un véritable défi. Les travaux entrepris dans cette thèse visaient à explorer les capacités et les limitations d'un élévateur d'état de charge commercial, l'injecteur ECR PHOENIX, pour la capture et l'élévation de l'état de charge des divers faisceaux d'ions radioactifs d'ISOLDE.

La plupart des mesures avec des ions stables furent effectuées par d'autres membres de la collaboration préalablement à ce travail, fournissant des informations importantes concernant les efficacités et temps d'élévation de l'état de charge et les conséquences liées à la masse sur la capture des isotopes. J'ai participé pendant ma thèse à des expériences en ligne pour étudier certains problèmes spécifiques qui ne peuvent être abordés qu'avec l'utilisation d'ions radioactifs:

- la validité de la méthode de "réglage à l'aveugle", c.a.d l'applicabilité du réglage du ΔV des ions stables aux espèces radioactives .
- les effets liés à la chimie des ions injectés sur la plage de capture plasma, indépendamment des effets liés à la masse, furent testés avec l'injection d'isobares (^{142}Xe , ^{142}Cs).
- les effets liés à la décroissance bêta des ions injectés dans le plasma ECR, et ses conséquences sur le piégeage ou le recyclage des noyaux-fils furent étudiés avec l'injection de ^{61}Mn décroissant vers le ^{61}Fe .

J'ai analysé les données des expériences effectuées en 2006, 2007 et 2008. Les résultats du programme complet d'étude ont montré que le dispositif était prêt à l'emploi pour des faisceaux intenses d'isotopes de masses intermédiaires à lourdes ($A > 40$). Il peut produire des faisceaux continus d'états de charge moyens ($4 < A/q < 7$) avec plusieurs pourcents d'efficacité, et des temps mesurés compatibles avec des temps de vie descendant jusqu'à 500 ms. On peut clairement identifier la plage de capture plasma comme dépendant principalement de la chimie de l'isotope injecté. J'ai pu apprécier tout au long de ce travail la reproductibilité des réglages dans une plage de quelques dizaines de Volts pour un ensemble cible-source donné.

Cependant, en raison d'une mauvaise configuration du mode ECRIT, les résultats obtenus précédemment pour l'extraction pulsée d'ions stables multichargés n'ont pas pu être reproduits avec les ions radioactifs. En outre, il n'a pas été possible de déterminer si les noyaux fils furent bien piégés dans le plasma ECR ou recyclés pendant longtemps des murs de la chambre plasma. Finalement, le concept actuel du PHOENIX ne semble pas convenir à l'injection d'ions légers ($A < 20$). De tels développements sont d'une grande importance pour la prochaine génération d'installations ISOL, comme dans le scénario EURISOL où l'élévateur d'état de charge choisi devra accepter un faisceau continu jusqu'à 10^{13} ions par seconde. Par exemple, de nouvelles solutions sont actuellement recherchées afin que les EBIS puissent accepter des faisceaux continus d'intensités aussi élevées.

Au cours de ma thèse, j'ai choisi d'aborder la question de la pureté des faisceaux multichargés par ECR. Je me suis efforcée de développer des moyens de réduction de la contamination intense provenant soit du gas résiduel du plasma, soit du faisceau injecté. Parmi les nombreuses solutions présentées, j'ai étudié l'installation d'un nouveau séparateur en masse et en énergie de haute résolution, pour lequel j'ai présenté un plan de conception. J'ai comparé des techniques existantes de manipulation du faisceau avec un élévateur d'état de charge ECR aux besoins des divers secteurs de la physique, et réuni une nouvelle collaboration pour tester les possibilités de purification du faisceau pour des études d'astrophysique. Au sein de cette collaboration, j'ai réalisé une expérience pour supprimer la contamination présente dans les faisceaux riches en neutrons de ^{84}Ge , un isotope impliqué dans le processus r , en injectant des molécules de $^{84}\text{Ge}^{34}\text{S}$ dans l'ECR, afin de casser les molécules dans le plasma ECR et extraire le ^{84}Ge multichargé seulement. La technique fut optimisée avec succès à l'aide de faisceaux propres de $^{134}\text{Sn}^{34}\text{S}^+$. Malheureusement, la méthode n'a pas pu être démontrée avec $^{84}\text{Ge}^{34}\text{S}$, car le pouvoir de résolution de l'analyseur en masse était insuffisant pour supprimer la contamination des états de charge intenses voisins.

Actuellement, l'élévateur de charge ECR semble plus approprié à la post-accélération avec un LINAC continu ou un cyclotron, et complète ainsi l'EBIS qui produit avec des efficacités similaires des faisceaux pulsés d'états de charge bien plus élevés pour les LINAC pulsés. Le développement des faisceaux ECR pour les expériences nécessite en priorité l'installation d'un

séparateur en masse et en énergie efficace afin de bénéficier de faisceaux multichargés par ECR aussi propres que possible. La disponibilité des faisceaux d'ISOLDE au banc de test du PHOENIX Booster est idéale pour de telles études.

Appendix A

Routines for GO4 and ROOT analysis

The basic operation of the ISOLDE DAQ system can be found in [146]. One had to adapt the existing routines developed by the ISOLDE collaboration to the needs of these experiments. Data acquisition through the VME is encoded according to the settings defined in the `f_user.c` routine (subsection A.1.1), and written to a `*.lmd` file (subsection A.1.2) on the disk. The module buffer stream (MBS) or the `*.lmd` file can be interpreted in GO4 GUI through the event reading routines [103] which will not be detailed here. Histograms of interest were constructed in one of these C++ routines for monitoring during the run. However, the GO4 framework is not adapted to the systematic analysis of a great number of files. Therefore, C++ routines were developed (section A.2) and compiled in the ROOT environment [102] for analysis after the run. An example of the data unpacking routine is given for the analysis of the daughter nuclide trapping run.

A.1 On-line monitoring with GO4

The GO4 GUI provides a ROOT browser, editing functions and fit panel, as shown on Figure A.1. Macros can be entered in the ROOT command line within the GO4 framework.

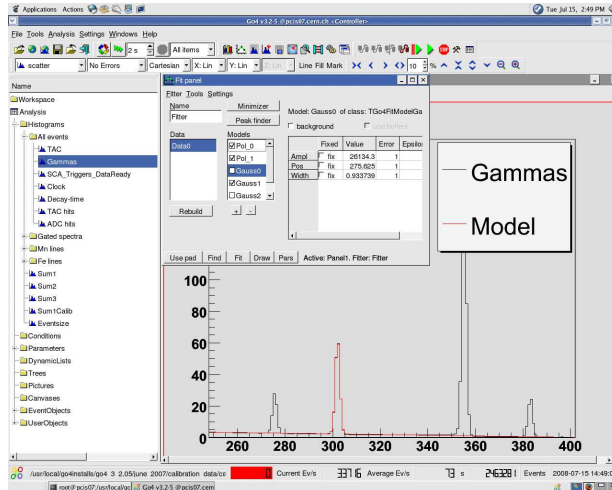


Figure A.1: GO4 graphical user interface. The ROOT browser allows online and offline analysis, and the fit panel provides basic fitting functions.

A.1.1 Data encoding with the f_user.c routine

The following f_user.c routine was used to encode data from the IS397 runs. Only three scaler channels and two ADC channels were needed.

```

1  #define DATA_W_BOE          0xFEFEFEFE
   #define DATA_W_EOE          0xEFEFEFEF
   #define WORD_TYPE_MAP        0xFF000000
   #define MODULE_HEADER        0xFA000000
   #define MODULE_DATA_WORD     0xF8000000
   #define MODULE_EOB           0xFC000000
   #define HEADER_CNT_MAP       0x0000FF00
   #define DATA_MAP             0x00000FFF
   #define DATA_CHN_MAP        0x001F0000
   #define EV_COUNTER_24bits     0x00FFFFFF
11 #define EV_COUNTER_26bits     0x03FFFFFF
   #define SCA_HEADER           0xFD000000

   static volatile unsigned short *ps_adc [NR_OF_ADCs];
   static volatile unsigned long *pl_adc [NR_OF_ADCs];

   static volatile unsigned short *ps_sca [NR_OF_SCAs];
   static volatile unsigned long *pl_sca [NR_OF_SCAs];

   static volatile unsigned short *ps_outreg;

21  /******
   /*Function that creates virtual pointers to the modules addresses*/
   int f_user_get_virt_ptr (long *pl_loc_hwacc, long pl_rem_cam [])
   {
       //ADC
       ps_adc [0] = (unsigned short *) (A24_BASE + 0x400000); //Short pointer to ADC
       pl_adc [0] = (unsigned long *) (A24_BASE + 0x400000); //Long pointer to ADC

       //OUTPUT REGISTER
31  ps_outreg = (unsigned short *) (A24_BASE + 0x600000);

       //SCALER
       ps_sca [0] = (unsigned short *) (A24_BASE + 0x300000); //Short pointer to SCALER
       pl_sca [0] = (unsigned long *) (A24_BASE + 0x300000); //Long pointer to SCALER
   }

   /******
   /*Function that initializes the ADC and SCALER channels*/
41  int f_user_init ( unsigned char bh_crate_nr,
                   long *pl_loc_hwacc,
                   long *pl_rem_cam,
                   long *pl_stat )
   {
       //Vetoing triggers: out register set low
       *(ps_outreg + OFFSET_NIM_OUT / sizeof(unsigned short)) = 0;

       //ADC
51  *(ps_adc [0] + OFFSET_CRATE_NR / sizeof(unsigned short)) = 1;
       //low threshold on two channels used
       *(ps_adc [0] + OFFSET_THRESHOLD / sizeof(unsigned short)) = 2;
       *(ps_adc [0] + OFFSET_THRESHOLD / sizeof(unsigned short) + 1) = 2;
       //high threshold on unneeded channels
       for (i = 2; i < 32; i++)
           *(ps_adc [0] + OFFSET_THRESHOLD / sizeof(unsigned short) + i) = 200;
       //ADC bitset 2
       *(ps_adc [0] + OFFSET_BITSET2 / sizeof(unsigned short)) = 0x4888;

61  //SCALER
       *(pl_sca [0] + OFFSET_ENABLE / sizeof(unsigned long)) = 0x1C; //channel 3,4,5 enabled
       *(ps_sca [0] + OFFSET_SCA_CTRL / sizeof(unsigned short)) = 0x45; //26 bit, clear, no header
       *(ps_sca [0] + OFFSET_SCA_CLEAR / sizeof(unsigned short)) = 0xFFFF; //clear scaler

       *(ps_adc [0] + OFFSET_EV_RESET / sizeof(unsigned short)) = 1; //reset event counters ADCs
   }

   /******
71  /*Function that reads the modules channels and encodes the events*/
   int f_user_readout (unsigned char bh_trig_typ, //trigger type
                     unsigned char bh_crate_nr,

```

```

        register long *pl_loc_hwacc,
                register long *pl_rem_cam,
                long *pl_dat,
                short *ps_veshe,
                long *l_se_read_len,
                long *l_read_stat)
{
81  unsigned short us_data_ready;
    unsigned short us_data_ready_bit;
    unsigned long l_data;
    unsigned long word_type;
    unsigned long nr_words;
    unsigned long l_adcdata;
    unsigned long l_adcchn;
    unsigned long l_tdcdata;
    unsigned long l_tdcchn;
91  unsigned long sca_cnt;
    long l_nrwords;

    *pl_dat=0;
    l_nrwords=1;
    *l_se_read_len=0;

    switch (bh_crate_nr) //switching between the crates
    {
101  case 0: //only one crate is used here

        switch (bh_trig_typ) { //switching between the triggers

            case 2: //running acquisition with one trigger signal
                *(ps_outreg+OFFSET_NIM_OUT/sizeof(unsigned short))=0; //veto input trigger
                *pl_dat=DATA_W_BOE; //encoding beginning of event

                pl_dat++;
                l_nrwords++;

111  //SCALER
                us_data_ready=*(ps_sca[0]+OFFSET_SCA_STAT/sizeof(unsigned short));
                us_data_ready_bit = us_data_ready & 1;

                if (us_data_ready_bit==1){
                    //channel 0
                    l_data = (*pl_sca[0]&EV_COUNTER_24bits);
                    *pl_dat=l_data|SCA_HEADER; //encoding scaler header word with first data word
                    pl_dat++;
                    l_nrwords++;

121  //channel 1
                    l_data = (*pl_sca[0]&EV_COUNTER_24bits);
                    *pl_dat = l_data; //second data word
                    pl_dat++;
                    l_nrwords++;

                    //channel 2
                    l_data = *(pl_sca[0]); //clock is taken on 26bits
                    *pl_dat = l_data; //third data word
131  pl_dat++;
                    l_nrwords++;
                }

                //ADC
                us_data_ready=*(ps_adc[0]+OFFSET_STATREG1/sizeof(unsigned short));
                us_data_ready_bit = us_data_ready & 1;

                if (us_data_ready_bit==1){
141  l_data = *pl_adc[0];
                    *pl_dat=l_data;
                    pl_dat++;
                    l_nrwords++;

                    word_type = l_data & WORD_TYPEMAP;
                    //decode header
                    if (word_type==MODULE_HEADER)
                        nr_words = (l_data & HEADER_CNT_MAP) >> 8; //getting number of ADC words to read

                    while(word_type!=MODULE_EOB){ //loop on number of ADC words
151  l_data = *pl_adc[0];
                        *pl_dat=l_data;
                        pl_dat++;

```

```

        l_nrwords++;

        word_type = l_data & WORD.TYPMAP;

        if (word_type==MODULEHEADER); //unexpected ADC header word

161      if (word_type==MODULEDATAWORD){
            l_adcdata = (l_data & DATA.MAP);
            l_adcchn = (l_data & DATA.CHN_MAP)>>16;
        }

        }//end of loop on ADC words
    }//end of ADC reading

    *pl_dat=DATA.WEOE; //encoding the end of event
    pl_dat++;
    l_nrwords++;
171    *l_se_read_len=l_nrwords*4;

    *(ps_outreg+OFFSET_NIM_OUT/sizeof(unsigned short))=0xFFFF; //removing register high to
        accept input triggers
    break; //end of case 2

    case 14: //start acquisition
        *(ps_sca[0] + OFFSET_SCA_CLEAR/sizeof(unsigned short)) = 0xFFFF; //clear scaler
        *(ps_outreg+OFFSET_NIM_OUT/sizeof(unsigned short))=0xFFFF; //accept input triggers
    break; //end of case 14

181    case 15://stop acquisition
        *(ps_outreg+OFFSET_NIM_OUT/sizeof(unsigned short))=0x0; //veto input trigger
    break; //end of case 15

    default: //running acquisition
    break; //end of case default

} /* end switch trigger */
break; //end of case one crate

191    default:
    break;

} /* end switch crate */

} /* end of function */

/******

```

A.1.2 Structure of the *.lmd data file

The event structures encoded in the f_user.c routine are emphasized in the following extract of an hexadecimal octal dump of the data. The first column gives the byte adress.

0100160	01000009	<u>fefefefe</u>	010000fd	01000000
0100200	77000020	000201fa	494000f8	ed4001f8
0100220	000000fc	<u>efefefef</u>	01000009	02000000
0100240	0a000100	01000109	1c000000	0a000100
0100260	00000200	e34f1f00	0e000000	0a000100
0100300	01000009	<u>fefefefe</u>	020000fd	02000000
0100320	7d090020	<u>efefefef</u>	0a000100	02000000
0100340	0a000100	01000109	1c000000	0a000100
0100360	00000200	e44f1f00	0e000000	0a000100
0100400	01000009	<u>fefefefe</u>	030000fd	03000000
0100420	f2170020	<u>efefefef</u>	10a504fc	02000000
0100440	0a000100	01000109	1c000000	0a000100
0100460	00000200	e54f1f00	0e000000	0a000100
0100500	01000009	<u>fefefefe</u>	040000fd	04000000
0100520	72200020	<u>efefefef</u>	5af0ef20	02000000

One notes that the bytes sequences are inversed compared to the specified encoding, as the VME stores data in a little-endian order (with the least significant value of the sequence first).

Therefore the reading routine written in ROOT includes a function that reorders the bytes (subsection A.2.1).

A.2 Analysis with ROOT

The various files read and produced by the routines are summarized on Figure A.2.

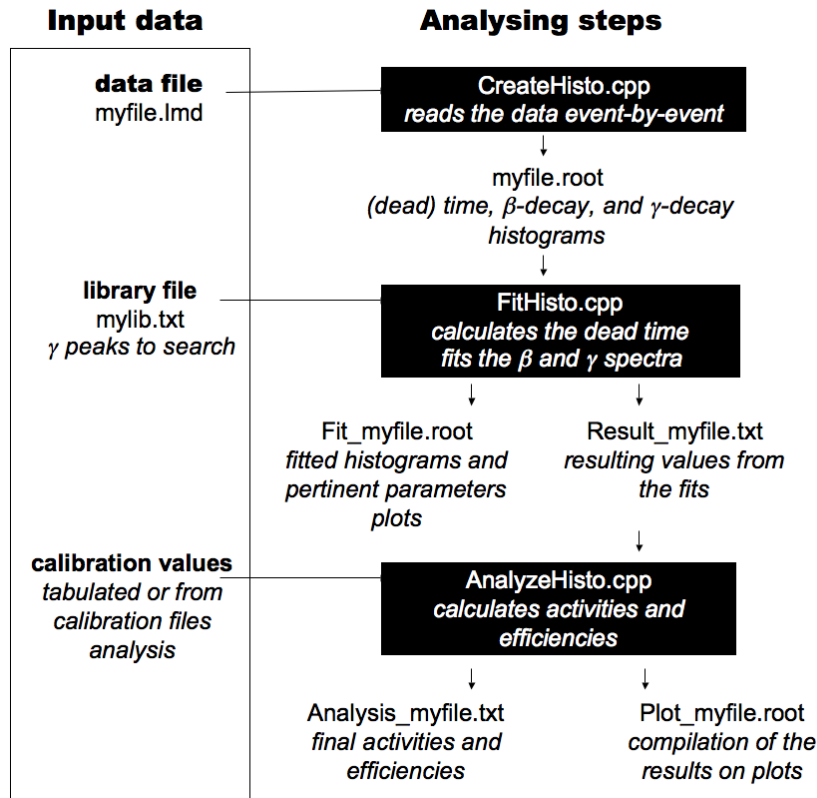


Figure A.2: Schematic representation of the analysis program.

Only the core of the routine is given, as proper C++ and ROOT libraries should be added to allow compilation. Some simple functions and static variable definitions were omitted to improve lisibility.

A.2.1 Unpacking the data with the CreateHisto.cpp routine

The CreateHisto.cpp (subsection A.2.1) routine reads the *.lmd file and unpacks events to build various histograms which are written to a corresponding file *.root. Special care had to be taken to suppress fake events generated by electronics and random incrementation of the scaler channels. The origin of such perturbations of the DAQ is not known.

```

//This class contains the various useful information about an event
class event: public TObject
{
5 public:
  event(); //constructor

  unsigned int event_nr; //index of the event in the list
  unsigned int cycle_nr; //index of the measurement cycle
  unsigned int scaler_clock; //clock value in microseconds
  unsigned int scaler_trigger; //number of triggers
  unsigned int scaler_ready; //number of accepted triggers
  unsigned int adc_TAC; //value of the TAC
  unsigned int adc_gamma; //gamma energy
15 unsigned int event_ok; //flag=1 if this event is correct
  unsigned int cycle_ok[2]; //cycle_ok[0]=0 if containing a wrong event indexed by
  // cycle_ok[1]
  unsigned int cycle_complete; //!=1 if the last event of this cycle is close to the
  // cycle_duration
  unsigned int acquisition_time; //time in microseconds over the file acquisition
  unsigned int live_time; //time in microseconds over the good events considered
  unsigned int cycle_time; //time in microseconds over the current cycle
  void MyPrint(); //function to print the list of values above
};

/* class event initialization and print functions*/
25 /*-----*/

//This class allows contains basic functions common to all is397 runs analysis
class is397
{
public:
35 is397(); //constructor
  ~is397(); //destructor

  long ReadWord(); //function to read a word from the data file
  long ByteSwap(long data_read); //function to reorganize the bytes in the big-endian
  // standard
  int EventCheck(); //function to check validity of an event
  int CycleCheck(); //function to check validity of a cycle
  int Write(const char * file); //function to write histograms to a *.root file

  FILE* data_file; //pointer to the *.lmd file to be read

45 //various histograms of interest
  TH1D* clockPlot;
  TH1D* triggers;
  TH1D* TAC;
  TH1D* gamma;
  TH1D* coincidence;
  TH1D* rebond_trigger;
  TH1D* rebond_accepted;

  TObjArray* Events; //dynamic list of the events read from the file
55 TObjArray* objectsToSave; //list of histograms to be written

  unsigned int prev_clock;
  unsigned int cycle_duration;
  unsigned int use_ALL_cycles;
  double coef[2];
  unsigned int gate[2];
};

/* class is397 initialization */
65 //*****Function that reads data words
long is397::ReadWord()
{
  long *read_ptr=(long*) malloc(sizeof(long));
  long bytes_read=0;
  long data=0;

  bytes_read=fread(read_ptr,sizeof(read_ptr),1,data_file);
75 data=*read_ptr;
  delete read_ptr;
}

```

```

    if(bytes_read != 1)
        return -1;
    else
        return ByteSwap(data);
}

//*****Function that organizes read data
85 long is397::ByteSwap(long data_read)
{
    int i=0;
    int bytes_number=4;
    long byte_part=0;
    long data=0;

    for(i=0;i<bytes_number;i++)
    { byte_part=(data_read>>(8*i))&0xFF;
95     data+=(byte_part<<(8*(3-i)));
    }

    return(data);
}

//*****Function that checks the read event
int is397::EventCheck()
{
    event* tempEvent;
    event* tempEvent_old;
105 unsigned int numEntries;
    unsigned int index_cycle=0;

    numEntries = Events->GetEntriesFast();
    printf("-----\n");
    printf("Checking %d events\n",numEntries);

    tempEvent_old = (event*)Events->At(0);

    if(tempEvent_old->adc_gamma) //one considers the first event is ok if it contains a gamma
115     tempEvent_old->event_ok=1;
        energy

    for(unsigned int i=1; i < numEntries; i++) //loop on all events read to suppress wrong
        increments due to electronics noise
    {
        tempEvent = (event*)Events->At(i);
        tempEvent->cycle_nr=index_cycle;

        if(tempEvent->scaler_ready>tempEvent_old->scaler_ready) //if the scaler was not reset
        {
            if((tempEvent->scaler_ready-tempEvent_old->scaler_ready)>50) tempEvent->event_ok=0;
            //too many triggers at once
125     else if((tempEvent->scaler_clock>tempEvent_old->scaler_clock)&&((tempEvent->
                scaler_clock-tempEvent_old->scaler_clock)>10000)) tempEvent->event_ok=0; //too
                much delay between two events
            else if ((tempEvent->scaler_clock<tempEvent_old->scaler_clock)&&((cycle_duration+
                tempEvent->scaler_clock-tempEvent_old->scaler_clock)>10000)) tempEvent->event_ok
                =0; //too much delay between two events
            else tempEvent->event_ok=1; //OK
        }
        else if(tempEvent->scaler_ready<tempEvent_old->scaler_ready) //scaler reset
        {
            if(tempEvent->scaler_clock<tempEvent_old->scaler_clock) index_cycle++; //if the
            clock was also reset, this is a new cycle
            if(tempEvent->scaler_ready>50) tempEvent->event_ok=0; //too many triggers at once
            else if(tempEvent->scaler_clock>tempEvent_old->scaler_clock) tempEvent->event_ok=0;
            //no reset of the clock means the triggers were incremented too much
            else if ((tempEvent->scaler_clock<tempEvent_old->scaler_clock)&&((cycle_duration+
                tempEvent->scaler_clock-tempEvent_old->scaler_clock)>10000)) tempEvent->event_ok
                =0; //too much delay between two events
135     else tempEvent->event_ok=1; //OK
        }
        else tempEvent->event_ok=0; //if no increment between two events, fake trigger

        //update acquisition clock
        if(!tempEvent->event_ok)
        {
            tempEvent->acquisition_time=tempEvent_old->acquisition_time+2500;
        }
    }
145     else
    {

```



```

    if(tempEvent->scaler_clock>=tempEvent_old->scaler_clock) tempEvent->acquisition_time=
        tempEvent_old->acquisition_time+tempEvent->scaler_clock-tempEvent_old->
        scaler_clock;
    else if(tempEvent->scaler_clock<tempEvent_old->scaler_clock) tempEvent->
        acquisition_time=tempEvent_old->acquisition_time+cycle_duration+tempEvent->
        scaler_clock-tempEvent_old->scaler_clock+1;
    }

    tempEvent_old=tempEvent;
} //fin du for
return 0;
}
155 //*****Function that checks the measurement cycle
int is397::CycleCheck()
{
    event* tempEvent;
    event* tempEvent_old;
    event* tempEvent_current;
    event* tempEvent_first;
    unsigned int numEntries;
    unsigned int bad_event_index;
    unsigned int good_cycle_nr=0;
    unsigned int total_cycle_nr=0;
165
    numEntries = Events->GetEntriesFast();
    tempEvent = (event*)Events->At(numEntries-1);
    total_cycle_nr=tempEvent->cycle_nr+1;
    printf("\n");
    printf("Checking %d cycles\n",total_cycle_nr);

    tempEvent_first = (event*)Events->At(0);
175 for(unsigned int i=0; i < numEntries; i++)
    {
        tempEvent_current = (event*)Events->At(i);
        if(tempEvent_current->cycle_nr!=tempEvent_first->cycle_nr)
        {
            for(unsigned int i=tempEvent_first->event_nr; i<tempEvent_current->event_nr; i++) //
                loop on events of the cycle to calculate the time in the cycle
                ((event*)Events->At(i))->cycle_time=((event*)Events->At(i))->acquisition_time-
                tempEvent_first->acquisition_time;

            if((tempEvent_current->acquisition_time-tempEvent_first->acquisition_time)>(
                cycle_duration-100000))
185 {
                //printf("cycle %u is complete\n",tempEvent_first->cycle_nr);
                for(unsigned int i=tempEvent_first->event_nr; i<tempEvent_current->event_nr; i++)
                    ((event*)Events->At(i))->cycle_complete=1;
            }
            //else
            //printf("cycle %u misses %u microseconds to be complete\n",tempEvent_first->cycle_nr
            ,cycle_duration-(tempEvent_current->acquisition_time-tempEvent_first->
            acquisition_time));

            tempEvent_first=tempEvent_current;
        }
    }
195 if(!tempEvent_current->event_ok)
    {
        bad_event_index=tempEvent_current->event_nr;
        unsigned int j=tempEvent_first->event_nr;
        tempEvent_current = (event*)Events->At(j); // back to beginning of the cycle
        while((j<numEntries)&&(tempEvent_current->cycle_nr==tempEvent_first->cycle_nr)) //loop
            on events of the cycle to indicate that the cycle is bad
            {
                tempEvent_current->cycle_ok[0]=0;
                tempEvent_current->cycle_ok[1]=bad_event_index;
                j++;
205 if(j<(numEntries-1)) tempEvent_current = (event*)Events->At(j);
            }

        if(tempEvent_current->cycle_nr!=tempEvent_first->cycle_nr)
        {
            for(unsigned int k=tempEvent_first->event_nr; k<tempEvent_current->event_nr; k++) //
                loop on events of the cycle to calculate the time in the cycle
                ((event*)Events->At(k))->cycle_time=((event*)Events->At(k))->acquisition_time-
                tempEvent_first->acquisition_time;

            if((tempEvent_current->acquisition_time-tempEvent_first->acquisition_time)>(

```

```

        cycle_duration - 100000))
    {
215 //printf("cycle %u is complete\n", tempEvent_first->cycle_nr);
        for (unsigned int k=tempEvent_first->event_nr; k<tempEvent_current->event_nr; k++)
            ((event*)Events->At(k)->cycle_complete=1;
        }
        //else
        //printf("cycle %u misses %u microseconds to be complete\n", tempEvent_first->
            cycle_nr, cycle_duration - (tempEvent_current->acquisition_time - tempEvent_first->
            acquisition_time));
    }
    tempEvent_first=tempEvent_current;
    i=j;
    }
225 else
    {
        tempEvent_current->cycle_ok[0]=1;
    }
}

//double checking number of good cycles
printf("-----\n");
printf("Number of good cycles ?\n");
tempEvent_old = (event*)Events->At(0);
235 for (unsigned int i=0; i < numEntries; i++)
    {
        tempEvent = (event*)Events->At(i);
        if (tempEvent->cycle_ok[0] && ((i==0) || (tempEvent->cycle_nr != tempEvent_old->cycle_nr)))
            good_cycle_nr++;
        tempEvent_old=tempEvent;
    }
    printf("%d good cycles over %d cycles\n", good_cycle_nr, total_cycle_nr);
    if ((double) good_cycle_nr / total_cycle_nr < 0.9)
    {
245 cout << "NOT enough statistics" << endl;
        use_ALL_cycles=1;
    }

return 0;
}

//*****Function that writes the histograms to a *.
    root file
int is397::Write(const char * file)
{
255 TFile* f =new TFile(file, "recreate");

    for (int i=0; i < objectsToSave->GetEntriesFast(); i++)
        objectsToSave->At(i)->Write();

    f->Close();
    return 0;
}

/*-----*/
265 class is397_runMn: public is397
{
public:
    is397_runMn();
    ~is397_runMn();

    int Unpack(const char * file);
    int Sort();
275 };

//*****Function that unpacks an event
int is397_runMn::Unpack(const char * file)
{
285 long tempData=0;
    unsigned int index_event=0;
    unsigned int fake_events=0;
    int i=0;
    event * tempEvent;

    printf("Unpacking...\n");
    fflush(stdout);

```

```

data_file = fopen(file,"rb");
if (data_file == NULL)
{
cout << "Error reading file" << endl;
return -1;
}
295
while(!feof(data_file))
{
tempData = ReadWord();
if(tempData == -1)
break;

/* Searching Beginning Of Event*/
if(((unsigned int)tempData) == DATA.W.BOE)
305
{
tempEvent = new event();
tempData = ReadWord();
//Searching for Scaler Header.
if((tempData&WORD.TYPE)==SCA_HEADER)
{
/* Scaler channel 1*/
tempEvent->scaler_trigger=tempData&SCA_EV_COUNTER_24bits;
tempData = ReadWord();

315
/* Scaler channel 2*/
tempEvent->scaler_ready=tempData&SCA_EV_COUNTER_24bits;
tempData = ReadWord();

/* Scaler channel 3*/
tempEvent->scaler_clock=tempData&SCA_EV_COUNTER_26bits;
if (tempEvent->scaler_clock>cycle_duration) cycle_duration=tempEvent->scaler_clock;
//searching for the cycle duration
tempData = ReadWord();

/* Searching for Module Header*/
if((tempData&WORD.TYPE)==MODULEHEADER)
325
{
tempData = ReadWord();
/*TAC*/
if((tempData&WORD.TYPE)==MODULEDATA.WORD)
{
tempEvent->adc_TAC=tempData&MODULEDATA;
tempData = ReadWord();

/*ADC*/
if((tempData&WORD.TYPE)==MODULEDATA.WORD)
335
{
tempEvent->adc_gamma=tempData&MODULEDATA;
tempData = ReadWord(); //reading end of module buffer
if((tempData&WORD.TYPE)==MODULE.EOB)
{
tempData = ReadWord(); //reading end of event after end of module buffer
if(((unsigned int)tempData) == DATA.W.EOE)
{
tempEvent->event_nr = index_event; //first event has index 0
Events->Add(tempEvent);
345
index_event++;
}
}
else
{
//cout<<"no end of event found\n"<<endl;
fake_events++;
delete tempEvent;
continue;
} //end of event
}
}
355
else
{
//cout<<"no end of module buffer found\n"<<endl;
fake_events++;
delete tempEvent;
continue;
} //end of buffer
}
}
else
365
{
//cout<<"missing second ADC channel\n"<<endl;
fake_events++;
delete tempEvent;

```

```

        continue;
    } //ADC channel 2
    }
    else
    {
        //cout<<"missing module content\n"<<endl;
        fake_events++;
        delete tempEvent;
        continue;
    } //ADC channel 1
    }
    else
    {
        //cout<<"Scaler but no module data"<<endl;
        fake_events++;
        delete tempEvent;
        continue;
    } //Module
}
else
{
    //printf("Missing scaler header\n");
    fake_events++;
    delete tempEvent;
    continue;
}
}
}
fclose(data_file);
printf("...done. %u events unpacked. %u fake events deleted.\n", (unsigned int)Events->
    GetEntriesFast(), fake_events);
return 0;
}

//*****Function that sorts events into the various
//*****histograms
int is397_runMn::Sort()
{
    event* tempEvent;
    event* tempEvent_old;
    unsigned int numEntries;
    unsigned int plot_triggers=0;
    unsigned int plot_ready=0;
    unsigned int total_clock=0;

    printf("Filling histograms...\n");
    numEntries = Events->GetEntriesFast();
    tempEvent_old = (event*)Events->At(0);

    for(unsigned int i=0; i < numEntries; i++)
    {
        tempEvent = (event*)Events->At(i);
        if(tempEvent->cycle_ok [0] || use_ALL_cycles)
        {
            //Clock
            if(tempEvent->event_ok)
            {
                if(tempEvent->scaler_clock >= tempEvent_old->scaler_clock) total_clock += tempEvent->
                    scaler_clock - tempEvent_old->scaler_clock;
                else total_clock += cycle_duration + tempEvent->scaler_clock - tempEvent_old->scaler_clock
                    + 1;
            }
            else total_clock += 2500; //when the event is wrong, one adds an average delay of 2500
                microseconds between two events

            //update live clock
            tempEvent->live_time = total_clock;

            if((total_clock/time_unit_in_micros) > (prev_clock/time_unit_in_micros))
            {
                clockPlot->Fill(total_clock/time_unit_in_micros);
                prev_clock = total_clock;
            }

            //Update triggers
            if(tempEvent->event_ok)
            {
                if(tempEvent->scaler_ready > tempEvent_old->scaler_ready)
                {
                    plot_triggers = tempEvent->scaler_trigger - tempEvent_old->scaler_trigger;

```

```

        plot_ready=tempEvent->scaler_ready-tempEvent_old->scaler_ready;
    }
445  else
    {
        plot_triggers=tempEvent->scaler_trigger+1;
        plot_ready=tempEvent->scaler_ready+1;
    }
    }
    else
    {
455  plot_triggers=1;
        plot_ready=1;
    }

    triggers->Fill(10,plot_triggers);
    triggers->Fill(20,plot_ready);

    //Check multiple counting
    rebond_trigger->Fill(plot_triggers);
    rebond_accepted->Fill(plot_ready);

    //TAC
465  TAC->Fill(tempEvent->adc.TAC);

    //Gamma spectrum
    gamma->Fill(coef[0]*(tempEvent->adc.gamma+(double)rand()/RANDMAX)+coef[1]);
    //Coincidence spectrum
    if((tempEvent->adc.TAC>=gate[0])&&(tempEvent->adc.TAC<=gate[1])) coincidence->Fill(
        coef[0]*(tempEvent->adc.gamma+(double)rand()/RANDMAX)+coef[1]);
    }
    tempEvent_old=tempEvent;
    }
    return 0;
475 }

/*-----*/
class is397_61Mn : public is397_runMn
{
    public:
    is397_61Mn();
    ~is397_61Mn();

485  int SortDecay();

    private:
    TH1D* beta_Mn;
    TH1D* beta_Fe;
    TH1D* betacycle_Fe;
    TH1D* corrected_beta_Mn;
    TH1D* corrected_beta_Fe;
};

495 //*****Function that sorts events into the decay
    histograms of 61Mn and 61Fe
    int is397_61Mn::SortDecay()
    {
        event* tempEvent;
        event* tempEvent_old;
        unsigned int numEntries;
        int Mn_gate=0;
        int Fe_gate=0;
        unsigned int plot_triggers=0;
        unsigned int plot_ready=0;
505  unsigned int total_clock=0;

        printf("Filling decay histograms...\n");
        numEntries = Events->GetEntriesFast();

        tempEvent_old = (event*)Events->At(0);

        for(unsigned int i=0; i < numEntries; i++)
        {
            tempEvent = (event*)Events->At(i);
515  if((tempEvent->cycle_ok[0]||use_ALL_cycles)&&tempEvent->cycle_nr)
            {
                //Clock
                if(tempEvent->event_ok)
                {

```

```

    if(tempEvent->scaler_clock>=tempEvent_old->scaler_clock) total_clock+=tempEvent->
        scaler_clock-tempEvent_old->scaler_clock;
    else total_clock+=cycle_duration+tempEvent->scaler_clock-tempEvent_old->scaler_clock
        +1;
}
else total_clock+=2500;
525 //update live clock
tempEvent->live_time=total_clock;

if((total_clock/time_unit_in_micros)>(prev_clock/time_unit_in_micros))
{
    clockPlot->Fill(total_clock/time_unit_in_micros);
    prev_clock=total_clock;
}

535 //Update triggers
if(tempEvent->event_ok)
{
    if(tempEvent->scaler_ready>tempEvent_old->scaler_ready)
    {
        plot_triggers=tempEvent->scaler_trigger-tempEvent_old->scaler_trigger;
        plot_ready=tempEvent->scaler_ready-tempEvent_old->scaler_ready;
    }
    else
545 {
        plot_triggers=tempEvent->scaler_trigger+1;
        plot_ready=tempEvent->scaler_ready+1;
    }
}
else
{
    plot_triggers=1;
    plot_ready=1;
}

555 triggers->Fill(10,plot_triggers);
triggers->Fill(20,plot_ready);

//Check multiple counting
rebond_trigger->Fill(plot_triggers);
rebond_accepted->Fill(plot_ready);

//TAC
TAC->Fill(tempEvent->adc_TAC);

565 //Gamma spectrum
gamma->Fill(coef[0]*(tempEvent->adc_gamma+(double)rand()/RANDMAX)+coef[1]);

//Coincidences only
if(((tempEvent->adc_TAC>=gate[0])&&(tempEvent->adc_TAC<=gate[1])))
{
    coincidence->Fill(coef[0]*(tempEvent->adc_gamma+(double)rand()/RANDMAX)+coef[1]);
    //Checking Mn gate
    if(((tempEvent->adc_gamma>=435)&&(tempEvent->adc_gamma<455))||((tempEvent->adc_gamma
        >=1220)&&(tempEvent->adc_gamma<1245))) Mn_gate=1;
    //Checking Fe gate
575 if(((tempEvent->adc_gamma>=273)&&(tempEvent->adc_gamma<293))||((tempEvent->adc_gamma
        >=605)&&(tempEvent->adc_gamma<625))||((tempEvent->adc_gamma>=1965)&&(tempEvent->
        adc_gamma<1990))||((tempEvent->adc_gamma>=2298)&&(tempEvent->adc_gamma<2320))
        ||((tempEvent->adc_gamma>=3118)&&(tempEvent->adc_gamma<3148))) Fe_gate=1;

    //Update beta_Mn
    if(Mn_gate) corrected_beta_Mn->Fill(tempEvent->cycle_time/time_unit_in_10micros);

    if(Fe_gate)
    {
        //Update beta_Fe
        corrected_beta_Fe->Fill(tempEvent->cycle_time/time_unit_in_10micros);
        //Update betacycle_Fe
585 betacycle_Fe->Fill(tempEvent->cycle_nr);
    }
}
tempEvent_old=tempEvent;
Mn_gate=0;
Fe_gate=0;
}

return 0;

```

```

595 }
/*-----*/
int main(int argc, char ** argv)
{
char* LMD_filename=(char*) malloc(60*sizeof(char*));
char* ROOT_filename=(char*) malloc(60*sizeof(char*));
int mycase=0;
605 if(argc < 2)
{
printf("Wrong input, usage: %s <path to data file without .lmd extension>\n",argv[0]);
return 0;
}

if((argv[1][0]=='c')&&(argv[1][1]=='a')&&(argv[1][2]=='1')) mycase=1;
else if((argv[1][0]=='m')&&(argv[1][1]=='n')&&(argv[1][2]=='6')&&(argv[1][3]=='1')) mycase
=2;

sprintf(LMD_filename, "%s.lmd", argv[1]);
615 sprintf(ROOT_filename, "%s.root", argv[1]);

ifstream input_file (LMD_filename);
if (input_file.is_open())
{
switch(mycase)
{
case 1 : {
//cout<<"It is a calibration file !\n"<<endl;
625 is397_runMn test_calib;
test_calib.Unpack(LMD_filename);
test_calib.EventCheck();
test_calib.CycleCheck();
test_calib.Sort();
test_calib.Write(ROOT_filename);
}
break;

case 2 : {
//cout<<"It is a run file !\n"<<endl;
635 is397_61Mn test_61;
test_61.Unpack(LMD_filename);
test_61.EventCheck();
test_61.CycleCheck();
test_61.SortDecay();
test_61.Write(ROOT_filename);
}
break;
}
}

645 input_file.close();
}

cout<< "Ending CreateHisto routine" << endl;

return 0;
}

```

A.2.2 Fitting the coincidence spectra with the FitHisto.cpp routine

The FitHisto.cpp routine reads the *.root file produced by CreateHisto.cpp and the corresponding *.txt libraries to fit the (beta-gated) gamma spectra with gaussian peaks. As the rough counts are Poisson-like distributed, errors are estimated from the log likelihood. Results of the fit are written to a Fit_*.txt file with the measurement time and the dead time.

A.2.3 Sorting the results with the Analyze.cpp routine

The Analyze.cpp routine calculates activities and efficiencies from the reported calibration source activities or yields and from the Fit_*.txt file. In the case of calibration measurements, efficiencies are fitted as in Figure 1.14 and a calib_param.txt file is produced with the parameters of the gamma calibration fitting curve. For other data, the existing calib_param.txt file is read to calculate charge bred efficiencies. In all cases, results are sorted versus the parameters of interest and plotted in a Plot_*.root file.

The combination of those three programs allowed an efficient sorting and analysis of the numerous data files, especially for the experiment with the charge breeding of isobars. In the case of the daughter nuclide trapping experiment, the ^{61}Mn and ^{61}Fe decay plots were independently fitted with the Origin software which allowed more flexibility to define fitting equations and parameters.

Appendix B

Beam calculations for the new mass and energy separator

A quick overview on the available equipment is given in section B.1. Then the routines used in COSY INFINITY to calculate the optimal positions of the beamline elements are detailed, and the beam separation is simulated with a program in Matlab. Finally, a control system was started to test the various power supplies performances.

B.1 Available beamline elements

Elements available from the dismantlement of Lund AMS setup are listed below in Table B.1. For the following beam calculations with COSY INFINITY, one used the correct specifications from the manufacturer for the magnetic and electrostatic sectors (Table B.2), and measured dimensions for the quadrupole triplets (Figure B.1).

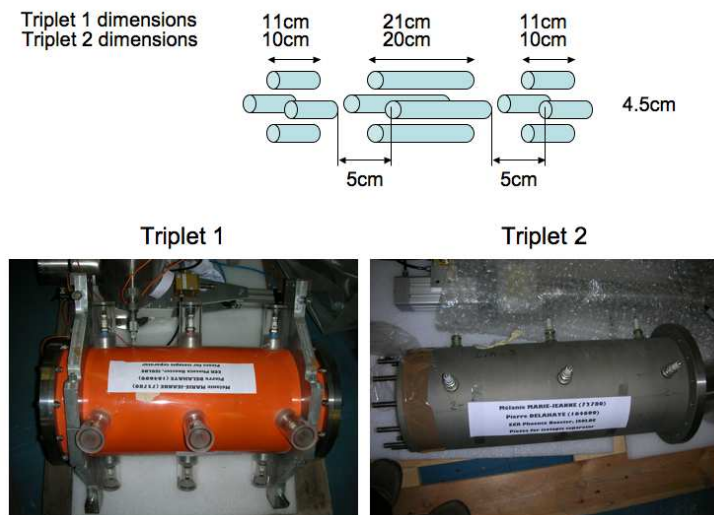


Figure B.1: Triplets measured dimensions.



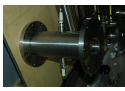
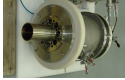





	Element	Item
	Magnetic bender	x1
	Electrostatic bender	x1
	Electrostatic quadrupole triplet	x2
	Electrostatic steerer	x1
	Sputter ion source	x1
	Faraday Cup	x2
	Slits	x2
	Cryopump	x2
	Compressor	x2
	Vacuum valve	x2

Table B.1: List of elements available for the separator.

Magnetic bender		Electrostatic bender	
Danfysik reference	98234	Danfysik reference	HOL 3555
Deflection angle	90°	Bending angle	90°
Bending radius	373.5 mm	Bending radius	435 mm
Induction	1.2 T	Field strength	4.6 kV/cm
Entrance angle	28.2°	Plate height	160 mm
Exit angle	28.2°	Effective length	683 mm
Pole gap	48 mm	Plate separation	43.5 mm
Nominal voltage	35 V		
Nominal current	159 A	Voltage	± 10kV
Waterflow rate	6.5 L/min	Plate material	stainless steel
Pressure drop	3 bar	Plate shape	spherical
Temperature rise	10 °C		
Total weight	1401 kg		
Manufactured in	1998	Manufacture year	1993

Table B.2: Specifications of the new magnetic and electrostatic sectors as given by the manufacturer (Danfysik).

B.2 Transfer matrices with COSY INFINITY

For a reference particle of velocity v_0 , of motion quantity p_0 , of kinetic energy K_0 , of mass m_0 and of flight time t_0 , one defines an ion with the following set of coordinates:

$$\begin{pmatrix} x \\ a = p_x/p_0 \\ y \\ b = p_y/p_0 \\ l = v_0 \cdot (t - t_0) \\ d = (K - K_0)/K_0 \\ g = (m - m_0)/m_0 \end{pmatrix}$$

where x and y are the positions according to the x and y axes on the plane perpendicular to the optical system axis, p_x and p_y are the projections of the ion motion quantity on the x and y axes, t is the flight time, K is the kinetic energy and m the mass of the ion. The COSY INFINITY program can calculate transfer matrices depending on the specified parameters: here the kinetic energy K , mass m and charge q of the ion. The parameters should be indicated in the input coordinates as deviations from the kinetic energy, mass and charge of the reference particle.

$$\begin{pmatrix} \langle x|x \rangle & \langle x|a \rangle & \langle x|y \rangle & \langle x|b \rangle & \langle x|t \rangle \\ \langle a|x \rangle & \langle a|a \rangle & \langle a|y \rangle & \langle a|b \rangle & \langle a|t \rangle \\ \langle y|x \rangle & \langle y|a \rangle & \langle y|y \rangle & \langle y|b \rangle & \langle y|t \rangle \\ \langle b|x \rangle & \langle b|a \rangle & \langle b|y \rangle & \langle b|b \rangle & \langle b|t \rangle \\ \langle K|x \rangle & \langle K|a \rangle & \langle K|y \rangle & \langle K|b \rangle & \langle K|t \rangle \\ \langle m|x \rangle & \langle m|a \rangle & \langle m|y \rangle & \langle m|b \rangle & \langle m|t \rangle \\ \langle q|x \rangle & \langle q|a \rangle & \langle q|y \rangle & \langle q|b \rangle & \langle q|t \rangle \end{pmatrix}$$

Values for currents or fields are not calculated by the program. More information about the algorithm for matrix elements calculations can be found in [147, 148].

The following M_T_T_E_T.fox program contains third order fitting routines to optimize the distances between elements for a five-element beamline. A magnetic analyzer is followed by two triplets, then by an electrostatic analyzer either in a Z or in a U fashion. This constitutes the spectrometer. A triplet is added after the setup. If the beam is perfectly symmetrical in X and Y after the first triplet, one can add an angle to the vertical plane that contains the upper stage of the separator. The calculations take into account chromatic effects. One aims at minimizing the non-diagonal terms of the matrix.

```

INCLUDE 'C:\COSY\COSY';
PROCEDURE RUN;

{*****}
{* VARIABLES *}
{*****}
8 VARIABLE MENU 1;
  VARIABLE CHOICE 1;
  VARIABLE X 1; VARIABLE A 1; VARIABLE M 1;
  {Beam half width, Beam half angle, Magnification between x & y focii}
  VARIABLE V1TRIP1 1; VARIABLE V2TRIP1 1; VARIABLE V3TRIP1 1;
  VARIABLE V1TRIP1bis 1; VARIABLE V2TRIP1bis 1; VARIABLE V3TRIP1bis 1;
  VARIABLE V1TRIP2 1; VARIABLE V2TRIP2 1; VARIABLE V3TRIP2 1;
  VARIABLE D_ES_b 1; VARIABLE D_ES_a 1;
  VARIABLE D_TRIP1_b 1; VARIABLE D_TRIP1_a 1;
  VARIABLE D_TRIP1bis_b 1; VARIABLE D_TRIP1bis_a 1;
  18 VARIABLE D_TRIP2_b 1; VARIABLE D_TRIP2_a 1;
  VARIABLE D_MS_b 1; VARIABLE D_MS_a 1;
  VARIABLE DL1 1; VARIABLE DL2 1; VARIABLE DL3 1; VARIABLE DL4 1;
  VARIABLE DL5 1; VARIABLE DL6 1;
  VARIABLE ELEMALONE 1;
  VARIABLE ZMODE 1;
  VARIABLE MASS 1; VARIABLE CHARGE 1; VARIABLE POTENTIAL 1;
  VARIABLE SECT1 1000 8; VARIABLE SECT2 1000 8; VARIABLE SECT3 1000 8;
  VARIABLE SECTSEP 1000 8; VARIABLE SECTALL 1000 8;
  28 {*****}
  {* END OF VARIABLES *}
  {*****}

  {*****}
  {* PROCEDURES *}
  {*****}
  38 PROCEDURE TRIPLET_GREY VA VB VC;
    EQ 0.1 -VA .0225; {FIRST QUADRUPOLE}
    DL 0.05;
    EQ 0.2 VB .0225; {SECOND QUADRUPOLE}
    DL 0.05;
    EQ 0.1 -VC .0225; {THIRD QUADRUPOLE}
  ENDPROCEDURE;

  PROCEDURE TRIPLET_ORANGE VA VB VC;
    EQ 0.11 -VA .0225; {FIRST QUADRUPOLE}
    DL 0.05;

```

```

EQ 0.21 VB .0225;{SECOND QUADRUPOLE}
DL 0.05;
EQ 0.11 -VC .0225;{THIRD QUADRUPOLE}
48  ENDPROCEDURE;

{*****}
{*  MAIN INITIALIZATION                               *}
{*****}
PROCEDURE INITIALIZE;
  {defines the beam}
  OV 3 3 3; {order 3, phase space dim 3, # of parameters 3}
  RP POTENTIAL*CHARGE*PARA(1) MASS*PARA(2) CHARGE*PARA(3);
  {kinetic energy 30 keV, mass 16 amu, charge 5}
58  SB X A 0 X*M A/M 0 0 0 0 0;
  {sets half width of the beam in the
  x, a, r12, y, b, r34, t, d, r56, g, z directions}
  UM; {sets map to unity}
  CR ; {clears all the rays previously set}
  SCDE; {plots the envelope and the dispersive rays}
  ENDPROCEDURE;

{*****}
{*  END OF MAIN INITIALIZATION                       *}
{*****}
68  PROCEDURE PLOT;
  PG -101 -102;
  ENDPROCEDURE;

PROCEDURE TRACK_ES_BENDER;
  {plot the electrostatic bender and its action on the beam}
  PS 0.0065; {focal plane of 0.0065m width}
  DL D_ES_b; {drift of length D_ES_b m}
  ES 0.435 90 0.02175 2 -3 4 -5 6;
78  {radius 435 mm, angle 90, aperture 21.75 mm, parameters for spherical plate}
  DL D_ES_a; {drift of length D_ES_a m}
  PS 0.0065; {focal plane of 0.0065m width}
  ENDPROCEDURE;

PROCEDURE TRACK_MS_BENDER;
  PS 0.0065; {focal plane of 0.0065m width}
  DL D_MS_b; {drift of length D_MS_b m}
  DI 0.3735 90 0.024 28.2 0 28.2 0; {angle 28.2}
  { radius 373.5 mm, angle 90, aperture 24 mm, entrance/exit angle 28.2}
88  DL D_MS_a; {drift of length D_MS_a m}
  PS 0.0065; {focal plane of 0.0065m width}
  ENDPROCEDURE;

PROCEDURE TRACK_TRIPLET1;
  PS 0.0065; {focal plane of 0.0065m width}
  DL D_TRIP1_b; {drift of length D_TRIP1_b m}
  TRIPLET_GREY V1TRIP1 V2TRIP1 V3TRIP1;
  DL D_TRIP1_a; {drift of length D_TRIP1_a m}
98  PS 0.0065; {focal plane of 0.0065m width}
  ENDPROCEDURE;

PROCEDURE TRACK_TRIPLET2;
  PS 0.0065; {focal plane of 0.0065m width}
  DL D_TRIP2_b; {drift of length D_TRIP2_b m}
  TRIPLET_ORANGE V1TRIP2 V2TRIP2 V3TRIP2;
  DL D_TRIP2_a; {drift of length D_TRIP2_a m}
  PS 0.0065; {focal plane of 0.0065m width}
  ENDPROCEDURE;

108  PROCEDURE TRACK_TRIPLET1bis;
  PS 0.0065; {focal plane of 0.0065m width}
  DL D_TRIP1bis_b; {drift of length D_TRIP1bis_b m}
  TRIPLET_GREY V1TRIP1bis V2TRIP1bis V3TRIP1bis;
  DL D_TRIP1bis_a; {drift of length D_TRIP1bis_a m}
  PS 0.0065; {focal plane of 0.0065m width}
  ENDPROCEDURE;

PROCEDURE TRACK;
  {plot the elements and their action on the beam}
118  INITIALIZE;
  BP; {begin to plot here}

{*****}
{*  BEAM LINE                                       *}
{*****}
  TRACK_MS_BENDER;
  TRACK_TRIPLET1;

```

```

TRACK_TRIPLET1bis;
IF ZMODE=1; CB; ENDIF;
TRACK_ES.BENDER;
128 TRACK_TRIPLET2;
{*****}
{* END OF BEAM LINE *}
{*****}
EP; {end plotting here}
{output is the picture}
PLOT;
ENDPROCEDURE;

138 {*****}
{* STEP-BY-STEP OPTIMIZATION *}
{*****}
PROCEDURE STEP_ONE;
VARIABLE D1 1 ; VARIABLE D2 1 ; VARIABLE OBJ 1 ;
VARIABLE X_DEV 1; VARIABLE CROSS_DEV 1;
WRITE 6
' Fitting a magnetic bender to perform stigmatic imaging by '
' adjusting the distance after using the Simplex algorithm';
D1:=D_MS.b; D2:=D_MS.a;
148 FIT D1 D2;
D_MS.b:=D1;
D_MS.a:=D2;
INITIALIZE;
BP;
TRACK_MS.BENDER;
EP;
PLOT;
X_DEV:=ABS(MA(1,1)-1)+ABS(MA(3,3)-1);
CROSS_DEV:=ABS(MA(1,2))+ABS(MA(3,4))+ABS(MA(2,1))+ABS(MA(4,3)) ;
OBJ := X_DEV + CROSS_DEV;
158 ENDFIT 1E-4 10000 1 OBJ ;
WRITE 6
' Distance D_MS.b D_MS.a'
(' Objective Function:' &SF(D_MS.b,'(F6.3)')&SF(D_MS.a,'(F6.3)')&S(OBJ));
PM 6 ;
ENDPROCEDURE;

PROCEDURE STEP.TWO;
VARIABLE D1 1 ; VARIABLE D2 1 ; VARIABLE VOLT1 1; VARIABLE VOLT2 1;
168 VARIABLE VOLT3 1;
VARIABLE OBJ 1 ;
WRITE 6 ' '
' Fitting a quadrupole triplet to perform stigmatic imaging by adjusting '
' various parameters using the Simplex algorithm' ' ' ;
D1:=D_TRIP1.b; D2:=D_TRIP1.a; VOLT1:=V1TRIP1; VOLT2:=V2TRIP1;
VOLT3:=V3TRIP1;{minimum 0.670 pour D_TRIP1.b}
FIT D1 {D2} VOLT1 VOLT2 {VOLT3};
D_TRIP1.b:=D1; D_TRIP1.a:=D1;V1TRIP1:=VOLT1; V2TRIP1:=VOLT2;
V3TRIP1:=VOLT1;
178 INITIALIZE;
BP;
IF ELEM.ALONE=0;
TRACK_MS.BENDER;
ENDIF;
TRACK_TRIPLET1;
EP;
PLOT;
OBJ := ABS(MA(1,2))+ABS(MA(3,4))+ABS(MA(1,1)-1)+ABS(MA(3,3)-1);
ENDFIT 1E-4 10000 1 OBJ ;
WRITE 6 ' '
188 ' Quad distance D_TRIP1.b, D_TRIP1.a'
(' Objective Function:' &SF(D_TRIP1.b,'(F6.3)')&SF(D_TRIP1.a,'(F6.3)'));
WRITE 6 ' '
' Quad voltage V1TRIP1, V2TRIP1, V3TRIP1'
(' Objective Function:' &SF(V1TRIP1,'(F6.3)')&SF(V2TRIP1,'(F6.3)')
&SF(V3TRIP1,'(F6.3)'));
WRITE 6 ' '
(' Fit precision' &S(OBJ));
PM 6 ;
ENDPROCEDURE;
198
PROCEDURE STEP.THREE;
VARIABLE D1 1 ; VARIABLE D2 1 ; VARIABLE VOLT1 1; VARIABLE VOLT2 1;
VARIABLE VOLT3 1;
VARIABLE OBJ 1 ;
WRITE 6 ' '
' Fitting a quadrupole triplet to perform stigmatic imaging by adjusting '

```

```

' various parameters using the Simplex algorithm' ' ' ;
D1:=D-TRIP1bis_b; D2:=D-TRIP1bis_a; VOLT1:=V1TRIP1bis; VOLT2:=V2TRIP1bis;
VOLT3:=V3TRIP1bis;{minimum 0.670 pour D-TRIP1_b}
208 FIT D1 {D2} VOLT1 VOLT2 {VOLT3};
      D-TRIP1bis_b:=D1; D-TRIP1bis_a:=D1;
      V1TRIP1bis:=VOLT1; V2TRIP1bis:=VOLT2;
      V3TRIP1bis:=VOLT1;
      INITIALIZE;
      BP;
      IF ELEMALONE=0;
      TRACK_MS.BENDER;
      TRACK_TRIPLET1;
      ENDIF;
218 TRACK_TRIPLET1bis;
      EP;
      PLOT;
      OBJ := ABS(MA(1,2))+ABS(MA(3,4))+ABS(MA(1,1)-1)+ABS(MA(3,3)-1);
      ENDFIT 1E-4 10000 1 OBJ ;
      WRITE 6 ' '
      ' Quad distance D-TRIP1bis_b, D-TRIP1bis_a'
      (' Objective Function:' &SF(D-TRIP1bis_b, '(F6.3)')
      &SF(D-TRIP1bis_a, '(F6.3)'));
      WRITE 6 ' '
228 ' Quad voltage V1TRIP1bis, V2TRIP1bis, V3TRIP1bis'
      (' Objective Function:' &SF(V1TRIP1bis, '(F6.3)')&SF(V2TRIP1bis, '(F6.3)')
      &SF(V3TRIP1bis, '(F6.3)'));
      WRITE 6 ' '
      (' Fit precision' &S(OBJ));
      PM 6 ;
      ENDPROCEDURE;

PROCEDURE STEP_FOUR;
VARIABLE D1 1 ; VARIABLE D2 1 ;
238 VARIABLE OBJ 1 ;
      WRITE 6 ' '
      ' Fitting an electrostatic bender to perform stigmatic imaging by '
      ' adjusting the distances before and after using the Simplex algorithm';
      D1:=D-ES_b; D2:=D-ES_a;
      FIT D1 D2;
      D-ES_b:=D1; D-ES_a:=D2;
      INITIALIZE;
      BP;
248 IF ELEMALONE=0;
      TRACK_MS.BENDER;
      TRACK_TRIPLET1;
      TRACK_TRIPLET1bis;
      ENDIF;
      IF ZMODE=1; CB; ENDIF;
      TRACK_ES.BENDER;
      EP;
      PLOT;
      OBJ := ABS(MA(1,2))+ABS(MA(3,4))+ABS(MA(1,1)-1)+ABS(MA(3,3)-1);
      ENDFIT 1E-4 10000 1 OBJ ;
258 WRITE 6 ' '
      ' Electrostatic bender distances D-ES_b, D-ES_a'
      (' Objective Function:' &SF(D-ES_b, '(F6.3)')&SF(D-ES_a, '(F6.3)'));
      {WRITE 6 ' '
      (' Fit precision' &S(OBJ));}
      PM 6 ;
      ENDPROCEDURE;

PROCEDURE STEP_FIVE;
VARIABLE D1 1 ; VARIABLE D2 1 ; VARIABLE VOLT1 1; VARIABLE VOLT2 1;
268 VARIABLE VOLT3 1;
VARIABLE OBJ 1 ;
      WRITE 6 ' '
      ' Fitting a quadrupole triplet to perform stigmatic imaging by adjusting '
      ' various parameters using the Simplex algorithm' ' ' ;
      D1:=D-TRIP2_b; D2:=D-TRIP2_a; VOLT1:=V1TRIP2; VOLT2:=V2TRIP2;
      {VOLT3:=V3TRIP2;}
      FIT {D1 D2} VOLT1 VOLT2 {VOLT3};
      D-TRIP2_b:=D1; D-TRIP2_a:=D1; V1TRIP2:=VOLT1; V2TRIP2:=VOLT2;
      V3TRIP2:=VOLT1;
278 INITIALIZE;
      BP;
      IF ELEMALONE=0;
      TRACK_MS.BENDER;
      TRACK_TRIPLET1;
      TRACK_TRIPLET1bis;
      IF ZMODE=1; CB; ENDIF;

```



```

                TRACK_ES_BENDER;
                ENDFIT;
                TRACK_TRIPLET2;
288      EP;
                PLOT;
                OBJ := ABS(MA(1,2))+ABS(MA(3,4))+ABS(MA(1,1)-1)+ABS(MA(3,3)-1);
                ENDFIT 1E-4 10000 1 OBJ ;
                WRITE 6 ' '
                ' Quad distance D_TRIP2_b, D_TRIP2_a'
                (' Objective Function:' &SF(D_TRIP2_b, '(F6.3)')&SF(D_TRIP2_a, '(F6.3)'));
                WRITE 6 ' '
                ' Quad voltage V1TRIP2, V2TRIP2, V3TRIP2'
298      (' Objective Function:' &SF(V1TRIP2, '(F6.3)')&SF(V2TRIP2, '(F6.3)')&
                SF(V3TRIP2, '(F6.3)'));
                WRITE 6 ' '
                (' Fit precision' &S(OBJ));
                PM 6 ;
                ENDPROCEDURE;

                PROCEDURE OPTIMIZE;
                VARIABLE GO_ON 1; VARIABLE STEPNUM 1;
                GO_ON:=1; STEPNUM:=0;
                WRITE 6 'NEXT STEP or STOP ? TYPE 1 or 0';
308      WHILE (GO_ON#0)*(STEPNUM<5);
                IF STEPNUM=0; STEP_ONE;
                ELSEIF STEPNUM=1; STEP_TWO;
                ELSEIF STEPNUM=2; STEP_THREE;
                ELSEIF STEPNUM=3; STEP_FOUR;
                ELSEIF STEPNUM=4; STEP_FIVE;
                ENDFIT;
                STEPNUM:=STEPNUM+1;
                WRITE 6 'THEN ?';
                READ 5 GO_ON;
318      ENDWHILE;
                ENDPROCEDURE;

                {*****}
                {* END OF STEP-BY-STEP OPTIMIZATION *}
                {*****}

                {*****}
                {* 2-SECTION OPTIMIZATION *}
                {*****}
                PROCEDURE FIRST_SECTION;
                INITIALIZE;
328      BP;
                TRACK_MS_BENDER;
                TRACK_TRIPLET1;
                EP;
                PLOT;
                SM SECT1;
                ENDPROCEDURE;

                PROCEDURE SECOND_SECTION;
                INITIALIZE;
338      BP;
                TRACK_TRIPLET1bis;
                TRACK_ES_BENDER;
                EP;
                MT MAP SECT2 0;
                AM SECT2;
                PLOT;
                ENDPROCEDURE;

                PROCEDURE THIRD_SECTION;
                INITIALIZE;
348      BP;
                TRACK_TRIPLET2;
                EP;
                MT MAP SECT3 0;
                AM SECT3;
                PLOT;
                ENDPROCEDURE;

                PROCEDURE SEPARATOR_SECTION;
                INITIALIZE;
358      BP;
                TRACK_MS_BENDER;
                TRACK_TRIPLET1;
                TRACK_TRIPLET1bis;

```

```

        TRACK_ES_BENDER;
        EP;
        ANM SECT1 SECT2 SECTSEP;
        AM SECTSEP;
        PLOT;
368  ENDPROCEDURE;

PROCEDURE ALL_SECTIONS;
INITIALIZE;
        BP;
        TRACK_MS_BENDER;
        TRACK_TRIPLET1;
        TRACK_TRIPLET1bis;
        TRACK_ES_BENDER;
378  TRACK_TRIPLET2;
        EP;
        ANM SECTSEP SECT3 SECTALL;
        AM SECTALL;
        PLOT;
ENDPROCEDURE;

PROCEDURE SECTION;
VARIABLE GO_ON 1; VARIABLE STEPNUM 1;
GO_ON:=1; STEPNUM:=0;
388  WRITE 6 'NEXT STEP or STOP ? TYPE 1 or 0';
        WHILE (GO_ON#0)*(STEPNUM<5);
                IF STEPNUM=0; FIRST_SECTION;
                        ELSEIF STEPNUM=1; SECOND_SECTION;
                        ELSEIF STEPNUM=2; THIRD_SECTION;
                        ELSEIF STEPNUM=3; SEPARATOR_SECTION;
                        ELSEIF STEPNUM=4; ALL_SECTIONS;
                        ENDIF;
                STEPNUM:=STEPNUM+1;
                WRITE 6 'THEN ?';
                READ 5 GO_ON;
398  ENDWHILE;
ENDPROCEDURE;

{*****}
{* END OF 2-SECTION OPTIMIZATION *}
{*****}

{*****}
{* END OF PROCEDURES *}
{*****}

408 {*****}
{* VARIABLES INITIALIZATION *}
{*****}
X:=0.0065; A:=0.002; M:=1; {6.5mm, 18mrad, magnification 1}
ELEMALONE:=0;
Z.MODE:=0;
MASS:=16; CHARGE:=5; POTENTIAL:=0.03;
D_ES_b:=0.437; D_ES_a:=0.437;
D_MS_b:=0.9; D_MS_a:=0.7;
418 D_TRIP1_b:=0.158; D_TRIP1_a:=0.158;
        D_TRIP1bis_b:=0.158; D_TRIP1bis_a:=0.158;
        D_TRIP2_b:=0.158; D_TRIP2_a:=0.158;
        V1TRIP1:=0.82; V2TRIP1:=0.62; V3TRIP1:=0.95;
        V1TRIP1bis:=0.8; V2TRIP1bis:=0.60; V3TRIP1bis:=0.8;
        V1TRIP2:=0.7; V2TRIP2:=0.6; V3TRIP2:=0.7;

{*****}
{* END OF VARIABLES INITIALIZATION *}
{*****}

428 {*****}
{* MENU *}
{*****}
OPENF 7 'C:\COSY\M_T_T_E_T.OUT' 'UNKNOWN' ;

MENU := 1 ; WHILE MENU#99 ;
WRITE 6 ' ' ;
        ' COSY INFINITY M_T_T_E_T '
        ' _____ '
        ' Please choose action '
        ' 1: Enter a beam characteristics '
438  ' 2: Enter an analyzer setup (default is U_mode)'
        ' 99: Quit ' ;
READ 5 MENU ;
IF MENU=99 ; QUIT 0 ;

```

```

ELSEIF MENU=1 ;
    WRITE 6 '      Enter atomic mass in AMU';
    READ 5 MASS;
    WRITE 6 '      Enter charge state in units';
    READ 5 CHARGE;
448    WRITE 6 '      Enter potential energy in MeV';
    READ 5 POTENTIAL;
ELSEIF MENU=2 ;
    WRITE 6 '      Enter analyzer type U(=0) or Z(=1)';
    READ 5 ZMODE;
ENDIF ;
    INITIALIZE;

CHOICE := 1 ; WHILE CHOICE#4;
458    WRITE 6
    '      M_T_T_E_T TUNING      '
    '      ====='
    '      Please choose action'
    '      1: Plot last result'
    '      2: Step-by-step optimization'
    '      3: Rotated sections calculation'
    '      4: Back to first menu' ;
    READ 5 CHOICE ;
    IF CHOICE=1 ; TRACK;
468    ELSEIF CHOICE=2 ; OPTIMIZE;
    ELSEIF CHOICE=3 ; SECTION;
    ENDF ;
ENDWHILE ;

ENDWHILE ;
{*****}
{* END OF MENU *}
{*****}
CLOSEF 7 ;
478 ENDPROCEDURE;
RUN;
END;

```

B.3 Ion distribution with Matlab

Programs were written in Matlab to simulate a gaussian ion beam distribution through the previously calculated matrixes. The ions can have different masses, charges or energies, given as full deviations from a reference ion. The example of a program to simulate the beam through the magnetic bender is given below. Other routines allowed to simulate the electrostatic bender or the successive steps of mass and energy separation, using various slits opening at the focal planes.

```

function plot_M_bender
%The user chooses the number of particles for each distribution
dim=input('Number of particles ? ');
if isempty(dim)
    dim = 10;
end
%The user chooses the number of A/Q distributions
8 dim_AQ=input('How many A/Q ? ');
if isempty(dim_AQ)
    dim_AQ = 1;
end
AQ_in=zeros(dim_AQ,2);
RefA=input('Enter A ref (AMU): ');
RefQ=input('Enter Q ref (units): ');
for i=1:dim_AQ
    AQ_in(i,1)=input(sprintf('Enter A %d (AMU): ',i));
    AQ_in(i,2)=input(sprintf('Enter Q %d (units): ',i));
18 end
%The user chooses the number of energy distributions
dim_E=input('How many potential energies ? ');
if isempty(dim_E)
    dim_E = 1;
end

```

```

end
E_in=zeros(dim_E,1);
RefE=input('Enter ref potential(MeV): ');
for i=1:dim_E
    E_in(i,1)=input(sprintf('Enter E %d (MeV): ',i));
28 end

Dinit=e_init(dim, dim_AQ, AQ_in, dim_E, E_in, RefE, RefA, RefQ);

%The user choses between a study of mass separation and a study of energy
%separation
choice=input('Mass (0) or energy (1) study ? For both type (2)');
if isempty(choice)
    choice = 0;
end
38 %The user choses the type of the separation setup
reply=input('U(=0) or Z(=1) separation ? ');
if isempty(reply)
    reply = 0;
end

%Calculations of the transformations on the beam
[tMb, tSys]=elem(reply);
[tDMb, tDSys]=distributions(Dinit, tMb, tSys, dim, dim_AQ, dim_E);
48 [tFoc2D, tFin2D]=plot_AQ_or_E(Dinit, tDMb, tDSys, dim_AQ, dim_E, choice, dim);

end %end of main function
%-----
%Subfunction to initialize the program.
function Dinit=initialize(dim, E0, M0, Z0, RefE, RefA, RefQ)
% Simple initialization
Ein=E0;
Min=M0;
Zin=Z0;
58 % Random coordinates initialization
randn('state',sum(100*clock));
RXin=normrnd(0,0.004/2.3548,dim,1);
RYin=normrnd(0,0.004/2.3548,dim,1);
RAin=((Min)/(RefA))*normrnd(0,0.001/2.3548,dim,1);
RBin=((Min)/(RefA))*normrnd(0,0.001/2.3548,dim,1);
RTin=zeros(dim,1);% initial time of flight is 0

% Multidimensional array initialization
68 REin=((Ein*Zin-RefE*RefQ)/(RefE*RefQ))*ones(dim,1);%input is dE/E
RMin=((Min-RefA)/(RefA))*ones(dim,1);%input is dm/m
RZin=((Zin-RefQ)/(RefQ))*ones(dim,1);%input is dq/q
Dinit=[RXin RAin RYin RBin RTin REin RMin RZin zeros(dim,112)];

end %end of initialize function
%-----
%Subfunction to create A/Q multidimensional array
function DAQ=aq_init(dim, E0, dim_AQ, AQ_in, RefE, RefA, RefQ)
78 DAQ=initialize(dim, E0, AQ_in(1,1), AQ_in(1,2), RefE, RefA, RefQ);

for i=2:dim_AQ
    D_new=initialize(dim, E0, AQ_in(i,1), AQ_in(i,2), RefE, RefA, RefQ);
    DAQ=cat(3,DAQ, D_new);
end

end %end of aq_init function
%-----
%Subfunction to create variable energy multidimensional array
88 function D_E=e_init(dim, dim_AQ, AQ_in, dim_E, E_in, RefE, RefA, RefQ)

D_E=aq_init(dim, E_in(1,1), dim_AQ, AQ_in, RefE, RefA, RefQ);

for i=2:dim_E
    D_new=aq_init(dim, E_in(i,1), dim_AQ, AQ_in, RefE, RefA, RefQ);
    D_E=cat(4, D_E, D_new);
end

end %end of e_init function
98 %-----
%Subfunction to read a matrix from a file.
function matrix=readmat(filename, para)
fid=fopen(filename);
if para==0

```

```

    [matrix , count]=fscanf(fid , '%14g' , [6 , 14]);
    %not complete
elseif para==1
    [matrix , count]=fscanf(fid , '%14g' , [6 , 120]);
    matrix(6 , :) = [];
108    complement=horzcat(zeros(3 , 5) , eye(3) , zeros(3 , 112));
    matrix=vertcat(matrix , complement , zeros(112 , 120));
end
matrix=matrix';
status = fclose(fid);
end %end of readmat function
%-----
%Subfunction to read matrices from elements calculated separately.
function [Mb, Sys]=elem(reply)
if reply==0
118    % Electrostatic bender transfer matrix
    Mb=readmat('E:\COSY\setup 3 U\Magnetic bender.txt', 1);
elseif reply==1
    % Electrostatic bender transfer matrix
    Mb=readmat('E:\COSY\setup 3 Z\Magnetic bender.txt', 1);
end;
    Sys=Mb;

end %end of separatelem function
%-----
128 %Subfunction to calculate distributions.
function [DMb, DSys]=distributions(Dinit , Mb, Sys , dim , dim_AQ , dim_E , all)
DMb=zeros(dim , 120 , dim_AQ , dim_E);
DSys=zeros(dim , 120 , dim_AQ , dim_E);

for i=1:dim_E
    for j=1:dim_AQ
        DMb(:, :, j , i)=Dinit(:, :, j , i)*Mb;
        DSys(:, :, j , i)=Dinit(:, :, j , i)*Sys;
    end
138 end

end %end of distributions function
%-----
%Subfunction to plot the distributions.
function [Foc2D, Fin2D]=plot_AQ_or_E(Dinit , DMb, DSys , dim_AQ , dim_E , choice , dim)
if choice==0
    figure;
    [Foc2D]=plotplanes(Dinit , DMb, DSys , dim_AQ , 1 , choice);
    figure;
148    [Fin2D]=plotfinal(DSys , dim , dim_AQ , 1);
elseif choice==1
    figure;
    [Foc2D]=plotplanes(Dinit , DMb, DSys , dim_AQ , dim_E , choice);
    figure;
    [Fin2D]=plotfinal(DSys , dim , 1 , dim_E);
elseif choice==2
    figure;
    [Foc2D]=plotplanes(Dinit , DMb, DSys , dim_AQ , dim_E , choice);
    figure;
158    [Fin2D]=plotfinal(DSys , dim , dim_AQ , dim_E);
end
end %end of plot_AQ_or_E function
%-----
%Subfunction to plot the focal planes.
function [Names]=plotplanes(Dinit , DMb, DSys , dim_AQ , dim_E , choice)
%Colormap
colormap(colorcube);
cm=colormap;
Names=zeros(6 , dim_AQ , dim_E);
168 %Image on the focal plane
for i=1:dim_E
    for j=1:dim_AQ
        if choice==2 j=i;end
%Plot initial space plane
subplot(3 , 2 , 1);
Names(1 , j , i)=plot(Dinit(:, 1 , j , i) , Dinit(:, 3 , j , i) , 'ks');set(Names(1 , j , i) , 'Color' , cm(2*i+j , :) ,
    'Marker' , '.' );title('1) initial space distribution');hold on;
%Plot final space plane
subplot(3 , 2 , 2);
Names(2 , j , i)=plot(DMb(:, 1 , j , i) , DMb(:, 3 , j , i) , 'ks');set(Names(2 , j , i) , 'Color' , cm(2*i+j , :) ,
    'Marker' , '.' );title('2) final space distribution');hold on;
178 %Plot initial X phase plane
subplot(3 , 2 , 3);

```

```

Names(3,j,i)=plot(Dinit(:,1,j,i),Dinit(:,2,j,i),'ks');set(Names(3,j,i),'Color',cm(2*i+j,:),
'Marker','.');title('1) initial X phase distribution');hold on;
%Plot final X phase plane
subplot(3,2,4);
Names(4,j,i)=plot(DMb(:,1,j,i),DMb(:,2,j,i),'ks');set(Names(4,j,i),'Color',cm(2*i+j,:),
'Marker','.');title('2) final X phase distribution');hold on;

%Plot initial Y phase plane
subplot(3,2,5);
188 Names(5,j,i)=plot(Dinit(:,3,j,i),Dinit(:,4,j,i),'ks');set(Names(5,j,i),'Color',cm(2*i+j,:),
'Marker','.');title('1) initial Y phase distribution');hold on;
%Plot final Y phase plane
subplot(3,2,6);
Names(6,j,i)=plot(DMb(:,3,j,i),DMb(:,4,j,i),'ks');set(Names(6,j,i),'Color',cm(2*i+j,:),
'Marker','.');title('2) final Y phase distribution');hold on;
end
end %end of plotplanes function
%
%Subfunction to plot the final planes.
function [Fin2D]=plotfinal(DSys,dim,dim_AQ,dim_E)
198 N=count(DSys,dim,dim_AQ,dim_E);
colormap(colorcube);
cm=colormap;
for k=1:size(N,4)
for l=1:size(N,3)
Fin2D=plot(N(:,1,l,k),N(:,2,l,k),'+');set(Fin2D,'Color',cm(2*k+l,:));title('final
I=f(x)');hold on;
end
end
end %end of plotfinal function
%
208 %Subfunction to count the number of particles at each deviation value on the X axis
function N=count(DSys,dim,dim_AQ,dim_E)
TempN=zeros(dim,4,dim_AQ,dim_E);
M=zeros(1,7);
m=zeros(1,7);
for k=1:dim_E
for l=1:dim_AQ
for p=1:7
218 M(1,p)=max(DSys(:,p,l,k));
m(1,p)=min(DSys(:,p,l,k));
end
Xmax=M(1,1);
Xmin=m(1,1);
Ymax=M(1,3);
Ymin=m(1,3);
TempN(:,1,l,k)=DSys(:,1,l,k);
TempN(:,3,l,k)=DSys(:,3,l,k);
step=100;
TempX=0;
TempY=0;
228 save_i=1;
last_save=1;
for i = 1:step
for j = 1:dim
if (Xmin+((Xmax-Xmin)*(i-1)/step) <= TempN(j,1,l,k)) & (TempN(j,1,l,k)<=
Xmin+((Xmax-Xmin)*i/step))
save_j(j,i)=j;
if i == save_i
TempX=TempX+1;
else
238 TempN(last_save,2,l,k)=TempX;
TempX=1;
save_i=i;
end
last_save=j;
end
end
end
TempN(last_save,2,l,k)=TempX;
end
end
248 end
for k=1:dim_E
for l=1:dim_AQ
i=1;
for j = 1:dim
if TempN(j,2,l,k)~=0

```

```

258         N(i,1,1,k)=TempN(j,1,1,k);
           N(i,2,1,k)=TempN(j,2,1,k);
           i=i+1;
           end
         end
       end
     for k=1:dim_E
       for l=1:dim_AQ
         N(:,:,1,k)=sortrows(N(:,:,1,k),1);
       end
     end
268 end %end of count function

```

One notes that the divergences a and b are expressed as p_x/p_0 and p_y/p_0 , and not p_x/p_z and p_y/p_z . Therefore when the mass or the energy of the ion is very different from the mass and energy of the reference particle, the divergence deviation is enhanced. Because of this effect, special care was taken to calculate the separator resolving power with ions of similar masses and energies.

B.4 Control system with LabView

The various power supplies were tested within a Summer Student project [131]. The aim of the project was to control analog command and readout signals of the voltage power supplies from the personal computer (PC) (Figure B.2). For this purpose, they were connected to the various channels of a WAGO function module that were coupled in the fieldbus to be programmed from the PC equipped with the adequate Profibus card. A server for Process Control by Object Linking and Embedding (OPC) was installed, allowing to adress the various channels of the WAGO function module through the Profibus.

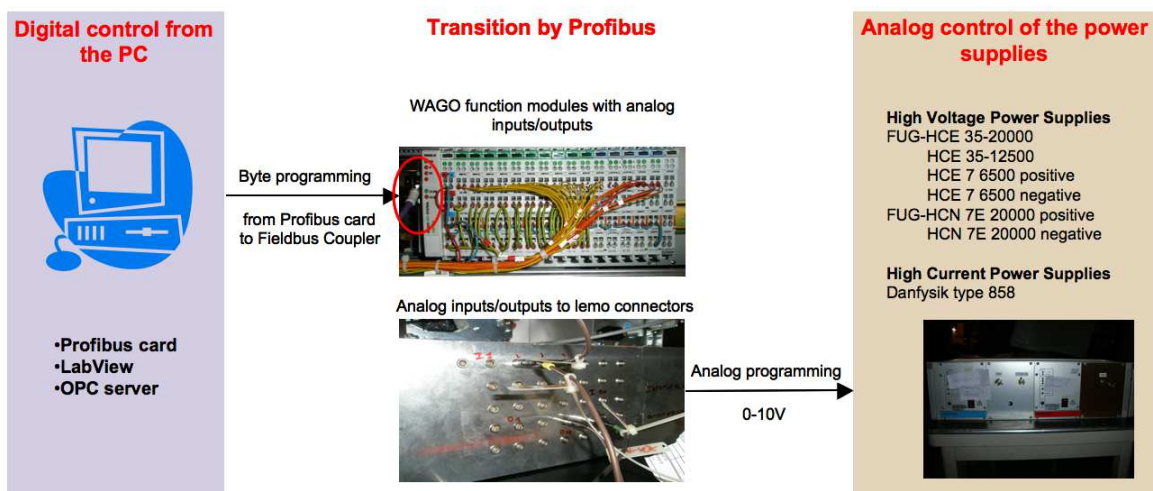


Figure B.2: Power supplies control via Profibus.

Functions were written in LabView to read and write bytes on the power supplies channels. The readout value was corrected for the deviation induced by the high resistance of the connector on the voltage supplies. The voltages were ramped up via a control loop of the readout value. The Danfysik current supply for the magnetic bender was controlled via a serial port directly adressable through the LabView program. The various read and write functions were grouped into modules for the control of the various beamline elements with user-friendly interfaces (Figure B.3).

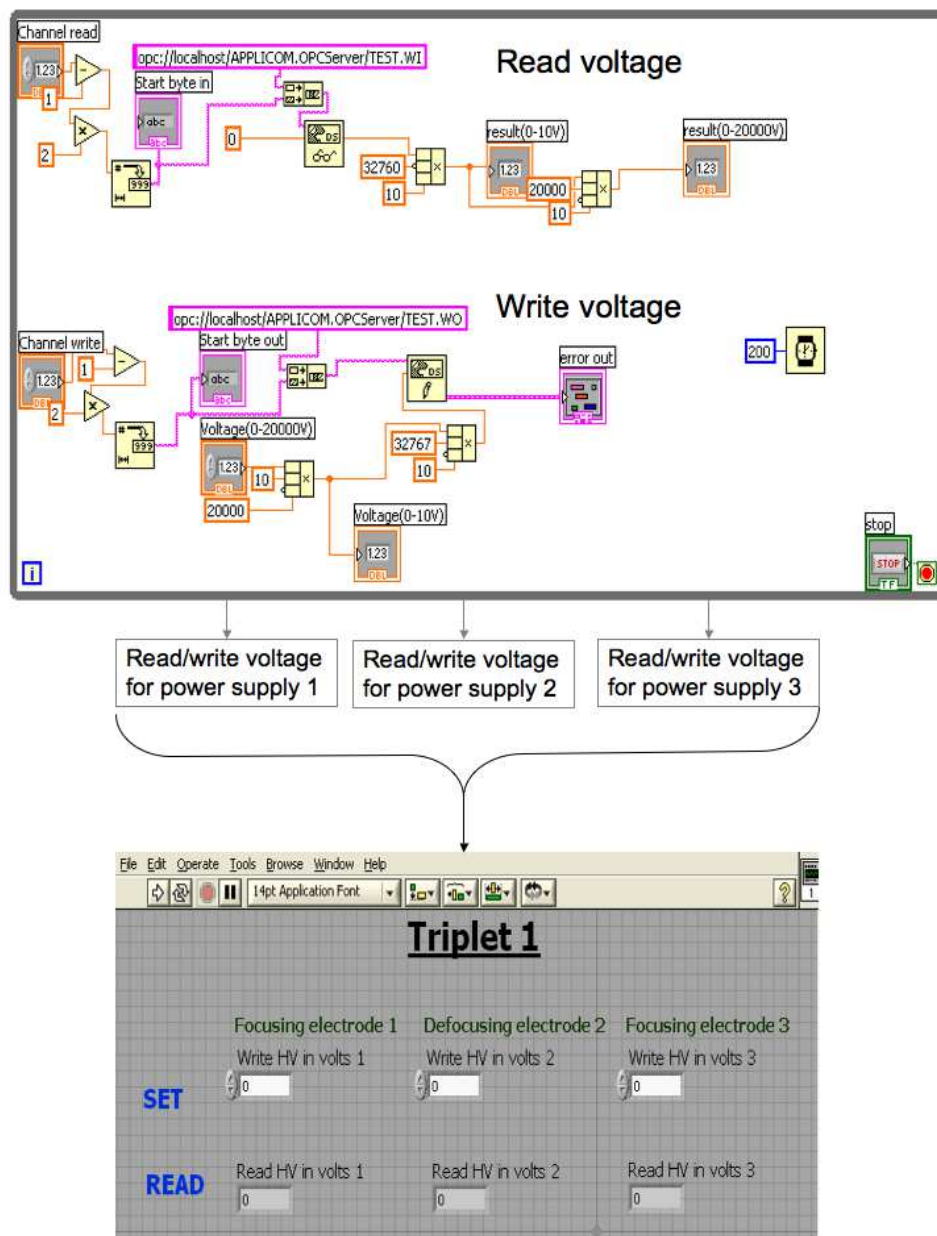


Figure B.3: LabView interface for the power supplies control system.

Appendix C

Latest proposal of experiment with the PHOENIX ECR charge breeder

EUROPEAN ORGANIZATION FOR NUCLEAR RESEARCH

CERN-INTC-2007-012

INTC-P-225

April 2007

Proposal to the INTC Committee

Measurement of ground state properties of neutron-rich nuclei on the r-process path between the N=50 and N=82 shells

Carmen Angulo¹, Charles Barton², Joakim Cederkall³, Pierre Delahaye³, Ulli Köster⁴,
Mélanie Marie-Jeanne³, Gabriel Martinez-Pinedo⁵, Alberto Mengoni^{3,6}, Karsten Riisager³,
John Simpson⁷, Olof Tengblad⁸

1. UCL, Louvain-la-Neuve, Belgium
2. University of York, Heslington, York, United Kingdom
3. CERN, Geneva, Switzerland
4. ILL, Grenoble, France
5. GSI, Darmstadt, Germany
6. IAEA Nuclear Data Section, Vienna, Austria
7. CCLRC Daresbury Laboratory, Warrington, Cheshire, United Kingdom
8. CSIC, Madrid, Spain

Spokesperson : Mélanie Marie-Jeanne

Contactperson : Pierre Delahaye

Abstract

The evolution of the unknown ground-state β -decay properties of the neutron-rich $^{84-89}\text{Ge}$, $^{90-93}\text{Se}$ and $^{102-104}\text{Sr}$ isotopes near the r-process path is of high interest for the study of the abundance peaks around the N=50 and N=82 neutron shells. At ISOLDE, beams of certain elements with sufficient isotopic purity are produced as molecular sidebands rather than atomic beams. This applies e.g. to germanium, separated as GeS^+ , selenium separated as SeCO^+ and strontium separated as SrF^+ . However, in case of neutron-rich isotopes produced in actinide targets, new "isobaric" background of atomic ions appears on the mass of the molecular sideband.

For this particular case, the ECR charge breeder, positioned in the experimental hall after ISOLDE first mass separation, can be advantageously used as a purification device, by breaking the molecules and removing the molecular contaminants.

This proposal indicates our interest in the study of basic nuclear structure properties of neutron-rich nuclei on the r-process path between the neutron magic numbers N=50 and N=82 at ISOLDE with the ECR Phoenix Booster. This first proposal should serve as a basis for the investigation of the potential applications of the ECR for nuclear astrophysics at ISOLDE. For instance, beam purification using molecular sidebands selection with the ECR is particularly suited for the study of the $^{84-89}\text{Ge}$, $^{90-93}\text{Se}$, $^{102-104}\text{Sr}$ isotopes, respectively produced as GeS^+ , SeCO^+ and SrF^+ molecular beams.



1. Motivation

We propose to determine the half lives and Pn-values of neutron rich isotopes located close to the r-process path between shells N=50 and N=82.

1.1. Astrophysics case

Approximately half of the heaviest isotopes in nature, beyond iron, are produced via neutron captures on very short time scales in neutron-rich environments, i.e. the so-called r-process.

At the high temperatures and neutron densities present in the r-process site, equilibrium between neutron captures and photo-dissociations is achieved. For each isotopic chain the series of neutron captures reaches equilibrium with photo-dissociation in what is known as "waiting point" nucleus as the flow of neutron captures "waits" for this nucleus to beta-decay. The r-process reaches the neutron shell closures at N = 50, 82, and 126 at such low Z values that the neutron separation energy is too small to allow the formation of still more neutron-rich isotopes; the isotopes then have to beta decay. To overcome the shell gap at the magic neutron numbers and produce heavier nuclei, the material has to undergo a series of alternating β -decays and neutron captures before it reaches a nucleus close enough to stability to have neutron separation energies large enough to allow for the continuation of the sequence of neutron capture reactions. As the β -decay half-lives are relatively long at the magic neutron numbers, the r-process network waits long enough at these neutron numbers to build up abundance peaks related to the mass numbers A = 80, 130, and 195. These abundance peaks are thus mainly shaped by the β -decay properties of the nuclei on the r-process path located between the neutron closed shells. Presently, most of these properties are not experimentally measured.

1.2. Comparison with models

The beta-decay half-lives ($T_{1/2}$) and the β -delayed neutron emission probabilities (P_n) combined provide a first rough characterization of the distribution of beta-strength in a beta-decay. In nuclei with N > 50 around and above Ni, first forbidden transitions will play an important role [1] and affect both experimental quantities. The correct theoretical description of these nuclei is an ongoing project (see for example [2], for a recent review).

2. Description of the PHOENIX ECR Booster

At ISOLDE, neutron-rich isotopes in the intermediate mass range (A=80 to 150) can be produced with high yields by fission of an actinide target associated to a chemically non-selective [3] plasma ion source. Thus, the whole isobaric chain is ionized, resulting sometimes in a high background of many different fission products that are extracted and mass-separated. This kind of problem can be addressed using an electron cyclotron ion source (ECRIS) to charge breed and remove isobaric contaminants with one of the beam purification techniques described later in this section.

The Daresbury PHOENIX ECRIS Booster is installed after the General Purpose Separator (GPS), on the High Mass (GHM) parasitic beam line at ISOLDE (see Fig.1) as an on-line test bench for charge breeding experiments described in a previous proposal [4].

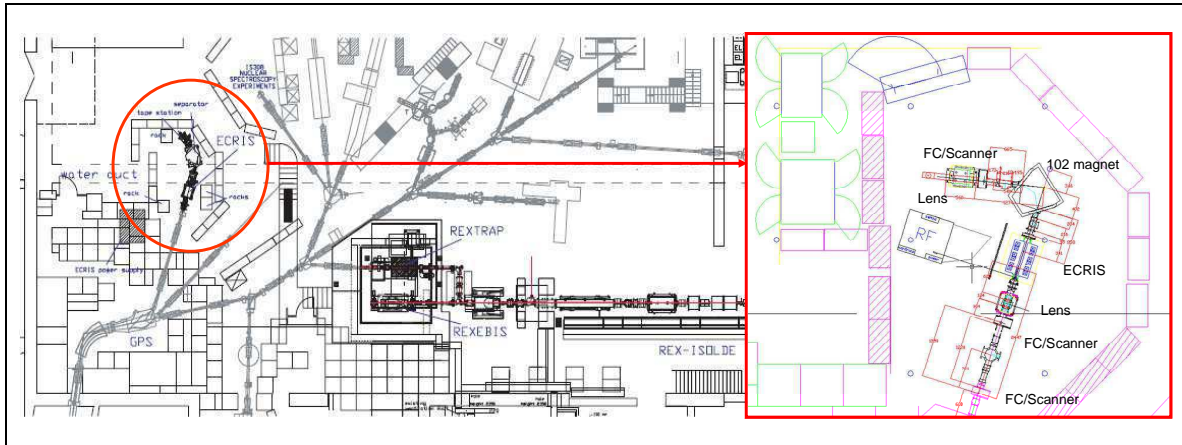


Fig.1 Current layout of the PHOENIX Booster ECRIS in ISOLDE hall

The singly charged ions from ISOLDE are injected into the PHOENIX Booster plasma chamber where they are slowed down by the ECRIS platform potential and stopped due to Coulomb interaction with the plasma (see Fig.2). The electrons of the plasma are confined in a so-called minimum-B-structure. A closed surface is created where the electron cyclotron resonance condition is fulfilled. The high mirror ratio of the magnetic field leads to long confinement times for the plasma electrons. They can pass thousands times the resonance region, stochastically gaining energy from a high frequency electromagnetic wave and ionizing plasma ions to high charge states via stepwise ionization.

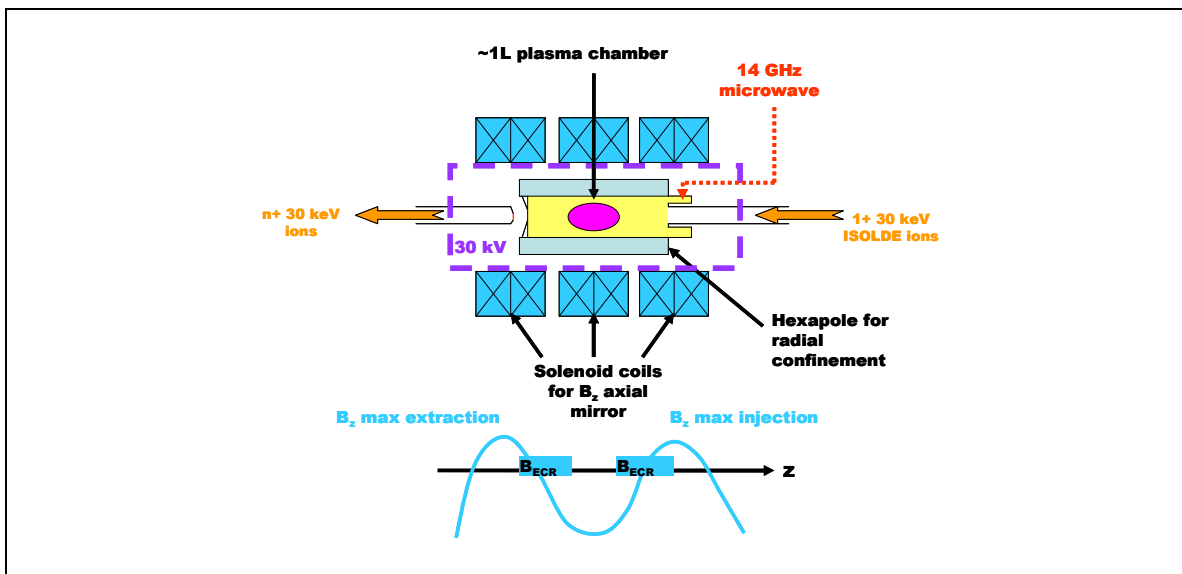


Fig.2 Ion motion inside the ECRIS

The latest on-line charge breeding results of the Phoenix booster are described in [5]. It is currently able to charge breed a wide range of nuclides for A/q values from 4 to 8, either in continuous or in pulsed mode. Efficiencies of the injected elements are similar to the ones measured for the REX beam preparation stage [6]. Charge bred ions are extracted and mass-separated by the 102^o analyzing magnet (see Fig.3) and can be sent towards a tape station around which β and γ detectors are set up.

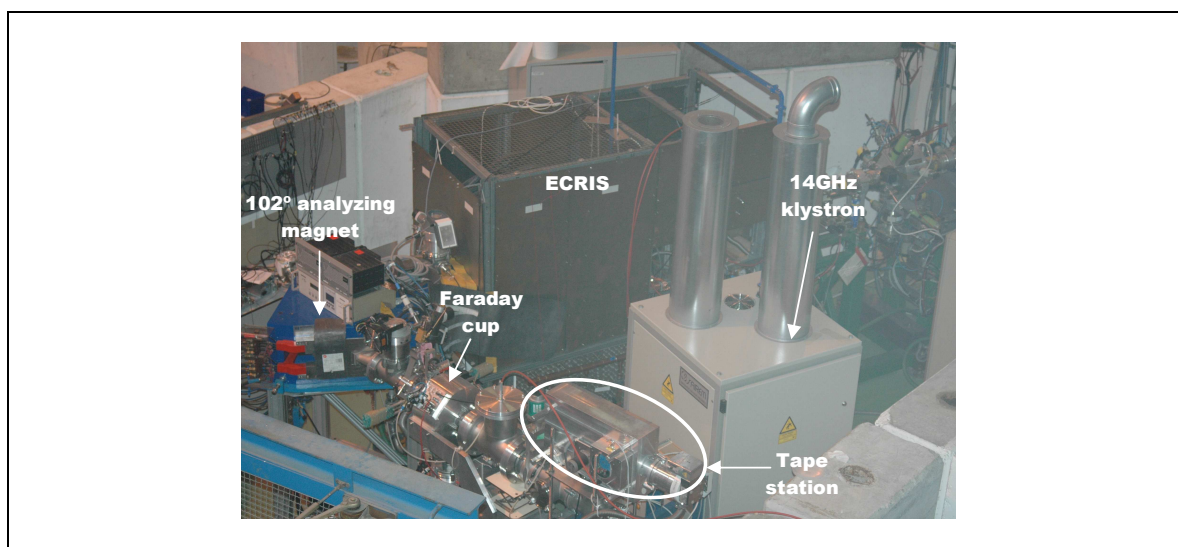


Fig.3 ECRIS experimental area

The PHOENIX Booster charge breeder offers two means for beam purification. The first one is the use of the charge state distribution generated inside the ECR plasma to extract ions with an optimized A/q -value so that the proportion of multiply charged contaminants is strongly suppressed. This method was already applied at ISOLDE to perform the study of ^{48}Ar decay [7].

The second method is the injection of the wanted species as molecules into the charge breeder where they are broken, extracted and mass selected, thus removing the molecular sidebands. Some elements are extracted from the ISOLDE target with a higher yield and less contamination as molecular beams.

As mentioned before, the question of isobaric contamination is crucial for the proper measurement of nuclear structure properties. As an example, the case of neutron-rich Ga was already studied at ISOLDE by K.-L. Kratz et al [8], where a ^{238}UC -graphite target was connected to a plasma ion source to produce the $^{81,82,83,84}\text{Ga}$ isotopes. According to reference [8], "*The determination of the Pn -values of the isotopes of major astrophysical interest was difficult due to the chemical nonselectivity of the plasma ion source. [...] Therefore, the Pn -values listed (in Tab. 1) have rather large uncertainties*". Now, a resonant laser ion source can be used at ISOLDE for selective ionization of many metallic elements. However, many non-metallic and some metallic elements can be better (i.e. more efficiently and/or more purely) separated in molecular form with a plasma ion source. The PHOENIX Booster charge breeding thus appears as an advantageous solution for cases where molecular sidebands can be injected.

3. Performances of the charge breeder

The PHOENIX Booster ECR charge breeder performances were studied in a previous proposal [4]. Charge breeding can be achieved within a continuous mode or a pulsed mode.

In continuous mode, the radiofrequency is applied permanently and the charge bred ions are extracted continuously from the source. The total time spent by the ions inside the plasma chamber is a global confinement time which includes the needed time for charge breeding [5]. Depending on the adjustments of the source, the global confinement time can go down to an average value of 100ms. Working in continuous mode, a charge breeding efficiency of typically 5% can be expected for one charge state.

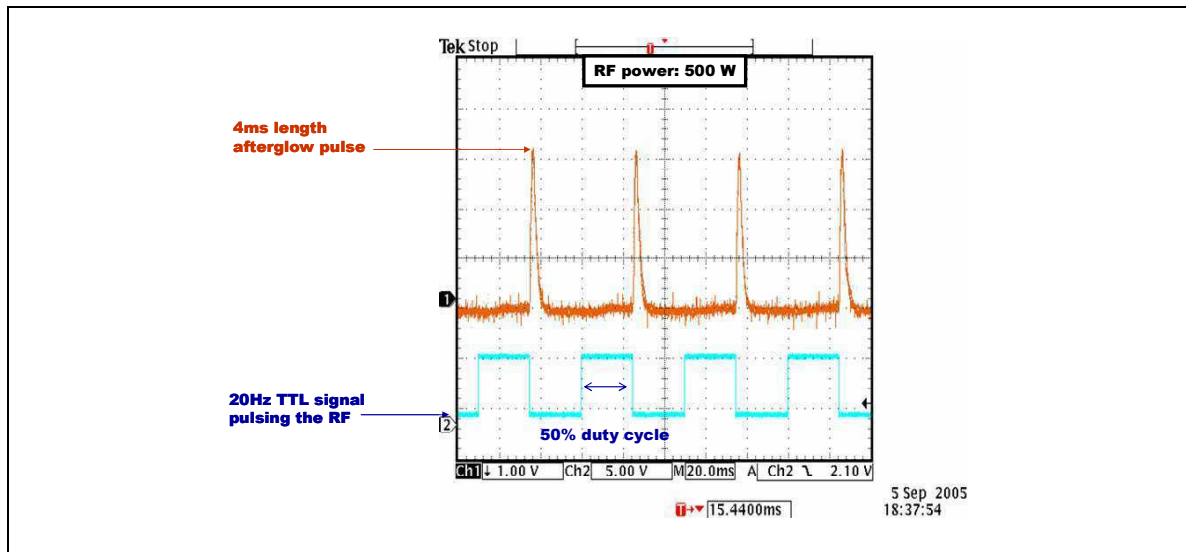


Fig.4 Pulsed mode principle

In pulsed mode, the radiofrequency (RF) is applied for a fixed time. As it is switched off, all ions are extracted as a single pulse or so-called “afterglow” pulse (see Fig.4). Therefore, the confinement time can be reduced to the minimum time necessary for charge breeding, which can go down to 20ms [9] (see Fig.5). The afterglow pulse can last up to 10ms. As a consequence, isotopes living down to 30ms can be studied in the afterglow mode. However, the charge breeding efficiency currently attainable in pulsed mode is half less than the one obtained in continuous mode, i.e. around 2.5% charge breeding efficiency for one charge state. An advantage of this method is the time reference that it gives for the half-life measurement.

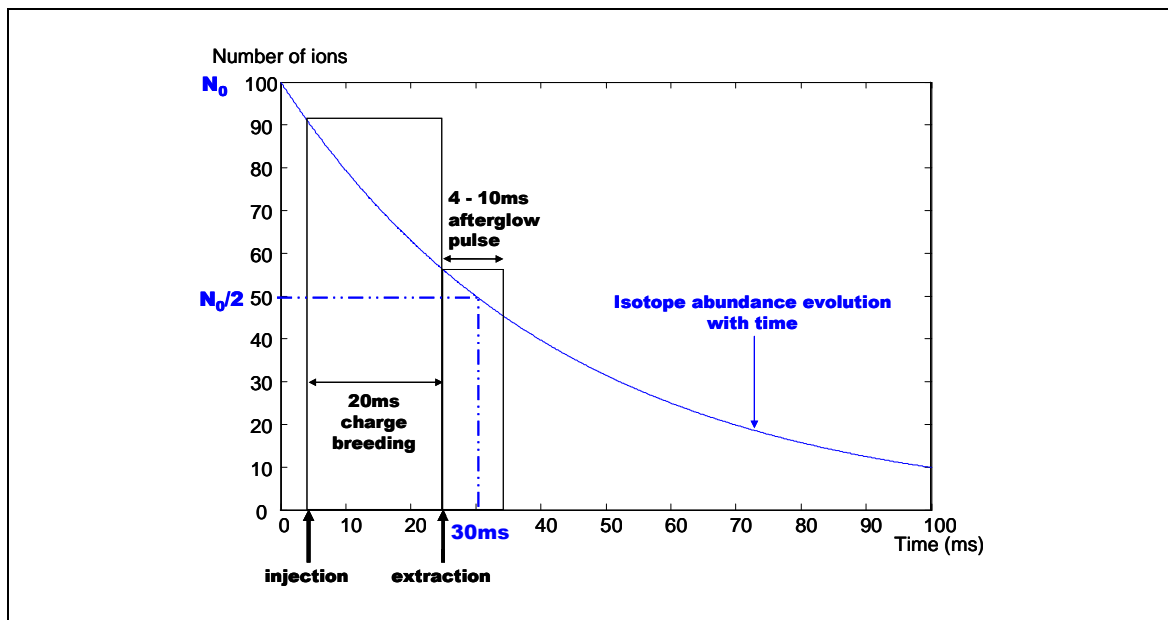


Fig.5 Tuning for short lived isotopes

4. Proposed experiment

4.1. Experimental setup

The experimental setup should consist of a tape station installed after the ECR test bench on GHM, a beta detector (NE102 scintillator cup) in coincidence with at least one HPGe detector for isotopes identification and background estimation, and a neutron counter described in [10].

The detection efficiency can be estimated to 30% for the betas, 19% for the neutrons [10] and about 1% for gamma energies in the range of 500keV-1MeV. The Phoenix Booster can be assumed to have a total injection and charge breeding efficiency of respectively 5% or 2.5% for one charge state in continuous mode or in pulsed mode.

4.2. Cycle description

For each $T_{1/2}$ and P_n measurement, one assumes the following procedure. One starts accumulating ions after the proton pulse, and one stops the accumulation on the tape at the maximum of the release curve with the use of an electrostatic deflector after the analyzing magnet. Doing so, the collection will be optimized according to the release time and expected half life of the isotope in question. The collection will be followed by a counting period $t_{measurement}$ over four half-lives in order to obtain a clean decay curve for both beta and neutrons. The tape is moved afterwards to get rid of the remaining activity. This induces a delay δt_{tape} of approximately 500ms. One has to wait for the next proton pulse coming every $\delta t_{protons}$ of 1.2s to start a new measurement cycle. Therefore, the cycle time t_{cycle} is given in seconds by (eq.1):

$$(eq.1) \quad t_{cycle} = \left(\text{trunc} \left(\frac{t_{measurement} + \delta t_{tape}}{\delta t_{protons}}, 0 \right) + 1 \right) \cdot \delta t_{protons}$$

One proton pulse every 2.4s was expected as the highest rate, and each proton pulse has maximum intensity, i.e. 4.8 μ C.

4.3. Estimated yields and measurement times

We would like to demonstrate first the performances of the cleaning by charge breeding with less exotic GeS^+ , SeCO^+ and SrF^+ beams, such as $^{82-83}\text{GeS}^+$, $^{86-89}\text{SeCO}^+$ and $^{98-101}\text{SrF}^+$. These have reasonable branching ratios for identification by gamma detection and are therefore easily detectable. The demonstration of feasibility of this method for beam purification, and the yield measurement for such beams would also help other experiments (e.g. REX). For these calibration measurements, we aim for 10% accuracy on the measured $T_{1/2}$ and P_n values.

Then we aim at studying the $^{84-87}\text{Ge}$ and $^{90-92}\text{Se}$ isotopes by charge breeding them with the continuous mode, and the $^{88-89}\text{Ge}$, ^{93}Se and $^{102-104}\text{Sr}$ isotopes with the pulsed mode. For these more exotic isotopes, in order to be competitive with the tabulated values [11] and [12], we aim at measuring $T_{1/2}$ and P_n with uncertainties reduced by a factor 2 compared to former measurements. In case no value was previously reported, we aim at measuring them for the first time with less than 20% uncertainty.

Table 1 gives the current tabulated values of the interesting isotopes for $T_{1/2}$ and P_n with their uncertainties.

The required beams are basically impossible to identify without the proposed additional mass separation after molecular breakup, due to a high background of well-produced isobars such as Ag, Cd, In...etc. The method we propose here was used in a similar way at Oak Ridge National Laboratory (ORNL) [12], where $^{80-86}\text{GeS}^+$ beams were produced with a target-ion source set comparable to what is used at ISOLDE. The molecules were post-accelerated and broken by stripping before undergoing mass and energy separation. Except for the yields measured through this experiment, there are obviously no measured yields available. Therefore we have to estimate probable yields from the measured yields [12], and from available information on less exotic isotopes produced at ISOLDE ([13] and [14]).

Contrary to the experiment at the ORNL, we plan to use a tungsten neutron converter to suppress part of the symmetric fission products. The induced loss factor in the production of the isotope of interest inside a

uranium carbide target was calculated using the fission cross-section that can be found in [15]. Hence, the expected yields for molecular beams of less exotic isotopes such as ^{80}Ge , ^{96}Se and ^{84}Sr could be extrapolated from the available information on measured yields ([13], [14] and [16]). Since the drop of fission yields towards very neutron-rich isotopes of a given element is rather universal, the expected ISOLDE yields could thus be derived (see Table 1).

Then, following the same development as in [17], one calculates the total measurement time. One assumes that a measurement of the total background rate is performed preceding or following the actual $T_{1/2}$ and P_n measurement, with all parameters remaining the same. The internal beta and neutron background is believed to arise mainly from two sources: from the possible neutral radioactive gas diffusing from the GPS target, and from the nearby A/q tails of well-produced isotopes extracted at the same mass as the molecules. For example, the well-produced ^{116}Ag , ^{118}Ag and ^{121}Ag isotopes will be respectively extracted at the same masses as the $^{82}\text{GeS}^+$, $^{90}\text{SeCO}^+$, $^{102}\text{SrF}^+$ molecules, with a yield of about $1\text{E}+8$ ions/s. The factor of suppression for the tails of nearby peaks measured with stable beam in our A/q separation is about 10^{-5} . This leads to a background rate of 20Hz for the betas, and 0.5Hz for the neutrons. For the calculation of the total measurement time, the total background rate was estimated to a maximum of 100Hz for the betas, and 1Hz for the neutrons as in [18].

From the total measurement time and the time for one cycle (eq.1), one can deduce the total time needed for the $T_{1/2}$ measurement and for the P_n measurement, given in Table 1. Detection limits of 1 beta per second and 1 neutron per second were assumed.

Nuclide	$T_{1/2}$	P_n (%)	Estimated yield (ions/ μC)	T for $T_{1/2}$	T for P_n
^{82}Ge	4.55s (0.05)	0	2E+03	<1h	-
^{83}Ge	1.85s (0.06)	0	1E+02	< 1 beta/s	-
^{84}Ge	947ms (11)	10.8(6)	6E+00	< 1 beta/s	< 0.1 neutron/s
^{85}Ge	535ms (47)	14 (3)	9E-02	< 1 beta/s	< 0.1 neutron/s
^{86}Ge	200ms (syst)	#?	4E-04	< 1 beta/s	< 0.1 neutron/s
$^{87-89}\text{Ge}$	#?	#?	-	-	-
^{86}Se	15.3s (0.9)	0	8E+03	<1h	< 0.1 neutron/s
^{87}Se	5.50s (0.12)	0.20 (4)	5E+03	<1h	3h
^{88}Se	1.53s (0.06)	0.99 (10)	2E+03	<1h	2h
^{89}Se	410ms (40)	7.8 (25)	3E+02	<1h	5h
^{90}Se	#300ms (>300ns)	#?	6E+01	<1h	< 0.1 neutron/s
^{91}Se	270ms (50)	21 (10)	3E+00	< 1 beta/s	< 0.1 neutron/s
$^{92-93}\text{Se}$	#?	#?	-	-	-
^{98}Sr	653ms (2)	0.25 (5)	2E+05	<1h	<1h
^{99}Sr	269ms (1)	0.100 (19)	7E+03	<1h	<1h
^{100}Sr	202ms (3)	0.78 (13)	1E+03	<1h	<1h
^{101}Sr	118ms (3)	2.37 (14)	5E+01	2h	< 0.1 neutron/s
^{102}Sr	69ms(6)	5.5 (15)	3E+00	< 1 beta/s	< 0.1 neutron/s
$^{103-104}\text{Sr}$	#?	#0 ?	-	-	-

Table 1 Gross properties of the interesting isotopes as in [11] and [12]

The symbol “#” shows estimated values

5. Summary and beam time requirements

Apart from the nuclear astrophysics interest, the measurement of the neutron-rich ^{84+x}Ge , ^{90+x}Se , $^{102+x}\text{Sr}$ isotopes gross properties ($T_{1/2}$, P_n) are so challenging that they were proposed as one of the EURISOL key experiments [19]. The measurement of any of these at an existing facility such as ISOLDE would be a great success. The development of the related techniques of production and separation is in this respect of high

interest. The validation of this purification method is a major step for beam development as it is the only way to determine precisely the yields of the more exotic neutron-rich isotopes.

The study of the gross properties also constitutes a first step towards a deeper investigation of these neutron-rich isotopes through other experiments, for example such as mass measurement or using post-acceleration with REX-ISOLDE.

5.1. Experimental setup

For the experimental setup, a tape station will be needed on the GHM beam line, as well as an HPGe detector, and a neutron counter. The use of the ISOLDE Data Acquisition System is required as well.

5.2. Beam time for on-line measurements

Sufficient beam intensity is expected to perform the $T_{1/2}$ and P_n measurements of the ^{82}Ge , $^{86-90}\text{Se}$ and $^{98-101}\text{Sr}$ isotopes with the estimated yields. As the identification and the estimation of the background is a major concern, we require more time than the necessary measurement time reported in the previous section.

For the cases where the count rate was estimated to be below the detection limits, shifts are required for yield investigation, as no precise yield can be measured without the proposed method of additional purification with the ECR.

We require for each element:

- two shifts of preparation, including a yield measurement on less exotic isotopes on the ISOLDE tape station and beam tuning with stable and radioactive ions from GHM to the ECR, four shifts if the conditioning of the afterglow mode is required.
- two shifts of calibration on less exotic but well-known isotopes.
- the shifts necessary for the measurement of the yields for the interesting nuclides, and possibly of $T_{1/2}$ and P_n when the measurement time estimate given in Table 1 is favourable.

Nuclide	Target	Gas leak or mass marker	Ion source	Shifts	Protons averaged current μA	Comments
Ge settings	UC_x ThO_2	^{34}S (mass marker)	MK5	2	-	Beam tuning
^{82}Ge	"	"	"	2	0.3	Calibration
$^{84-87}\text{Ge}$	"	"	"	4	1.0-2.0	Investigation of the yields
Se settings	UC_x ThO_2	CO_2	MK5	2	-	Beam tuning
$^{86-89}\text{Se}$	"	"	"	2	0.1-2.0	Calibration
^{90}Se	"	"	"	1	2.0	Continuous mode
$^{91-92}\text{Se}$	"	"	"	3	2.0	Investigation of the yields
Sr settings	UC_x	CF_4	W surface tungsten	(4)	-	Beam tuning and afterglow conditioning
$^{98-101}\text{Sr}$	"	"	"	(2)	1.3-2.0	Calibration
$^{102-104}\text{Sr}$	"	"	"	(4)	2.0	Investigation of the yields

Table 2 Beam request for the interesting nuclides
As the Sr case is challenging, no shift is required at this stage

As a summary, a total of 16 shifts is required to perform an extensive study of yields and gross properties for neutron-rich $^{84-87}\text{Ge}$ and $^{90-92}\text{Se}$ nuclei on the r-process path for neutron shells between $N=50$ and $N=82$.

Preferably, the Ge and Se measurements could be done with the same target, using respectively for the former a mass marker filled with ^{34}S and for the latter a gas leak of CO_2 . Moreover, we know from the release of neutron deficient Se [20] that oxide targets would allow a more rapid release and, hence, higher beam intensities. This conclusion might also be applied to the production of Ge, i.e. a test of a ThO_2 target could give significantly higher yields compared to the conservative estimates used in the previous section for UC_x target. This study would strongly benefit from such a target, as the number of accessible isotopes could be significantly increased.

At this stage, no shift is required for the study of $^{102-104}\text{Sr}$ because these measurements appear quite challenging considering the technique to be used, i.e. the pulsed mode, or so-called afterglow, which still needs to be studied. For the same reason, no shift is required for $^{88-89}\text{Ge}$ and ^{93}Se either. However, as Sr beam developments are planned for the beginning of the year, one might consider the possibility of performing some test measurements with the ECR in parasitic mode. A beam request might be formulated later.

References

- [1] I.N. Borzov, Phys. Rev. C71 (2005) 065801
- [2] I.N. Borzov, Nucl. Phys. A777 (2006) 645
- [3] S. Sundell et al., Nucl. Inst. Meth. B **70** (1992) 160
- [4] CERN-INTC-2001-023 (INTC-P-143), addendum CERN-INTC-2005-022
- [5] P. Delahaye et al., Rev. Sci. Instrum. **77** 03B105 (2006)
- [6] F. Wenander et al., Rev. Sci. Instrum. **77**, 03B104 (2006)
- [7] T. Fritioff et al., Nucl. Inst. Meth. A **556** (2006) 31-37
- [8] K.-L. Kratz et al., Z. Phys. A – Hadrons and Nuclei **340**, 419-420 (1991)
- [9] P. Sortais et al., Rev. Sci. Instrum. **71**, 617 (2000)
- [10] U.C. Bergmann et al., Nucl. Phys. A **658** (1999) 129-145
- [11] The 2003 nubase evaluation and the 2003 atomic mass evaluation, Nucl. Phys. A **729**, No.1 (2003) 1-676
- [12] P. A. Hausladen et al., Int. J. Mass spectrom. 251 (2006) 119–124
- [13] U. Köster et al., to be published
- [14] SC ISOLDE yields for Sr: <http://isolde.web.cern.ch/ISOLDE/>
- [15] Fission yields for a ^{238}U target: <http://ie.lbl.gov/fission.html>
- [16] HRIBF yields for Se : http://www.phy.ornl.gov/hribf/beams/ribs_total.shtml
- [17] U. Köster, PhD thesis, Technische Universität München, Bavaria, 2000
- [18] U.C. Bergmann et al., Nucl. Phys. A **714** (2003) 21-43
- [19] R.D. Page et al., EURISOL DS Task 10, Internal Task Note (2007)
- [20] A. Joinet, PhD thesis IPNO-T-03-03, Universite Paris-Sud/IPN Orsay, France (2003)

Bibliography

- [1] EURISOL. The scientific need for high-intensity RIBs using the ISOL method. Result for the EURISOL feasibility study RTD, 2003. http://www.ganil.fr/eurisol/Final_Report.html.
- [2] Atomic Mass Data Center CSNSM-Orsay (In2p3/CNRS). A driver program for nuclear data visualisation. Nucleus-Win (version 2.1), 1997.
- [3] G. Werth, J. Alonso, T. Beier, K. Blaum, S. Djekic, H. Häffner, N. Hermanspahn, W. Quint, J. Verdù, T. Valenzuela, and M. Vogel. Highly charged ions, quantum-electrodynamics, and the electron mass. *International Journal of Mass Spectrometry*, 251:152–158, 2006.
- [4] G. Bollen, D. Davies, M. Facina, J. Huikari, E. Kwan, P. A. Lofy, D. J. Morrissey, A. Prinke, R. Ringle, J. Savory, P. Schury, S. Schwarz, C. Sumithrarachchi, T. Sun, and L. Weissman. Experiments with thermalized rare isotope beams from projectile fragmentation: a precision mass measurement of the superallowed β emitter ^{38}Ca . *Physical Review Letters*, 96:152501–1–4, 2006.
- [5] A. Herlert, S. Baruah, K. Blaum, P. Delahaye, M. Dworschak, S. George, C. Guénaut, U. Hager, F. Herfurth, A. Kellerbauer, M. Marie-Jeanne, S. Schwarz, L. Schweikhard, and C. Yazidjian. Towards high-accuracy mass spectrometry of highly charged short-lived ions at ISOLTRAP. *International Journal of Mass Spectrometry*, 251:131–137, 2006.
- [6] Thomas Beier, Hartmut Häffner, Nikolaus Hermanspahn, Savely G. Karshenboim, H.-Jürgen Kluge, Wolfgang Quint, Stefan Stahl, José Verdú, and Günther Werth. New determination of the electron’s mass. *Physical Review Letters*, 88:011603–1–4, 2002.
- [7] F. Bosch, T. Faestermann, J. Friese, F. Heine, P. Kienle, E. Wefers, K. Zeitelhack, K. Beckert, B. Franzke, O. Klepper, C. Kozhuharov, G. Menzel, R. Moshhammer, F. Nolden, B. Reich, H. Schlitt, M. Steck, T. Stöhlker, T. Winkler, and K. Takahashi. Observation of bound-state β^- decay of fully-ionized ^{187}Re : ^{187}Re - ^{187}Os cosmochronometry. *Physical Review Letters*, 77:5190–5193, 1996.

- [8] E. Silver, H. Schnopper, S. Bandler, N. Brickhouse, S. Murray, M. Barbera, E. Takacs, J. D. Gillaspay, J. V. Porto, I. Kink, J. M. Laming, N. Madden, D. Landis, J. Beeman, and E. E. Haller. Laboratory astrophysics survey of key X-ray diagnostic lines using a microcalorimeter on an electron beam ion trap. *The Astrophysical Journal*, 541:495–500, 2000.
- [9] E.W. Schmidt, S. Schippers, C. Brandau, D. Bernhardt, A. Müller, M. Lestinsky, F. Sprenger, J. Hoffmann, D.A. Orlov, M. Grieser, R. Repnow, A. Wolf, D. Lukić, M. Schnell, and D.W. Savin. Electron-ion recombination measurements of Fe^{7+} , Fe^{8+} , Fe^{13+} motivated by active galactic nuclei x-ray absorption features. *Journal of Physics: Conference Series*, 58:223–226, 2007.
- [10] H.P. Winter. HCI issues in tokamak fusion plasmas. *Journal of Physics: Conference Series*, 58:33–40, 2007.
- [11] M. Folkard, K. M. Prise, and B. Vojnovic. Status of charged particle microbeams for radiation biology. *Journal of Physics: Conference Series*, 58:62–67, 2007.
- [12] Daniela Schulz-Ertner, M.D., Anna Nikoghosyan, Christoph Thilmann, M.D., Thomas Haberer, Ph.D., Oliver Jäkel, Ph.D., Christian Karger, Ph.D., Gerhard Kraft, Ph.D., Michael Wannemacher, M.D. D.D.S., and Jürgen Debus, M.D. Ph.D. Results of carbon ion radiotherapy in 152 patients. *International Journal of Radiation Oncology Biology Physics*, 58:631–640, 2004.
- [13] M. Torikoshi. Heavy-ion cancer therapy. *Laser Physics*, 16:654–659, 2006.
- [14] P. Fehsenfeld, C. Eifrig, and R. Kubat. Application of RNB for high sensitive wear diagnostics in medicine technique and industry. *Nuclear Physics A*, 701:235c–239c, 2002.
- [15] T. Schenkel, I.W. Rangelow, R. Keller, S.J. Park, J. Nilsson, A. Persaud, V.R. Radmilovic, P. Grabiec, D.H. Schneider, J.A. Liddle, and J. Bokor. Open questions in electronic sputtering of solids by slow highly charged ions with respect to applications in single ion implantation. *Nuclear Instruments and Methods in Physics Research B*, 219-220:200–205, 2004.
- [16] G. Pasold, F. Albrecht, U. Reislöhner, M. Dietrich, M. Deicher, W. Witthuhn, and the REX-ISOLDE Collaboration. Production of rare earth isotope beams for radiotracer - DLTS on SiC. CERN INT-C proposal 167, 2003.
- [17] E. Sideras-Haddad, T. Schenkel, D.B. Rebuli, A. Persaud, S. Shrivastava, D.H. Schneider, and B. Mwakikunga. Electron emission and defect formation in the interaction of slow, highly charged ions with diamond surfaces. *Nuclear Instruments and Methods in Physics Research B*, 256:464–467, 2007.

- [18] M. Hass, F. Ames, L.T. Baby, C. Bordeanu, Th. Delbar, J.A. Dooley, R.H. France III, M. Gai, D. Habs, O. Kester, J.E. McDonald, B.S. Nara Singh, S.O. Nelson, A. Ninane, T. Sieber, and P. Thirolf. Measurement of the ${}^8\text{Li}(\alpha, n){}^{11}\text{B}$ reaction. CERN INTC proposal 165, 2003.
- [19] T. Fritioff, J. Cederkäll, L. Weissman, C. J. Barton, K. A. Connell, D. Duniec, O. Kester, T. Lamy, T. Nilsson, P. Jardin, P. Sortais, G. Tranströmer, ISOLDE Collaboration, and IS397 Collaboration. Purification of radioactive neutron-rich argon beams using an ion source in charge breeding mode. *Nuclear Instruments and Methods in Physics Research A*, 556:31–37, 2006.
- [20] P. A. Hausladen, J.R. Beene, A. Galindo-Uribarri, Y. Larochele, J.F. Liang, P.E. Mueller, D. Shapira, D.W. Stracener, J. Thomas, R.L. Varner, and H. Wollnik. Opportunistic mass measurements at the Holifield Radioactive Ion Beam Facility. *International Journal of Mass Spectrometry*, 251:119–124, 2006.
- [21] T. Nilsson and M. Lindroos. HIE-ISOLDE: the technical options. CERN Report, 2006.
- [22] EURISOL. Targets, beams and intensities. The EURISOL Report Appendix C - Targets and Ion Sources for EURISOL, 2003. http://www.ganil.fr/eurisol/Final_Report.html
http://www.eurisol.org/site01/tasks_details.php?tID=13&ttk=13.
- [23] T. Lamy, R. Geller, P. Sortais, and T. Thuillier. Status of charge breeding with electron cyclotron resonance ion sources. *Review of Scientific Instruments*, 77:03B101, 2006.
- [24] Fredrik J.C. Wenander. *Charge breeding and production of multiply charged ions in EBIS and ECRIS*. PhD thesis, Chalmers University of Technology, 2001.
- [25] F. Ames, R. Baartman, P. Bricault, K. Jayamanna, M. McDonald, M. Olivo, P. Schmor, and D. H. L. Yuan. Charge state breeding of radioactive ions with an electron cyclotron resonance ion source at TRIUMF. *Review of Scientific Instruments*, 77:03B103–1–3, 2006.
- [26] F. Ames, J. Cederkäll, F. J. C. Wenander, B. H. Wolf, and the REX-ISOLDE Collaboration. REXEBIS operation and developments. *Review of Scientific Instruments*, 75:1607–1609, 2004.
- [27] GANIL. The scientific objectives of the SPIRAL 2 project, 2006. <http://www.ganil.fr/research/developments/spiral2/index.html>.
- [28] H. L. Ravn. Status and future development of ion sources for on-line mass separators. *Nuclear Instruments and Methods in Physics Research B*, 70:107–117, 1992.
- [29] P. Delahaye, C. J. Barton, K. Connell, T. Fritioff, O. Kester, T. Lamy, M. Lindroos, P. Sortais, G. Tranströmer, and F. Wenander. Recent results with the Phoenix Booster at ISOLDE. *Review of Scientific Instruments*, 77:03B105, 2006.

- [30] T. Lamy, J. L. Bouly, J. C. Curdy, R. Geller, A. Lacoste, P. Sole, P. Sortais, T. Thuillier, J. L. Vieux-Rochaz, K. Jayamanna, M. Olivo, P. Schmor, and D. Yuan. Charge state breeding applications with the ECR PHOENIX source: from low to high current production. *Review of Scientific Instruments*, 73:717–719, 2002.
- [31] T. Lamy, J. Angot, and T. Thuillier. European research activities on charge state breeding related to radioactive ion beam facilities. *Review of Scientific Instruments*, 79:02A909–1–5, 2008.
- [32] O. Kester. Joint research activity 3: Advanced charge breeding of radioactive ions. European activity report, 2005. <http://user.uni-frankfurt.de/~okester/jra03cb/>.
- [33] EURISOL. Bunching and charge breeding. The EURISOL Report Appendix C-Targets and Ion Sources for EURISOL, 2003. http://www.ganil.fr/eurisol/Final_Report.html http://www.eurisol.org/site01/tasks_details.php?tID=13&ttk=13.
- [34] O. Kester. Charge breeding. European commission-RTD project contract HPRI-CT-1999-50003 final report, 2004. <http://user.uni-frankfurt.de/~okester/jra03cb/>.
- [35] Antonio C.C. Villari and the SPIRAL group. First results at SPIRAL-GANIL. *Nuclear Instruments and Methods in Physics Research B*, 204:31–41, 2003.
- [36] V. Jaggi, R. A. Pavan, and S. K. Zeisler. Production of carbon stripper foils for high-power cyclotrons. *Nuclear Instruments and Methods in Physics Research A*, 561:1–3, 2006.
- [37] B. Hartmann, S. Kalbitzer, and Ch. Klatt. Energy spread of ion beams passing a gas stripper. *Nuclear Instruments and Methods in Physics Research B*, 124:490–499, 1997.
- [38] Jorge O. Fernández Niello, Alfred Priller, Andres Arazi, Denia Djokič, Robin Golser, Walter Kutschera, Peter Steier, Christof Vockenhuber, and Anton Wallner. A study of the tandem-terminal-stripper reaction ${}^1\text{H}({}^{12}\text{C},\gamma){}^{13}\text{N}$ with accelerator mass spectrometry. *Nuclear Instruments and Methods in Physics Research B*, 240:495–499, 2005.
- [39] Hans-Dieter Betz. Charge states and charge-changing cross sections of fast heavy ions penetrating through gaseous and solid media. *Review of Modern Physics*, 44:465–539, 1972.
- [40] A. B. Wittkower and H. D. Betz. Equilibrium-charge-state distributions of energetic ions ($Z > 2$) in gaseous and solid media. *Atomic Data and Nuclear Data Tables*, 5:113–166, 1973.
- [41] Kunihiro Shima, Takashi Mikumo, and Hiroyuki Tawara. Equilibrium charge state distributions of ions ($Z_1 \geq 4$) after passage through foils: Compilation of data after 1972. *Atomic Data and Nuclear Data Tables*, 34:357–391, 1986.

- [42] Kunihiro Shima, Noriyoshi Kuno, Mikio Yamanouchi, and Hiroyuki Tawara. Equilibrium charge fractions of ions of $Z = 4-92$ emerging from a carbon foil. *Atomic Data and Nuclear Data Tables*, 51:173–241, 1992.
- [43] D.W. Stracener. Status of radioactive ion beams at the HRIBF. *Nuclear Instruments and Methods in Physics Research B*, 204:42–47, 2003.
- [44] Uwe Greife, Ellen Simmons, Luke Erikson, Cybele Jewett, Jake Livesay, and Kelly Chipps. Possibilities for beam stripping solutions at a rare isotope accelerator (RIA). *Nuclear Instruments and Methods in Physics Research B*, 261:9–12, 2007.
- [45] Lu Hao-Lin, Walter F. Sommer, and Michael J. Borden. Review of carbon stripper foil lifetime. *Nuclear Instruments and Methods in Physics Research A*, 362:239–244, 1995.
- [46] Atsushi Yoshida, Kousuke Morita, Kouji Morimoto, Daiya Kaji, Toshiyuki Kubo, Yutaka Takahashi, Akira Ozawa, and Isao Tanihata. High-power rotating wheel targets at RIKEN. *Nuclear Instruments and Methods in Physics Research A*, 521:65–71, 2004.
- [47] Karl von Reden, Mei Zhang, Martha Meigs, Enid Sichel, Shaoli Fang, and Ray H. Baughman. Carbon nanotube foils for electron stripping in tandem accelerators. *Nuclear Instruments and Methods in Physics Research B*, 261:44–48, 2007.
- [48] B. Gavin, P. Batson, B. Leemann, and B. Rude. A continuous liquid sheet generator for ion stripping. *Nuclear Instruments and Methods in Physics Research B*, 10/11:788–791, 1985.
- [49] A. Leon, S. Melki, D. Lisfi, J. P. Grandin, P. Jardin, M. G. Suraud, and A. Cassimi. Charge state distributions of swift heavy ions behind various solid targets ($36 \leq Z_p \leq 92$, $18 \text{ MeV/u} \leq E \leq 44 \text{ MeV/u}$). *Atomic Data and Nuclear Data Tables*, 69:217–238, 1998.
- [50] P.N. Ostroumov, R.C. Pardo, G.P. Zinkann, K.W. Shepard, and J.A. Nolen. Simultaneous acceleration of multiply charged ions through a superconducting linac. *Physical Review Letters*, 86:2798–2801, 2001.
- [51] F. Wenander. Charge breeding techniques. CERN-AB Internal note, 2004.
- [52] R. Becker. EBIS/EBIT: Electron Beam Ion Source/Trap. In B. H. Wolf, editor, *Handbook of Ion Sources*, chapter 2, pages 157–182. CRC Press Inc., 1995.
- [53] E. N. Beebe and V. O. Kostroun. An electron beam ion source for laboratory experiments. *Review of Scientific Instruments*, 63:3399–3411, 1992.
- [54] Fredrik Wenander. EBIS as charge breeder for radioactive ion beam accelerators. *Nuclear Physics A*, 701:528c–536c, 2002.
- [55] F. Ames, G. Bollen, P. Delahaye, O. Forstner, G. Huber, O. Kester, K. Reisinger, and P. Schmidt. Cooling of radioactive ions with the Penning trap at REXTRAP. *Nuclear Instruments and Methods in Physics Research A*, 538:17–32, 2005.

- [56] U. Köster, O. Kester, and D. Habs. Ion sources for fission fragment accelerators. *Review of Scientific Instruments*, 69:1316–1321, 1998.
- [57] Evgeni D. Donets. Historical review of electron beam ion sources. *Review of Scientific Instruments*, 69:614–619, 1998.
- [58] Reinard Becker. Electron beam ion sources and traps. *Review of Scientific Instruments*, 71:816–819, 2000.
- [59] F. Wenander, P. Delahaye, R. Scrivens, R. Savreux, and the REX-ISOLDE Collaboration. The REX-ISOLDE charge breeder as an operational machine. *Review of Scientific Instruments*, 77:03B104–1–5, 2006.
- [60] D. Habs, O. Kester, T. Sieber, H. Bongers, S. Emhofer, P. Reiter, P.G. Thirolf, G. Bollen, J. Aystö, O. Forstner, H. Ravn, T. Nilsson, M. Oinonen, H. Simon, J. Cederkall, F. Ames, P. Schmidt, G. Huber, L. Liljeby, O. Skeppstedt, K.G. Rensfelt, F. Wenander, B. Jonson, G. Nyman, R. von Hahn, H. Podlech, R. Repnow, C. Gund, D. Schwalm, A. Schempp, K.-U. Kühnel, C. Welsch, U. Ratzinger, G. Walter, A. Huck, K. Kruglov, M. Huyse, P. Van den Bergh, P. Van Duppen, L. Weissman, A.C. Shotter, A.N. Ostrowski, T. Davinson, P.J. Woods, J. Cub, A. Richter, G. Schrieder, and the REX-ISOLDE Collaboration. The REX-ISOLDE project. *Hyperfine Interactions*, 129:43–66, 2000.
- [61] O. Kester, R. Becker, J. Pfister, A. Sokolov, G. Vorobjev, M. Vogel, D. Winters, and H. Zimmermann. The MAXEBIS at GSI as a test ion source for charge breeding and for HITRAP. *Review of Scientific Instruments*, 79:02A705–1–4, 2008.
- [62] J.G. Alessi, E.N. Beebe, O. Gould, A. Kponou, R. Lockey, A. Pikin, K. Prelec, D. Raparia, J. Ritter, and L. Snyderstrup. Progress on TEST EBIS and the design of an EBIS-based RHIC preinjector. In *Proc. of 2005 Particle Accelerator Conference*, pages 363–365. IEEE, 2005.
- [63] S. Schwarz, G. Bollen, M. Kostin, F. Marti, P. Zavodszky, J. R. Crespo López-Urrutia, J. Dilling, and O. Kester. A high-current electron beam ion trap as a charge breeder for the reacceleration of rare isotopes at NSCL. *Review of Scientific Instruments*, 79:02A706–1–5, 2008.
- [64] Pierre Delahaye, Oliver Kester, Thierry Lamy, Fredrik Wenander, and Holger Zimmermann. Preliminary report on the charge-breeding techniques study. EURISOL DS task 9 internal task note 09-25-2008-0003, 2008. http://www.eurisol.org/site01/preliminary_report_on_the_charge_breeding_techniques-813.html.
- [65] B. Blank, A. Bey, G. Cancel, J. Giovinazzo, J. Huikari, I. Matea, J. Souin, M.J.G. Borge, A. Meira, O. Tengblad, M. Turrion, D. Lunney, P. Delahaye, L. Fraile, and S. Sturm. Precision measurement of the half-life of the superallowed $0^+ \rightarrow 0^+$ β decay of ^{38}Ca . CERN INTC proposal 196, 2007.

- [66] P. Delahaye, B. Blank, and S. Sturm. Trap assisted spectroscopy with REXTRAP. *Nuclear Instruments and Methods in Physics Research B*, 266:4647–4651, 2008.
- [67] P. Delahaye, I. Ames, F. ad Podarera, R. Savreux, and F. Wenander. Recent developments of the radioactive beam preparation at REX-ISOLDE. *European Physics Journal A*, 25:739–741, 2005.
- [68] A. M. Hurst, D. G. Butler, P. A. and. Jenkins, P. Delahaye, F. Wenander, F. Ames, C. J. Barton, T. Behrens, A. Bürger, J. Cederkäll, E. Clément, T. Czosnyka, T. Davinson, G. de Angelis, J. Eberth, A. Ekström, S. Franchoo, G. Georgiev, A. Görgen, R.-D. Herzberg, M. Huysse, O. Ivanov, J. Iwanicki, G. D. Jones, P. Kent, U. Köster, T. Kröll, R. Krücken, A. C. Larsen, M. Nespolo, M. Pantea, E. S. Paul, M. Petri, H. Scheit, T. Sieber, S. Siem, J. F. Smith, A. Steer, I. Stefanescu, N. U. H. Syed, J. Van de Walle, P. Van Duppen, R. Wadsworth, N. Warr, D. Weisshaar, and M. Zielińska. Measurement of the sign of the spectroscopic quadrupole moment for the 2_1^+ state in ^{70}Se : no evidence for oblate shape. *Physical Review Letters*, 98:072501–1–4, 2007.
- [69] F. Wenander. Charge state breeders: on-line results. *Nuclear Instruments and Methods in Physics Research B*, 266:4346–4353, 2008.
- [70] B. H. Wolf. ECR Ion Sources >2.4 GHz. In B. H. Wolf, editor, *Handbook of Ion Sources*, chapter 2, pages 121–148. CRC Press Inc., 1995.
- [71] R. Geller. Specified elements of plasma physics applied to electron cyclotron resonance ion sources (ECRIS). In *Electron cyclotron resonance ion sources and ECR plasmas*, chapter 1, pages 1–146. Bristol: IOP, 1996.
- [72] C. Tamburella. *Projet PIAFE: production d'états de charge élevée pour des ions radioactifs*. PhD thesis, Université Denis Diderot PARIS VII, 1996. chapter 3: Production d'états de charge élevées: injection directe des ions monochargés à très basse énergie dans le plasma ECR, pages 69–113.
- [73] R. Geller, T. Lamy, and P. Sortais. Charge breeding of isotope on-line-created radioactive ions using an electron cyclotron resonance ion trap. *Review of Scientific Instruments*, 77:03B107–1–3, 2006.
- [74] T. Lamy, J.-F. Bruandet, N. Chauvin, J.-C. Curdy, M. Fruneau, R. Geller, G. Gimond, P. Sole, J.-L. Vieux-Rochas, G. Gaubert, L. Maunoury, P. Sortais, and A. C. C. Villari. Production of multicharged radioactive ion beams: new results for the $1+ \rightarrow n+$ method with the MINIMAFIOS and SARA-CAPRICE electron cyclotron resonance ion sources. *Review of Scientific Instruments*, 69:1322–1326, 1998.
- [75] P. Sortais, J. F. Bruandet, J. L. Bouly, N. Chauvin, J. C. Curdy, R. Geller, T. Lamy, P. Sole, and J. L. Vieux-Rochaz. Electron cyclotron resonance charge breeder. *Review of Scientific Instruments*, 71:617–622, 2000.

- [76] P. Sortais. Pulsed ECR ion source using the afterglow mode. *Review of Scientific Instruments*, 63:2801–2805, 1992.
- [77] Reinard Becker. Collision physics in ECR and EBIS/T. *Review of Scientific Instruments*, 73:693–695, 2002.
- [78] S. C. Jeong, M. Oyaizu, E. Tojyo, H. Kawakami, H. Ishiyama, H. Miyatake, K. Enomoto, Y. Watanabe, I. Katayama, T. Nomura, M. Matsuda, A. Osa, and S. Ichikawa. Test results of 18 GHz ECR charge breeder for KEK-JAERI RNB facility. *Review of Scientific Instruments*, 75:1631–1633, 2004.
- [79] M. Cavenago, O. Kester, T. Lamy, and P. Sortais. Model of accumulation, multi-ionization, and extraction of ions in ecr ion sources. *Review of Scientific Instruments*, 73:537–540, 2002.
- [80] Claude M. Lyneis, D. Leitner, D. S. Todd, G. Sabbi, S. Prestermon, S. Caspi, and P. Ferracin. Fourth generation electron cyclotron resonance ion sources. *Review of Scientific Instruments*, 79:02A321–1–4, 2008.
- [81] P. Suominen. *Modified multipole structure for electron cyclotron resonance ion sources*. PhD thesis, Faculty of Mathematics and Science of the University of Jyväskylä, 2006. chapter 5: Modified MultiPole Structure - MMPS, chapter 6: Experiments with the MMPS plasma chamber, pages 45-79.
- [82] N. Imai, S. C. Jeong, M. Oyaizu, S. Arai, Y. Fuchi, Y. Hirayama, H. Ishiyama, H. Miyatake, M. H. Tanaka, M. Okada, Y. X. Watanabe, S. Ichikawa, H. Kabumoto, A. Osa, Y. Otokawa, and T. K. Sato. KEKCB electron cyclotron resonance charge breeder at TRIAC. *Review of Scientific Instruments*, 79:02A906–1–3, 2008.
- [83] D. Leitner, M. L. Galloway, T. J. Loew, C. M. Lyneis, I. Castro Rodrigue, and D. S. Todd. High intensity production of high and medium charge state uranium and other heavy ion beams with VENUS. *Review of Scientific Instruments*, 79:02C710–1–4, 2008.
- [84] H. W. Zhao, L. T. Sun, X. Z. Zhang, X. H. Guo, Y. Cao, W. Lu, Z. M. Zhang, P. Yuan, M. T. Song, H. Y. Zhao, T. Jin, Y. Shang, W. L. Zhan, B. W. Wei, and D. Z. Xie. Intense beam production of highly charged heavy ions by the superconducting electron cyclotron resonance ion source SECRA. *Review of Scientific Instruments*, 79:02A315–1–6, 2008.
- [85] T. Thuillier, T. Lamy, L. Latrasse, I. V. Izotov, A. V. Sidorov, V. A. Skalyga, V. G. Zorin, and M. Marie-Jeanne. Study of pulsed electron cyclotron resonance ion source plasma near breakdown: the preglow. *Review of Scientific Instruments*, 79:03A314–1–4, 2008.
- [86] L. T. Sun, Z. M. Zhao, B. Wei, X. Z. Zhang, X. H. Guo, X. W. Ma, Y. Cao, W. He, and H. Y. Zhao. Brief review of multiple charge state ECR ion sources in Lanzhou. *Nuclear Instruments and Methods in Physics Research B*, 235:524–529, 2005.

- [87] N. Chauvin. *La transformation d'état de charge $1+/n+$ pour l'accélération des ions radioactifs*. PhD thesis, Institut des Sciences Nucléaires de Grenoble - IN2P3, Université Joseph-Fourier - Grenoble I, 2000. chapter 4: Les résultats expérimentaux de la transformation d'état de charge $1^+ \rightarrow n^+$, pages 87-132.
- [88] V. Banerjee, A. Chakrabarti, A. Bandyopadhyay, S. Chattopadhyay, A. Polley, T. Nakagawa, O. Kamigaito, A. Goto, and Y. Yano. Design of a two-ion-source (2-IS) beam transport line for the production of multi charged radioactive ion beams. *Nuclear Instruments and Methods in Physics Research A*, 447:345–349, 2000.
- [89] C. Eléon, G. Gaubert, P. Jardin, M.-G. Saint-Laurent, J. Alcantara, R. Alvès Condé, C. Barué, D Boilley, J. Cornell, P. Delahaye, M. Dubois, B. Jacquot, P. Leherissier, R. Leroy, R. Lhersonneau, M. Marie-Jeanne, L. Maunoury, J. Y. Pacquet, F. Pellemoine, C. Pierret, J. C. Thomas, and A. C. C. Villari. Development of a $1+/N+$ setup for the production of multicharged radioactive alkali ions in SPIRAL. *Review of Scientific Instruments*, 79:02A904–1–3, 2008.
- [90] T. Lamy, J.-L. Bouly, J.-C. Curdy, P. Sole, P. Sortais, T. Thuillier, J.-L. Vieux-Rochaz, and D. Voulot. ECRIS charge breeding: high resolution spectra and emittance. *Review of Scientific Instruments*, 75:1624–1626, 2004.
- [91] D. Habs, F. Ames, M. Cavenago, K. Connell, G. Nyman, G. Huber, B. Jonson, O. Kester, T. Lamy, M. Lindroos, K. Reisinger, T. Sieber, P. Sortais, L. Tecchio, A. Villari, D. Warner, F. Wenander, and B. Wolf. Charge breeding of radioactive ions in an electron cyclotron resonance ion source (ECRIS) at ISOLDE. CERN INT-C proposal 143, 2001.
- [92] F. Ames, R. Baartman, P. Bricault, K. Jayamanna, M. McDonald, P. Schmor, T. Spanjers, and D. H. L. Yuan. The ECRIS charge state breeding project at TRIUMF. *Review of Scientific Instruments*, 79:02A902–1–3, 2008.
- [93] P. Delahaye and M. Marie-Jeanne. Potentials of the ECR $1+n+$ charge breeding for radioactive ions. *Nuclear Instruments and Methods in Physics Research B*, 266:4429–4433, 2008.
- [94] N. Chauvin, J. F. Bruandet, J. C. Curdy, R. Geller, T. Lamy, and P. Sortais. Electron cyclotron resonance ion trap, a multicharged ion breeder/buncher. *Nuclear Instruments and Methods in Physics Research A*, 419:185–188, 1998.
- [95] P. Sortais, J.L. Bouly, N. Chauvin, J.C. Curdy, R. Geller, T. Lamy, P. Sole, and J.L. Vieux-Rochaz. ECRIS as ion source and charge breeder. *Nuclear Physics A*, 701:537c–549c, 2002.
- [96] T. Lamy, J. C. Curdy, R. Geller, C. Peaucelle, P. Sole, P. Sortais, T. Thuillier, D. Voulot, K. Jayamanna, M. Olivo, P. Schmor, and D. Yuan. Charge breeding method results with the PHOENIX Booster ECR ion source. *Proceedings of EPAC 2002, Paris, France*, pages 1724–1726, 2002.

- [97] E. Kugler. The ISOLDE facility. *Hyperfine Interactions*, 129:23–42, 2000.
- [98] M. Lindroos. Review of the ISOL method. CERN-AB Internal report, 2004.
- [99] R. Kirchner. Review of ISOL target-ion-source systems. *Nuclear Instruments and Methods in Physics Research B*, 204:179–190, 2003.
- [100] National Instruments. LabView 7, 2006. <http://www.ni.com/labview/>.
- [101] Charles Barton, Joakim Cederkäll, Pierre Delahaye, Oliver Kester, Thierry Lamy, and Mélanie Marie-Jeanne. Status of the PHOENIX electron cyclotron resonance charge breeder at ISOLDE. *Review of Scientific Instruments*, 79:02A905–1–3, 2008.
- [102] Rene Brun and Fons Rademakers. ROOT - an object oriented data analysis framework. *Nuclear Instruments and Methods in Physics Research A*, 389:81–86, 1997. <http://root.cern.ch/>.
- [103] J. Adamczewski, M. Al-Turany, D. Bertini, H.G. Essel, and S. Linev. The GO4 analysis framework, 2006. <http://www-win.gsi.de/go4/>.
- [104] IS397. <http://is397-collaboration.web.cern.ch/is397-collaboration/>.
- [105] C. Barton, P. Butler, K. Connell, P. Delahaye, T. Fritioff, D. Habs, C. Hill, O. Kester, H. Koivisto, P. Jardin, T. Lamy, R. Leroy, M. Lindroos, P. Sortais, P. Suominen, G. Tranströmer, A. Villari, D.D. Warner, and F. Wenander. Addendum to experiment IS397 INTC-P-143. CERN INTC proposal 143, 2005.
- [106] S. Sundell, H. Ravn, and the ISOLDE Collaboration. Ion source with combined cathode and transfer line heating. *Nuclear Instruments and Methods in Physics Research B*, 70:160–164, 1992.
- [107] V. I. Mishin, V. N. Fedoseyev, H.-J. Kluge, V. S. Letokhov, H. L. Ravn, F. Scheerer, Y. Shirakabe, O. Tengblad, and the ISOLDE Collaboration. Chemically selective laser ion-source for the CERN-ISOLDE on-line mass separator facility. *Nuclear Instruments and Methods in Physics Research B*, 73:550–560, 1993.
- [108] K.-L. Kratz, W. Böhmer, C. Freiburghaus, P. Möller, B. Pfeiffer, T. Rauscher, and F.-K. Thielemann. On the origin of the Ca-Ti-Cr isotopic anomalies in the inclusion EK-1-4-1 of the Allende-meteorite. *Memorie della società astronomica italiana*, 72:453–466, 2001.
- [109] G. Audi, O. Bersillon, J. Blachot, and A. H. Wapstra. The NUBASE evaluation of nuclear and decay properties. *Nuclear Physics A*, 729:3–128, 2003.
- [110] M. Turrión, M. Eller, R. Catherall, L. M. Fraile, U. Herman-Izycka, U. Köster, J. Lettry, K. Riisager, and Th. Stora. Management of ISOLDE yields. *Nuclear Instruments and Methods in Physics Research B*, 266:4674–4677, 2008.

- [111] J. Lettry, R. Catherall, P. Drumm, P. Van Duppen, A.H.M. Evensen, G.J. Focker, A. Jokinen, O.C. Jonsson, E. Kugler, H. Ravn, and the ISOLDE Collaboration. Pulse shape of the ISOLDE radioactive ion beam. *Nuclear Instruments and Methods in Physics Research B*, 126:130–134, 1997.
- [112] S. Lukić, F. Gevaert, A. Kelić, M.V. Ricciardi, K.-H. Schmidt, and O. Yordanov. Systematic comparison of ISOLDE-SC yields with calculated in-target production rates. *Nuclear Instruments and Methods in Physics Research A*, 565:784–800, 2006.
- [113] Canberra Industries. Genie 2000 - gamma acquisition and analysis. V2.1, 2002.
- [114] A. Herlert, S. Baruah, D. Beck, K. Blaum, M. Breitenfeldt, P. Delahaye, M. Dworschak, S. George, C. Guénaut, U. Hager, F. Herfurth, A. Kellerbauer, H.-J. Kluge, D. Lunney, D. Neidherr, R. Savreux, S. Schwarz, L. Schweikhard, and C. Yazidjian. High-precision mass measurements on neutron-rich nuclides with ISOLTRAP. *GSI Scientific Report 2006*, 1:255, 2007.
- [115] ISOLDE. Isolde psb yields, 2008. https://oraweb.cern.ch/pls/isolde/query_tgt.
- [116] Liviu Penescu. *ISOL Ion Source Development for 100kW Beam Power*. PhD thesis, University Politehnica of Bucharest, to be published.
- [117] J. Van de Walle, V. Bildstein, N. Bree, J. Cederkäll, E. Clément, J. Diriken, P. Delahaye, V.N. Fedosseev, R. Gernhauser, M. Huyse, O. Ivanov, T. Kröll, R. Krücken, N. Patronis, P. Van Duppen, D. Voulot, F. Wenander, K. Wimmer, and the MINIBALL collaboration. Investigation of beam purity after in-trap decay and Coulomb excitation of ^{62}Mn - ^{62}Fe . CERN INTC proposal 237, 2008.
- [118] J. Van de Walle. Production and coulomb excitation of neutron rich isotopes near ^{78}Ni at REX-ISOLDE. Proceedings of the Fifth International Conference on Exotic Nuclei and Atomic Masses - ENAM'08, to be published.
- [119] Anna Gustafsson. Investigation of beta-decay induced ion recoil effects at REX-ISOLDE and mass separation methods with REXTRAP. Master's thesis, Wiesbaden University of Applied Science, to be published.
- [120] S.C. Jeong, M. Oyaizu, E. Tojyo, H. Kawakami, H. Ishiyama, H. Miyatake, K. Enomoto, Y. Watanabe, I. Katayama, T. Nomura, M. Matsuda, A. Osa, and S. Ichikawa. The development of an ECR charge breeder for KEK-JAERI joint RNB facility. *Nuclear Instruments and Methods in Physics Research B*, 204:420–427, 2003.
- [121] D. Voulot, F. Wenander, E. Piselli, R. Scrivens, M. Lindroos, H.B. Jeppesen, L. Fraile, S. Sturm, Delahaye P., and the REX-ISOLDE collaboration. Radioactive beams at REX-ISOLDE: Present status and latest developments. *Nuclear Instruments and Methods in Physics Research B*, 266:4103–4107, 2008.

- [122] P. Sortais, J.-L. Bouly, J.-C. Curdy, T. Lamy, P. Sole, T. Thuillier, J.-L. Vieux-Rochaz, and D. Voulot. ECRIS development for stable and radioactive pulsed beams. *Review of Scientific Instruments*, 75:1610, 2004.
- [123] Seventh Framework Program. http://ec.europa.eu/research/fp7/index_en.cfm?pg=understanding.
- [124] D. Leitner, C. M. Lyneis, T. Loew, D. S. Todd, S. Virostek, and O. Tarvainen. Status report of the 28 Ghz superconducting electron cyclotron resonance ion source VENUS. *Review of Scientific Instruments*, 77:03A302–1–6, 2006.
- [125] C. Lyneis, D. Leitner, D. Todd, S. Virostek, T. Loew, A. Heinen, and O. Tarvainen. Measurements of bremsstrahlung production and x-ray cryostat heating in VENUS. *Review of Scientific Instruments*, 77:03A342, 2006.
- [126] M. Marie-Jeanne and P. Delahaye. Recent developments on the Phoenix ECR Booster at ISOLDE, CERN. *Chinese Physics C (formerly High Energy Physics and Nuclear Physics)*, 31-S1:216–218, 2007.
- [127] H. Wollnik. *Optics of Charged Particles*. Orlando, FL : Academic Press, 1987.
- [128] R. Hellborg, S. Bazhal, M. Faarinen, K. Håkansson, C.-E. Magnusson, P. Persson, G. Skog, and K. Stenström. A high resolution AMS-injector for the Pelletron in Lund. *PRAMANA journal of physics*, 59:1061–1073, 2002.
- [129] Kyoko Makino and Martin Berz. COSY INFINITY version 8. *Nuclear Instruments and Methods in Physics Research A*, 427:338–343, 1999.
- [130] R. Rao, O. Kester, T. Sieber, D. Habs, K. Rudolph, and REX-ISOLDE Collaboration. Beam optics design of the REX-ISOLDE q/m-separator. *Nuclear Instruments and Methods in Physics Research A*, 427:170–176, 1999.
- [131] C. Yin Vallgren. Charge breeding of radioactive ions in an Electron Cyclotron Resonance Ion Source(ECRIS) at ISOLDE: control system for HV power supplies. CERN Summer Student Program - internal PH report, 2007.
- [132] Fredrik Wenander. Charge breeding techniques. *Nuclear Physics A*, 746:40c–46c, 2004.
- [133] B.H. Wolf, J. Cederkäll, O. Forstner, F. Wenander, F. Ames, K. Reisinger, L. Liljeby, Ö. Skeppstedt, B. Jonson, G. Nyman, and The REX-ISOLDE Collaboration. First radioactive ions charge bred in REXEBIS at the REX-ISOLDE accelerator. *Nuclear Instruments and Methods in Physics Research B*, 204:428–432, 2003.
- [134] T. Kroyer. RF measurements on the DC block of the CERN ECR4 ion source. CERN-AB Internal note, 2005.

- [135] M. Marie-Jeanne and P. Delahaye. Charge breeding ions for nuclear astrophysics experiments at ISOLDE. In *Proc. of Ninth International Symposium on Nuclei In the Cosmos*, page 87. POS, 2007.
- [136] Mélanie Marie-Jeanne and Pierre Delahaye. Charge breeding ions for nuclear physics with the PHOENIX ECRIS. *Nuclear Instruments and Methods in Physics Research B*, 266:4387–4390, 2008.
- [137] Mélanie Marie-Jeanne, Carmen Angulo, Charles Barton, Joakim Cederkäll, Pierre Delahaye, Ulli Köster, Gabriel Martinez-Pinedo, Alberto Mengoni, Karsten Riisager, John Simpson, and Olof Tengblad. Measurement of ground state properties of neutron-rich nuclei on the r-process path between the N=50 and N=82 shells. CERN INTC proposal 225, 2007.
- [138] IS458. <http://is458-collaboration.web.cern.ch/is458-collaboration/>.
- [139] K.-L. Kratz, H. Gabelmann, P. Möller, B. Pfeiffer, H.L. Ravn, A. Wöhr, and the ISOLDE Collaboration. Neutron-rich isotopes around the r-process “waiting-point” nuclei $^{79}_{29}\text{Cu}_{50}$ and $^{80}_{30}\text{Zn}_{50}$. *Zeitschrift für Physik A*, 340:419–420, 1991.
- [140] H Grawe, K Langanke, and G Martínez-Pinedo. Nuclear structure and astrophysics. *Reports on Progress in Physics*, 70:1525–1582, 2007.
- [141] K.-L. Kratz, H. Gabelmann, W. Hillebrandt, B. Pfeiffer, K. Schlösser, F.-K. Thielemann, and the ISOLDE Collaboration. The beta-decay half-life of $^{130}_{48}\text{Cd}_{82}$ and its importance for astrophysical r-process scenarios. *Zeitschrift für Physik A*, 325:489–490, 1986.
- [142] R.D. Page. Selection of key experiments with the associated instrumentation. EURISOL DS Task 10: Physics and instrumentation, 2007. Internal task note.
- [143] G. Penessot. Montage et tests d’un dérouleur de bande et du dispositif de détection associé. Rapport de stage ENSICAEN - internal PH report, 2008.
- [144] O. Tengblad. Efficiency calibration of a neutron counter. Diploma thesis, Chalmers University of Technology, 1982.
- [145] N. Nica. *Nuclear Data Sheets*, 108:1287, 2007.
- [146] J. Van De Walle. internal ISOLDE report, 2008.
- [147] M. Berz and H. Wollnik. The program HAMILTON for the analytic solution of the equations of motion through fifth order. *Nuclear Instruments and Methods in Physics Research A*, 258:364–373, 1987.
- [148] M. Berz, H. C. Hoffmann, and H. Wollnik. COSY 5.0 - the fifth order code for corpuscular optical systems. *Nuclear Instruments and Methods in Physics Research A*, 258:402–406, 1987.